Alla mia famiglia e

alla mia cara amica

Elena Bertacco

“We must not forget that when radium was discovered no one knew that it would prove useful in hospitals. The work was one of pure science. And this is a proof that scientific work must not be considered from the point of view of the direct usefulness of it. It must be done for itself, for the beauty of science, and then there is always the chance that a scientific discovery may become like the radium a benefit for humanity.”

Marie Sklodowska-Curie (1867-1934)
The first woman to be awarded a Nobel Prize
The only woman who has been honoured twice

UNIVERSITÀ DEGLI STUDI DI PADOVA

DIPARTIMENTO DI SCIENZE CHIMICHE

SCUOLA DI DOTTORATO DI RICERCA IN SCIENZE MOLECOLARI
INDIRIZZO: SCIENZE CHIMICHE
CICLO XXIV

AEROSOL CHARACTERIZATION BY PMF ANALYSIS OF SINGLE PARTICLE ATOFMS SPECTRA

Direttore della Scuola: Ch.mo Prof. Maurizio Casarin
Supervisore: Ch.mo Prof. Andrea Tapparo

Dottorando: Chiara Giorio

2009-2011

Index

Preface

The present work of thesis, dealing with the chemical characterization of aerosol by factor analysis of ATOFMS spectra, has been carried out in collaboration with the research group of professor Roy M. Harrison of the Department of Geography, Earth & Environmental Sciences, University of Birmingham (UK). In particular, the two aerosol sampling campaigns were conducted by his research group while I have worked mainly on data treatment.

During my PhD I had the opportunity to work also in other research groups and to participate to different research projects, all concerning aerosol. A brief description of them is reported in the annex 3, 4 and 5 even if they are not related to the main project.

The project described in annex 3 (Study of atmospheric particles deposition into human lungs) was conducted during a visit of 6 months to professor Roy M. Harrison's research group. The project described in annex 4 (SOA aging experiment in a smog chamber-preliminary results) was conducted during a visit of 3 months at LISA (Laboratoire Interuniversitaire des Systèmes Atmosphériques, Université de Paris Diderot, Université de Paris Est-Créteil, CNRS, Créteil-France) working both with the research group of prof. Jean-François Doussin (LISA) and dr. Paola Formenti (LISA) and the research group of professor Anne Monod of the University of Provence. The project described in annex 5 (Assessment of the environmental exposure of honeybees to neonicotinoid insecticides used in corn seeds treatment) was conducted at the University of Padova, in collaboration with the research group of professor Vincenzo Girolami, of the Department of Environmental Agronomy and Crop Production of the University of Padova.

Abstract (EN)

Atmospheric particles are especially problematic to characterize because of the multiple sources, transport and transformation processes and, consequently, for their chemical composition. In this connection, on-line aerosol mass spectrometers are the most promising techniques able to provide both size and chemical composition in real time on a wide range of substances. ATOFMS - Aerosol Time of Flight Mass Spectrometer - is one of the most powerful state-of-the-art techniques which allows both size and chemical characterization of single airborne particles.

Conversely, data treatment is still a challenge and it is habitually performed using clustering algorithms, i.e. traditional k-means, or more powerful Art-2a (Adaptive Resonance Theory neural network) analysis. Otherwise, factor analysis, i.e. Positive Matrix Factorization (PMF), has been applied to data obtained from off-line techniques to perform source apportionment studies and to ATOFMS data *after* clustering with another technique but never *before* clustering.

In the present work of thesis, for the first time, Positive Matrix Factorization (PMF) has been directly applied to single particle ATOFMS spectra collected during two field campaigns conducted in Harwell (UK), a rural background site in the Oxfordshire and in a kerbside site, at Marylebone Road, a major traffic route in London (UK) city centre.

The results show that PMF analysis applied to single particles makes a deconvolution of their mass spectra and it extracts factors with very well defined and characterized chemical profiles, representing inorganic species, i.e. NIT (nitrate), SUL (sulphate), NaCl, and different elemental and organic carbon families including fresh EC, aged EC, oxidized organic aerosol, aromatic, and two organic nitrogen factors. Moreover, for each extracted component (PMF factor), its temporal trend, both in terms of scores, equivalent number of particles and volume, is obtainable contemporarily with its size distribution.

In order to validate the approach adopted, PMF results were compared to k-means cluster analysis results, and independent ion and non-refractory organic aerosol measurements, finding in general a good agreement.

Additionally, PMF analysis, applied to single particles, has been revealed as a powerful tool to study the mixing state of particles through a correlation analysis among temporal trends of PMF factors.

Abstract (IT)

Il particolato atmosferico è una miscela complessa di particelle solide e liquide di sostanze organiche ed inorganiche sospese in aria, le cui caratteristiche dimensionali, morfologiche e chimiche variano sensibilmente in funzione delle sorgenti emissive e dei processi chimico-fisici di trasformazione e di trasporto su brevi e lunghe distanze.

Tra le tecniche di analisi on-line del particolato quelle che impiegano la spettrometria di massa sembrano essere le più promettenti, al fine di ottenere una caratterizzazione chimica su un ampio spettro di sostanze. A questo proposito, l'ATOFMS (Aerosol Time of Flight Mass Spectrometer) è uno degli strumenti più potenti attualmente in commercio che permette di ottenere informazioni chimiche e dimensionali in tempo reale su singola particella. Tuttavia, il trattamento dei dati ottenuti da tale strumentazione è molto impegnativo e viene tradizionalmente effettuato attraverso l'analisi di classificazione, utilizzando procedure dedicate quali ad esempio K-means o la più sofisticata Art-2a (Adaptive Resonance Theory neural network). Al contrario, l'analisi fattoriale, come ad esempio la PMF (Positive Matrix Factorization), che viene ampiamente utilizzata per studi di assegnazione di sorgenti da dati di caratterizzazione ottenuti da tecniche di campionamento off-line, è stata fino ad ora applicata a dati ATOFMS preventivamente classificati attraverso l'utilizzo di un'altra tecnica.

Nel presente lavoro di tesi, per la prima volta, l'analisi PMF è stata applicata agli spettri di massa su singola particella ottenuti in due campagne di campionamento condotte ad Harwell, un sito di fondo rurale nell'Oxfordshire (UK), e in un sito ad elevato traffico veicolare, a Marylebone Road, nel centro di Londra (UK).

L'analisi PMF, applicata agli spettri di massa su singola particella, consente di estrarre fattori rappresentativi delle principali specie chimiche o di classi importanti di sostanze presenti nelle particelle. Tra queste, il carbonio elementare primario da poco emesso in atmosfera (fattore EC-), il carbonio elementare che ha subito dei processi ossidativi di invecchiamento (fattore EC+), i composti aromatici, il particolato organico ossidato (OOA), due componenti di particolato organico azotato (una primaria e una ossidata) e diverse specie inorganiche, come ad esempio il nitrato (fattore NIT), il solfato (fattore SUL) e il cloruro di sodio (fattore NaCl). Infatti, l'analisi

PMF effettua una deconvoluzione degli spettri di massa ed estrae fattori molto ben caratterizzati sotto il profilo chimico.
Inoltre, per ogni componente estratta (fattore PMF) è possibile calcolare l'andamento temporale in segnale strumentale, volume e numero equivalente di particelle, unitamente alla sua distribuzione dimensionale.
Al fine di validare l'approccio adottato, i risultati dell'analisi PMF sono stati confrontati con i risultati dell'analisi di classificazione k-means evidenziando in generale una buona correlazione. Inoltre l'analisi PMF, in particolare attraverso lo studio delle correlazioni fra gli andamenti temporali dei fattori, si è rivelata uno strumento utile per lo studio dello stato di mescolamento delle particelle presenti in atmosfera.

1. Introduction

Clean air is considered to be a basic requirement for human health and well-being. However, air pollution continues to pose a significant threat to health worldwide. According to a WHO assessment of the burden of disease due to air pollution more than 2 million premature deaths each year can be attributed to the effects of urban outdoor and indoor air pollution. More than half of this disease burden is borne by the populations of developing countries [WHO 2005].

Air pollution is the contamination of indoor or outdoor environment by any chemical, physical or biological agent that modifies the natural characteristics of the atmosphere. Household combustion devices, motor vehicles and industrial facilities are common sources of air pollution. Pollutants of major public health concern include particulate matter, carbon monoxide, ozone, nitrogen dioxide and sulphur dioxide [WHO 2005].

Perhaps, the first air pollution incident recorded took place in the 1930s in the Meuse Valley of Belgium. A heavy smog (the combination of smoke and fog) blanket settled over the valley, sickening more than 6000 and killing 63 people [Sportisse 2010]. Although the most famous air pollution event happened when a dense smog formed over London on December 4, 1952.

Estimates of PM_{10} concentrations during the December of that year range between 3000 and 14000 μg/m³, being approximately 50 times higher than normal levels at that time [De Angelo 2008]. The weather in Greater London was unusually cold for several weeks. Households were, therefore, burning more coal than usual to keep warm. The smoke from approximately one million coal-fired stoves, in addition to the emissions from local industry, was released into the atmosphere. Thousands of tons of black soot, tar particles, and sulphur dioxide had accumulated in the air from the heavy coal combustion and a light fog had lingered in the city throughout the day of 5th December. As night came, light winds, cool air, and high humidity at ground-level were ideal conditions for the formation of thick, smoky fog (smog). The smoke and fumes from the heavy coal combustion settled close to the ground and, due to a temperature inversion, remained motionless and created dense smog.

A temperature inversion occurs when the air closer to the ground is cooler than the air above it. This cool air is denser than the warmer air above it and does not rise and remains trapped in the inversion layer. In the opposite situation, warmer air at contact

with ground lifts up leading to circulation and dispersion of pollutants eventually emitted. Temperature inversions occur more frequently on cold winter nights because the ground cools and water vapour precipitates on low-level dust particles, forming a mist. This caused the thick, smoke-polluted air to be trapped under the inversion.
The implications of smog were not immediately clear until the deaths peaked at 900 per day on the 8th and 9th of December. During the smog and for two weeks following, approximately 4000 people were killed. Some reports indicate that death rates remained above-normal for the entire winter and it is now thought that approximately 12000 deaths can be linked to the great smog in winter 1952. The death toll could have been thousands higher with the knowledge of how many people died from complications of smog-related illnesses in the following months and years [De Angelo 2008].
Although this is the most famous air pollution event, the term “smog” was coined almost half a century earlier by H.A. Des Voeux, who first used it in 1905 to describe the conditions of sooty fog - fog intensified by smoke - which occurred often over British urban areas, and it was popularised in 1911 at the Manchester Conference of the Smoke Abatement League of Great Britain.

1.1. Atmospheric aerosols

The term particulate matter (PM) or atmospheric aerosols defines a suspension of airborne solid particles and/or droplets whose diameters are in the range of 10^{-9}-10^{-4} m. The lower limit comprehends molecules and molecular clusters while the upper limit is referred to particles subjected to rapid sedimentation (figure 1.1).
In atmospheric science, the term aerosol traditionally refers to suspended particles that contain a large proportion of condensed matter other than water, whereas clouds are considered as separate phenomena [Pöschl 2005].
Atmospheric aerosol particles originate from a wide variety of natural and anthropogenic sources. Primary particles are directly emitted as liquids or solids from sources such as biomass burning, incomplete combustion of fossil fuels, volcanic eruptions, and wind-driven or traffic-related suspension of road, soil, and mineral dust, sea salt, and biological materials (plant fragments, microorganisms, pollen, etc.). Secondary particles, on the other hand, are formed by gas-to-particle conversion in the atmosphere. Primary gaseous species undergo chemical reaction

which convert them into low-volatility products, which then partition to the particulate phase, i.e. new particles are formed by nucleation and condensation of gaseous precursors [Aiken 2008].

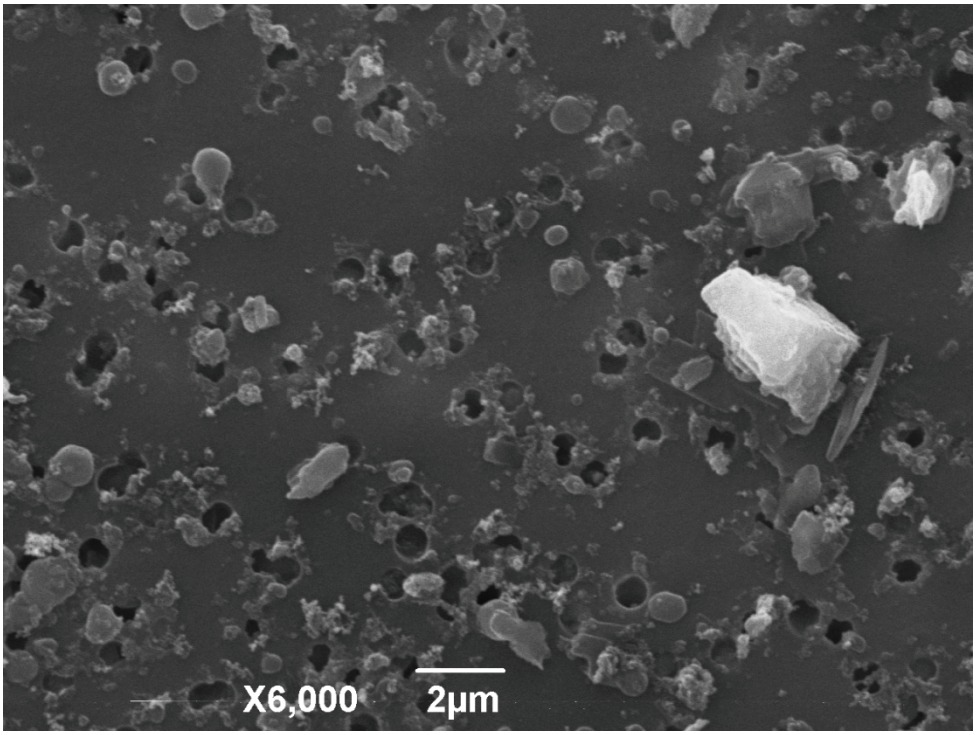

Figure 1.1. SEM image of Padova (Italy) urban $PM_{2.5}$ collected on a polycarbonate filter

1.2. Size distributions

Atmospheric particles emitted from air pollution sources and formed by natural processes have a multitude of different shapes and densities. That is why in air pollution control, it is necessary to use a particle size definition that directly relates to how the particle behaves in a fluid such as air. For this purpose the aerodynamic diameter is defined as the diameter of a spherical particle having a density of 1 g/cm^3 that has the same inertial properties (i.e. terminal settling velocity) in air as the particle of interest.

Depending on the physical and chemical processes involved in the particle formation and growth, the particles are conventionally divided into different size fractions, generally called “modes” (figure 1.2), the denomination of which mostly refers to how the particles are formed: nucleation, Aitken, accumulation, and coarse modes [CAFE 2004].

The nucleation (or ultrafine) mode resides in the range below 0.02 μm of particle diameter and usually presents its maximum number-density around 5-15 nm of particle diameter. New particles are formed by homogenous nucleation from chemical conversion of gaseous precursors into low volatility vapours. These particles have hours lifetime in the atmosphere as they rapidly coagulate with larger particles or grow into larger sizes due to condensation. Classical nucleation theory shows that the nucleation highly depends on the concentrations of the gaseous precursors, relative humidity and temperature. In particular, the nucleation is favoured by decreases in the temperature and/or increases in the relative humidity [Easter and Peter, 1994].

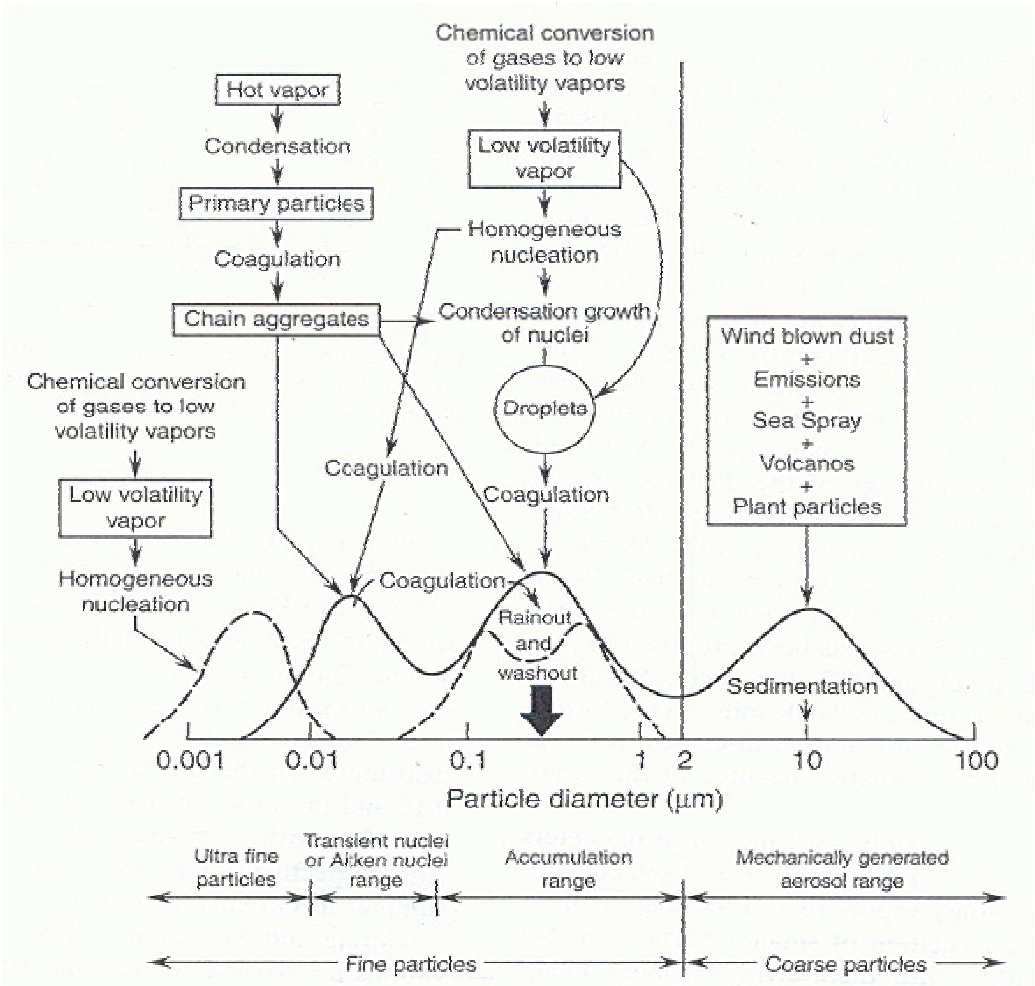

Figure 1.2. Atmospheric aerosol typical polimodal size distribution [Finlayson-Pitts 1999, Whitby 1976]

Aitken mode particles range from 0.02 to 0.1 μm and originate from either primary particles, natural and anthropogenic, or by growth of nucleation mode particles. It is likely that secondary Aitken mode particles are formed by coagulation of ultrafine

particles, by condensation and by liquid phase reactions. Primary sources that have very large emissions of Aitken mode particles are combustion processes.
The accumulation mode covers the range between 0.1 and up to 1 μm. In the atmosphere Aitken mode particles grow to accumulation mode particles primarily by coagulation and liquid phase reactions occurring in cloud droplets.
The coarse mode includes particles >1 μm. Most particles in the coarse mode range are formed by mechanical processes, such as the erosion of the earth's crust (mineral dust) or other materials, or the bursting bubbles on the ocean surface (sea spray).
Coagulation processes do not affect the particle number concentration of coarse particles. The processes of formation and growing of particles in the range <1 μm do not tend to produce particles >1 μm. On the other hand, mechanical processes forming primary particles cannot easily reduce the size of particles to diameters <1 μm owing to energetic limitations. Thus, the transfer of particles from different modes of the size spectrum presents a barrier around 1 μm.

1.3. Emission sources and chemical composition

Aerosol concentration and composition vary dramatically from one site to another as a consequence of the presence of different natural and anthropogenic sources contributing to it, formation mechanisms, medium and long-range transport mechanisms. The major PM_{10} and $PM_{2.5}$ components are sulphate, nitrate, ammonium, sodium, chloride, organic and elemental carbon, mineral dust and water.
PM_{10} means particulate matter which passes through a size-selective inlet as defined in the reference method for sampling of PM_{10}, EN 12341, with a 50% efficiency cut-off at 10 μm aerodynamic diameter [EU 2008/50/CE]. On the same basis, $PM_{2.5}$ and PM_1 are defined.
Natural particles originate mainly from sea spray, volcanic emission, mineral dust from long-range transport or erosion processes, forest fires and biogenic sources. Primary particle fraction of sea spray is mainly constituted by sodium chloride and some sulphates. The sea spray is generated by bubble bursting on the ocean/marine surface and by the breaking of waves in the coastal areas [Warneck 1987]. Sea spray primary particles undergo chemical processes in the atmosphere in which nitrate and sulphate could substitute chloride in the particles. This phenomenon is

known as “chlorine depletion” [Zhao 2008]. Volcanic emission are sources of primary particles but perhaps mainly secondary sulphur compounds from SO_2 emission. Although the contribution of such events to bulk particle mass levels in ambient air is generally limited. Crustal and mineral dust could be subject to regional variation as a function of the geology of the source areas, but in general they are composed of silicates, carbonates, aluminium, iron and metals in traces. They are originated by erosion processes, e.g. by the wind, or transported from desert region (e.g. Saharan dust events in south Europe). Forest fires are sources of both organic primary emission and gaseous precursors of particles. The biomass burning sources could be traced by some specific markers: levoglucosan, mannosan, galactosan which are degradation products of lignin burning [Zhang 2011, Reisen 2011]. Biogenic sources emit vegetal debris, pollen, spores which have sizes extending into the coarse mode and minor amounts of micro-organism (e.g. viruses, bacteria, fungi, protozoa or algae) contributing to particles in the size range < 2 μm. The natural secondary aerosol is constituted mainly by sulphate - originated from the oxidation of SO_2 emitted by volcanoes -, nitrate - originated from the oxidation of NO_x from soil transpiration and lightning - and organic aerosol originated from organic gaseous precursors such as biogenic emissions of terpenes from large forested areas.

In urban environments primary particles are emitted as a result of traffic-related combustion processes, house heating and industrial processes. Industrial activities such as building, mining, manufacturing of cement, ceramic and bricks, and smelters are typical sources of primary particles. Smelters produce mostly fine particles formed by condensation of hot vapours, often Ni, V, Mn and Cu are emitted. The other industrial sources mostly emit coarse primary mineral particles. Traffic-related combustion processes emit particles constituted by elemental carbon, various inorganic and organic compounds and gaseous precursors of secondary aerosol. Particles mechanically generated by road traffic, such as erosion of the pavement (road dust) and abrasion of brakes and tires, are coarse particles whereas particles emitted by vehicles exhaust are fine particles. Oxidation of SO_2 emitted by fossil fuel combustion and metal smelting [Charlson 1992] produces sulphuric acid which could be incorporated as it is or neutralised by ammonia or by reaction with calcium carbonate or sodium chloride. NO_x are emitted by traffic in urban environments and by some industrial processes. By oxidation of NO_x, nitric acid is formed, which may be neutralised and then incorporated into particles phase. Nitrate and sulphate size

distributions depends mainly on the neutralising agent. Therefore ammonium nitrate and sulphate are present in the fine fraction while sodium and calcium nitrate and sulphate are in the coarse fraction. Large agricultural areas, combustion of biomass and fossil fuels are important sources of organic gaseous precursors of anthropogenic secondary aerosol. These vapours are mainly emitted by gasoline evaporation (fugitive emission) and combustion processes. Human activities may also generate anthropogenic bio-aerosols. Bacteria and fungi generated in solid waste recycling and composting plants [Marchand 1995].

1.3.1. Carbonaceous particles

Carbonaceous particles are principally produced during combustion of liquid or gaseous fuels. Particles produced in this way consist of both EC (elementary carbon) and OC (organic carbon) and are known as soot. Soot particles are agglomerates of small roughly spherical elementary carbonaceous particles, which sizes vary from 20 to 30 nm. These elementary carbon particles cluster with each other, forming straight or branched chains. Soot particles absorb organic vapours when the combustion products cool down, accumulating significant amounts of organic compounds [Seinfeld and Pandis 1998]. Soot particles, as they aged, are mixed with other particles through coagulation, condensation of secondary aerosol compounds and cloud processing. Soot particles usually contain compounds other than pure graphitic carbon, e.g. particles emitted from spark-ignition engines consist of a core of EC covered with a layer of PAHs and an outermost shell of volatile compounds. Ambient carbonaceous aerosol in urban areas has been found to consist of aggregated spherules, with a range of carbon structures from amorphous to graphitic within aggregates. These aggregates could be coated with inorganic materials during aging processes [Seinfeld and Pandis 1998].

The organic component of ambient particles in both polluted and remote areas is a complex mixture of hundreds of organic compounds such as alkanes and alkenes, alkanoic acids, alkanals, aliphatic and aromatic di- and poly-carboxylic acids, diterpenoid acids, polycyclic aromatic hydrocarbons and polycyclic nitro-aromatic hydrocarbons, polycyclic aromatic ketones and quinones, steroids, N-containing compounds. OC concentrations are usually given as merely the concentration of carbon without including the contribution to the aerosol mass of the other elements

(oxygen, nitrogen and hydrogen) constituting the particles. Various studies have used factor of 1.2 to 1.6 for the calculation of the total organic mass associated with the OC [El-Zanan 2009, Bae 2006, Simon 2011]. Contributions of the primary and secondary organic aerosol are difficult to quantify. Lack of direct chemical analysis method for the identification of either of these components has led researchers to utilize several indirect methods (e.g. tracer compounds, emission and dispersion models). Elemental carbon has often been used as tracer of primary OC. The underlying hypothesis is that EC and primary OC often have the same sources, and so it is possible to extract a representative OC/EC ratio for the primary aerosol [Pio 2011].

Sources of primary carbonaceous particles in urbanized areas are fossil fuel burning (transportation and energy production), domestic burning (cooking and heating), biomass burning, including deforestation and agricultural waste fires [Kanakidou 2005].

A group of the most harmful substances for human health present in aerosol is the family of polycyclic aromatic hydrocarbons (PAHs). They are formed during the incomplete combustion of organic matter such as coal, oil, wood and gasoline fuels. Whereas some atmospheric PAHs result from natural forest fires and volcanic eruptions, anthropogenic emissions are the predominant source. Mobile sources are the major contributors in urban areas [Ravindra 2008].

Secondary organic aerosol is formed in the atmosphere by the mass transfer to the aerosol phase of low vapour pressure products from the oxidation of organic gaseous precursors. In the atmosphere, organic gases are mainly oxidized by the hydroxyl radical, ozone, NO_x and nitrate radical. The ability of a given volatile organic compound (VOC) to produce aerosol depends on its atmospheric abundance, its chemical reactivity and the volatility of its oxidation products. Low volatility compounds transfers to particulate phase by condensation or nucleation. Thus secondary aerosol implies both gas-phase reactions and a change of phase.

Oxidation of VOCs (volatile organic compounds) leads to the formation of more highly substituted products, i.e. addition of carboxylic acid, alcohol, aldehyde, ketone, alkyl nitrate, nitro groups, and therefore less-volatile products.

In general, small VOCs give a negligible contribution to SOA production, because of their high volatility, with the exception of isoprene, whose photooxidation products have been studied in smog chamber experiments and they have been detected in

ambient aerosols. On the contrary, large VOCs containing one or more double bonds are expected to be good SOA precursors. Aromatic hydrocarbons are the most significant anthropogenic precursors while terpenes are the major biogenic contributors.

SOA compounds, once formed, partition in particle phase, a process affected by temperature, relative humidity and the existence of other organics. After that, SOA compounds may undergo further chemical reaction in particle phase, to produce more oxidized and less-volatile compounds.

1.4. Particles lifetime and removal processes

Once aerosol is suspended in the atmosphere, it undergoes chemical and physical processes that transform and remove it. Particles lifetime depends on their size, but average lifetimes are of the order of a few hours to a few days.

The lifetime of an individual aerosol particle within a size range is difficult to determine, as it is function of the whole aerosol size distribution. Moreover, an aerosol particle undergoes physical and chemical processes that could modify its size and than its lifetime will change [Williams 2002]. Sinks processes and long-range transport influence its lifetime too.

The first attempts to measure a general residence time of atmospheric particles were made using radioisotopes as tracers. Values of the order of 5 days were deduced for mid-latitudes from the ratio of short-lived to long-lived radon daughters in surface air [Blifford 1952, Haxel 1955]. In a recent study of Williams et al. 2002, the variability in aerosol number and mass concentration over the Indian Ocean was used to measure the particles lifetime in different size ranges using an empirical relationship [Jobson 1998, Jobson 1999]. The results shows that particles of size less than 0.02 μm are affected by one dominant process, coagulation, for which particle residence times, in the order of a couple of hours, may be calculated based on temperature, pressure and number concentration. In the boundary layer, a troposphere layer of ~1 km of altitude at contact with the earth surface, the lifetimes of particles between 0.02 μm and 0.165 μm increases from 1 to 2.5 days while particle lifetime decreases from 2.5 to 0.5 days for particles between 0.165 μm and 2.5 μm [Williams 2002].

Above the boundary layer particle lifetimes increase from 6 days at 0.02 μm to a maximum lifetime at 0.065 μm of 15 days at 4-8 Km of altitude and 35 days at 8-13

Km. Accumulation mode particles have longer lifetime above the boundary layer, approximately 5 days [Williams 2002].

The principal removal mechanisms are divided in wet and dry depositions. Wet depositions is the name given to deposition pathways involving water. They include rainout, washout, sweepout and occult deposition but the first two mechanism are the most important [Seinfeld and Pandis 1998, Wang 2012]. The rainout process takes place in clouds producing rain. Aerosols act as nuclei for the condensation of cloud droplets, in which drops grow to such a large size that they fall (gravitationally settle) to the surface as rain drops. Washout describes the removal of aerosol by cloud droplets. If an aerosol is incorporated into an already existing cloud drop, and that drop grows large enough to fall as rain, the particle is said to have been washed out. Sweepout is the process which involves aerosol remaining below the cloudbase of a raining cloud that can impact into falling raindrops. If the impact leads to incorporation of the aerosol into the drop, the aerosol is deposited with the raindrop. In occult deposition, aerosol can be incorporated into droplets in clouds making contact with the surface of the ground (e.g. fog, orographic clouds). The impaction efficiency of droplets is higher than that of the aerosol they nucleate on. This produces an enhanced probability of impaction for such aerosol incorporated into drops [Trautner 1990, Norton 1988].

Dry deposition pathways are the group of deposition mechanisms that transport pollutants (in this case particles) directly to the surface without the aid of precipitation. Through the boundary layer there are two dry deposition mechanisms: gravitational settling and turbulent settling. Gravitational settling simply means particles falling under gravity and it interests large particles. Turbulence is the most effective dry vertical transport mechanism in the boundary layer. During turbulent fluid motions, particles are transported by the turbulence eddies and the Brownian diffusion.

Relative to rainout and washout, dry deposition is not very effective and influences only a very small fraction of the atmospheric aerosol [Williams 2002].

1.5. Human health effects

Several worldwide epidemiological and toxicological studies have proven that PM cause adverse health effects. A recent meta-analysis of epidemiological data and $PM_{2.5}$ concentration in Europe by that Clean Air For Europe (CAFE) depicted the

estimated loss of life expectancy due to exposure to fine particulate matter (figure 1.3) [Zimmermann 2011].

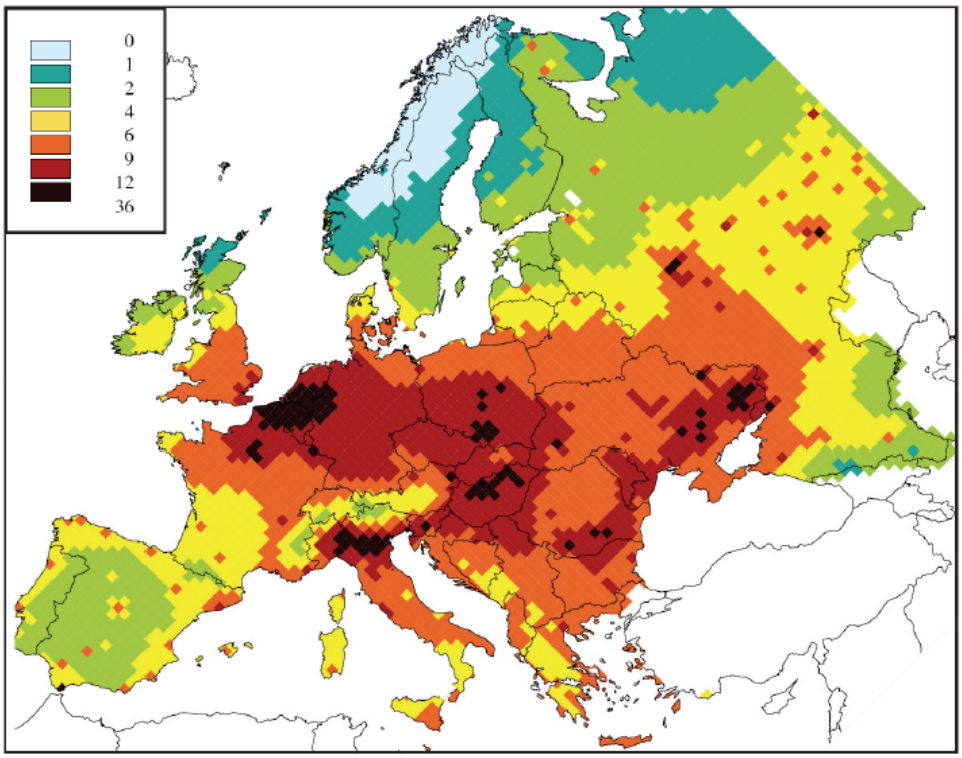

Figure 1.3. Loss in statistical life expectancy in months that can be attributed to the identified anthropogenic contribution to $PM_{2.5}$ (months), for the emissions of the year 2000. Calculation results for the meteorological conditions of 1997 [CAFE 2011].

A consistent increasing of cardiovascular and respiratory morbidity and mortality is currently associated to PM exposure [Nel 2005]. Effects of PM that have experimental support are inflammation, cytokine and chemokine release, production of white blood cells, oxygen free-radical production in the lungs, endotoxin mediated cellular and tissue responses, stimulation of irritant receptors and covalent modification of key cellular enzymes [Nel 2005]. In order to prevent adverse health effects we need to understand which particle properties are important and related to them. Parameters and components potentially relevant for these adverse effects are the specific surface area, the particle size, transition metals and strong acids content and some organic compounds [Pöschl 2005, Harrison 2000].

Particle size and surface area are important characteristics from a toxicological point of view. As the size of a particle decreases its surface area increases allowing a greater proportion of its atoms or molecules to be displayed on the surface, rather than inside the material, and the contact surface with lung tissues increases [Nel 2006]. Moreover, particle size is crucial for penetration and deposition efficiency into

human lungs, with ultrafine particles ability to penetrate the membranes of the respiratory tract and enter the blood circulation. The occupational health community has defined size fractions to be used in human health protection. This convention classifies particles into inhalable, thoracic, and respirable particles according to their upper size cuts characterized in terms of their entrance into various respiratory system regions (figure 1.4). Accordingly, inhalable particles enter the respiratory tract, including the head airways. Thoracic particles travel past the larynx and reach the lung airways and the gas-exchange regions of the lung. Respirable particles are a subset of thoracic particles that are more likely to reach the gas-exchange region of the lung [Wilson 2002].

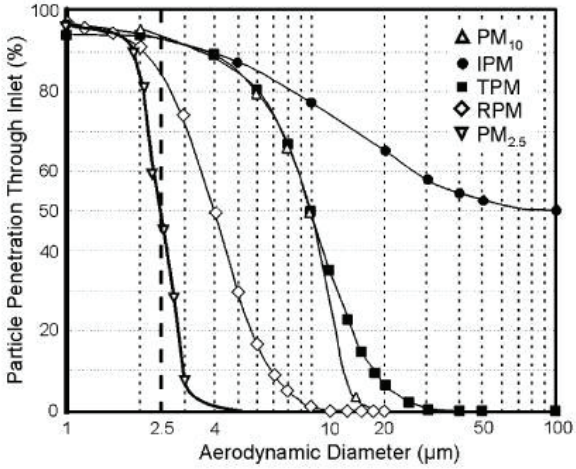

Figure 1.4. Occupational health sizecuts [Wilson 2002]

Besides particle size and surface area, it is difficult to imagine that chemical composition does not play a role in determining human adverse health effects. Transition metals, and particularly iron, may contribute to the production of hydroxyl radicals through the Fenton reaction [Harrison 2000, Nel 2006]. Important aspects to be considered are particles chemical speciation and hence their bioavailability and potential to participate in specific reactions rather than determining their total concentrations. Some studies revealed that sulphate content is strongly related to mortality rates [Dockery 1993, Pope 1995]. Sulphuric acid is non-volatile, and once formed, is immediately incorporated into airborne particles which are only subsequently neutralised by atmospheric ammonia. Thus, in environment with low ammonia concentrations, airborne particles may have an appreciable strong acid content that could explain the sulphate toxic action [Harrison 2000]. More recent studies indicate that there are not epidemiological and toxicological evidences of a

direct health risk of sulphate alone. There are indeed some possible indirect processes through which sulphate and nitrate in PM may affect health-related endpoints, including interaction with metals and participation to secondary organic matter production [Reiss 2007].

Particulate organic matter in ambient air is a complex mixture of chemicals, i.e. polycyclic aromatic hydrocarbons (PAHs). The International Agency for Research on Cancer (IARC) classified some PAHs, i.e. benzo[a]pirene, as human carcinogens. Carcinogenic PAHs are known to bind covalently to DNA, forming DNA adducts, after metabolic activation by cytochrome P450 enzymes and they can also induce oxidative lesions resulting from the production of reactive oxygen species (ROS). The assessment of the risk associated with exposure to PAHs is still a challenge because they are present in ambient air as a complex mixture and the interactions among components may lead to additively, synergistic or antagonistic effects. In a recent study, Topinka et al. clearly demonstrated that organic matter extracted from PM2.5 induce DNA adducts and oxidative DNA damage in *in vitro* cell-free assay experiments [Topinka 2011].

Several studies have indicated that the biogenic fraction might play a key role in determining inflammation and irritation. In addition, the presence of pathogenic bacteria and bacterial endotoxins are of great concern for their potential harmful effects [Franzetti 2011]. Even though atmosphere is an extreme environment for microorganisms because of its chemical and physical characteristics and its large dispersing capability. First investigations demonstrated that bioaerosol in the atmosphere can be not only dead or dormant but also actively reproducing [Fuzzi 1997]. The results of Franzetti et al. showed large seasonal variations in the microbial communities in PM_{10} and $PM_{2.5}$ with a high species richness [Franzetti 2011].

Fujii et al. postulated that adverse health effects associated to PM_{10} exposure are related to proinflammatory mediators, like interleukins (IL-6 and IL-8), produced in the lung and released into the circulation where they initiate a systemic inflammatory response [Fujii 2002]. *In vitro* testing on human monocytes, showed that water extracts of urban $PM_{2.5-10}$ induces 20 times the amounts of IL-6 and IL-8 than $PM_{2.5}$, suggesting the role of gram-negative bacteria and/or endotoxins in systemic inflammation [Monn 1999]. Furthermore, circulating levels of cytokines were elevated in subjects exposed to high levels of PM_{10} during an episode of acute air pollution [van Eeden 2001].

Moreover, reactions involving microorganisms might occur, i.e. absorption/desorption and releasing of organic matter and molecules because of cell lysis [Cote 2008].

1.6. Environmental and climate effects

Climate change is strongly influenced by both gaseous and aerosol anthropogenic emissions and, in the past decades, it has become a problem of serious concern [Rasool 1971]. Human activities result in emissions of four principal greenhouse gases: carbon dioxide (CO_2), methane (CH_4), nitrous oxide (N_2O) and the halocarbons [Forster 2007]. While knowledge about green-house gases is well advanced, the influence of aerosol particles to climate change is far less understood [Pósfai 2010].

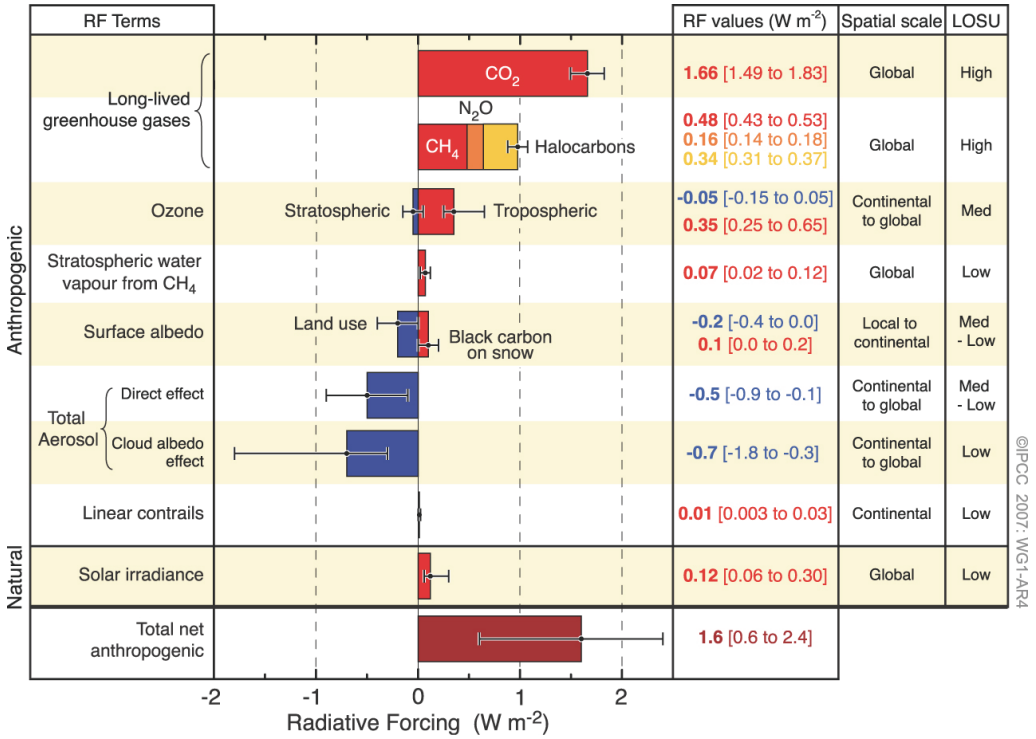

Figure 1.5. Summary of the principal components of the radiative forcing of climate between 1750 and 2005 [Forster 2007]

For several decades in the 20th century the solar intensity at the earth's surface has registered a gradual decreasing which has been named global dimming. It is likely that aerosol is one of the cause that contributes to this trend, which has reversed since 1980s (global brightening) when sulphate aerosol has declined significantly with the Clean Air Act in the USA and similar policies in Europe [Pósfai 2010]. Example of a dimming event is a marked drop in sunlight at the surface of the Indian

Ocean relative to areas far from the continents, corresponding to a tenfold increase in airborne soot and other aerosol particles [Pósfai 2010, Ramanathan 2007].

While greenhouse gases absorb upwelling infrared radiation at the top of the atmosphere, aerosols increase the reflection of solar radiation back to space through a variety of both radiative and physical processes [Ramanathan 2001]. Global estimates of radiative forcing, which is “the change in net (down minus up) irradiance at the tropopause after allowing for stratospheric temperatures to readjust to radiative equilibrium, but with surface and tropospheric temperatures and state held fixed at the unperturbed values” [Forster 2007], due to anthropogenic aerosols indicate a cooling effect (figure 1.5). Changes arising from the aerosol scattering and absorption of radiation are referred to as directive radiative forcing [Ramanathan 2001].

Moreover aerosols exert indirect effects on the radiative forcing through their important role as cloud condensation nuclei (CCN) and ice nuclei (IN). Increasing concentration of CCN results in increased concentrations of cloud droplets but smaller in size, resulting in enhanced shortwave albedo of clouds. Nevertheless, the perturbation in longwave absorption by tropospheric clouds arising from an increase in cloud-droplet concentration is much less important because tropospheric clouds are already optically thick at infrared wavelengths. Accordingly to Kelvin and Raoult effects, heterogeneous nucleation is thermodynamically favoured over homogenous nucleation of water. The result is that in aerosol polluted cloud the tendency is to form more but smaller droplets. Cloud albedo or Twomey effect consists of more-numerous and smaller cloud particles reflect more solar radiation leading to climate cooling [Pöschl 2005, Ramanathan 2001, Stevens 2009]. Moreover the decreasing in droplet radius leads to a decrease in precipitation efficiency, and so an increase in cloud lifetime and in turn the amount of clouds. This increase in cloudiness will lead to a further increase in the reflection of solar radiation, giving rise to the second indirect effect on radiative forcing [Albrecht 1989].

Aerosol particles could induce the formation of ice particles by acting as ice nuclei (IN) and, according to Bergeron-Findeisen theory [Koop 2004], because the vapour pressure of ice is lower than that of water, ice particles grow faster than water droplets and thus will initiate precipitation leading to a decrease in the solar radiation reflection [Pósfai 2010].

The major impact of the large reductions in the surface solar radiation along with the precipitation suppression is to spin down the hydrogeological cycle. Moreover the

interaction between aerosols effects and greenhouse gases effects is largely unknown because the former are concentrated regionally and the latter are distributed globally. This asymmetric nature of the aerosol forcing can also lead to a multitude of feedback effects [Charlson 1992, Ramanathan 2001].
Aerosol particles may contain chemically distinct species or they can be a complex mixture. Pure sulphate aerosols primarily scatter solar radiation and cause cooling. Carbonaceous aerosols indeed, absorb and scatter solar radiation. Black carbon or soot, strongly absorb solar radiation leading to a warming of the atmosphere and a cooling of the earth surface because of a reduction of the solar radiation reaching the surface [Quaas 2011, Zhuang 2011].

1.7. On-line sampling techniques

The major limits of off-line sampling techniques, which means collecting particles on filters and analyzing them in the laboratories, are the low time resolution (24 hours in general), the modifications of samples that could occur during the transport, i.e. reactions between particles and substrate, reactions between particles, loss of semivolatile compounds and absorption of volatile compounds.
On-line aerosol measurement techniques provide integrals of specified variables or size segregated quantification. Condensation Particles Counter (CPC) provides the total aerosol number concentration. Particles are grown by condensation of water or alcohol (usually n-butyl alcohol) until they are sufficiently large to be detected optically [Sinclair 1975, Bricard 1976]. CPCs can detect individual particles as small as 3 nm and the response is typically insensitive to the composition of the measured particles. CPCs are also used as detectors for other instruments [McMurry 2000]. The automated methods most in use for measurement of aerosol mass concentrations are beta-gauge and oscillating element instruments. The first is based on the measurement of attenuation of beta radiation from a radioactive source through a particle-laden filter. Particle mass loading is determined from the increase in attenuation that is measured as particles are added to the filter [Husar 1974]. The latter is constituted by a tapered tube, the wide end of which is mounted to a rigid base. Particles are collected on a filter that is mounted on the narrow end of the tapered element, which is free to oscillate. The element vibrates at a frequency that

depends on its geometrical and mechanical properties and on the mass of the filter [McMurry 2000, Patashnick 1991].

The instruments able to do size-resolved measurements are: OPC, APS and SMPS. Optical particle counters (OPC) measure the amount of light scattered by individual particles traversing a tightly focused beam of light. Particle size is determined from the intensity of the light scattered in a certain direction by using a calibration curve typically obtained from measurements using spherical particles of known size [McMurry 2000, Biswas 1987, Cooke 1975, Willeke 1976]. OPC could detect particles with diameters larger than 0.05 μm (laser OPC) or 0.3 μm (white light/incandescent source OPC) [Gebhart 1976]. Aerodynamic particle sizer (APS) utilizes measurements of particle speed in an accelerating gas flow to determine size [Baron 1993]. Aerodynamic size is inferred from particle velocity which is determined by measuring the time of flight of the particles between two lasers separated by a known distance [Dahneke 1973, Dahneke 1977]. Light scattered is used to detect particles and not to measure the size. APS could detected particles with diameters larger than 0.5 μm. Scanning electrical mobility particle sizer (SMPS) classifies particles according to their mobility in an electrical field [Hinds 1982, Whitby 1966, Liu 1974]. Electrical mobility depends on gas properties, particle charge and geometric particle size but is independent from density. The SMPS include an electrostatic classifier (differential mobility analyzer, DMA) and a particle detector (CPC) and it can measure size distributions in the 3-500 nm diameter range [Liu 1974, Knutson 1975]. In the DMA aerosol is exposed to a bipolar cloud of ions, where it achieves Boltzmann charge equilibrium [Liu 1974, Adachi 1983]. The mean charge of particles leaving the charger is close to zero, but with a fraction of multiple charged particles which increases with increasing size. Subsequently, particles, in a narrow mobility range, follow an annular flow through two coaxial cylinders and are delivered to the detector. Particle size is selected by the classifying voltage and the complete size range is obtained by ramping the classifying voltage continuously [Wang 1990].

Beside particle number and mass concentrations on-line chemical speciation is possible for the major components of PM.

Elemental and organic carbon content could be measured in real time by an automated carbon analyzer [Turpin 1990]. It collects PM on quartz filters, after removing coarse particles by an impactor. Samples are analyzed by sequentially heating the filters, firstly in helium at 650°C to volatilize organic carbon. The gases

evolving from the filter are converted to CO_2 in a MnO_2 catalyst at 1000°C and then converted to CH_4 in a nickel-firebrick methanator at 500°C. Methane is then detected using a FID. Elemental carbon is thereafter obtained by filter exposure to a 2% mixture of O_2 in He and ramping from 350 to 750°C.

Water soluble aerosol compounds can be analysed in real time through a GRAEGOR [Thomas 2009] which uses ion chromatography (IC) for anions and flow injection analysis (FIA) for NH_4^+ and NH_3 within an hour.

Particle hygroscopicity could be measured by HTDMA (hygroscopic tandem differential mobility analyzer). The instrument is constituted by two DMAs in series [Rader 1986, McMurry 1989]. Aerosol classified by the first DMA is humidified at a particular %RH and then measured with the second DMA. HTDMA can provide information on the effect of humidity on particle size and water uptake among particle of a given size.

1.7.1. Mass spectrometric techniques

Atmospheric particulate matter is especially problematic to be characterized because of the multiple compositions, size ranges and a wide spectrum of both natural and anthropogenic sources. In this connection on-line measurement deploying mass spectrometric techniques are the most promising in order to characterise both aerosol size and chemical composition for a wide range of substances.

Aerosol mass spectrometry instruments could be classified according to the sample introduction mechanism, aerosol sizing techniques, ionization techniques and mass spectrometer type (figure 1.6).

The sample introduction method is a crucial parameter for single particle analysis because it has to avoid any sample alteration, contamination, volatilization or crystallization. The particle beam characteristics are of fundamental importance [Murphy 1964, Dahneke 1970]. A particle beam is formed when an aerosol expands through a capillary or converging nozzle into vacuum. The maximum velocity of each particle depends on its size, mass, shape and density. Divergence in the particle beam is another important characteristic, in which smaller particles, less massive, follow gas flow more than particles with greater mass. More recently, aerodynamic lenses have been introduced to focus particle beams [Suess 1999, Liu 1995, Zhang 2004].

Aerodynamic lens typically consist of a hole in the centre of a plate blocking the flow and could be considered as a short capillary [Kulkarni, Baron, Willeke 2011]. A series of aerodynamic lenses is used to focus particle beam. At the end, the final exit orifice controls the supersonic gas and particle acceleration into vacuum.

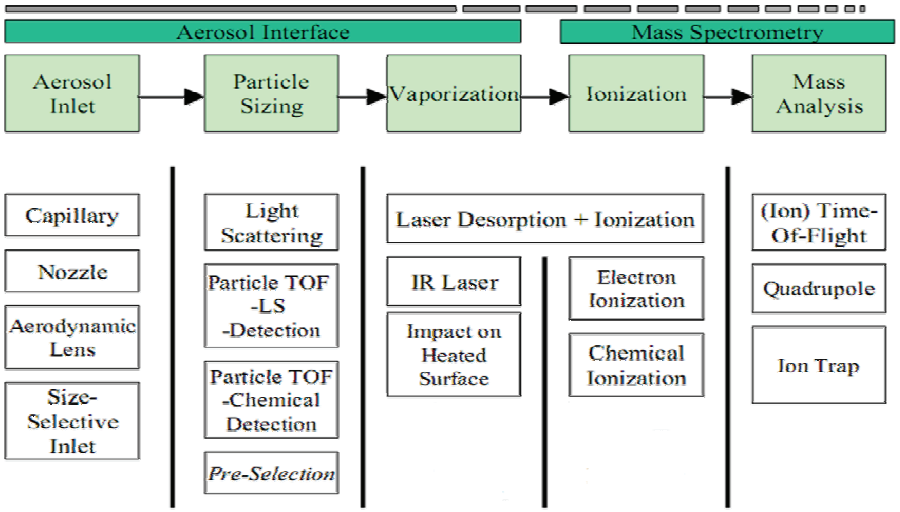

Figure 1.6. Aerosol Mass Spectrometers most used building blocks [Jimenez 2002]

The joint determination of both size and chemical composition is one of the major goal in which recently there have been developments in aerosol MS community. In the sizing region, one or two continuous wave lasers to either measure the light scattering intensity from single particles or the particles time of flight between two fixed position lasers, are the most used techniques to size single particles. Particles time of flight is also measured between a mechanic chopper and the MS detector, in AMS (Aerosol Mass Spectrometer) instruments, in order to measure PM size distributions in mass.

A variety of ionization techniques have been applied to particle analysis, surface or thermal, electron impact (EI) and laser desorption/ionization (LDI) are the most used in on-line mass spectrometers instruments. Electron impact ionization (EI) requires that the analyte be in its gaseous phase, therefore, surface volatilization/ionization must be the preceding step. Particles volatilization is not always easy to achieve, thus only the non-refractory aerosol component could be analysed with thermal desorption with EI ionization. Laser desorption/ionization (LDI) is the most utilized techniques for on-line single particles analysis. The laser could be either focused on a particle, as with LAMMS (Laser Microprobe Mass Spectrometry), or is triggered to

fire at a single particle, as with on-line instruments. The particle absorbs photons and undergoes both desorption and ionization by the same pulse. Although the details of this process are still not completely understood, the thermal process seems to be favoured as opposed to an electronic one [Heinen 1981]. LDI efficiency not only depends on the ionization potential and the lattice energy of the substance but also on the absorption cross section and the wavelength utilized. It can perform the analysis on a wide range of materials from elemental and organic carbon species, to inorganic salts and metals. Quantification of LDI spectra is still a challenge due to differences in sensitivity between species, i.e. it is highly sensitive to alkali metals, and reproducibility of the laser power density absorbed from particle to particle [Gross 2000, Cotter 1997, Thomson 1993, Thomson 1997].

Throughout the development of aerosol MS, different mass analyzers have been utilized. Magnetic sector instruments were utilized in the first on-line surface ionization instruments. In general, the use of magnetic sector instruments have been limited in single particle analysis because of their scanning nature, as a complete mass spectra cannot be obtained from a single particle [Stoffel 1994]. Quadrupole mass spectrometer were widely employed in aerosol on-line MS instruments. However, they cannot be used to obtain a complete mass spectrum with single particle analysis as the time needed to scan the full mass range is too long [Miller 1986]. Another type of mass spectrometer utilized for particles analysis is the ion trap MS. A limitation of this technique for single particle analysis includes space charge effects. Ion traps can only hold a certain number of ions until repulsive, or space charge, forces cause ion leakage limiting mass resolution as ion density increases, causing calibration problems and non-linearity response [Guan 1994, Eades 1993]. This could be a major problem in particles analysis. Time of flight mass spectrometer (TOFMS) are widely utilized for single particle analysis [Gard 1997]. In general, because of its speed, simplicity, high sensitivity and the ability to provide a complete mass spectrum of each individual particle, TOFMS has been the mass spectrometer of choice for recent on-line single particle MS instruments.

Concerning single particle analysis, ATOFMS (Aerosol Time of Flight Mass Spectrometer) is perhaps the most in used, commercially, available instrument.

The ATOFMS (TSI Model 3800–100) collects bipolar mass spectra of individual aerosol particles. Briefly, particles are sampled through an orifice and accelerated through the aerodynamic lens to the sizing region of the instrument. Here, the

aerodynamic diameter of particles sizes between 100 nm and 3 μm is calculated based on their time-of-flight between two orthogonally positioned continuous wave lasers (λ=532 nm) [Gard 1997, Su 2004]. Particles are then transmitted to the mass spectrometry region where a pulsed high power desorption and ionization laser (λ=266 nm, 1 mJ/pulse) is triggered and it desorbs and ionizes the particle's components in the centre of the ion source of a bipolar reflectron ToF-MS.
Of course, particulate matter has been widely analysed with off-line mass spectrometric techniques both with direct sample injection or with an extraction preceding step. ICP-MS, GC-MS and LC-MS have been used with traditional sample introduction which requires the dissolution of an aerosol from a filter sample leading both to an alteration of the original analyte and a limitation of the analysis to bulk samples. Secondary ion mass spectrometry (SIMS) has been applied to off-line single particle analysis of filter samples [Christie 1981]. It utilizes an ionization process, usually in conjunction with a microscope, in which detailed surface analysis is achieved.

1.8. Source apportionment and factor analysis

In environmental studies, factor analysis techniques (PCA, PCFA, PMF) are widely used to perform source apportionment from data taken at receptor sites. Positive Matrix Factorization is the most used techniques in this field as it does not require a priori knowledge about source profiles and in the most cases it is not subjected to inconsistencies like rotational ambiguity, lack of uniqueness of the solutions because of the non negativity constraint of factor solutions. It relies on the accuracy of error estimates to produce reliable non negative results and uses data error estimates to provide both variables and samples weighting. This is particularly important when less robust datasets have to be used because of the presence of many missing or below detection limits values, as the case of mass spectra, that could have indeed the ability to define real sources or even be source markers [Owega 2004, Paatero 1994, Paatero 1998, Zhang 2008]. PMF analysis has been successfully applied for source apportionment studies of 24h averaged data from analysis of particles collected on filters [Stortini 2009, Jia 2010, Dogan 2008, Bari 2009, Alleman 2010]. The principal limit of source apportionment studies applied to 24h averages data is the loss of point sources contribution because the characteristic times of this features

requires higher temporal resolution. Thus, the results obtained are usually limited to the extraction of the 3-4 main sources like crustal, marine, combustion sources and secondary particulate matter while other sources, which have a shorter characteristic time and could be characterized by peak events, could be extracted only with a wide range chemical analysis, size segregation and more frequent measurement [Pekney 2006, Wexler 2008]. PMF applied to data obtained from on-line techniques could be a useful tool to reach this purpose. In fact, PMF analysis was successfully applied to 1h semi-continuous characterization data of both particulate and gas phase species leading to the extraction of 6 main sources, while by adding ATOFMS and AMS (aerosol mass spectrometry) data to the original dataset the PMF was able to identify 16 factors during a field campaign in Riverside, CA [Eatough 2008]. In situ measurements of volatile organic carbon measurements coupled with other gas and particles phase measurements subjected to PMF analysis are able to apportion the anthropogenic sources in urban background locations or in roadside locations [Lanz 2009, Thornhill 2010]. Moreover PMF was successfully applied to AMS dataset to characterise the organic component of PM_1. In these cases PMF was able to separate the contribution of chemically reduced urban primary emissions, oxygenated organic aerosol, and the biomass burning component [Aiken 2009, DeCarlo 2010, Tsimpidi 2010]. Moreover, Ng et al. reported the application of full CMB (Chemical Mass Balance) modeling to AMS data using experimentally determined aerosol source profiles as fixed input mass spectra. CMB is a simple linear decomposition algorithm which can separate factors that correlate strongly in time. However, CMB is applicable only with an appropriate and complete source characterization [Ng 2011, Zhang 2011]. Recently, Ulbrich et al applied 3D factorization to full AMS mass spectra and size distributions acquired with a time-of-flight spectrometer, obtaining the size distributions of four factors HOA (Hydrocarbon-like organic aerosol), OOA (oxygenated organic aerosol), BBOA (biomass-burning organic aerosol) and nitrogen rich factor [Ulbrich 2011, Zhang 2011].

Factor analysis techniques could also be utilized to obtain a multivariate curve resolution in infrared and fluorescence spectroscopy [Liu 2009] and mass spectrometry [Vlasenko 2009]. Vlasenko et al. for the first time applied PMF analysis to the full mass spectrum to allow individual PTR-MS (Proton Transfer Reaction Mass Spectrometry) signals to be apportioned to different source factors [Vlasenko 2009]. PMF was also applied to ATOFMS data previously clustered by k-means analysis in

a study in Cork (Ireland) by combining them with semi-continuous $PM_{2.5}$ aerosol measurements obtaining 6 factors representing vehicular traffic, marine, long-range transport, power generation, domestic solid fuel combustion and shipping traffic [Healy 2010]. In another study conducted in Toronto, $PM_{2.5}$ was characterized by laser ablation mass spectrometry and the single particles mass spectra obtained where classified with art-2a (Adaptive Resonance Theory neural network) and the hourly temporal trends - in number of particles appertaining to each cluster - were subjected to PMF analysis to obtain 9 source factors representing both crustal and secondary sources and some episodic events [Owega 2004]. Moreover, PMF analysis was applied to hourly aggregated single particles mass spectra to obtain 7 source factors in a rural site in Harrow, Ontario (Canada). The factors obtained were compared with AMS data finding a good correlation between the PMF ATOFMS sulphate factor and AMS sulphate concentrations and between the PMF ATOFMS organic factor and OOA1 (oxidized organic aerosol) AMS PMF factors [McGuire 2009]. Hourly temporal trends of previously classified particles with Art-2a were also subjected to PMF analysis and 9 factors that identify both local and regional transport sources in three sites in south-west Ontario (Canada) were extracted [McGuire 2011].

2. Aim of the work

The current work of thesis has been conducted in collaboration with the research group of Professor Roy M. Harrison OBE, of the Department of Geography, Earth & Environmental Sciences, University of Birmingham (UK).

Atmospheric aerosol is especially problematic to characterize because of the multiple compositions, size ranges and a wide spectrum of both natural and anthropogenic sources; on-line measurement deploying mass spectrometric techniques are the most promising in order to characterise both aerosol size and chemical composition for a wide range of substances. Aerosol time of flight mass spectrometry (ATOFMS) is particularly attractive as it allows size and chemical characterisation by measuring the aerodynamic diameter and both positive and negative ion mass spectra of individual particles in real time within the diameter range of 0.1-3 μm [Rebotier 2007, Gard 1997, Dall'Osto 2004, Drewnick 2008]. ATOFMS provides in a single campaign hundreds of thousand single particle mass spectra which are unlikely to be manually analysed. Therefore single particles data are usually treated with clustering algorithm, such as K-means or Art-2a, in order to group particles of similar size range and chemical composition [Rebotier 2007, Gross 2010, Healy 2009, Pekney 2006]; while factor analysis techniques, i.e. PMF, have been applied to ATOFMS data previously clustered or temporally aggregated in order to perform source apportionment studies.

In the current work of thesis, for the first time, Positive Matrix Factorization (PMF) has been directly applied to single particle ATOFMS mass spectra. The aim of the work of thesis is to extract the major components (chemical species) contributing to particles, their temporal trends and size distributions, and to study particle mixing state.

The work started from a laboratory experiment in which the aim was the evaluation of ATOFMS instrumental precision and data uncertainties. In fact, data uncertainty is a crucial aspect in PMF analysis which relies on the accuracy of error estimate in order to provide both variables and samples weights. After that, PMF analysis was optimized and applied to two ambient sampling campaigns. The first campaign was conducted in October 2008 in Harwell (UK), a rural background site in the Oxfordshire. The second campaign was conducted in May-June 2009 in London (UK), at Marylebone Road, a kerbside site in London city centre.

In details, for each campaign, PMF analysis has been applied to a *n*x*m* data matrix **X**, in which every row represents a single particle mass spectra and every column represents the instrumental response at specific m/z value: every datum in the matrix represents the corresponding absolute area under the peak in the mass spectrum. As this is the first time in which PMF is directly applied to single particle mass spectra, PMF analysis was also applied to temporally aggregated data in order to compare the approach adopted with results of literature studies. Moreover, PMF analysis results were compared to k-means cluster analysis results in order to draw differences and similarities between the two data treatment techniques. PMF and k-means results were then compared with independent measurements in order to validate the approach adopted and to evaluate data quality. Results obtained were then utilized to characterize ambient PM of the two sampling campaigns and to study the mixing-state of airborne particles.

3. Materials and methods

3.1. Sampling campaigns

The first sampling campaign was conducted (by David C.S. Beddows and Roy M. Harrison) in Harwell (51°34'32"N, 1°18'49"W), a rural background site in the Oxfordshire (UK) from the 4th October to the 17th October 2008 deploying two on-line mass spectrometric instruments, an Aerosol Time of Flight Mass Spectrometer (ATOFMS TSI Model 3800-100) and an aerosol mass spectrometer (Aerodyne high-resolution-ToF-AMS) [Drewnick 2005, DeCarlo 2006, Canagaratna 2007, Jimenez 2003], and a GRAEGOR [Thomas 2009] for the quantification of inorganic species. Moreover, hourly data about gaseous pollutants concentration and local weather were obtained from the UK national air quality archive (www.airquality.co.uk).

Figure 3.1. Maps of (a) Harwell and (b) London Marylebone Road.

The second sampling campaign was conducted (by Johanna K. Gietl and Roy M. Harrison) at Marylebone Road (51°31'22.8"N, 0°9'18"W), a kerbside site in the city-centre of London (UK), from the 22nd May 2009 to the 11th June 2009 deploying an ATOFMS TSI Model 3800-100. PM characterization, primary gaseous pollutants concentration and local weather were obtained from the UK national air quality archive (www.airquality.co.uk). Five days air masses back-trajectories arriving in London Marylebone Road and in Harwell at three different highs (100, 500 and 1000 meters) above the ground were obtained using HYSPLIT (Hybrid Single Particle Lagrangian Integrated Trajectory Model) [Draxler, Rolph 2003].

3.2. Instruments

3.2.1. ATOFMS

The ATOFMS (TSI Model 3800-100) collects, in real-time, mass spectra of individual aerosol particles in the size region 100-3000 nm of aerodynamic diameter.
The instrument is constituted by an aerosol inlet, a sizing region and a mass spectrometer detector. In the aerosol inlet, particles are introduced into a vacuum system region through a converging nozzle then particles are focused through aerodynamic lenses into a narrow particle beam [Zhang 2002, Zhang 2004], which travels through the sizing region.

Figure 3.2. TSI Aerosol Time Of Flight Mass Spectrometer instrument

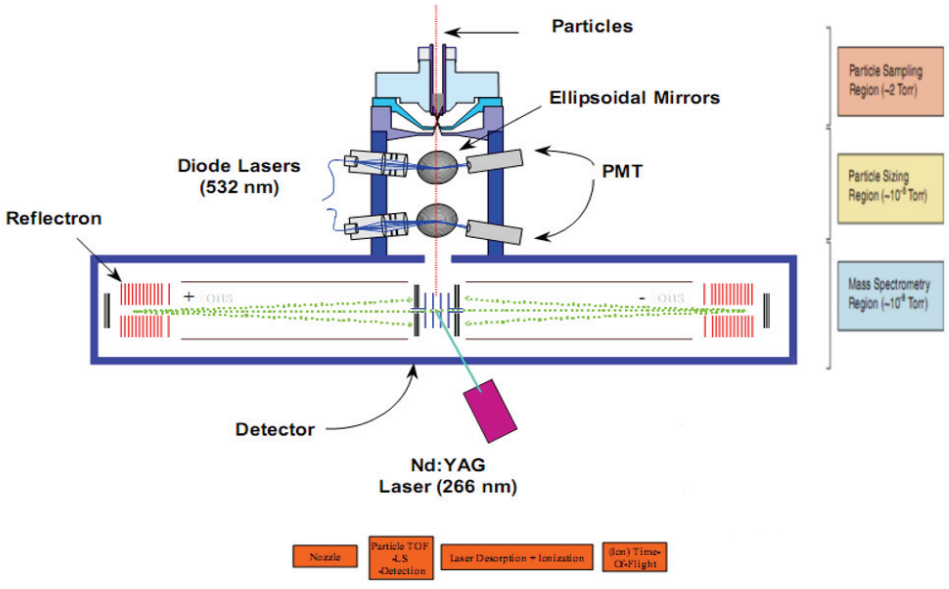

Figure 3.3. ATOFMS operating scheme

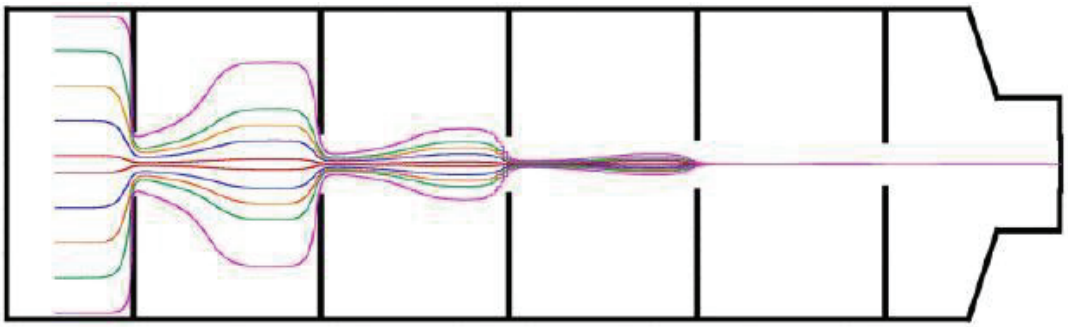

Figure 3.4. Particle trajectories inside the Aerodynamic Focusing lenses system [Zhang 2004].

Here, the aerodynamic diameter of particles sizes between 100 nm and 3 μm is calculated based on their time-of-flight between two orthogonally positioned continuous wave lasers (λ=532 nm). After that particles enter into the mass spectrometer region where a pulsed high power desorption ionization laser (λ=266 nm) is triggered on the basis of the transit time of the particle measured in the sizing region. Mass analysis is then provided by a bipolar time of flight reflectron mass spectrometer [Gard 1997, Dall'Osto 2004, Drewnick 2008]. The principal limits of the ATOFMS analyzer reside in the size-dependent transmission losses [Allen 2000, Wenzel 2003], laser intensity shot-to-shot variations [Bhave 2002], ionization matrix effects [Reilly 2000], different sensitivities among chemical species that make a semi-quantitative analysis possible to achieve only beside independent sampling measurements [Bhave 2002, Gross 2000, McGuire 2011].

During the campaign, the ATOFMS sampled aerosol through a 3/4 inch diameter copper pipe mounted vertically and in-line with the Aerosol Focussing Lens (AFL) [Su 2004]. The inlet of the copper pipe (roughly 4m above the ground) was protected using a simple hockey stick rain cap. The ATOFMS itself was fitted with a TSI 3800-100 AFL (Aerodynamic Focusing Lenses) which admitted the aerosol at nominal volumetric flow rate of 0.1 L/min operating at a pressure of 2 Torr.

3.3. Data pre-treatment

Before the analysis, single particle mass spectra were exported using the TSI MS-Analyze software. The peak-list were done using the following parameters: minimum peak height of 20 units above the baseline, minimum area under the peak of 20 units and representing at least the 0.005% of total area in particle mass spectra. These are

standard values to use in ATOFMS dataset [Dall'Osto 2004]. The data obtained were analysed using Positive Matrix Factorization (PMF) and K-means cluster analysis.
Regarding PMF analysis, single particle mass spectra exported from MS-Analyze into MS-Access database were treated to obtain the final matrix to be subjected to PMF as detailed in Annex 1, section 1. The *nxm* data matrix obtained ***X***, in which x_{ij} is the absolute area under the peak at m/z *j* in the particle *i*, is ordered respect to particle collection time and were subjected to PMF analysis. The original noise of the data (random number between 0 and 8) was added to the matrix to avoid multiple zero entries (details in section 4.1).

3.4. PMF

The PMF analysis was performed using the program PMF2 by Pentti Paatero [Paatero 1994, Paatero 1998]. The positive matrix factorisation model, developed by Paatero from Multivariate Curve Resolution-Alternating Least Squares procedure first proposed in Barcelona by Tauler et al. [Tauler 1995], solves the following equation: $\boldsymbol{X} = \boldsymbol{GF} + \boldsymbol{E}$, $x_{ij} = \sum_{h=1}^{p} g_{ih} f_{hj} + e_{ij} = y_{ij} + e_{ij}$ where **X** is the original *n*×*m* data matrix (in this case *n* single particles, and *m* variables -m/z values-), **G** is the *n*×*p* scores matrix (factors weight – weight of *p* factors to *n* single particles) and **F** is the *p*×*m* loadings matrix (factors profile – *p* factors and *m* m/z values-), **E** represents the *n*×*m* residuals matrix and **Y** represents the model predicted data matrix. The PMF routine starts from a pseudorandom starting point [Paatero 1998] and minimizes the following variable through an iteration process:

$$Q = \sum_{i=1}^{n}\sum_{j=1}^{m}\left[\frac{x_{ij} - \sum_{h=1}^{p} g_{ih} f_{hj}}{s_{ij}}\right]^2 = \sum_{i=1}^{n}\sum_{j=1}^{m}\left[\frac{e_{ij}}{s_{ij}}\right]^2$$

PMF analysis goodness resides on the accuracy of error data estimate, which are utilized to give a reliable weight to every sample and variable. Data uncertainties of absolute area under the peaks in mass spectra were evaluated during a laboratory experiment and optimized on the dataset, considering all variability inherent the measurement, as described in details in section 4.1 (Results and Discussion), obtaining $s_{ij} = 64 + 0.4 x_{ij}$. The exact number of factors *p* to use was determined by monitoring the following parameters: *Q*, the explained variation of the residuals

$$EV(E) = \frac{1}{n}\sum_{i=1}^{n}\left(\frac{\sum_{j=1}^{m}\left|e_{ij}\right| / s_{ij}}{\sum_{j=1}^{m}\left(\sum_{h=1}^{p}\left|g_{ih}f_{hj}\right| + \left|e_{ij}\right|\right) / s_{ij}}\right), \quad IM = max_{j=1\ldots m}\left(\frac{1}{n}\sum_{i=1}^{n}\frac{e_{ij}}{s_{ij}}\right) \quad \text{and}$$

$$IS = max_{j=1\ldots m}\left(\sqrt{\frac{1}{n-1}\sum_{i=1}^{n}\left(r_{ij} - \bar{r}_j\right)^2}\right), \text{ where } IM \text{ is the maximum individual column}$$

mean and *IS* is the maximum individual column standard deviation of the scaled residual matrix and they are utilized as indicators to identify the species having the least fit and the most imprecise fit [Lee 1999]. Besides the aforementioned parameters the chemical interpretation of the factors profile was used for the purpose. The definitive solution was chosen from the results of the PMF analysis conducted by starting from 50 different seeds (pseudorandom starting point). This step is mandatory because, in PMF, the function Q may possess local minima. This may be caused by the individual weighting of the elements x_{ij}, by the non-negativity constraints, or by the combined action of both. The PMF2 algorithm can find a minimum of Q(G,F) but it does not indicate whether the minimum is local or global. Therefore, different sets of pseudorandom numbers can be used as starting points (G_0,F_0) in order to identify the global minimum of Q among the local minima [Paatero 1994].

Robustness of factor solution was investigated by comparing factor loadings and scores through the different factor solutions. The rotational ambiguity was also tested by modifying the Fpeak parameter from -2.5 to 2.5. The effect of this variation was not significant with values in the range ±0.5 while PMF routine did not converge with larger Fpeak values (400 iterations). Thus the PMF solution obtained could be considered unique and Fpeak=0 was used for the final analysis.

After the PMF analysis, factor loadings (**F**) and scores (**G**) obtained were respectively normalized and weighted as follows: each factor loading vector was normalized by dividing it for a scalar value $b_h = \sum_{j=1}^{m} f_{hj}$ and the corresponding score vector was weighted by multiplying it for the same scalar b_h.

Hourly aggregated data were subjected to the PMF analysis too. The aggregation was made by summing the absolute area of peaks in the mass spectra of particles collected in the same hour of sampling $x_{ij,hour} = \sum_{hour} x_{ij}$.

The uncertainties were evaluated using the following equation $s_{ij,hour} = 64 + \frac{\sqrt{n_{i,hour}}}{n_{i,hour}} x_{ij,hour} + 0.05\, max\left(\left|x_{ij,hour}\right|, \left|y_{ij,hour}\right|\right)$ [McGuire 2009].

3.5. K-means

Single particle data are usually treated with clustering algorithms, such as K-means, in order to group particles of similar mass spectra, or more powerful Art-2a (Adaptive Resonance Theory neural network) which groups particles of similar size range and chemical composition [Rebotier 2007, Gross 2010, Healy 2009, Pekney 2006].

ATOFMS particle mass spectra were directly imported into ENCHILADA, an open source single particle mass spectra software package [Gross 2010], and single particle mass spectra were clustered using the K-means/Euclidean square algorithm [McQueen 1967]. K-means is a non hierarchical clustering technique which starts with the random subdivision of objects (in this case single particles) among *c* clusters defined by the operator. The algorithm computes the total heterogeneity of the system $E_T = \sum_{c=1}^{C} \sum_{i=1}^{I_c} \sum_{v=1}^{V_c} \left(x_{ivc} - \bar{x}_{vc}\right)^2$, which is related to the Euclidean distance of every object to the cluster centre, and moves objects from a cluster to the others until it finds the minimum of system heterogeneity [Forina 2010, Gross 2010].

The analysis was performed several times using different numbers of clusters. In order to find the right number of cluster the average distances of all points from their cluster centre were registered. Clusters obtained from miscalibrated mass spectra were eliminated and clusters with similar profiles and temporal trends were recombined to generate the definitive clusters.

4. Harwell 2008 campaign

4.1. PMF analysis optimization and validation

A correct evaluation of data uncertainties is a very critical aspect of PMF analysis, which uses data uncertainties to give a reliable weight to each variable and sample [Paatero 1994]. For this reason, a laboratory experiment was set up (by David C.S. Beddows and Roy M. Harrison, unpublished results), in which ATOFMS instrument measured the aerosol (with poly-disperse size distribution) generated through nebulisation of two equimolar aqueous solutions of various salts:

- KI, KNO_2, KBr, KCl, K_2SO_4, K_2CO_3 for the negative ions;
- NaCl, $Pb(NO_3)_2$, $Ni(NO_3)_2$, $CuCl_2$, CuO, $FeCl_3$, $CrCl_3$ for the positive ions.

The low precision of the instrumental signal (absolute area under the peaks in the MS spectra) appeared very clearly. The uncertainty, in term of relative standard deviation, was of about 50% for positive ions and about 80% for negative ions, without considering the cases in which the instrument did not reveal signals. Moreover it emerged very clearly that diameter of particles does not influence the signal intensity. In fact, particles of similar size were grouped together and the average signal intensities were calculated for each group. The average signal intensities were compared using a *t*-test which showed that the average signals of particles appertaining to different groups are statistically equals. Furthermore, the laboratory experiment showed that there is an extremely different sensitivity among ions and, in particular, between positive and negative ions [Gross 2000]. This low reproducibility reflects the limitation of single particles laser ionization-mass spectrometry analysis which reside in the size-dependent transmission losses [Allen 2000, Allen 2006, Wenzel 2003], laser intensity shot-to-shot variations [Bhave 2002], ionization matrix effects [Reilly 2000], different sensitivities among chemical species that make a semi-quantitative analysis possible to achieve only beside independent sampling measurements [Bhave 2002, Gross 2000, McGuire 2011].

Before the PMF analysis on Harwell 2008 campaign, the dataset was reduced to 106 major m/z values (-146, -144, -124, -121, -119, -104, -101, -99, -98, -97, -96, -95, -89, -88, -85, -84, -81, -80, -79, -76, -73, -72, -71, -64, -63, -62, -61, -60, -59, -49, -48, -46, -45, -44, -43, -42, -37, -36, -35, -27, -26, -25, -24, -17, -16, -15, -14, -13, -12, 7, 12, 15, 18, 23, 24, 27, 36, 37, 39, 41, 43, 46, 48, 49, 50, 51, 52, 53, 54, 55, 56, 57, 58,

59, 60, 61, 62, 63, 64, 69, 70, 71, 72, 73, 74, 75, 77, 81, 83, 84, 85, 86, 87, 88, 91, 94, 96, 108, 115, 118, 120, 128, 132, 138, 139, 207) and 55357 particles by eliminating the bad variables (the ones that have more than 55000 zero point values on a total number of particles of 56898) and the particles with a diameter below the calibration range. Absolute area under the peaks was considered for the analysis, which was directly applied to single particle mass spectra (*n*x*m* data matrix of *n* single particles, *m* variables - m/z values -, in which each datum is the absolute area under the peak in the mass spectra corresponding to the n_i particle and m_j m/z). The original noise of the data ($\bar{x}_b = 4$, $\sigma_b = 4$), evaluated in zones of particle mass spectra without peaks, was added to the input matrix by simulating it with random numbers between 0 and 8, to avoid multiple zero entries. In fact, circa the 70% of data in the input matrix are null values. From this evaluation it does not seem that the noise varies with m/z, but lower m/z were not considered and only a few spectra were analyzed. The detection limit was evaluated as $DL = \bar{x}_b + 3\sigma_b = 4 + 3 \cdot 4 = 16$ (blank value plus three times its standard deviation) by integrating the mass spectra signals in several regions without peaks. The data uncertainties to use in the PMF analysis were then optimized in a series of PMF trials, taking in mind the results of the aforementioned laboratory experiment.

The first PMF trial was done using the following uncertainties $s_{ij} = t + v \cdot x_{ij}$ with *t=DL=16* and by varying *v*, which represent the percentage fraction uncertainty, from 0.05 to 0.8. In this PMF trial the number of factors was set to 10 because in preliminary tests it was found that 10 could be considered a reliable number of factors for this dataset. The results show that using uncertainty values larger than the real ones, the analysis does not improve in terms of Q value decreasing (Figure 4.1). An uncertainty of 40%, which is similar to the one evaluated from the laboratory experiment, seems to be the optimum, thus *v=0.4* was chosen for the complete analysis.

The second PMF trial was done using the following data uncertainties $s_{ij} = 16 + 0.4 \cdot x_{ij}$ by changing the number of factors from 3 to 25. From factors profile (loadings) inspection, the presence of a “noise” factor appeared. The noise factor is made up of almost every m/z value but presents very low loadings and scores (Figure 4.2) and it explains the noise fluctuations added to the input matrix. This factor is always present on the analysis, even if a low number of factors is set. The

"noise" factor explains about the 20% of the data variation. In order to downweight the noise, which is not physically meaningful for the analysis, and to obtain only useful factors (related to chemical/physical processes) a third PMF trial was done changing the *t* value from the data uncertainties equation from *t=DL=16* to *t=8DL=128*. With *t=4DL=64* the noise factor disappears and the explained variation by factors decreases of only about the 5%, which is much less than the explained variation of the noise factor (20%). Using a *t>4DL* the analysis does not improve anymore.

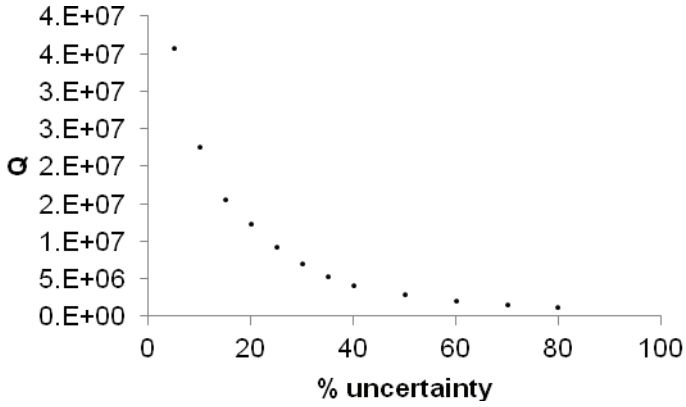

Figure 4.1. Q values of the PMF trials with different percentage of the uncertainties

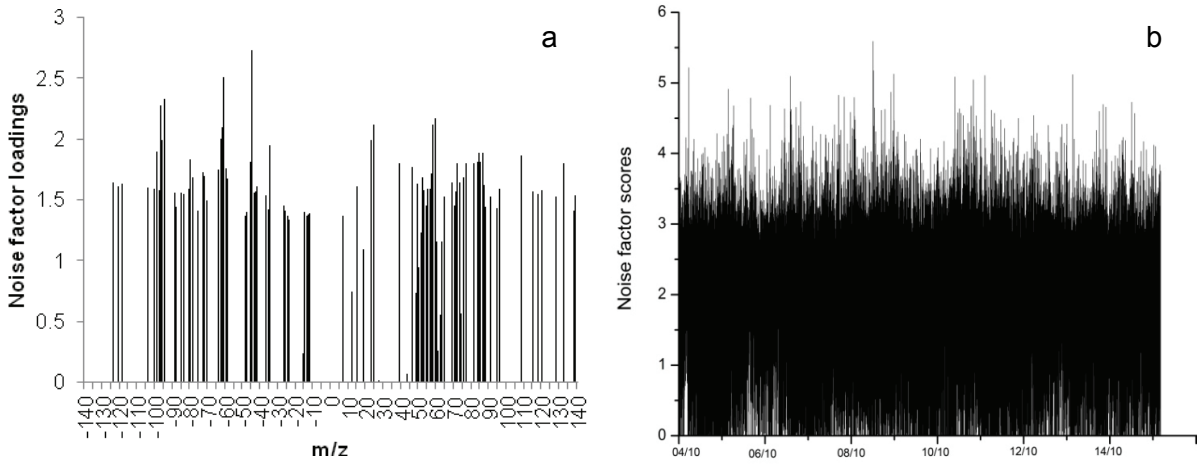

Figure 4.2. Noise factor (a) loadings and (b) scores for PMF solution obtained using an uncertainty calculated from $s_{ij} = DL + 0.4x_{ij}$

The definitive PMF analysis on the Harwell dataset was done using the optimized uncertainties ($s_{ij} = 4DL + 0.4x_{ij} = 64 + 0.4x_{ij}$) and by changing the number of factors from 3 to 21. The exact number of factors to be used was determined by monitoring the parameters suggested by Lee et al. [Lee 1999] (see Material and Methods) and

the chemical interpretation of factors profile. In figure 4.3 and 4.4 the Q/Qexp and the explained variation by the residues through the different factor solutions are reported. Moreover, PMF solutions robustness was investigated by comparing the factor loading and score of every single factor through the different factor solutions.

The last PMF trial was done by adding the column with information on particle diameters to the input data matrix, as an extra variable. Different units (μm and nm) and different diameter uncertainties were tried but the results always showed a factor which explains the variation of the particle size through the samples without any other correlation with other variables. In fact, particles of many different sizes are present in the dataset, and a factor which explain the variation of the size through the different particles is not useful as it does not give any extra information. Thus, the size information was not further utilized in the PMF analysis, however it has been used after the analysis for factors and data interpretation (section 4.2, page 42). Probably a step forward could be done by using a 3 dimensional PMF model [Zhang 2011].

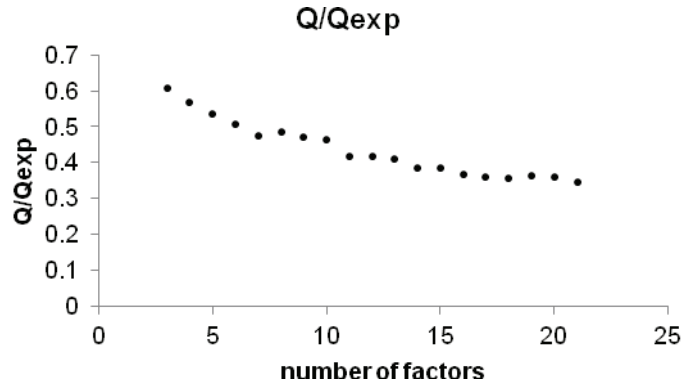

Figure 4.3. Plot of the Q/Qexp values vs number of PMF factors.

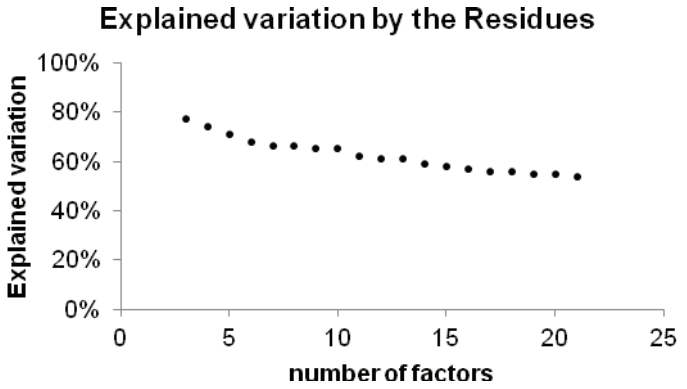

Figure 4.4 Plot of the explained variation by the residues vs number of PMF factors.

4.2. PMF analysis on Single Particles

From the PMF analysis on single particle mass spectra the 10 factors solution was selected according to both mathematical parameters [Lee 1999] (details in section 3.4) and chemical interpretation of factors profiles. In fact, using a solution with 11 factors, the split of a factor into two factors with nearly identical mass spectra is observed accompanied with no improvement in data explained variation. The factors extracted are: F1 “CNO-COOH” explaining the 2% of variance, F2 “SUL” explaining the 2 % of variance, F3 “NH4-OOA” with an explained variation of 4%, F4 “NaCl” explaining the 6% of variance, F5 “EC+” explaining the 7% of data variation, F6 “OC-Arom” explaining the 5% of variance, F7 “EC-” explaining the 3%, F8 “K” explaining the 7%, F9 “NIT” explaining the 4% and F10 “OC-CHNO” with an explained variation of the 5%. The 10 factors obtained can explain only the 45% of the total data variation [Table 4.1]. Despite the poor explained variation the main signals constituting the factors are well represented in the factors: for example potassium reaches explained variation of the 89%, sulphate is explained at the 84%, while the majority of the bad variables (i.e. m/z=-146, -144, -124, -121, -119, -104, -101) are not explained at all. Moreover, the factors obtained are characterized by clear and well defined chemical patterns [Figure 4.5].

Table 4.1. PMF factors obtained from the analysis on single particles and their explained variation

Factors	**EV %**
F1 CNO-COOH	2
F2 SUL	2
F3 NH4-OOA	4
F4 NaCl	6
F5 EC+	7
F6 OC-Arom	5
F7 EC-	3
F8 K	7
F9 NIT	4
F10 OC-CHNO	5
residues	55
total	100

The first factor “CNO-COOH” presents peaks of [CN^-] (m/z -26), [CNO^-] (m/z -42), [$CHOO^-$] (m/z -45) and [CH_3COO^-] (m/z -59). The second factor “SUL” is characterized by the main peak of sulphate (m/z -97). The third factor “NH4-OOA” is

characterized by peaks of [NH_4^+] (m/z 18), [$C_2H_3^+$] (m/z 27) and [$C_2H_3O^+$] (m/z 43). The fourth factor “NaCl” is characterized by peaks of [Na^+] (m/z 23), [Na_2^+] (m/z 46), [Na_2O^+] (m/z 62), [Na_2OH^+] (m/z 63) and [Na_2Cl^+] (m/z 81/83). The fifth factor “EC+” contains the elemental carbon positive ions; the sixth factor “OC-Arom” contains signals related to organic carbon and the benzene fragment (m/z 27, 41, 43, 51, 53, 55, 57, 63, 69, 77, 87, 91, 115). The seventh factor “EC-” is characterized by elemental carbon signals in the negative mass spectra; the eight factor “K” contains the potassium signals (m/z 39/41). The ninth factor “NIT” is characterized by the nitrate peaks (m/z -46/-62) and the tenth factor “OC-CHNO” is characterized by organic carbon and organic carbon related to nitrogen signals (m/z -26, 27, 37, 49-52, 60-63, 73-77, 84-87).

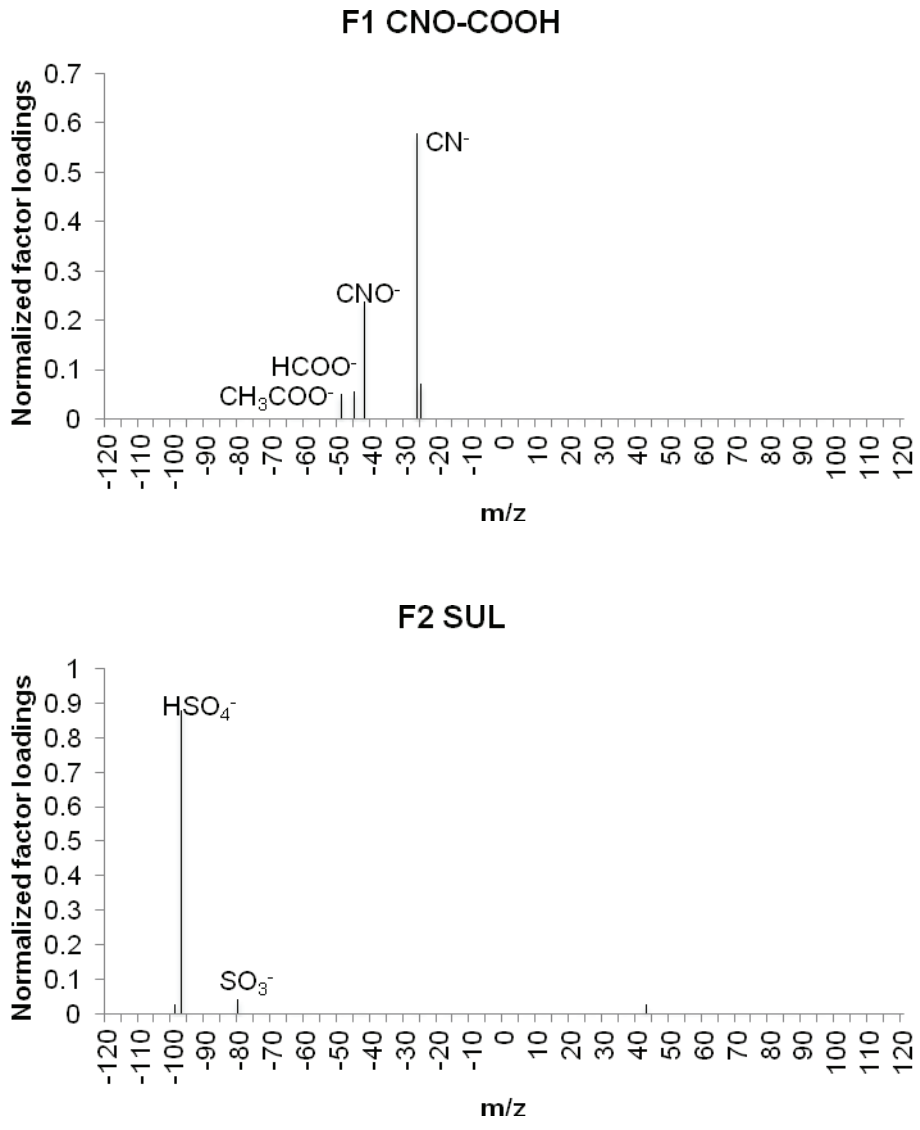

Figure 4.5

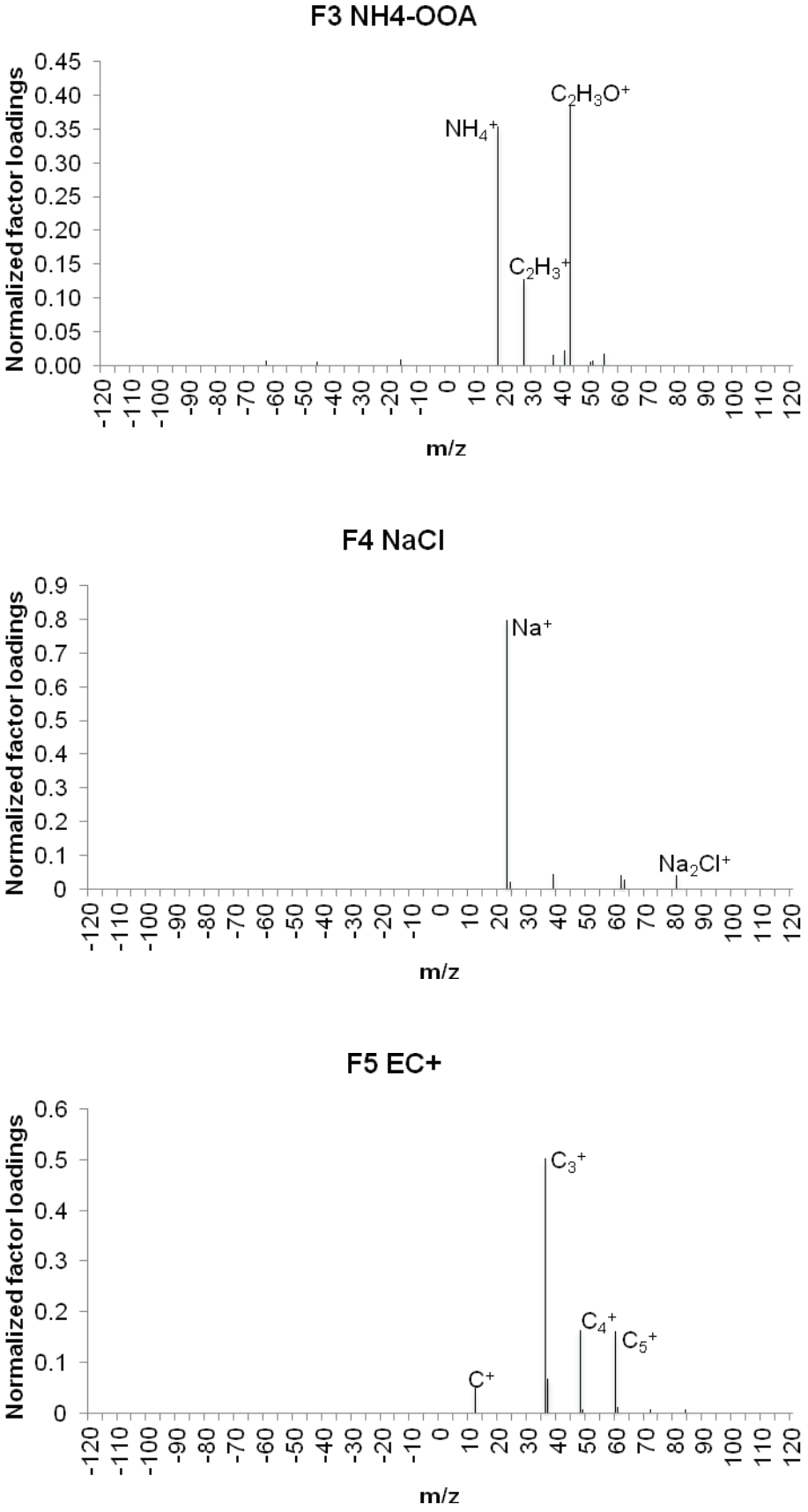
F3 NH4-OOA
Normalized factor loadings
m/z
NH4+
C2H3O+
C2H3+
F4 NaCl
Normalized factor loadings
m/z
Na+
Na2Cl+
F5 EC+
Normalized factor loadings
m/z
C+
C3+
C4+
C5+

Figure 4.5

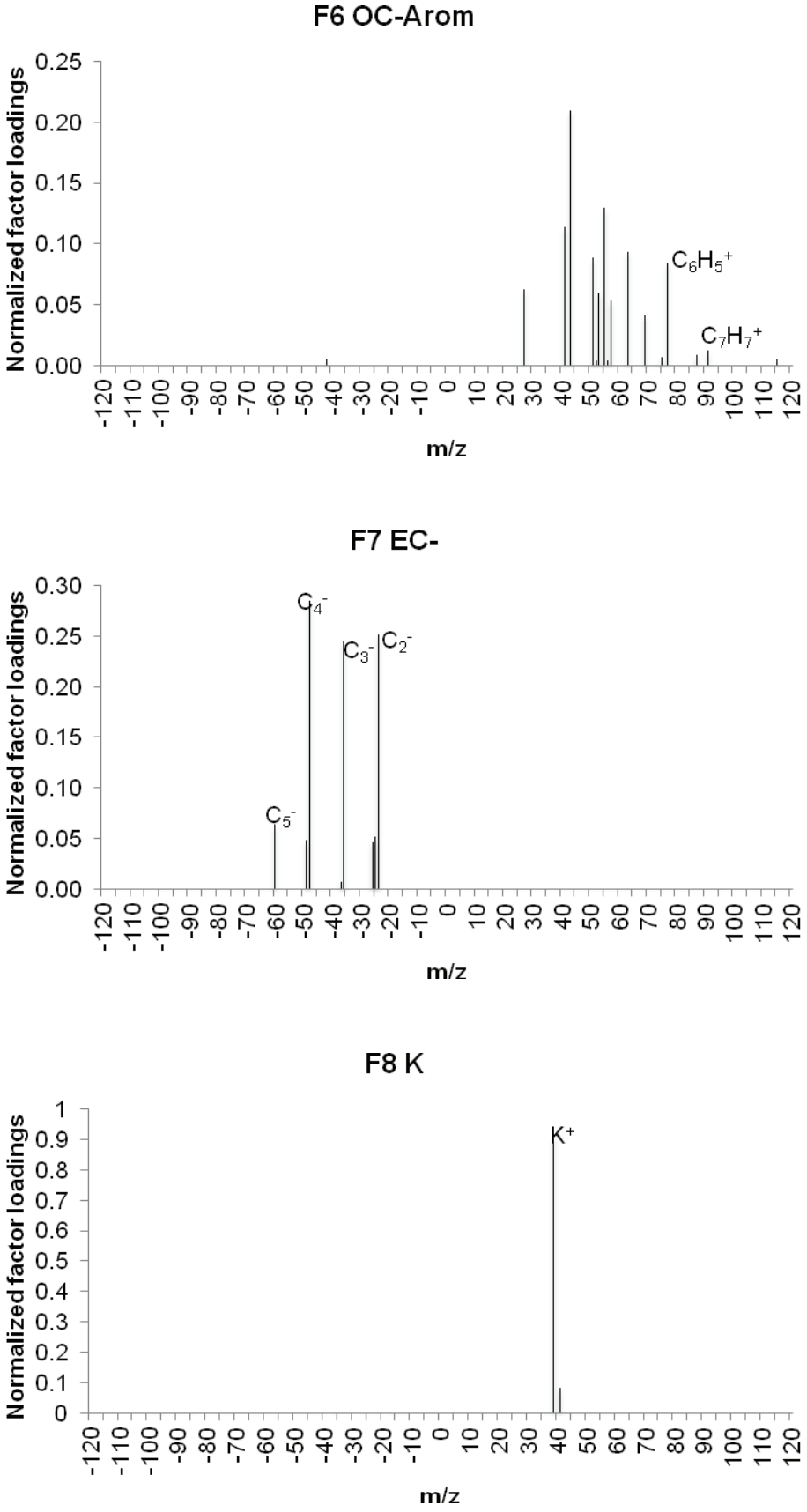
F6 OC-Arom
Normalized factor loadings
0.25
0.20
0.15
0.10
0.05
0.00
$C_6H_5^+$
$C_7H_7^+$
-120 -110 -100 -90 -80 -70 -60 -50 -40 -30 -20 -10 0 10 20 30 40 50 60 70 80 90 100 110 120
m/z
F7 EC-
Normalized factor loadings
0.30
0.25
0.20
0.15
0.10
0.05
0.00
C_4^-
C_3^-
C_2^-
C_5^-
-120 -110 -100 -90 -80 -70 -60 -50 -40 -30 -20 -10 0 10 20 30 40 50 60 70 80 90 100 110 120
m/z
F8 K
Normalized factor loadings
1
0.9
0.8
0.7
0.6
0.5
0.4
0.3
0.2
0.1
0
K^+
-120 -110 -100 -90 -80 -70 -60 -50 -40 -30 -20 -10 0 10 20 30 40 50 60 70 80 90 100 110 120
m/z

Figure 4.5

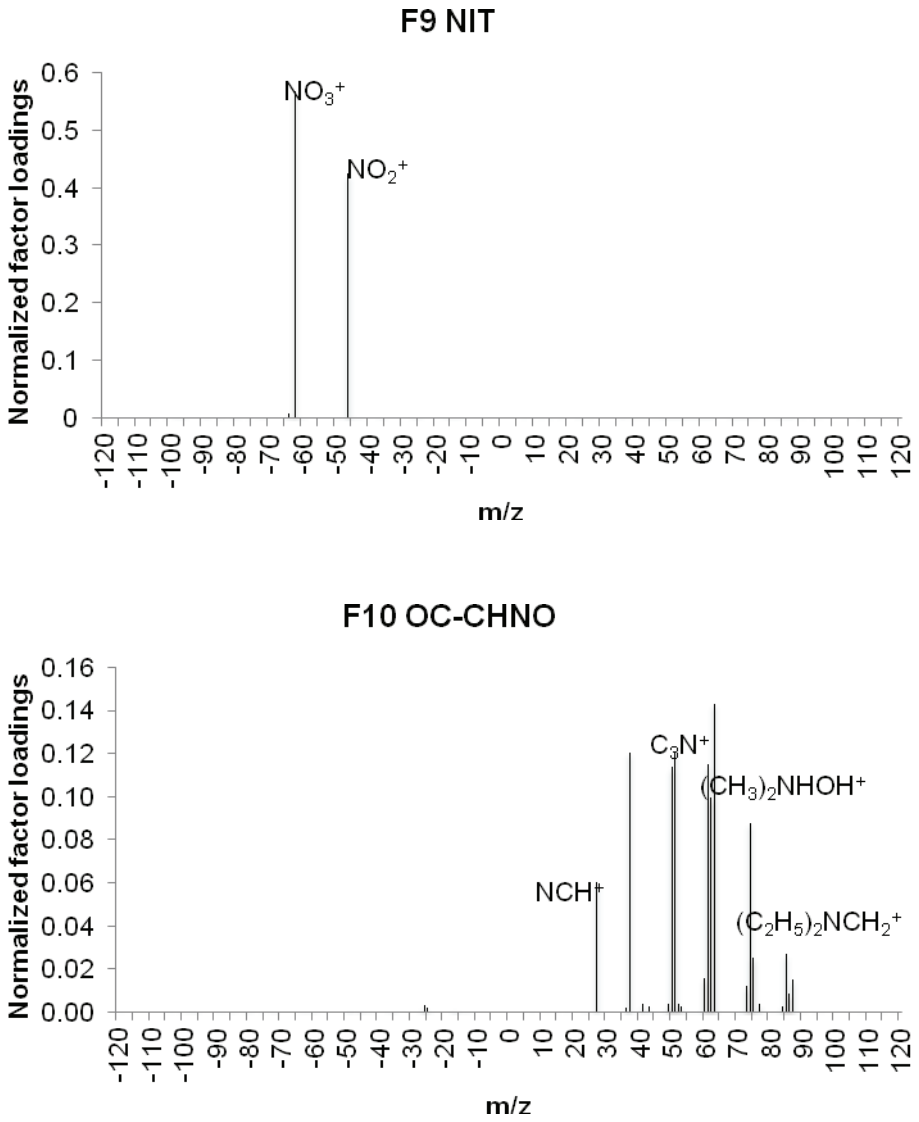

Figure 4.5. PMF factor mass spectra (loadings), single particles analysis.

It is worth to notice that positive and negative m/z signals are split in different factors (EC+ and EC-, K, NIT, SUL for example) probably due to different temporal trends, multiple sources contribution or different ionization efficiencies [Bhave 2002, Dall'Osto 2006, Gross 2000].

In order to understand if the splitting of positive and negative ions in different factors is only due to a different signal intensity, the PMF analysis has been applied to single particle mass spectra considering the relative area instead of the absolute area under the peaks. Moreover, relative areas were calculated differently for the positive and the negative mass spectra.

Using this approach, a limited improvement of the analysis was achieved in terms of explained variation, which rises from 45 to 47%. This is due to the appearance of a

few elemental carbon negative fragments [-24/-36/-48] in the EC+ factor, and chloride [-35/-37] and water signals [-16/-17] in the NaCl factor [Figure 4.6]. The splitting of positive and negative ions in different factor remains and thus the PMF analysis on relative signals was not further considered.

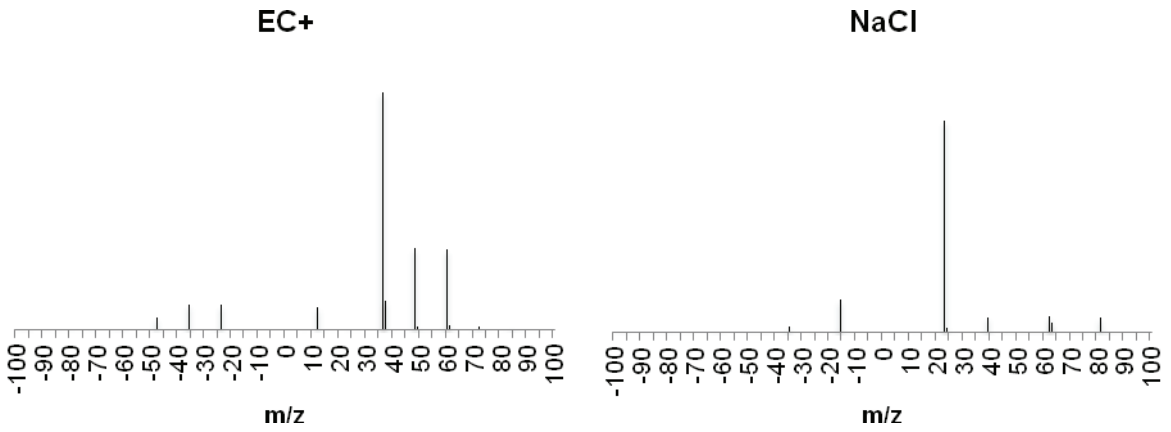

Figure 4.6. Mass spectra of PMF factor (a) EC+ and (b) NaCl from PMF analysis on single particle relative signals.

It is worthwhile to notice that, despite the poor explained variation which could be harmful in the case of quantification purposes, the chemical profiles of the factors obtained are cleared and well defined, thus the consideration on qualitative base are not affected by it. Moreover the signals extracted are in the majority of the cases well represented, with good explained variation and good correlations with the original signals.

In addition, the hourly temporal trends of the factors, obtained by summing the scores (absolute peak area) within an hour, are very strongly correlated with their original m/z signals. The results of the multiple linear regressions made to compare each factor with its constituting m/z signals are very encouraging. In all cases the correlation between the factors and their constituting variables is statistically significant with p-values less than $4 \cdot 10^{-151}$ for the Pearson correlation test. The weakest signals are partially explained by the factors while the strongest ones, in terms of hourly temporal trends, present explained variations up to 99% for potassium, 97% for sulphate and 98% for nitrate. On the contrary, the chloride signal (m/z=-35/-37) which is weakly correlated to the NaCl factor remain almost totally unexplained and in fact it is not present in the factor profile.

From the results obtained, we can state that the positive matrix factorization analysis applied to individual particles mass spectra has the effect of deconvolving the mass

spectra into the contributing chemical components (K, NIT, SUL) or important classes of components (EC+, EC-, OC-Arom, OC-CHNO, CNO-COOH, NH4-OOA, NaCl). In Figure 4.7, it is possible to notice that every particle mass spectra could be reconstructed by adding the contribution of the constituting factors. For instance, particle mass spectrum reported in figure 4.7a is reconstructed by 10% CNO-COOH, 3% SUL, 6% NH4-OOA, 26% OC-Arom, 10% EC-, 8% K, 8% NIT while the 29% remains unexplained.

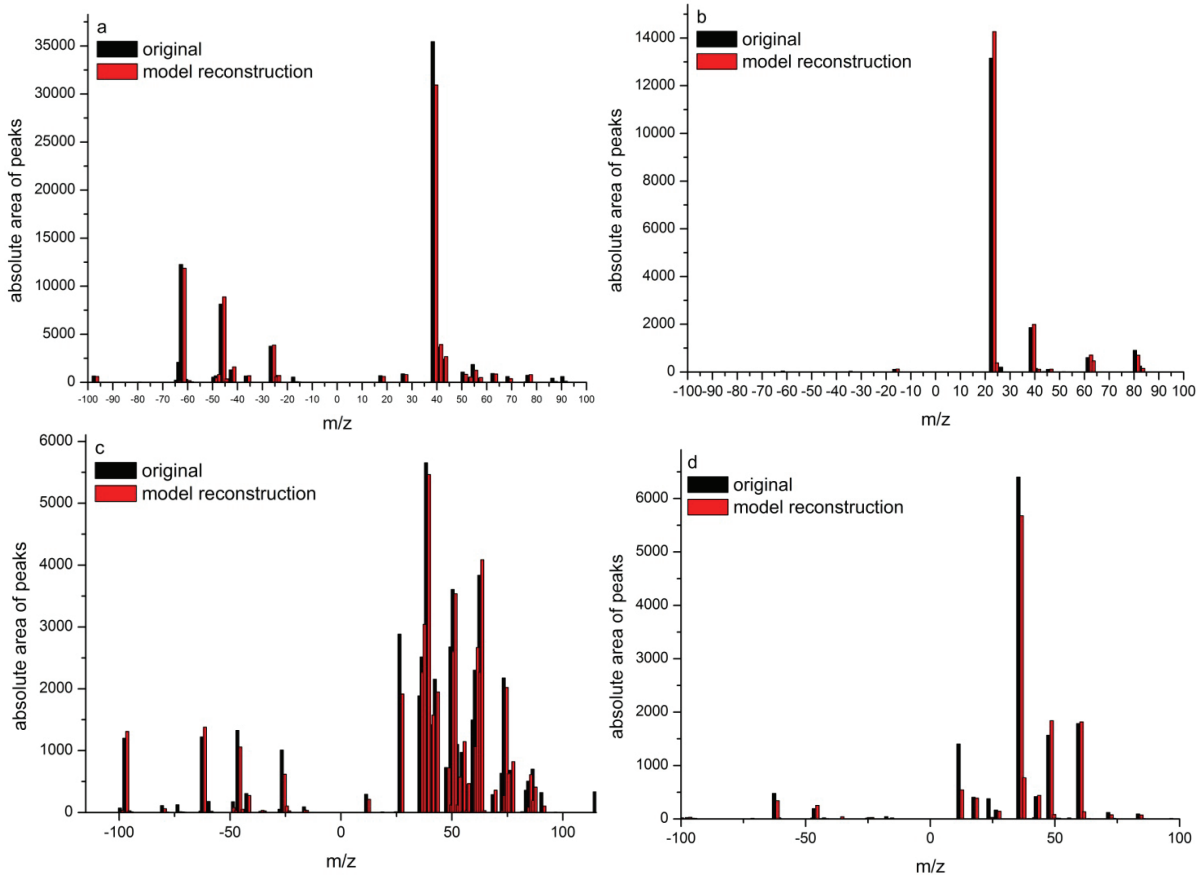

Figure 4.7. Comparison between original and model reconstructed mass spectra of (a) particle made of 10% CNO-COOH, 3% SUL, 6% NH4-OOA, 26% OC-Arom, 10% EC-, 8% K, 8% NIT AND 29% unexplained; (b) particle made of 1% NH4-OOA, 55% NaCl, 2% OC-Arom, 1% EC-, 8% K, 3% OC-CHNO and 30% unexplained; (c) particle made of 4% CNO-COOH, 3% SUL, 9% EC+, 17% OC-Arom, 1% EC-, 3% K, 4% NIT, 27% OC-CHNO and 31% unexplained; (d) particle made of 1% CNO-COOH, 1% SUL, 15% NH4-OOA, 42% EC+, 8% NIT, 1% OC-CHNO and 32% unexplained.

By comparing the original mass spectra and the model reconstructed ones, it appears that some particle mass spectra are well reconstructed (Figure 4.7) while some others remain totally unexplained. Moreover, from residuals inspection (Figure 4.8) it appears that the analysis made failed to extract a few components, for example the chloride signals (m/z=-35,-37), which are not present in the NaCl factor, water signals and some other signals probably related to m/z miscalibration problems

[Dall'Osto 2006]. In fact, the majority of the not explained signals do not influence factor interpretation.

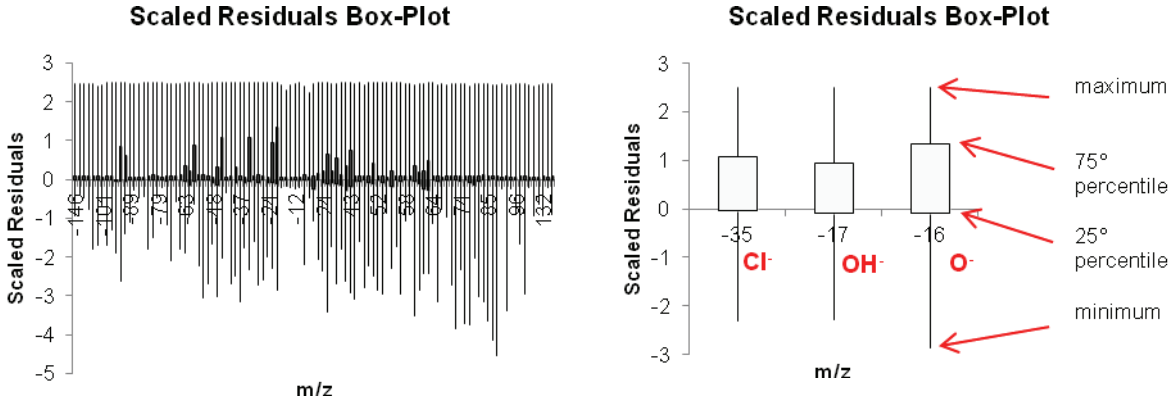

Figure 4.8. Scaled residuals box-plot of every variable (m/z)

The PMF analysis allows the extraction of the chemical species constituting the particles and their temporal trends and size distributions. In effect, the temporal trends of the factors were calculated in scores (instrumental signal), in equivalent number of particles and in volume. Factor temporal trends in scores were calculated as hourly sum of factor scores $G_{h,hour} = \sum_{hour} g_{ih}$ (Figure 4.a). Factor temporal trends in equivalent number of particles were calculated as hourly sum of particle fractions attributable to each factor (Figure 4.c):

-fraction of particle attributable to factor h $fF_{ih} = \frac{\sum_{j=1}^{m} g_{ih} f_{hj}}{\sum_{j=1}^{m} \left(g_{ih} f_{hj} + e_{ij} \right)}$;

- sum over each hour of particle fractions attributable to factor h $NfF_{h,hour} = \sum_{hour} fF_{ih}$.

The temporal trends of the factors were also calculated in volume, under the assumptions that all particles are homogenous, spherical and a constant mass of material is ionized from each particle, irrespective of its size [Dall'Osto 2006a]. Particle volume - calculated from the aerodynamic diameter - was multiplied by the percentage contribution of each factor to it. The factor hourly temporal trends (in volume) were then calculated by summing the partial volume of each particle attributable to each factor (Figure 4.9b).

- particle volume $V_i = \frac{\pi}{6} d_a^3$;

- particle volume attributable to factor h $V_{ih} = V_i f F_{ih}$;

- hourly sum of partial volumes attributable to factor h $V_{h,hour} = \sum_{hour} V_{ih}$.

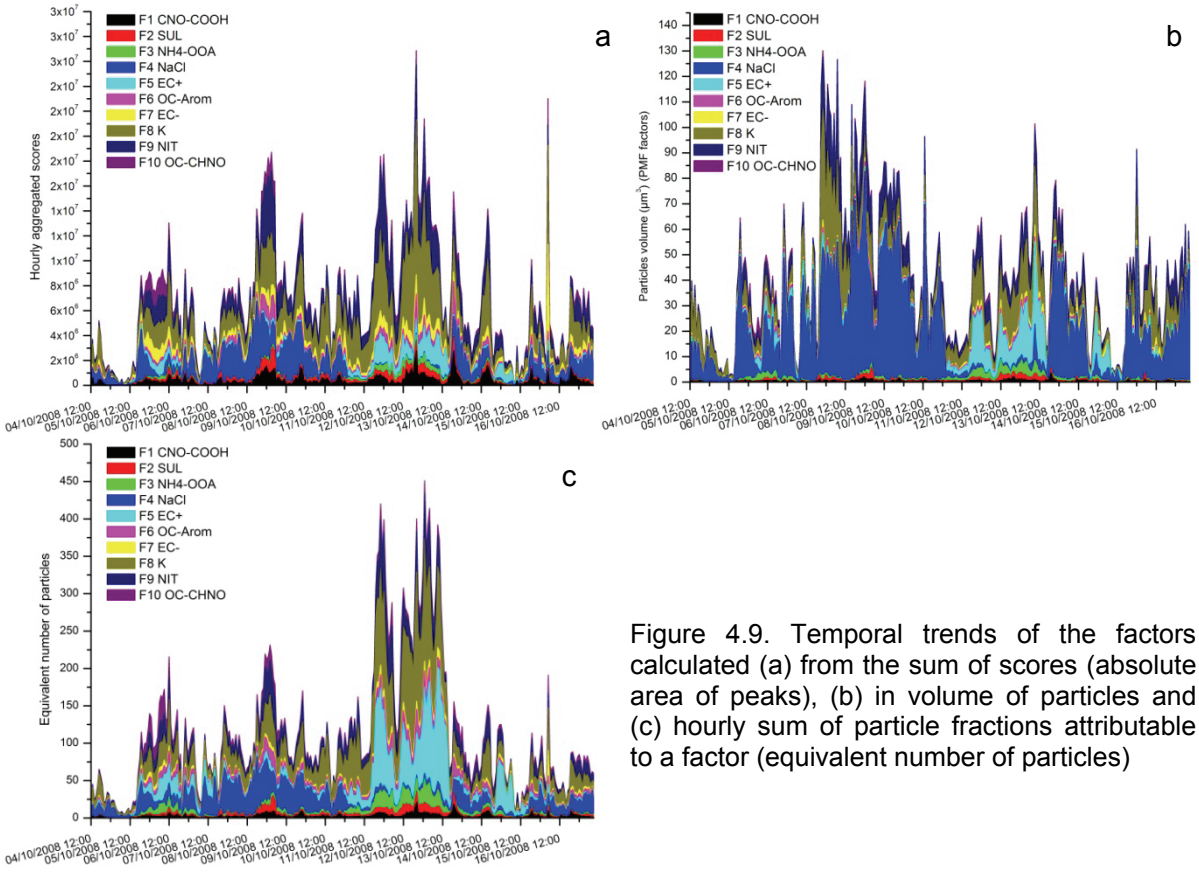

Figure 4.9. Temporal trends of the factors calculated (a) from the sum of scores (absolute area of peaks), (b) in volume of particles and (c) hourly sum of particle fractions attributable to a factor (equivalent number of particles)

The size distributions were indeed calculated by summing the factor scores of particles appertaining at the same size bin (size bin width of 0.01 µm) (Figure 4.10):

$$G_{h,size} = \sum_{size\ bin\ (0.01\mu m)} g_{ih}$$

The factors CNO-COOH, SUL, NH4-OOA and EC+ size distributions present an accumulation mode centred at 0.6 µm particle aerodynamic diameter. The factors OC-Arom and K present an accumulation mode centred at 0.5 µm particle aerodynamic diameter. Smaller diameter could indicate more freshly emitted particles. OC-CHNO and EC- factors seems to be much finer, with an accumulation mode centred at 0.5 µm diameter but with a tail in the direction of the Aitken mode. NIT presents a bimodal size distribution centred at 0.6 and 1.5 µm particle diameters, due to a double source contribution from secondary processes and from chloride displacement in aged sea spray particles. NaCl, indeed, presents a coarse distribution centred at 1.5 µm diameter confirming the sea spray origin.

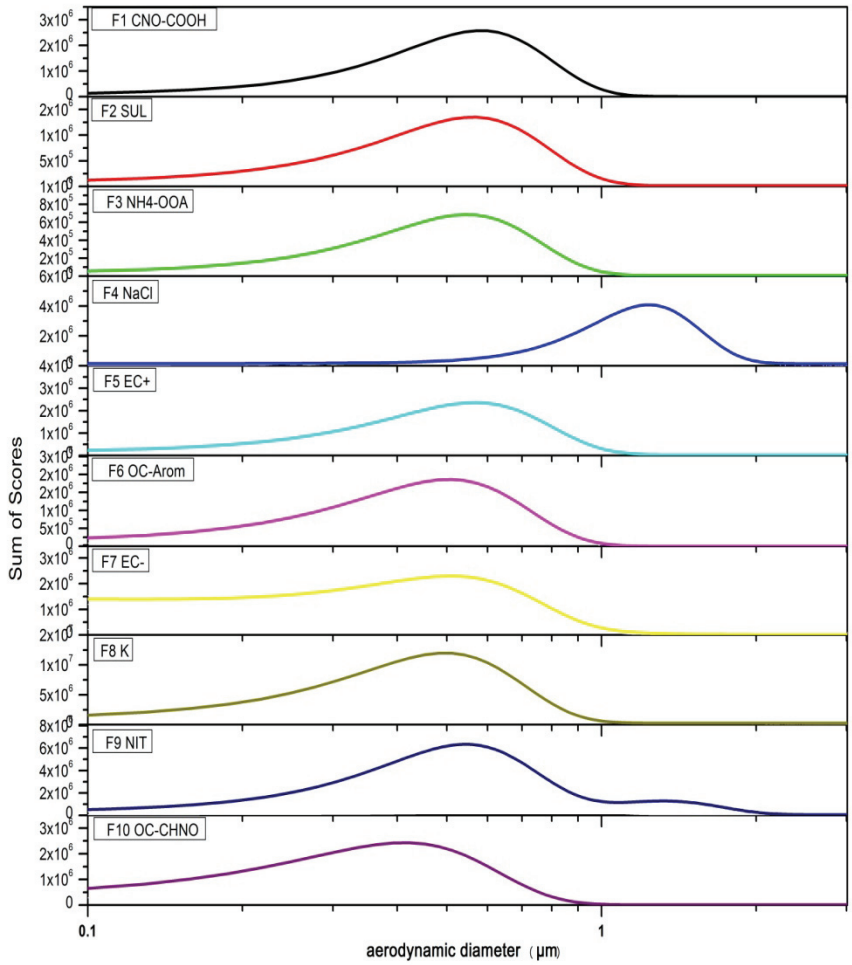

Figure 4.10. Size distributions of the 10 factors obtained from the PMF analysis on individual particle mass spectra

A study of the correlations between hourly temporal trends (sum of scores) of the factors could give deeper insight into particle components and their sources. Correlations between factors were studied through the r correlation coefficients and the Pearson correlation test (Figure 4.11, Tables 4.2 and 4.3). It has to be said that almost every correlation is statistically significant (p-value<0.05) but with different intensity. The NaCl seems to be an independent factor because it has not strong correlations with the other factors according to Cohen classification (which indicates 0.1<r<0.29 as a small correlation, 0.3<r<0.49 as a medium correlation and r>0.5 as a large correlation) [Cohen 1988] and it is not correlated to sulphate, EC-, potassium, nitrate and OC-CHNO (p-value>0.05). Sulphate is strongly correlated to potassium (r=0.635), nitrate (r=0.754) and the organic carbon factors, OC-Arom (r=0.826) in particular. Potassium and nitrate are strongly correlated with almost every factor and in fact they are dominant species, present in the majority of the particles collected.

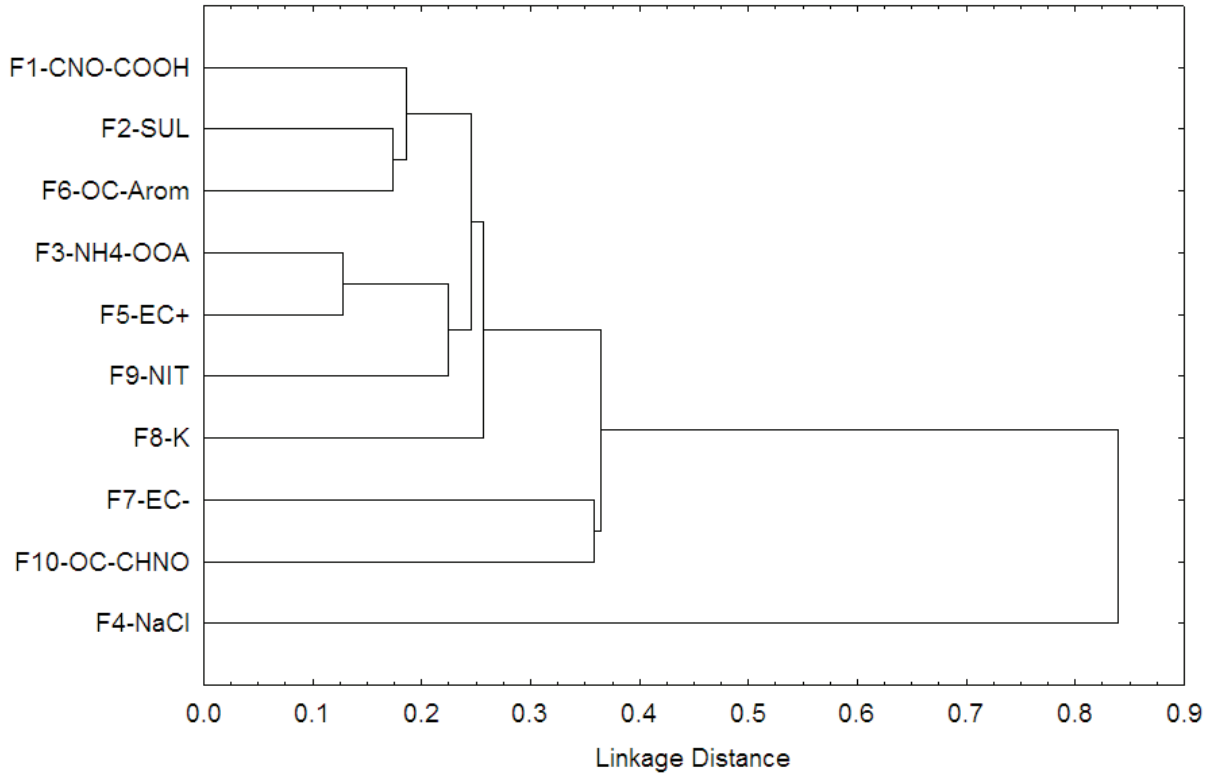

Figure 4.11. Tree diagram of the hourly temporal trends (sum of scores) of the 10 factors extracted from PMF analysis on single particle mass spectra, single linkage, distance measure r-Pearson correlation coefficient

EC- and EC+ hourly temporal trends present only a correlation of medium intensity (r=0.406). EC- is strongly correlated to OC-CHNO (r=0.641) while EC+ is correlated more with secondary species (r coefficients for NH4-OOA 0.872, K 0.578 and NIT 0.612). This result suggests that the splitting of elemental carbon signals in two factors could be not only due to different ionization and detection efficiencies between positive and negative ions. It seems that the ionization pattern is influenced by the matrix composition [Reilly 2000] delineating two different elemental carbon components: one probably freshly emitted (EC-) and one more aged (EC+) internally mixed with secondary species. In fact, as advanced by Reinard and Johnston [Reinard 2008] secondary species like nitrate and sulphate could limit the electron availability, leading to a suppression of elemental carbon fragments negatively charged, while potassium and sodium, on the contrary, could lead to an enhancement of them. Moreover, the EC- temporal trends is characterized by a peak event at 16/10/2008 probably due to a combustion event near the sampling site.

On the whole, the deconvolution made by the PMF analysis directly applied to single particle mass spectra could turn to be very useful to separate the contribution of the different inorganic species (NIT, K, SUL, NaCl) and elemental carbon and organic

families including fresh EC (EC-), aged EC (EC+), aromatic (OC-Arom), oxidized organic aerosol (NH4-OOA), and two organic nitrogen factors, fresh (OC-CHNO) and aged (CNO-COOH).

Table 4.2. Coefficient of correlation for linear regression between PMF factor temporal trends in scores

r	F1 CNO-COOH	F2 SUL	F3 NH4-OOA	F4 NaCl	F5 EC+	F6 OC-Arom	F7 EC-	F8 K	F9 NIT	F10 OC-CHNO
F1 CNO-COOH	1	0.63	0.34	0.15	0.19	0.81	0.48	0.74	0.60	0.47
F2 SUL	0.63	1	0.63	0.00	0.45	0.83	0.41	0.64	0.75	0.51
F3 NH4-OOA	0.34	0.63	1	0.37	0.87	0.40	0.44	0.72	0.78	0.39
F4 NaCl	0.15	0.00	0.37	1	0.39	0.16	0.02	0.10	0.03	0.09
F5 EC+	0.19	0.45	0.87	0.39	1	0.24	0.41	0.58	0.61	0.29
F6 OC-Arom	0.81	0.83	0.40	0.16	0.24	1	0.43	0.57	0.71	0.64
F7 EC-	0.48	0.41	0.44	0.02	0.41	0.43	1	0.63	0.48	0.64
F8 K	0.74	0.64	0.72	0.10	0.58	0.57	0.63	1	0.73	0.38
F9 NIT	0.60	0.75	0.78	0.03	0.61	0.71	0.48	0.73	1	0.61
F10 OC-CHNO	0.47	0.51	0.39	0.09	0.29	0.64	0.64	0.38	0.61	1

Table 4.3. p-value of Pearson correlation test for linear regression between PMF factor temporal trends in scores

p-value	F1 CNO-COOH	F2 SUL	F3 NH4-OOA	F4 NaCl	F5 EC+	F6 OC-Arom	F7 EC-	F8 K	F9 NIT	F10 OC-CHNO
F1 CNO-COOH	0									
F2 SUL	1.2E-35	0								
F3 NH4-OOA	6.1E-10	1.1E-34	0							
F4 NaCl	1.1E-02	0.96	3.7E-11	0						
F5 EC+	6.2E-04	2.3E-16	3.6E-96	2.0E-12	0					
F6 OC-Arom	1.3E-73	2.3E-77	5.2E-13	4.9E-03	2.5E-05	0				
F7 EC-	1.0E-18	1.8E-13	4.6E-16	0.78	1.5E-13	3.2E-15	0			
F8 K	6.9E-55	7.4E-36	5.3E-50	0.09	1.4E-28	2.7E-27	1.1E-34	0		
F9 NIT	4.0E-31	2.4E-57	2.1E-62	0.59	1.1E-32	6.9E-48	4.1E-19	4.1E-51	0	
F10 OC-CHNO	3.1E-18	1.1E-21	1.8E-12	0.10	3.5E-07	7.3E-36	1.0E-36	1.2E-11	6.9E-32	0

4.3. PMF analysis on hourly aggregated data

Hourly aggregated mass spectra (hourly sum of absolute peak area, data matrix of 106 m/z and 305 hours) were analyzed by PMF following the aforementioned criteria (see Materials and Methods). A 7 factors solution was selected, characterized by a good explained variation, 72% (Table 4.4, Figure 4.12).

The factors extracted are: F1 “K-OC-CN-NIT” explaining the 14% of data variation, F2 “K-NIT” explaining the 10% of data variation, F3 “NaCl” explaining the 13% of data variation, F4 “Na/K-EC” explaining the 9% of data variation, F5 “K-CN” explaining the

10% of data variation, F6 “OC-NIT-SUL” and F7 “K” both characterized by the 8% of explained variation.

Table 4.4. PMF factors obtained from the analysis on hourly aggregated data

Factors	**EV %**
F1 K-OC-CN-NIT	14
F2 K-NIT	10
F3 NaCl	13
F4 Na/K-EC	9
F5 K-CN	10
F6 OC-NIT-SUL	8
F7 K	8
residues	28
total	100

The hourly aggregated data produced factors characterized by a high amount of potassium which dominates in almost every factor. Potassium and other dominant species, nitrate for example, make the factors difficult to interpret. The first factor “K-OC-CN-NIT” is characterized by potassium, nitrate and organic carbon signals, the second factor “K-NIT” is characterized by potassium and nitrate signals, the third factor “NaCl” is characterized by sodium, chloride, potassium and nitrate signals, the fourth factor “Na/K-EC” is characterized by sodium, potassium and elemental carbon signals, the fifth factor “K-CN” is characterized by potassium and CN-/CNO- signals, the sixth factor “OC-NIT-SUL” is characterized by aromatic organic carbon signals, nitrate and sulphate and the seventh factor “K” is characterized by a strong potassium signal. In effect, the factors obtained are difficult to describe from a chemical point of view because they are constituted by many chemical species mixed to each other and difficult to outline.

The analysis on hourly aggregated data produce a 7 factors solution with an explained variation of the 72% while the PMF analysis on single particles produces a 10 factors solution which can explain the 45% of the variation of single particle data. Despite the poor explained variation, the factors obtained from the analysis on single particles are very clear and chemically identified while the hourly aggregated data produced factors characterized by high amounts of a few dominant species, potassium and nitrate for example, that yield the other components difficulty to emerge. Moreover the chemical profile of the factors is mixed and difficult to define.

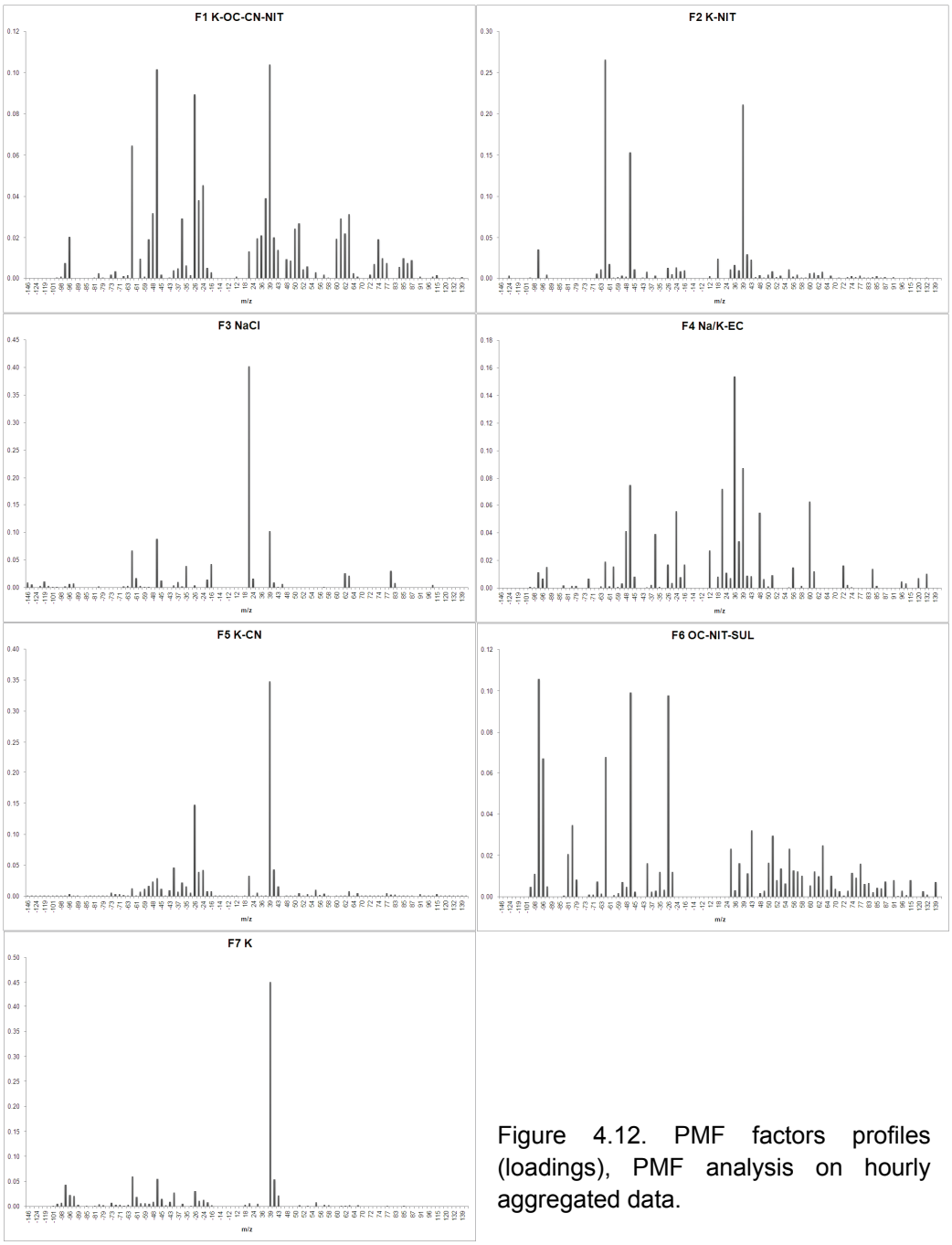

Figure 4.12. PMF factors profiles (loadings), PMF analysis on hourly aggregated data.

The PMF analysis, directly applied to single particle mass spectra, presents several advantages. In fact its result consists in a deconvolution of the mass spectra into the different components or classes of chemical species whose size distributions and temporal trends could then be extracted. Moreover, despite the low total explained variation, the main components are well represented and explained by the corresponding factors (i.e. potassium is explained at the 89% and sulphate is explained at the 84%). The correlation between the factor and the corresponding original m/z signals is even higher if we consider hourly aggregated temporal trends (i.e. the correlation between the potassium factor and m/z=+39 is statistically

significant with r=0.99, p-value 1.4E-198). The particle mass spectra reconstruction is perfectly achieved for some particles while other particles are not explained at all.
The analysis on hourly aggregated data presents a good explained variation, but the information on single particles is completely lost. The factors obtained are chemically mixed, they could give information on the correlation between species but they cannot be disaggregated to have single species temporal trends. In conclusion PMF on single particle mass spectra could be a powerful tool to extract qualitative information from the dataset and, for the main components which are the best explained, also semi-quantitative considerations could be done.
Beside PMF analysis on hourly aggregated data, analyses on data aggregated with different time resolutions were done, i.e. half an hour and ten minutes. The analysis on aggregated data within half of a hour shows the same results as the analysis on hourly aggregated data. The results obtained from the analysis of data aggregated within ten minutes were in between a hourly aggregated analysis and an analysis on single particles in terms of factor mass spectra definition and data explained variation. Moreover, the PMF analysis was applied to a matrix of frequencies - hourly count of signal in single particle mass spectra corresponding to each m/z value - without obtaining useful results in terms of data explained variation and chemical profile of factors definition.

4.4. K-means cluster analysis

The K-means analysis, applied to a total of 56898 particles, outlined 9 clusters (Table 4.5, Figure 4.13). The main clusters are “K” (14140 particles, 25%), “K-EC” (3252 particles, 6%), “NaCl” (10872, 19%), “EC” (9436 particles, 17%), “K-SUL-OC-NIT” (1832 particles, 3%), “OC” (4625 particles, 8%) and “K-NIT” (6829 particles, 12%). Another cluster made of signals corresponding to OC and carboxylic acids is called “OOA” (2006 particles, 4%). The ninth cluster is characterized by signals at m/z=+51/+56/+67 that could be assigned respectively to V^+, Fe^+ and VO^+ and by signals at m/z=+58/+60 that could be assigned to nickel. The cluster is named “Fe-V” (840 particles, 1%). The K-means clusters chosen include the 95% of particles but this is not a parameter that can be used to evaluate the quality of the results. In fact, K-means cluster analysis assigns every object (particles) to a cluster. The choice is then on the operator who selects the number of clusters and eventually eliminates some of them.

Table 4.5. Clusters obtained from K-means analysis, their number of particles and % contribution.

Cluster names	number of particles	%
K	14140	25
NaCl	10872	19
EC	9436	17
K-NIT	6829	12
OC	4625	8
K-EC	3252	6
OOA	2006	4
K-SUL-OC-NIT	1832	3
Fe-V	840	1
miscalibrated	3066	5
total	56898	100

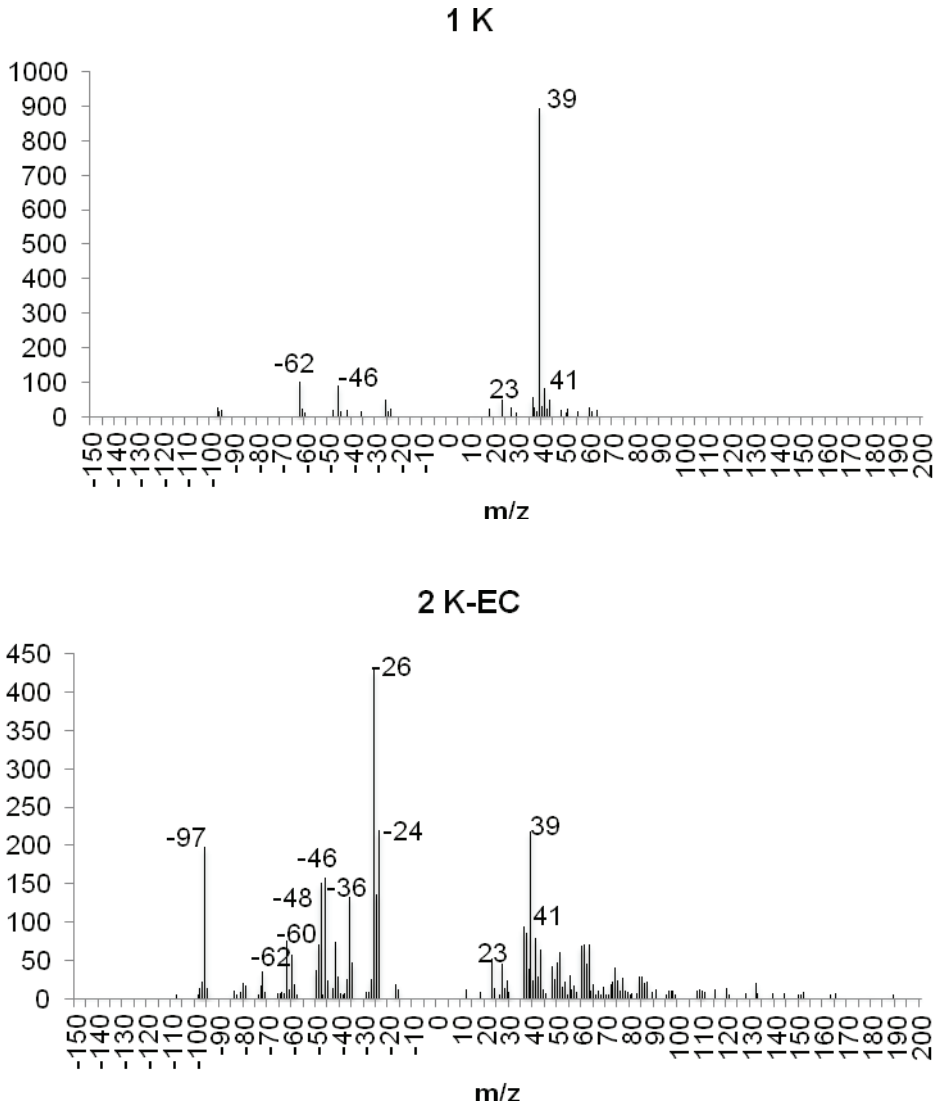

Figure 4.13

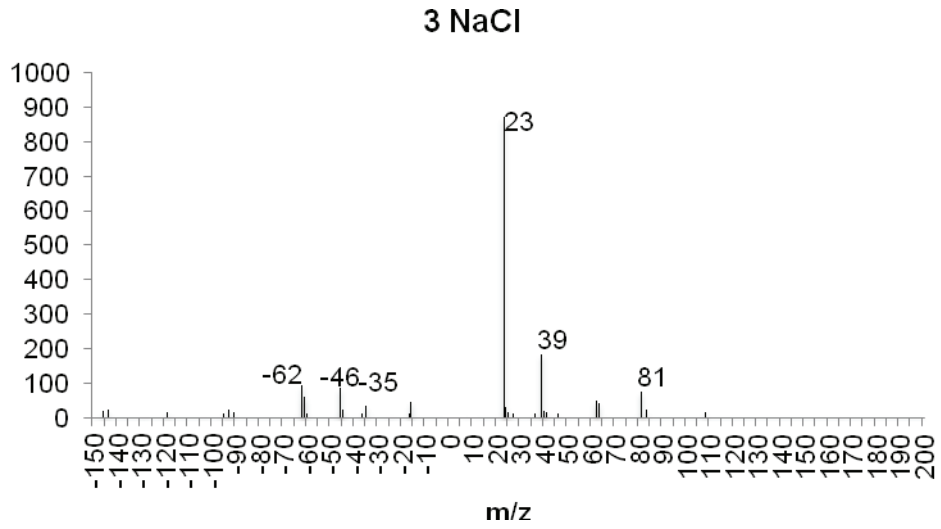
3 NaCl
1000
900
800
700
600
500
400
300
200
100
0
23
39
81
-62
-46
-35
-150 -140 -130 -120 -110 -100 -90 -80 -70 -60 -50 -40 -30 -20 -10 0 10 20 30 40 50 60 70 80 90 100 110 120 130 140 150 160 170 180 190 200
m/z

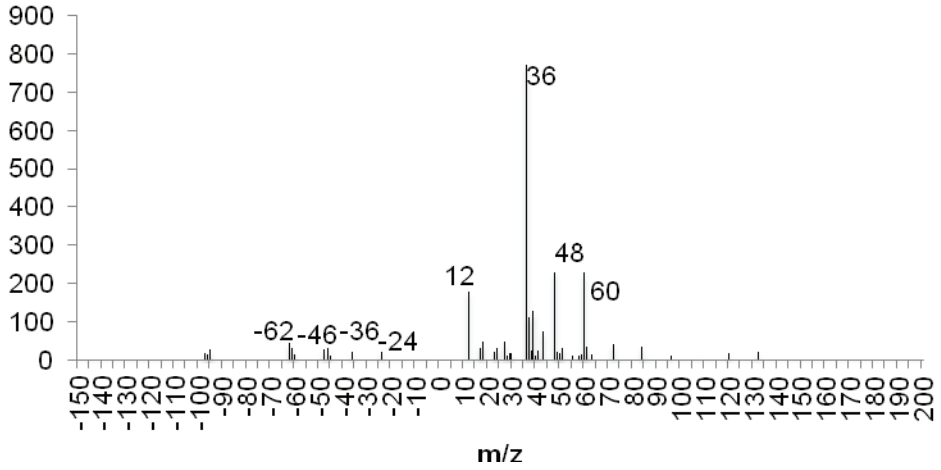
4 EC
900
800
700
600
500
400
300
200
100
0
36
48
60
12
-62
-46
-36
-24
-150 -140 -130 -120 -110 -100 -90 -80 -70 -60 -50 -40 -30 -20 -10 0 10 20 30 40 50 60 70 80 90 100 110 120 130 140 150 160 170 180 190 200
m/z

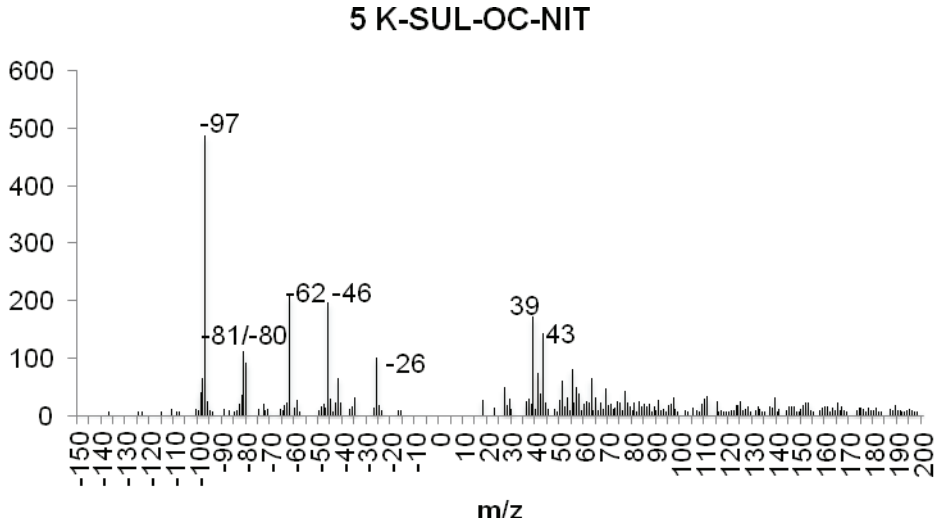
5 K-SUL-OC-NIT
600
500
400
300
200
100
0
-97
-81/-80
-62
-46
-26
39
43
-150 -140 -130 -120 -110 -100 -90 -80 -70 -60 -50 -40 -30 -20 -10 0 10 20 30 40 50 60 70 80 90 100 110 120 130 140 150 160 170 180 190 200
m/z

Figure 4.13

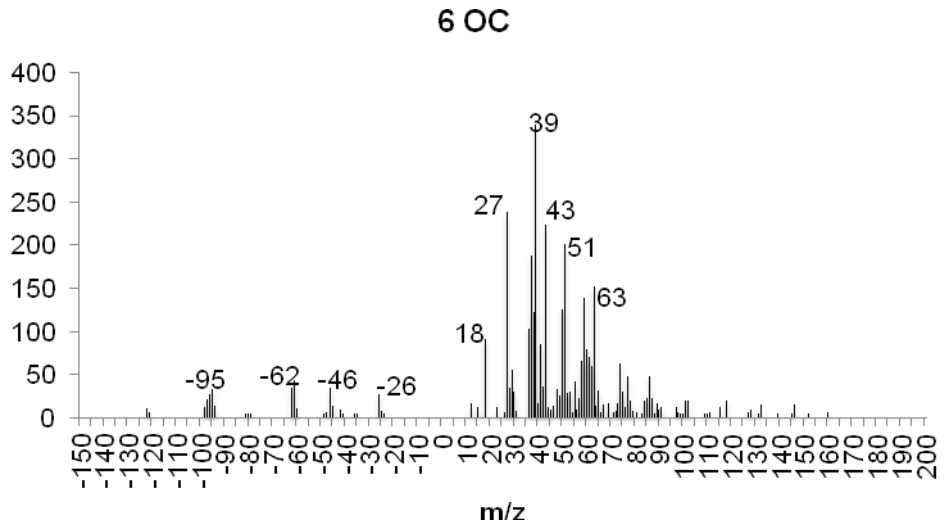
6 OC
400
350
300
250
200
150
100
50
0
39
27
43
51
63
18
-95
-62
-46
-26
-150 -140 -130 -120 -110 -100 -90 -80 -70 -60 -50 -40 -30 -20 -10 0 10 20 30 40 50 60 70 80 90 100 110 120 130 140 150 160 170 180 190 200
m/z

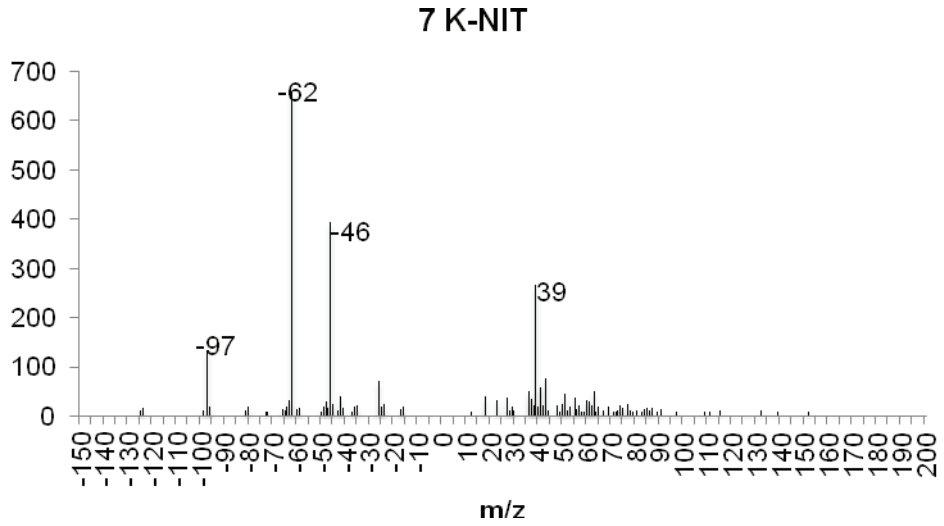
7 K-NIT
700
600
500
400
300
200
100
0
-62
-46
39
-97
-150 -140 -130 -120 -110 -100 -90 -80 -70 -60 -50 -40 -30 -20 -10 0 10 20 30 40 50 60 70 80 90 100 110 120 130 140 150 160 170 180 190 200
m/z

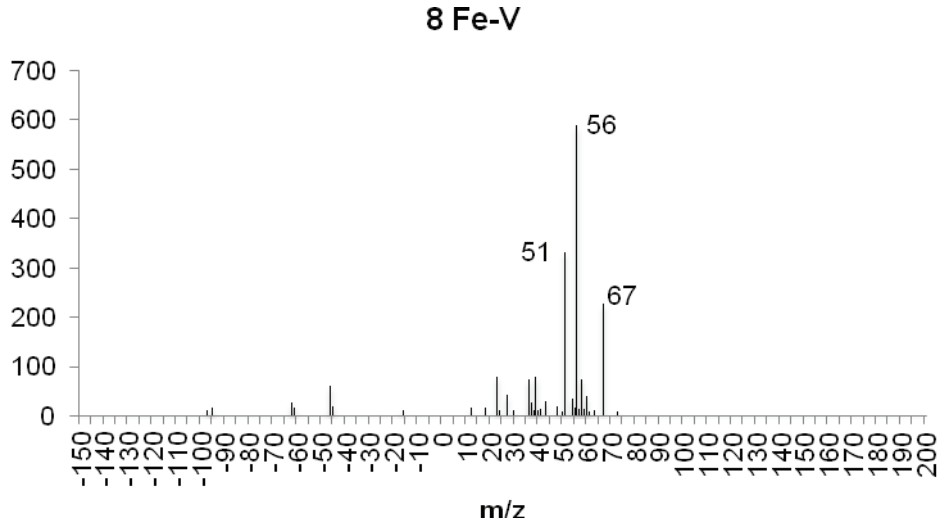
8 Fe-V
700
600
500
400
300
200
100
0
56
51
67
-150 -140 -130 -120 -110 -100 -90 -80 -70 -60 -50 -40 -30 -20 -10 0 10 20 30 40 50 60 70 80 90 100 110 120 130 140 150 160 170 180 190 200
m/z

Figure 4.13

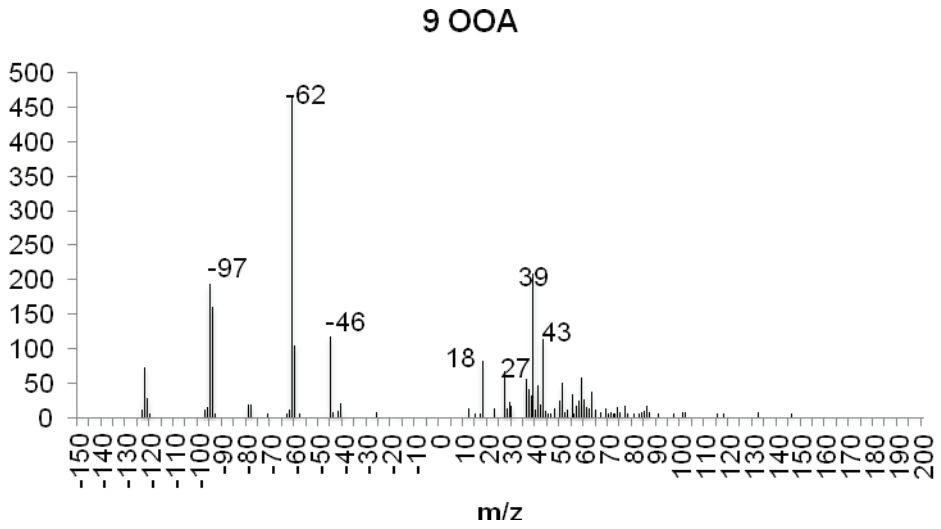

Figure 4.13. K-means cluster mass spectra.

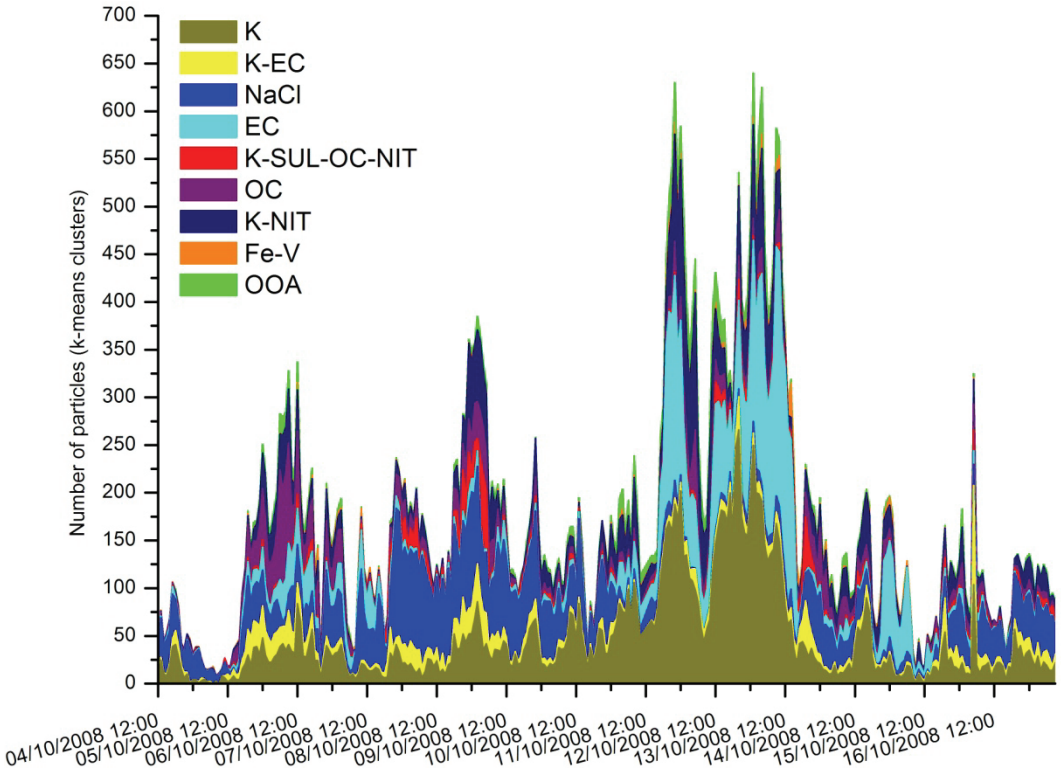

Figure 4.14. Hourly temporal trends of the 9 k-means cluster (number of particles)

The K cluster presents high potassium signals and some negative ion signals with a low intensity. The K-EC cluster presents negative ion signals related to elemental carbon and positive ion signals, with a lower intensity, related to organic carbon, potassium and sodium. The NaCl cluster presents signals of sodium, chloride, potassium and nitrate mainly. The EC cluster presents both positive and negative signals related to elemental carbon. The OC cluster presents both aromatic, ammine and oxygenated carbon signals. K-NIT is mainly characterized by potassium and

nitrate signals while K-SUL-OC-NIT presents sulphate and nitrate signals in the negative mass spectra and OC aromatic signals in the positive mass spectra. Hourly temporal trends of clusters in number of particles are reported in Figure 4.14.
ATOFMS data could be clustered with other algorithms, i.e. Art-2a (Adaptive Resonance Theory, neural network analysis), obtaining similar results [Giorio 2012].

4.5. Comparison between PMF and K-means analysis

PMF and cluster analysis could be used as complementary techniques. While k-means give a rapid outcome about the heterogeneity of particles by dividing them into classes of similarity the PMF analysis on single particle mass spectra permits the extraction of the chemical species constituting the particles by disaggregating their contribution to single particle mass spectra. In fact, the two techniques together, because they have a different approach and different outcomes, could be successfully used to study the mixing-state of particles.
The results of the correlation analysis show a good agreement between PMF factor temporal trends in scores and the corresponding cluster temporal trend: for example F8 K is correlated to the K cluster with r=0.92 and p-value=3E-125 (Pearson correlation test), F4 NaCl is correlated to the NaCl cluster (r=0.86, p-value=4E-91) and F3 NH4-OOA is correlated to the OOA cluster (r=0.90, p-value=9E-112). The cross correlations between factor and cluster temporal trends confirm the conclusion made from the cross correlations between PMF factors (Tables 4.2 and 4.3, Figure 4.11). The NaCl cluster presents a strong correlation only with the NaCl factor. The EC+ factor is strongly correlated with clusters characterized by secondary aerosol (F3 NH4-OOA r=0.79, F8 K-NIT=0.71) while EC- is not strongly correlated to any cluster (except K-EC). The cluster Fe-V is strongly correlated with the EC+ factor (r=0.67) probably because of a common origin from petroleum based fuel combustion [Korn 2007]. Moreover, K-EC cluster which is correlated to organic factors as well as EC-, could represent a biomass burning signature [Bi 2011]. Fe-V cluster does not present a corresponding PMF factor with similar mass spectrum. In fact iron and vanadium signals are not extracted by PMF and they remain confined in the residuals probably because the number of particles containing those signals are insufficient.
PMF factor temporal trends in equivalent number of particles could be a better quantity to correlate with cluster temporal trends which are in number of particles

appertaining to each cluster. The correlation analysis (Table 4.8-4.9) show a better agreement between factors and clusters by expressing factors in equivalent number of particles. For example, K cluster is better correlated with K factor in number (r=0.99) than in scores (r=0.92) and NaCl cluster is better correlated with NaCl factor in equivalent number (r=0.96) than in scores (r=0.86), with the exceptions of K-EC cluster which is better correlated to EC- factor in scores (r=0.74) than in equivalent number (r=0.59) and K-SUL-OC-NIT which is better correlated to SUL factor as hourly sum of scores (r=0.80) than in number (r=0.71). In general, the differences between the two correlation analyses made are very little, confirming that the instrumental signal better represent particle number concentration rather than mass concentration.

Table 4.6. Correlation coefficients of the linear regression between PMF factors (hourly sum of scores) and K-means clusters

	1-K	2-K-EC	3-NaCl	4-EC	5-K-SUL-OC-NIT	6-OC	7-K-NIT	8-Fe-V	9-OOA
G-F1-CNO-COOH	0.53	0.57	0.13	0.15	0.56	0.25	0.38	0.06	0.21
G-F2-SUL	0.59	0.46	0.04	0.37	0.80	0.36	0.61	0.21	0.49
G-F3-NH4-OOA	0.87	0.16	0.34	0.77	0.15	0.37	0.86	0.49	0.90
G-F4-NaCl	0.29	0.25	0.86	0.39	0.23	0.02	0.23	0.29	0.32
G-F5-EC+	0.78	0.13	0.35	0.95	0.05	0.30	0.71	0.67	0.79
G-F6-OC-Arom	0.41	0.67	0.19	0.14	0.81	0.38	0.53	0.06	0.28
G-F7-EC-	0.49	0.74	0.01	0.27	0.30	0.38	0.42	0.11	0.34
G-F8-K	0.92	0.38	0.07	0.53	0.29	0.22	0.58	0.24	0.59
G-F9-NIT	0.71	0.41	0.08	0.49	0.43	0.46	0.89	0.27	0.69
G-F10-OC-CHNO	0.23	0.80	0.15	0.07	0.46	0.79	0.56	0.03	0.32

Table 4.7. r-Pearson correlation test between PMF factors (hourly sum of scores) and K-means clusters

	1-K	2-K-EC	3-NaCl	4-EC	5-K-SUL-OC-NIT	6-OC	7-K-NIT	8-Fe-V	9-OOA
G-F1-CNO-COOH	2.5E-23	2.3E-27	2.9E-02	9.9E-03	4.8E-26	1.4E-05	9.3E-12	3.1E-01	1.8E-04
G-F2-SUL	1.6E-29	1.4E-17	4.6E-01	4.7E-11	4.4E-68	7.0E-11	3.6E-32	2.4E-04	8.5E-20
G-F3-NH4-OOA	1.3E-93	4.1E-03	1.2E-09	3.1E-62	8.1E-03	2.3E-11	4.0E-89	5.5E-20	9.1E-112
G-F4-NaCl	4.0E-07	9.0E-06	4.2E-91	2.3E-12	4.6E-05	6.8E-01	6.8E-05	1.7E-07	1.3E-08
G-F5-EC+	1.0E-62	2.1E-02	1.8E-10	2.1E-150	4.1E-01	1.3E-07	9.6E-49	2.4E-40	5.0E-67
G-F6-OC-Arom	5.4E-14	2.0E-41	7.6E-04	1.3E-02	2.9E-73	3.5E-12	6.6E-24	3.3E-01	9.7E-07
G-F7-EC-	1.3E-19	2.5E-54	8.5E-01	2.0E-06	1.3E-07	4.2E-12	2.1E-14	5.4E-02	1.0E-09
G-F8-K	3.3E-125	1.1E-11	2.2E-01	3.0E-23	2.3E-07	9.2E-05	2.3E-29	1.7E-05	3.8E-30
G-F9-NIT	3.7E-47	1.1E-13	1.5E-01	2.1E-19	4.1E-15	1.2E-17	4.0E-108	2.3E-06	5.0E-44
G-F10-OC-CHNO	5.1E-05	7.5E-68	7.5E-03	2.4E-01	2.2E-17	1.8E-66	1.4E-26	5.6E-01	1.5E-08

Table 4.8. Correlation coefficients (r) of the linear regression between PMF factors in equivalent number of particles and K-means clusters

	1-K	2-K-EC	3-NaCl	4-EC	5-K-SUL-OC-NIT	6-OC	7-K-NIT	8-Fe-V	9-OOA
N-F1-CNO-COOH	0.66	0.59	0.05	0.30	0.53	0.30	0.50	0.14	0.35
N-F2-SUL	0.73	0.45	0.05	0.53	0.71	0.35	0.67	0.31	0.61
N-F3-NH4-OOA	0.87	0.12	0.34	0.83	0.08	0.41	0.80	0.51	0.91
N-F4-NaCl	0.25	0.25	0.96	0.34	0.24	0.06	0.17	0.25	0.28
N-F5-EC+	0.77	0.00	0.37	1.00	0.01	0.15	0.60	0.70	0.73
N-F6-OC-Arom	0.73	0.55	0.00	0.50	0.60	0.54	0.77	0.28	0.64
N-F7-EC-	0.73	0.59	0.14	0.65	0.24	0.41	0.64	0.40	0.63
N-F8-K	0.99	0.18	0.21	0.75	0.17	0.19	0.69	0.41	0.78
N-F9-NIT	0.77	0.34	0.06	0.60	0.35	0.44	0.96	0.34	0.80
N-F10-OC-CHNO	0.37	0.63	0.03	0.29	0.34	0.91	0.70	0.16	0.55

Table 4.9. r-Pearson correlation test between PMF factors in equivalent number of particles and K-means clusters

	1-K	2-K-EC	3-NaCl	4-EC	5-K-SUL-OC-NIT	6-OC	7-K-NIT	8-Fe-V	9-OOA
N-F1-CNO-COOH	5.5E-39	1.7E-29	4.0E-01	1.0E-07	3.5E-23	1.5E-07	1.6E-20	1.5E-02	2.4E-10
N-F2-SUL	4.4E-51	1.4E-16	3.9E-01	7.4E-24	5.7E-49	3.5E-10	5.8E-41	2.5E-08	4.5E-32
N-F3-NH4-OOA	4.1E-97	3.3E-02	1.6E-09	2.7E-77	1.5E-01	9.2E-14	5.4E-69	4.7E-22	4.0E-118
N-F4-NaCl	1.3E-05	6.6E-06	7.7E-163	1.0E-09	3.0E-05	2.8E-01	3.7E-03	1.5E-05	6.0E-07
N-F5-EC+	7.8E-61	9.9E-01	1.7E-11	0.0E+00	9.3E-01	9.4E-03	3.8E-31	9.3E-47	4.0E-52
N-F6-OC-Arom	1.2E-52	8.4E-26	9.8E-01	2.5E-20	2.2E-31	3.1E-24	1.2E-60	6.0E-07	3.1E-37
N-F7-EC-	7.6E-52	6.6E-30	1.3E-02	4.7E-38	2.3E-05	6.0E-14	3.0E-37	3.4E-13	1.2E-34
N-F8-K	9.3E-296	1.6E-03	2.4E-04	1.2E-56	2.3E-03	6.5E-04	3.5E-44	8.4E-14	3.2E-63
N-F9-NIT	1.2E-61	6.6E-10	3.0E-01	7.8E-32	4.1E-10	1.3E-15	3.2E-168	6.8E-10	8.5E-69
N-F10-OC-CHNO	1.4E-11	2.9E-35	6.4E-01	2.2E-07	1.7E-09	2.1E-118	1.7E-46	5.1E-03	5.0E-25

4.6. Comparison with independent measurements

During all the sampling campaign, beside ATOFMS, inorganic ion concentrations in TSP and $PM_{2.5}$ were measured by GRAEGOR and non-refractory inorganic and organic concentrations in PM_1 by the AMS. In order to validate the PMF factor temporal trends, a correlation analysis (r-Pearson test) was made between them and the independent measurements (Table 4.10). In figure 4.15 sulphate, nitrate, chloride, ammonium and organic concentrations are reported compared to the corresponding PMF ATOFMS factors in volume and k-means clusters. For comparison with species concentration measured in PM_1 by AMS, PMF factor partial volumes and PMF factors in scores were integrated for particle of diameter < 1μm.

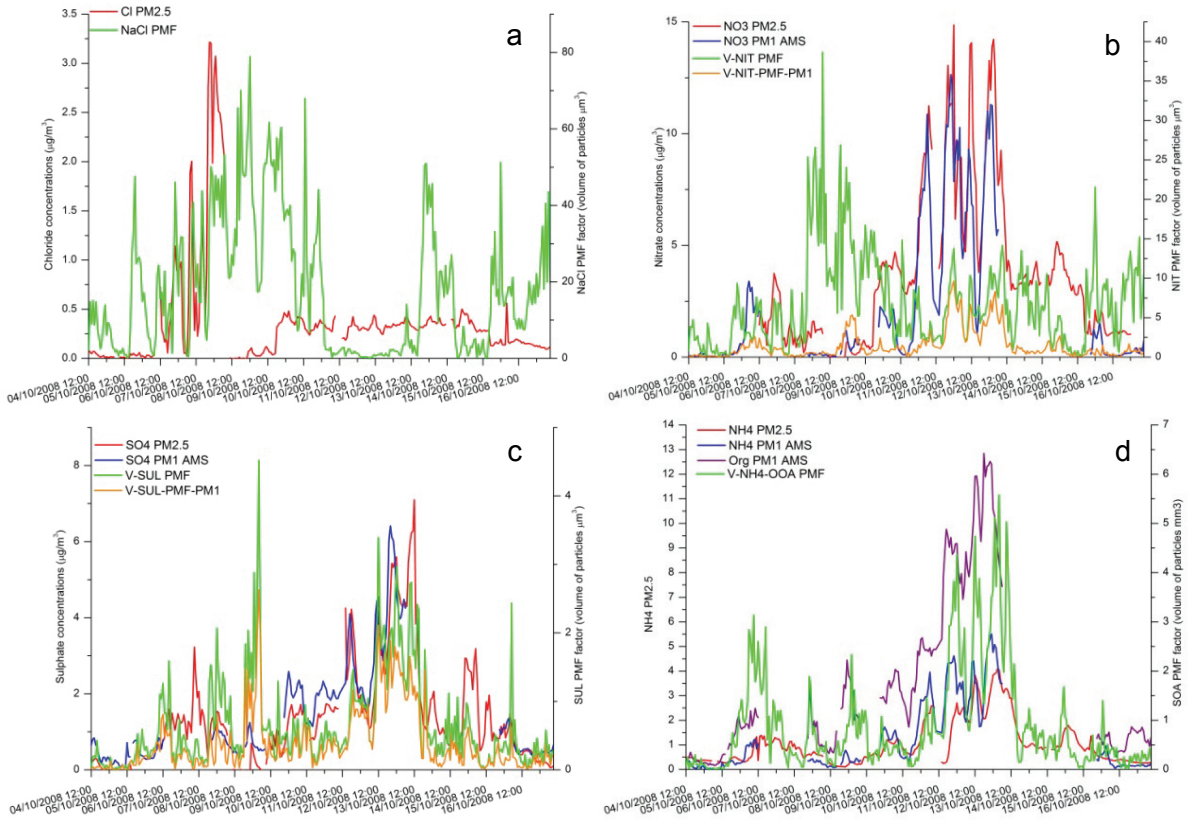

Figure 4.15. Hourly temporal trends of (a) chloride concentrations and NaCl factor, (b) nitrate concentrations and NIT factor, (c) sulphate concentrations and SUL factor, (d) ammonium and organic concentrations and NH4-OOA factor.

The nitrate (NIT) and sulphate (SUL) factors (expressed in volume of particles) are correlated with the nitrate and sulphate concentrations measured in TSP (r=0.30, p-value=4E-4 for nitrate and r=0.56, p-value=8E-15 for sulphate), $PM_{2.5}$ (r=0.26, p-value=2E-4 for nitrate and r=0.58, p-value=6E-16 for sulphate) and AMS PM_1 (r=0.74, p-value=3E-24 for nitrate and r=0.64, p-value=6E-20 for sulphate). In the case of nitrate, NIT PMF factor temporal trend presents a weak correlation with TSP and $PM_{2.5}$ concentrations while it is strongly correlated to nitrate concentration in PM_1. This could be explained by an overestimation of the largest particles contribution in the volume temporal trends, which does not influence PMF factor integrated for particles with diameter <1 µm. In fact nitrate presents both an accumulation and a coarse mode, the last due to its presence in sea spray particles.

The NaCl factor is correlated to the chloride measurements in TSP (r=0.46, p-value=5E-11) and $PM_{2.5}$ (r=0.33, p-value=5E-6). On the contrary AMS chloride is not correlated to the other chloride measurements (p-value=0.32 for TSP and 0.46 for $PM_{2.5}$) because the AMS could only analyse the non-refractory aerosol. The NH4-OOA factor, which contains both OOA and ammonium signals, is correlated to the

ammonium concentration in TSP (r=0.77, p-value=4E-38), in $PM_{2.5}$ (r=0.77, p-value=5E-40) and in PM_1 (r=0.77, p-value=3E-38) and to the organic component measured by the AMS (r=0.77, p-value=3E-39).

Table 4.10. Correlation coefficient, determination coefficient and p-values of r-Pearson correlation tests of PMF factors*, as sum of scores (G-PMF) and in volume (V-PMF), k-means clusters and independent measurements in TSP, $PM_{2.5}$ and PM_1**.

	r correlation coefficients			r^2			p-values of r-Pearson test		
	G-PMF SUL	**V-PMF SUL**	**k-means K-SUL-OC-NIT**	**G-PMF SUL**	**V-PMF SUL**	**k-means K-SUL-OC-NIT**	**G-PMF SUL**	**V-PMF SUL**	**k-means K-SUL-OC-NIT**
SO_4^{2-} TSP	0.45	0.56	0.01	0.20	0.32	0.00	3.0E-09	7.6E-15	0.93
SO_4^{2-} $PM_{2.5}$	0.43	0.58	0.00	0.19	0.34	0.00	1.2E-08	6.4E-16	0.95
SO_4^{2-} PM_1	0.44	0.64	0.01	0.20	0.41	0.00	3.9E-09	5.6E-20	0.88
	G-PMF NIT	**V-PMF NIT**	**k-means K-NIT**	**G-PMF NIT**	**V-PMF NIT**	**k-means K-NIT**	**G-PMF NIT**	**V-PMF NIT**	**k-means K-NIT**
NO_3^- TSP	0.47	0.30	0.58	0.22	0.09	0.34	9.7E-09	4.5E-04	2.2E-13
NO_3^- $PM_{2.5}$	0.48	0.26	0.60	0.23	0.07	0.36	3.5E-09	2.1E-03	2.0E-14
NO_3^- PM_1	0.65	0.74	0.67	0.42	0.54	0.46	1.8E-17	3.0E-24	3.8E-19
	G-PMF NaCl	**V-PMF NaCl**	**K-means NaCl**	**G-PMF NaCl**	**V-PMF NaCl**	**K-means NaCl**	**G-PMF NaCl**	**V-PMF NaCl**	**K-means NaCl**
Cl^- TSP	0.40	0.46	0.56	0.16	0.21	0.31	1.3E-08	4.6E-11	9.2E-17
Cl^- $PM_{2.5}$	0.32	0.33	0.49	0.10	0.11	0.24	9.0E-06	5.1E-06	9.2E-13
	G-PMF NH4-OOA	**V-PMF NH4-OOA**	**K-means OOA**	**G-PMF NH4-OOA**	**V-PMF NH4-OOA**	**K-means OOA**	**G-PMF NH4-OOA**	**V-PMF NH4-OOA**	**K-means OOA**
NH_4^+ TSP	0.85	0.77	0.82	0.72	0.59	0.68	2.2E-53	4.4E-38	3.3E-48
NH_4^+ $PM_{2.5}$	0.84	0.78	0.79	0.70	0.61	0.62	2.9E-51	5.4E-40	4.4E-41
NH_4^+ PM_1	0.82	0.77	0.76	0.67	0.59	0.58	3.6E-47	2.6E-38	1.2E-37
Org PM_1	0.83	0.77	0.73	0.68	0.60	0.53	1.7E-48	2.6E-39	7.2E-33

*PMF factor were integrated for particles of diameter <1µm for comparison with PM_1 data while they have been integrated for all particles for the other comparisons

**measured in PM_1 by AMS

Regarding the cluster analysis, K-SUL-OC-NIT k-means cluster is not correlated to the sulphate concentrations. NaCl clusters and factor present a similar correlation to chloride concentrations. NIT factor and K-NIT cluster present a similar correlation to nitrate concentration.

PMF factors are strongly correlated to the corresponding chemical species concentrations, with a better agreement with PM_1 fraction. Cluster temporal trends are correlated to independent measurements too, with the exception of K-SUL-OC-NIT cluster which is not correlated to sulphate concentrations. In conclusion, cluster temporal trends are in good agreement to species concentrations when their chemical profile is clear, or mixed with substances that present the same temporal

profile. Otherwise, for K-SUL-OC-NIT k-means clusters, in which sulphate is mixed with many other substances, the correlation between the cluster and the concentration of one of its substances is weaker or even lost. Thus, the disaggregation of species made by the PMF analysis (on single particle) turn to be very useful for quantification purposes of the principal substances or classes of substances constituting the particles. On the whole, the results of the present correlation study suggest that, for some species i.e. ammonium, nitrate, sulphate and non-refractory organic in PM_1, PMF factors could be utilized for reliable quantification purposes. In this connection, a first attempt to obtain quantitative data from PMF ATOFMS factors were done by a linear regression between them and the ion and organic measurements in PM_1. It is worth to specify that ATOFMS data were not corrected for size dependent transmission losses because there were not enough APS and SMPS data available. Nevertheless, the results reported in table 4.11 seem encouraging.

Table 4.11. Intercept, slope and determination coefficient of the linear regression between PMF factor hourly temporal trends in scores (G-PMF) and in volume (V-PMF), and the corresponding species concentration in PM_1* (y=a+bx, with y=PMF factor temporal trend and x=species concentration).

	G-PMF (corresponding hourly factor scores)**			**V-PMF** (corresponding hourly factors in volume)**		
	a	**b**	**r^2**	**a**	**b**	**r^2**
SO_4^{2-} PM_1	114000±33000	95000±15000	0.20	0.08±0.05	0.25±0.02	0.41
NO_3^- PM_1	75000±120000	244000±25000	0.42	0.81±0.18	0.46±0.04	0.54
NH_4^+ PM_1	19800±8800	87800±4500	0.67	0.11±0.06	0.50±0.03	0.59
Org PM_1	-4700±9400	38200±1900	0.68	-0.03±0.06	0.22±0.01	0.60

*PM1 measurements by AMS

**PMF factors integrated for particles of diameter <1µm

The closed to zero intercepts (however in many cases not statistically zero) and the low standard deviations of the slopes seem to indicate that quantitativity is possible to achieve besides independent measurements which so far are still necessary. In fact, Jeong et al. obtained mass concentrations of sulphate, nitrate, ammonium, organic carbon and elemental carbon by scaling the ion peak intensities using APS and SMPS size distribution, and by applying linear regression parameters between them and independent species measurements [Jeong 2011]. He demonstrated that the correlation coefficients r increase significantly when ATOFMS data were corrected for transmission losses. For example, for sulphate, the r increased from 0.30 to 0.80 using unscaled and scaled ATOFMS data (peak area scaled using APS and SMPS

measurements) respectively in a campaign conducted in Harrow, Ontario, Canada [Jeong 2011].

In this context, the results obtained could be considered encouraging even though a deeper assessment and investigation are needed taking into account that so far, ATOFMS data need to be adjusted and correlated to independent sampling measurements. In fact, low reproducibility due to size-dependent transmission losses [Allen 2000, Allen 2006, Wenzel 2003], laser intensity shot-to-shot variations [Bhave 2002], ionization matrix effects [Reilly 2000], different sensitivities among chemical species makes a semi-quantitative analysis possible to achieve only beside independent sampling measurements [Bhave 2002, Gross 2000, McGuire 2011].

4.7. Air masses back-trajectories and local meteorological data

During the entire campaign, Harwell was influenced by low speed winds coming from south and west directions. In figure 4.16 the bivariate polar plots which show the PMF factor abundance (hourly sum of scores) in relation to wind direction and speed are reported. The majority of PMF factors present the highest abundance when low-speed wind coming from east direction are present. The exception are: CNO-COOH and OC-Arom factors which present the highest abundance when the wind blows from west and south direction and NaCl factor which is more abundant when the wind blows from N/NW and S directions. More information could be extracted by the study of air masses back-trajectories.

During the EMEP08 campaign, the contributions of the air masses back-trajectories could be divided into four periods: the marine polar (MP), two continental-marine (MC1 and MC2) and the continental (C) contribution periods. In table 4.12, the sampling campaign is divided into time periods corresponding to the different contributions of air masses and in Figure 4.17 the air masses back-trajectories are reported.

Table 4.12. Contributions of the air mass transports during Harwell October 2008 campaign.

Time	Type
04/10/2008 12.00 – 06/10/2008 0.00	MP
06/10/2008 0.00 – 07/10/2008 0.00	MC1
07/10/2008 0.00 – 10/10/2008 0.00	MP
10/10/2008 0.00 – 14/10/2008 0.00	C
14/10/2008 0.00 – 15/10/2008 12.00	MC2
15/10/2008 12.00 – 17/10/2008 12.00	MP

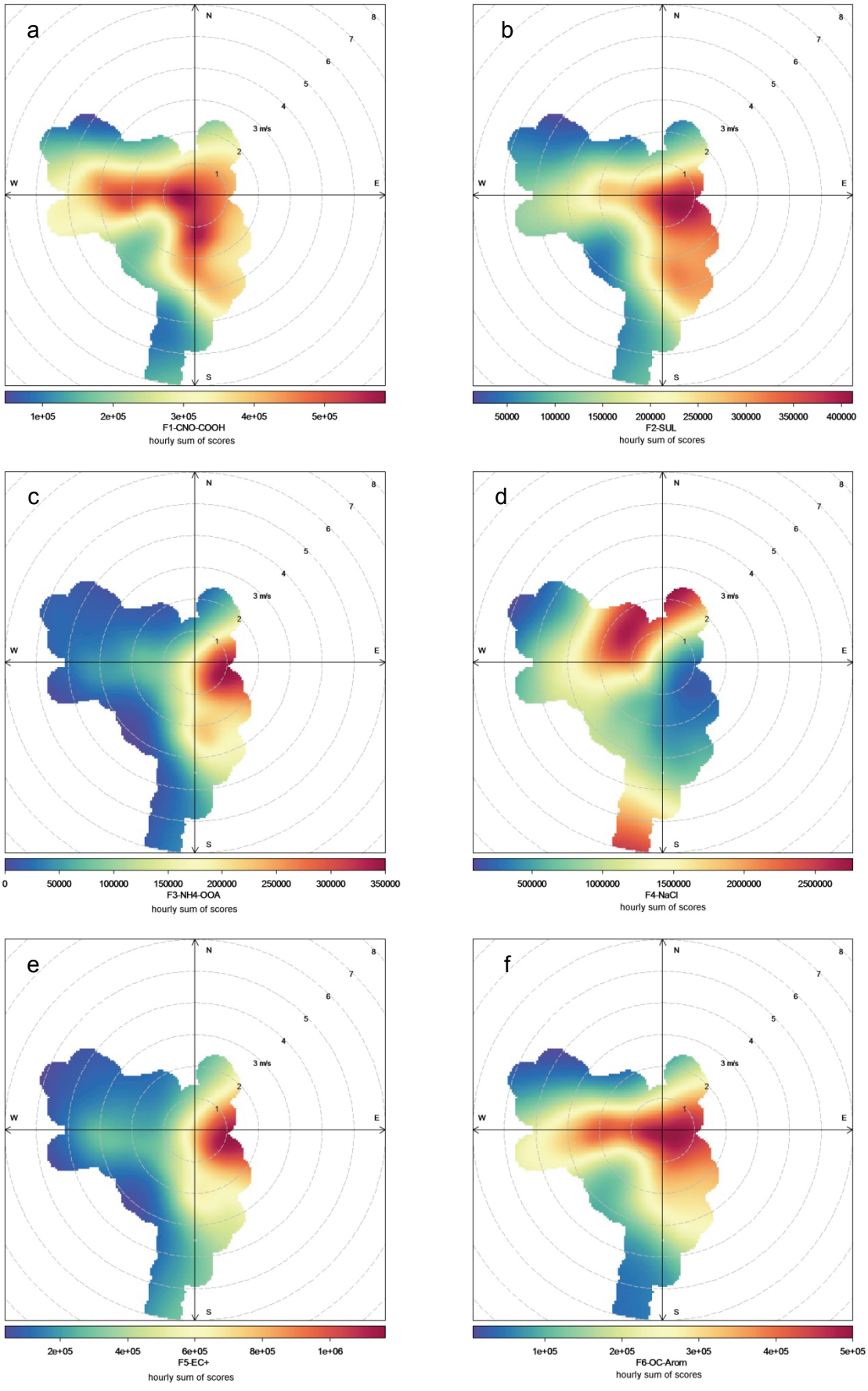
a
N
S
W
E
3 m/s
1e+05 2e+05 3e+05 4e+05 5e+05
F1-CNO-COOH
hourly sum of scores
b
50000 100000 150000 200000 250000 300000 350000 400000
F2-SUL
hourly sum of scores
c
0 50000 100000 150000 200000 250000 300000 350000
F3-NH4-OOA
hourly sum of scores
d
500000 1000000 1500000 2000000 2500000
F4-NaCl
hourly sum of scores
e
2e+05 4e+05 6e+05 8e+05 1e+06
F5-EC+
hourly sum of scores
f
1e+05 2e+05 3e+05 4e+05 5e+05
F6-OC-Arom
hourly sum of scores

Figure 4.16

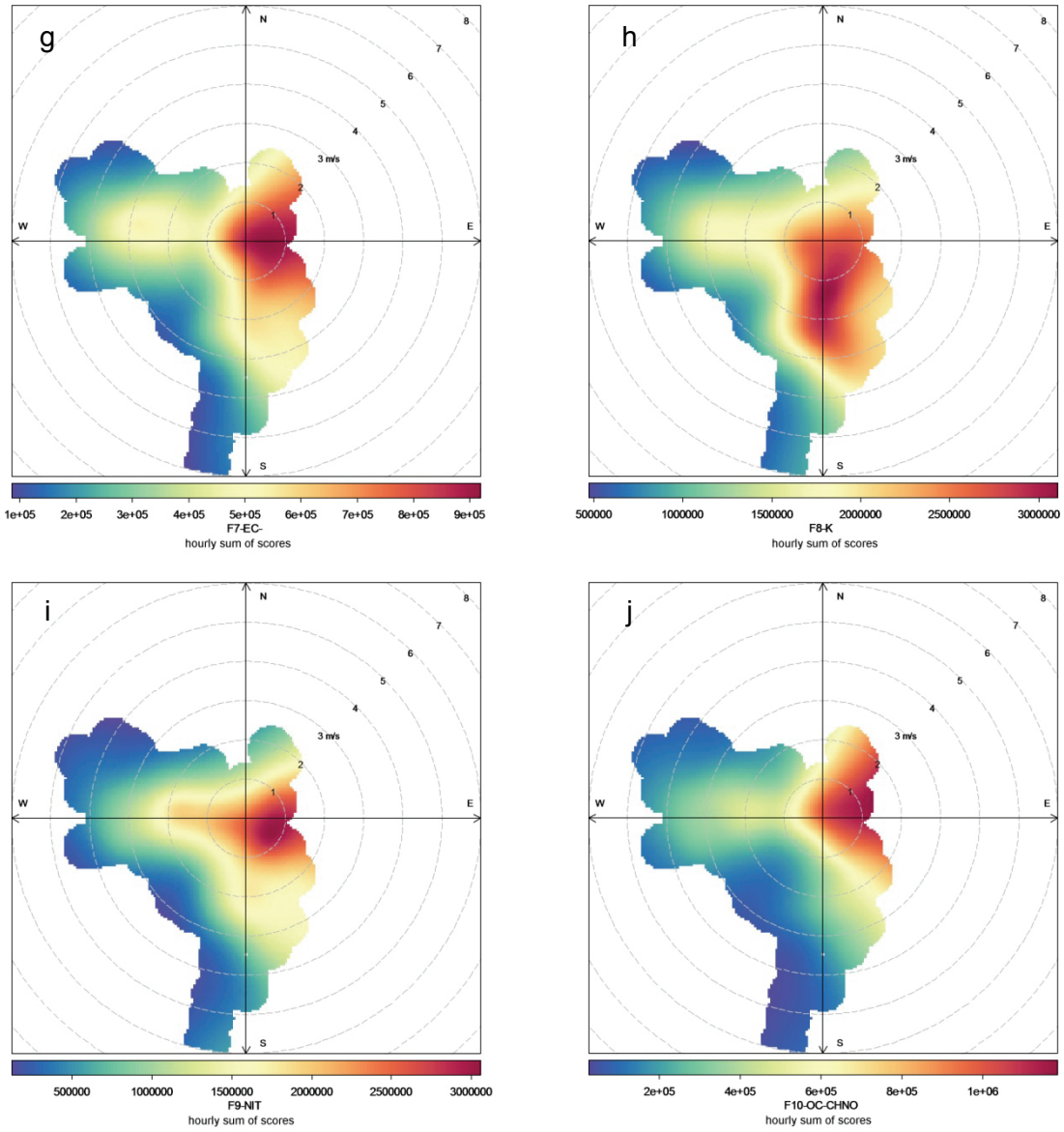

Figure 4.16. Bivariate polar plots of PMF factors (hourly sum of scores), (a) F1 CNO-COOH, (b) F2 SUL, (c) F3 NH4-OOA, (d) F4 NaCl, (e) F5 EC+, (f) F6 OC-Arom, (g) F7 EC-, (h) F8 K, (i) F9 NIT and (j) F10 OC-CHNO, respect to wind direction and speed.

In Figure 4.18, the pie chart of the ionic component in TSP, $PM_{2.5}$ and PM_1 divided during the three different contributions from long range transports are reported. During the marine polar contribution the chloride concentration is enhanced, while during the continental contribution there is a major contribution of other species like nitrate, sulphate, ammonium and organic fraction.

The cluster and PMF factor contributions lead to similar conclusions (Figures 4.18 and 4.19). During the continental contribution there is an enhancement of the potassium, nitrate, sulphate, EC and OC fractions.

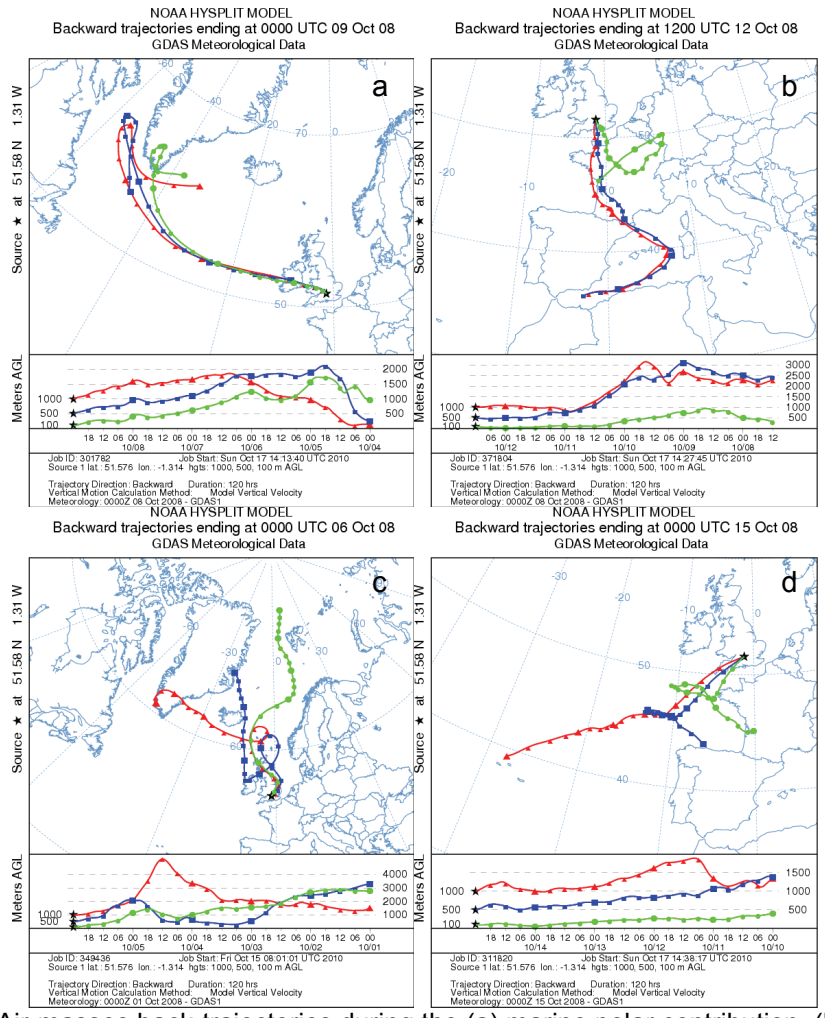

Figure 4.17. Air-masses back-trajectories during the (a) marine polar contribution, (b) continental contribution and the two (c) MC1, (d) MC2 mixed marine-continental contributions.

The two marine continental periods are different (table 4.13 and Figure 4.16). The first one is characterized by air masses coming from the ocean, crossing Scotland and England before arriving at the Harwell site. It is also characterized by a high amount of NO_x, alkanes, unsaturated aliphatics and BTEX concentrations. The second one is characterized by air masses coming from the west-coast of France. The first period is characterized by a relative high amount of the OC-CHNO and EC-PMF factors while the second period is characterized by a relative high amount of the CNO-COOH acids and EC+ PMF factors.

Table 4.13. Primary gaseous pollutants concentration and PMF factor abundance during the two marine-continental polar periods.

		PMF factors (average equivalent number of particles/hour)				Total concentration (µg/m^3)			
		F1 CNO-COOH	**F2 EC+**	**F10 OC-CHNO**	**F7 EC-**	**BTEX**	**alkanes**	**unsaturated**	**NOx (as NO2)**
MC1	06/10/2008 0.00 – 07/10/2008 0.00	3.4	18.0	18.4	5.2	2.65	7.22	1.47	24.4
MC2	14/10/2008 0.00 – 15/10/2008 12.00	4.0	21.7	3.8	2.8	1.77	3.03	0.94	6.4

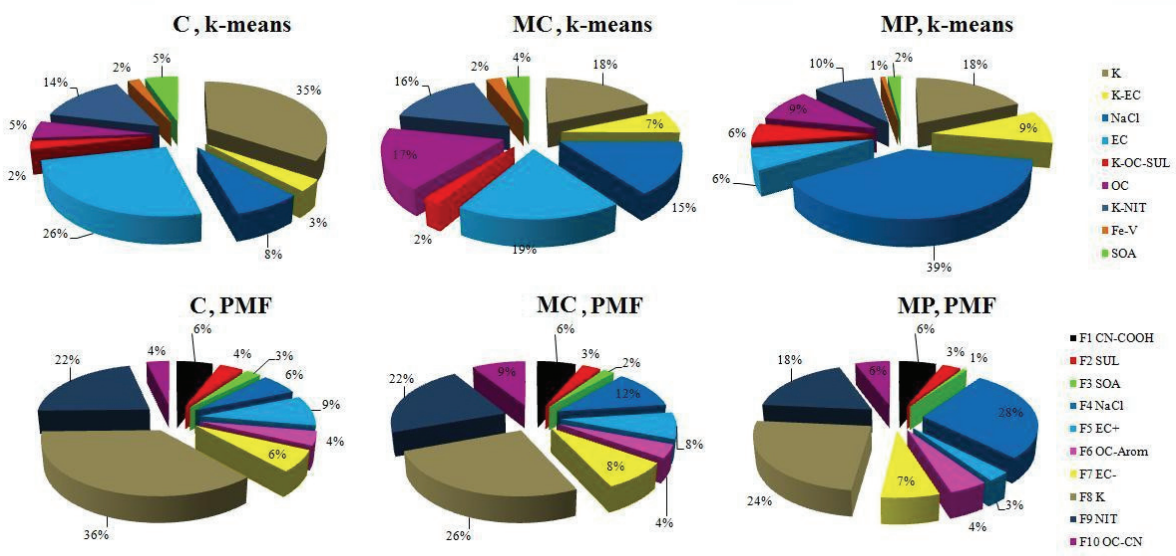

Figure 4.18. Factors and clusters abundance during the three different air masses long-range transports

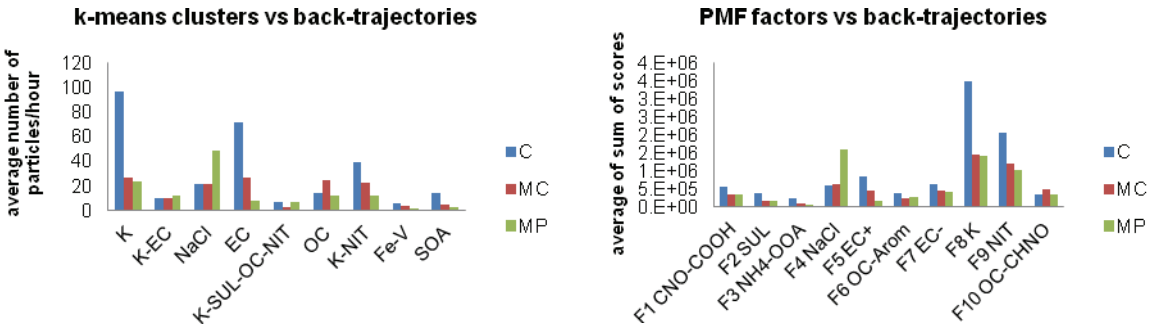

Figure 4.19. Clusters and factors abundance during the three different contributions from long-range transport of air masses

In conclusion, from the cross correlation analysis among PMF factor temporal trends it was possible to outline two elemental carbon components: the EC- factor, correlated to OC-CHNO, probably related to anthropogenic primary emissions and the EC+ factor present in aged particles internally mixed with secondary species. In fact, PMF analysis can successfully disaggregate the contribution of different component types: primary species, like EC- and OC-CHNO and secondary species like CNO-COOH, NIT and SUL. In Harwell (UK), a rural background site, the particles chemical composition is strongly influenced by long-range transports of air masses and it is interesting to notice two different marine-continental polar contributions. The first one, regional, characterized by freshly emitted particles and relatively high concentrations of gaseous pollutants and the second one, more continental, characterized by aged (more oxidized) aerosol.

Moreover, PMF factors temporal trends are strongly correlated to the corresponding chemical species concentrations measured by independent instruments even in the

case of highly internally mixed particles, while the correlation between cluster temporal trends and corresponding chemical species concentration could be affected and highly dependent by particle mixing state. Thus PMF analysis could turn useful for the quantification of the main components of PM in view of a future development of the ATOFMS instrument. In fact, the results of the first attempt to provide quantitative data from PMF factors could be considered encouraging even though a deeper assessment and investigation are needed.

5. London Marylebone Road 2009 campaign

5.1. PMF analysis optimization

During London Marylebone Road campaign the ATOFMS sized and hit 693462 particles in 21 days of continuous sampling (22/05/2009-11/06/2009). The particles sampled constitute a huge dataset, which is difficult to analyse all at once with PMF2 software [Paatero 1998] installed on state-of-the-art personal computers. So far, to the author's knowledge, there are not UNIX versions or other platform versions of the PMF algorithm, which could be used into more powerful computers or cluster of computers in order to analyse huge datasets all at once. For this reason, a further optimization step was needed, which was performed adopting the following approaches:

- PMF analysis on the dataset divided by groups of days;
- PMF analysis on sub-datasets selected through a random sampling of particles (10%);
- PMF analysis on hourly aggregated data.

Besides these approaches, different metrics, i.e. wind direction or air masses long range transports, could be used to select or divide the dataset in order to reach a specific purpose.

5.1.1. Data pre-treatment

The mass spectra of the particles were treated as aforementioned (chapter 3, Materials and Methods) in order to obtain the matrix to be subjected to the PMF analysis. Briefly, particles with a diameter of 0.1-3 μm were held for the analysis (681626 particles in total). The variables (m/z) considered were 121: -162, -146, -144, -124, -121, -119, -104, -101, -99, -98, -97, -96, -95, -89, -88, -85, -84, -83, -81, -80, -79, -76, -73, -72, -71, -64, -63, -62, -60, -59, -49, -48, -47, -46, -44, -43, -42, -37, -36, -35, -32, -27, -26, -25, -24, -17, -16, -15, -14, -13, -12, 7, 12, 15, 18, 23, 24, 27, 28, 29, 30, 36, 37, 39, 41, 43, 46, 48, 49, 50, 51, 52, 53, 54, 55, 56, 57, 58, 59, 60, 61, 62, 63, 64, 65, 69, 70, 71, 72, 73, 74, 75, 77, 81, 83, 84, 85, 86, 87, 88, 91, 94, 95, 96, 97, 99, 100, 101, 103, 105, 108, 115, 118, 120, 128, 132, 138, 139, 140, 173, 207.

Absolute area under the peaks was considered for PMF analysis, which was directly applied to single particle mass spectra (*nxm* data matrix of *n* single particles, *m* variables - m/z values - in which each datum is the absolute area under the peak in the mass spectra corresponding to the n_i particle and m_j m/z signal).
For the PMF analysis on the entire dataset divided by groups of days, 5 periods of time were selected on the basis of the number of particles sampled:
- sub-dataset “Time1” 22-25/05/2009, made up of 126607 particles;
- sub-dataset “Time2” 26-29/05/2009, made up of 134354 particles;
- sub-dataset “Time3” 30/05-04/06/2009, made up of 137448 particles;
- sub-dataset “Time4” 05-08/06/2009, made up of 144019 particles;
- sub-dataset “Time5” 09-11/06/2009, made up of 139198 particles.

For the PMF on sub-datasets obtained from random sampling of particles, 3 matrices representing the 10% of the entire dataset (68159 particles) were random selected using the software R as detailed in annex 1, section 2.
The hourly aggregated data matrix to be subjected to PMF analysis was obtained as explained in chapter 3 “Material and Methods”. For all the PMF analyses the matrix **S** of the data uncertainties was calculated as aforementioned (see chapter 3 Materials and Methods and chapter 4 Harwell 2008 campaign).

5.2. PMF analysis on the entire dataset divided by groups of days

Because of the huge amount of data, PMF analysis requires a lot of computing time. For this reason, a preliminary PMF analysis was performed on each “Time” matrix, using a single seed starting solution, and varying the number of factors from 3 to 20. For each matrix, the 15 factors solution contains all the main components contributing to particles, with some of them split in two or three factors. Despite this is a sub-optimal choice of factors, it is the one which allow the extraction of the main components in all the matrices. In fact, repeating the number of factors optimization for all the matrices would be a time consuming step. Thus the 15 factors solution was selected and the analysis was refined for all the five matrices by repeating the PMF routine starting from 50 different seeds (pseudorandom starting points). In table 5.1, the 15 factors extracted from the PMF analysis applied to the 5 sub-datasets are reported.

The results reveal that the main factors split into two or three factors, differently from one matrix to the other. In fact, because of the elevated number of factors chosen, the main factors split into more factors accordingly to their contribution to the particles of the sub-dataset. EC+ factor, splits into three factors regardless the sub-dataset used. On the contrary, OC-Arom splits into three factors during the PMF analysis applied to the matrices "Time1", "Time2" and "Time3" where its contribution is respectively 14%, 13% and 10% on average; while it splits into two factors during the PMF analysis on the matrices "Time4" and "Time5" where its contribution is 7% and 6% respectively.

For all the sub-datasets, factors extracted were manually merged accordingly to their chemical profile in order to obtain 10 factors explaining the 55% of variance (calculated on the entire dataset). It is worth to say that the chemical profiles of the factors extracted from the different "Time" matrices are absolutely equals, and therefore their temporal trends were manually merged. The 10 factors obtained are: K (6.6%), NIT (1.8%), NaCl (3.0%), OOA (4.8%), NH4 (2.1%), CNO-COOH (1.6%), EC+ (18.9%), EC- (2.5%), OC-arom (10.0%) and OC-CHNO (3.9%).

Table 5.1. Factors extracted from the PMF analysis on the dataset divided by days.

	sub-datasets				
	Time1	**Time2**	**Time3**	**Time4**	**Time5**
F1	CNO-COOH	CNO-COOH	NIT_2	CNO-COOH	EC-_1
F2	EC-	NaCl	OC-Arom_1	EC+_2	CNO-COOH
F3	m/z=-95	EC-_1	OC-Arom_2	EC-_1	EC-_2
F4	NH4	NH4	CNO-COOH	NaCl	m/z=-60
F5	EC+_2	OC-Arom_2	NH4	EC-_2	EC+_1
F6	OC-Arom_2	EC+_2	EC+_3	EC+_3	NaCl
F7	OC-Arom_3	OOA	EC-	NH4	NH4
F8	OC-Arom_1	EC-_2	EC+_1	OOA	EC+_2
F9	NIT	NIT	NIT_1	OC-Arom_3	K
F10	NaCl	K	NaCl	K	OOA
F11	K	EC+_1	K	EC+_4	OC-CHNO
F12	OOA	OC-Arom_3	EC+_2	EC+_1	NIT
F13	EC+_1	EC+_3	OC-Arom_3	NIT	OC-Arom_1
F14	OC-CHNO	OC-Arom_1	OOA	OC-Arom_2	OC-Arom_2
F15	EC+_3	OC-CHNO	OC-CHNO	OC-CHNO	EC+_3

5.3. PMF analysis on the random selected sub-datasets

Matrices selected from random samplings of particles (10%), named “Random1”, “Random2” and “Random3”, were subjected to PMF analysis, using a 15 factors solution and repeating the routine starting from 50 different seeds in order to reach the global minimum. The 15 factors extracted are reported in table 5.2. It is worth to notice that the 15 factors extracted are different from one sub-dataset to the others. For example, OC-Arom splits into three factors in the analysis on “Random1” and “Random2” matrices, where its explained variance is 13%, and into two factors in the analysis on “Random3” matrix, where its explained variance is 10%. EC- splits into two factors during the analysis on “Random1”, where its explained variance is 4%, while it remains unsplit in the analysis on the other two datasets (explained variance of 3% in “Random2” and 2% in “Random3”).
Thus, the three random selected matrices containing 10% of the total dataset, could not be considered representative of the entire dataset (see section 5.4).

Table 5.2. Factors extracted from the PMF analysis on three sub-datasets obtained by random sampling of particles

	Random1	**Random2**	**Random3**
F1	OC-Arom_2	CNO-COOH	EC-
F2	OC-Arom_1	EC-	m/z=-95
F3	OC-Arom_3	NaCl	CNO-COOH
F4	EC+_3	EC+_2	NIT_1
F5	K	EC+_1	NaCl
F6	NaCl	OC-Arom_3	NH4
F7	NH4	EC+_3	NIT_2
F8	EC+_2	NH4	EC+_2
F9	EC-_2	NIT_2	OOA
F10	EC+_1	OOA	K
F11	CNO-COOH	NIT_1	EC+_1
F12	NIT	K	OC-Arom_3
F13	EC-_1	OC-Arom_2	OC-CHNO
F14	OOA	OC-Arom_1	OC-Arom_2
F15	OC-CHNO	OC-CHNO	EC+_3

The 15 factors extracted were manually re-aggregated, by merging factors of similar profiles and temporal trend, in order to obtain 10 factors. The temporal trends (hourly sum of scores) of the 10 factors obtained through different approaches were then compared using a *r*-Pearson correlation test. In table 5.3 the correlation coefficients among temporal trends of factors, obtained from the whole dataset and the three random sub-datasets, are reported.

The temporal trends of factors obtained through different approaches are always in good agreement (p-value<0.0001). Correlation coefficients between factors obtained from the entire dataset (analysis on the dataset divided by groups of days) and the sub-datasets of random samplings vary from 0.69 (EC- vs EC- from “Random2”) to 0.95 (EC+ vs EC+ from all the three “Random” matrices).

On the whole, the random samplings could not be considered representative of the entire dataset, because the PMF solutions present different factors accordingly to the sub-dataset. However, once these factors are manually recombined to generate the 10 main factors, their hourly temporal trends could be a good surrogate for hourly temporal trends of factors extracted from the entire dataset. In this manner, random samplings of the 10% of the dataset could be used to preliminarily extract the main factors and their hourly temporal trends.

Table 5.3. Correlation analysis between factors temporal trends extracted from the PMF analysis on the entire dataset and the 3 random selected sub-datasets

	K	K_R1	K_R2	K_R3
K	1			
K_R1	0.93	1		
K_R2	0.92	0.87	1	
K_R3	0.92	0.88	0.85	1
	NIT	NIT_R1	NIT_R2	NIT_R3
NIT	1			
NIT_R1	0.87	1		
NIT_R2	0.89	0.81	1	
NIT_R3	0.88	0.81	0.85	1
	NaCl	NaCl_R1	NaCl_R2	NaCl_R3
NaCl	1			
NaCl_R1	0.85	1		
NaCl_R2	0.86	0.78	1	
NaCl_R3	0.88	0.77	0.77	1
	OOA	OOA_R1	OOA_R2	OOA_R3
OOA	1			
OOA_R1	0.93	1		
OOA_R2	0.94	0.91	1	
OOA_R3	0.94	0.91	0.91	1
	NH4	NH4_R1	NH4_R2	NH4_R3
NH4	1			
NH4_R1	0.94	1		
NH4_R2	0.95	0.90	1	
NH4_R3	0.94	0.92	0.90	1

	CNO-COOH	CNO-COOH_R1	CNO-COOH_R2	CNO-COOH_R3
CNO-COOH	1			
CNO-COOH_R1	0.86	1		
CNO-COOH_R2	0.87	0.75	1	
CNO-COOH_R3	0.87	0.76	0.77	1
	EC+	EC+_R1	EC+_R2	EC+_R3
EC+	1			
EC+_R1	0.95	1		
EC+_R2	0.95	0.91	1	
EC+_R3	0.95	0.91	0.91	1
	EC-	EC-_R1	EC-_R2	EC-_R3
EC-	1			
EC-_R1	0.67	1		
EC-_R2	0.69	0.57	1	
EC-_R3	0.71	0.55	0.61	1
	OC-Arom	OC-Arom_R1	OC-Arom_R2	OC-Arom_R3
OC-Arom	1			
OC-Arom_R1	0.91	1		
OC-Arom_R2	0.92	0.87	1	
OC-Arom_R3	0.89	0.84	0.85	1
	OC-CHNO	OC-CHNO_R1	OC-CHNO_R2	OC-CHNO_R3
OC-CHNO	1			
OC-CHNO_R1	0.91	1		
OC-CHNO_R2	0.91	0.86	1	
OC-CHNO_R3	0.92	0.88	0.88	1

5.4. Different random samplings and autocorrelation analysis

Accordingly to the results obtained from the PMF analysis on sub-datasets of random sampling of the 10% of the total dataset, two approaches were adopted in order to understand if the random samplings done were not numerous enough to represent the dataset or if the dataset is intrinsically not representable through random sampling because its distribution is not stochastic. Because of computational limits, for both approaches, the tests were made considering only the first half day of field campaign as initial screening.

The first approach adopted consisted in applying the PMF analysis to sub-datasets of random samplings of increasing numerousity.

PMF analysis was performed on the original dataset (1st half day of field campaign) and on sub-datasets of random samplings representing the 5%, 10%, 20%, 30%, 40%, 50%, 60%, 70%, 80% and 90% of the original dataset.

The analysis was conducted starting from 50 seeds and using a 15 factors solution. Although the increasing numerousity of the sub-datasets, factors obtained did not converged to a unique solution equal to the one obtained from the original data matrix (1st half day of sampling campaign). In table 5.4 factors obtained from the analysis on the original data matrix and on the sub-dataset representing the 90% of the original dataset are reported.

In conclusion, even a random sampling of the 90% of particles is not representative of the entire dataset in PMF analysis.

Table 5.4. Factors extracted from the PMF analysis on the data of the 1st half day of field campaign and the PMF analysis on a sub-dataset representing the 90% of the 1st half day of field campaign

	Random 90%	**Entire dataset**
F1	OOA_1	OOA_2
F2	EC+_2	NaCl
F3	EC+_3	CNO-COOH
F4	NaCl	OOA_1
F5	OOA_2	EC+_3
F6	OC-Arom_2	OC-Arom_1
F7	OC-Arom_3	EC+_2
F8	CNO-COOH	EC+_1
F9	K	OC-Arom_2
F10	EC+_1	OC-CHNO
F11	NIT	NIT
F12	OC-Arom_1	EC-
F13	OC-CHNO_2	K
F14	EC-	OC-CHNO_3
F15	OC-CHNO_1	OC-CHNO_2

The second approach consisted in making an autocorrelation test (correlation between observations separated by the same time span) for a few principal variables (m/z) which reveal the possible presence of drifts and periodicities in the timeseries, which make the variables not representable through random samplings.

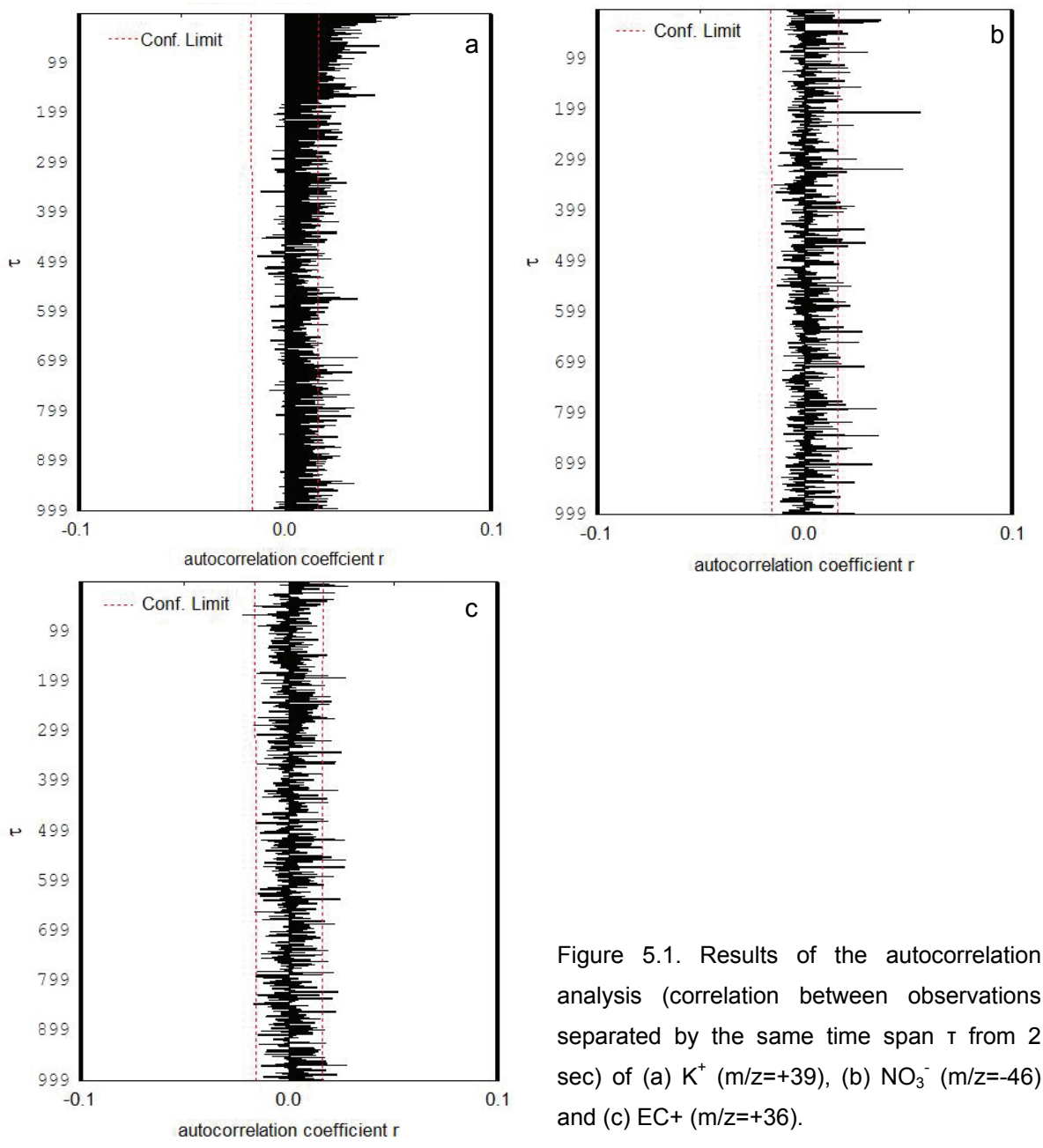

Figure 5.1. Results of the autocorrelation analysis (correlation between observations separated by the same time span τ from 2 sec) of (a) K^+ (m/z=+39), (b) NO_3^- (m/z=-46) and (c) EC+ (m/z=+36).

In fact, it is very likely that the timeseries of the variables are affected by drifts and periodicity, because of weather variability, sources variability and particle-to-particle variability.

Autocorrelation analysis (figure 5.1), applied to a few principal variables, i.e. K^+ (m/z=+39), EC+ (m/z=+36) and NO_3^- (m/z=-46) shows that the timeseries present both drifts and periodicities with a high contribution of noise. Even if the correlation coefficient is small, the timeseries could be considered statistically autocorrelated. As a consequence, ATOFMS data are not representable through random samplings of particles.
Despite half a day is an insufficient period of time which could not be considered representative of the entire campaign, it is likely that the autocorrelation would be even stronger if the entire campaign is considered. In fact, air masses change on timescale longer than half a day and sources change over several hours, so the data variation would be even higher if all the campaign is considered. In this way, the results of the first screening could be considered reliable, while if the test had given a negative response it would have been repeated on the entire campaign.

5.5. PMF analysis on hourly aggregated data

The analysis was performed starting from 25 different pseudorandom starting points and using different numbers of factors. The 7 factors solution was selected from both a mathematical [Lee 1999] and chemical point of view. The explained variation for the 7 factors solution is of about the 84%. The factors extracted are: F1-NaCl, F2-K-CN, F3-Na-EC, F4-K-NIT, F5-K, F6-K-NIT-OC and F7-EC+-NIT. As previously found for the Harwell dataset, potassium and nitrate are dominant signals, present almost in each factor and so the chemical interpretation of the chemical profiles of the factors is very difficult (not shown). Moreover as previously seen for the Harwell dataset, PMF analysis on hourly aggregated data does not give any extra information respect to the analysis on single particles.

5.6. PMF analysis on single particles (entire dataset)

The 10 factors obtained are: K (6.6%), NIT (1.8%), NaCl (3.0%), OOA (4.8%), NH4 (2.1%), CNO-COOH (1.6%), EC+ (18.9%), EC- (2.5%), OC-arom (10.0%) and OC-CHNO (3.9%), explaining the 55% of the variance. The chemical profiles of the factors (figure 5.2) are very clear and chemically well defined: each factor represents a specific chemical species (K, NIT, NH4 and CNO-COOH) or an important class of

components (OOA, NaCl, EC+, EC-, OC-Arom and OC-CHNO). The factors extracted present chemical profiles comparable to the ones obtained from the Harwell dataset. The two main differences reside on ammonium signal, which is separated from OOA and constitute an unique factor (NH4), and sulphate, which is not extracted by PMF analysis. In fact, sulphate is scarcely represented in this dataset, contributing for about 1% in total. Ammonium is principally considered a secondary component of aerosol. However, vehicles running under rich air-fuel conditions, with three-way catalytic converters designed to reduce NO_x to N_2 and O_2 could emit in addition NH_3 [Fraser 1998, Sutton 2000, Tanner 2009]. Other differences that could be noted are the scarce presence of carboxylic acids in CNO-COOH factor, and OOA and OC-Arom mass spectra which both present aromatic signals. In fact, the former is characterized by a high contribution of m/z=+27/+43 signals and a low contribution of aromatics while the latter is characterized by high contributions of m/z=+43 and aromatic fragments including m/z=+77/+91 associated to $C_6H_5^+$ and $C_7H_7^+$.

Despite the characteristics of the sampling site, which is a kerbside site characterized by a street canyon with highly intense vehicular traffic, PMF analysis seems to have not been able to extract other than the main components. The explained variation, in this case is 10% higher than the previous one (Harwell dataset), in particular the EC and OC contributions are significantly higher. However, it seems that possible source markers contribution was not isolated by the analysis. The ATOFMS precision and the PMF performances are probably not efficient enough to discriminate the source markers contribution if they have a low concentration.

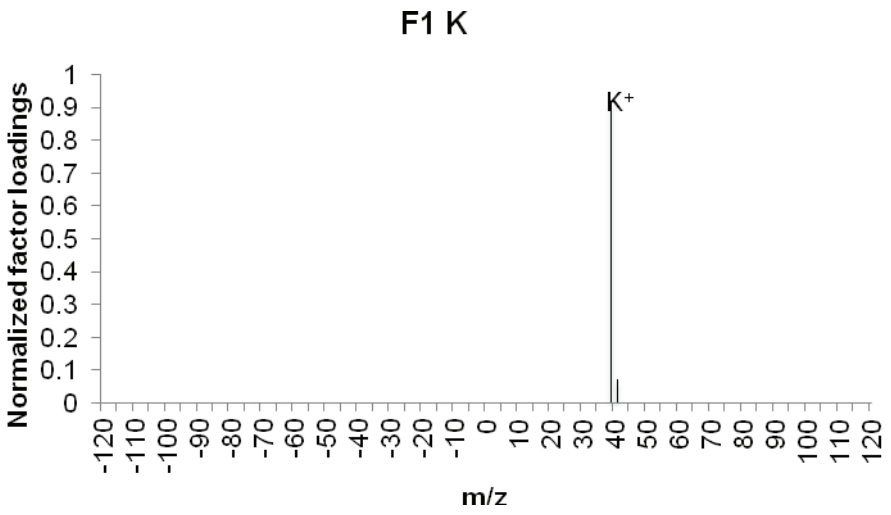

Figure 5.2

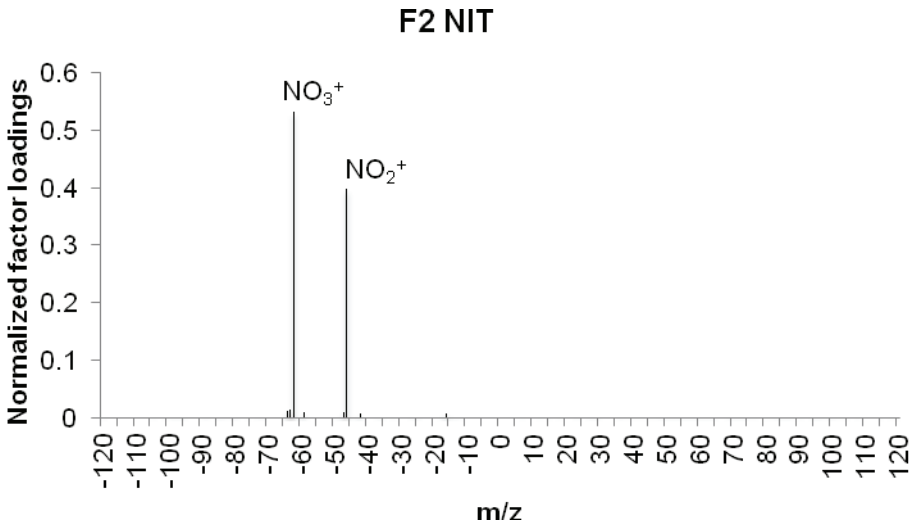
F2 NIT
Normalized factor loadings
0.6
0.5
0.4
0.3
0.2
0.1
0
NO3+
NO2+
-120 -110 -100 -90 -80 -70 -60 -50 -40 -30 -20 -10 0 10 20 30 40 50 60 70 80 90 100 110 120
m/z

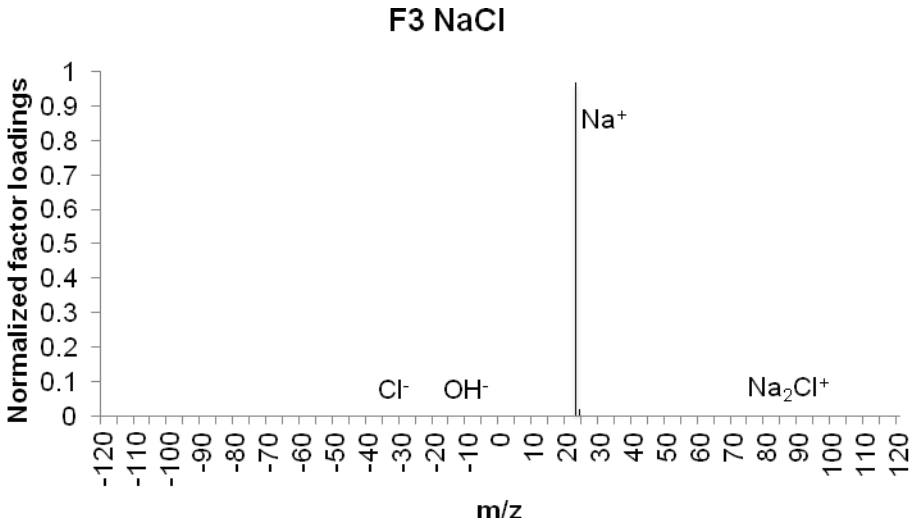
F3 NaCl
Normalized factor loadings
1
0.9
0.8
0.7
0.6
0.5
0.4
0.3
0.2
0.1
0
Na+
Cl-
OH-
Na2Cl+
-120 -110 -100 -90 -80 -70 -60 -50 -40 -30 -20 -10 0 10 20 30 40 50 60 70 80 90 100 110 120
m/z

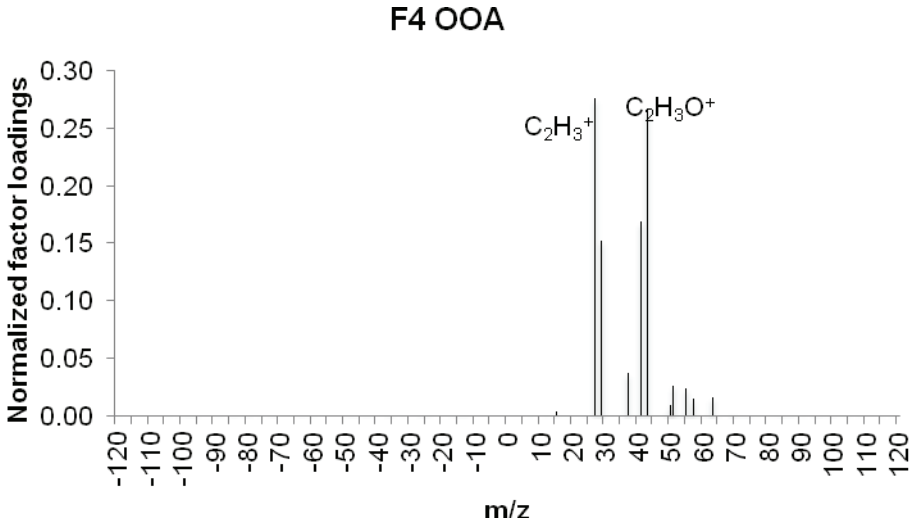
F4 OOA
Normalized factor loadings
0.30
0.25
0.20
0.15
0.10
0.05
0.00
C2H3+
C2H3O+
-120 -110 -100 -90 -80 -70 -60 -50 -40 -30 -20 -10 0 10 20 30 40 50 60 70 80 90 100 110 120
m/z

Figure 5.2

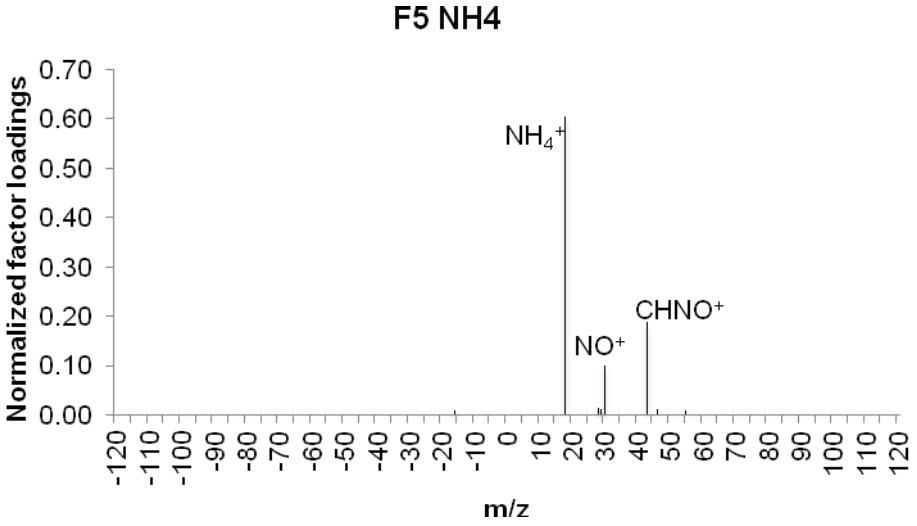
F5 NH4
Normalized factor loadings
0.70
0.60
0.50
0.40
0.30
0.20
0.10
0.00
NH4+
CHNO+
NO+
-120 -110 -100 -90 -80 -70 -60 -50 -40 -30 -20 -10 0 10 20 30 40 50 60 70 80 90 100 110 120
m/z

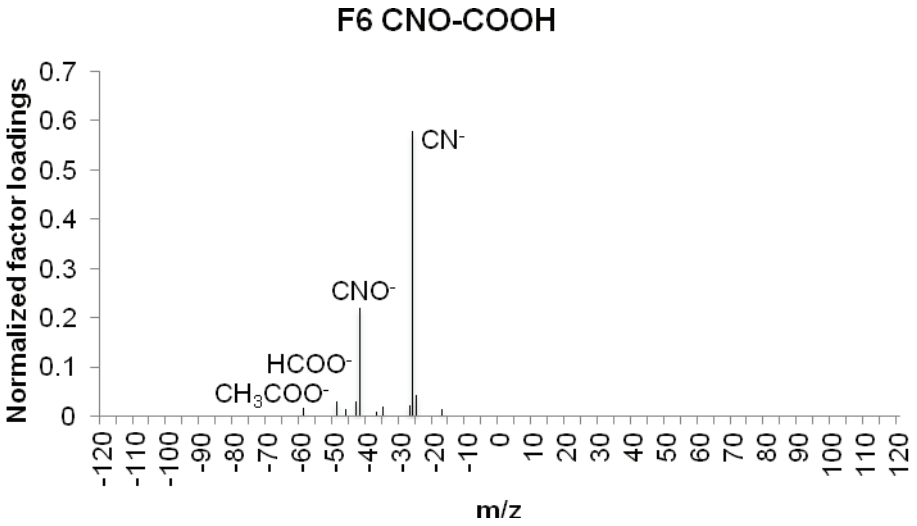
F6 CNO-COOH
Normalized factor loadings
0.7
0.6
0.5
0.4
0.3
0.2
0.1
0
CN-
CNO-
HCOO-
CH3COO-
-120 -110 -100 -90 -80 -70 -60 -50 -40 -30 -20 -10 0 10 20 30 40 50 60 70 80 90 100 110 120
m/z

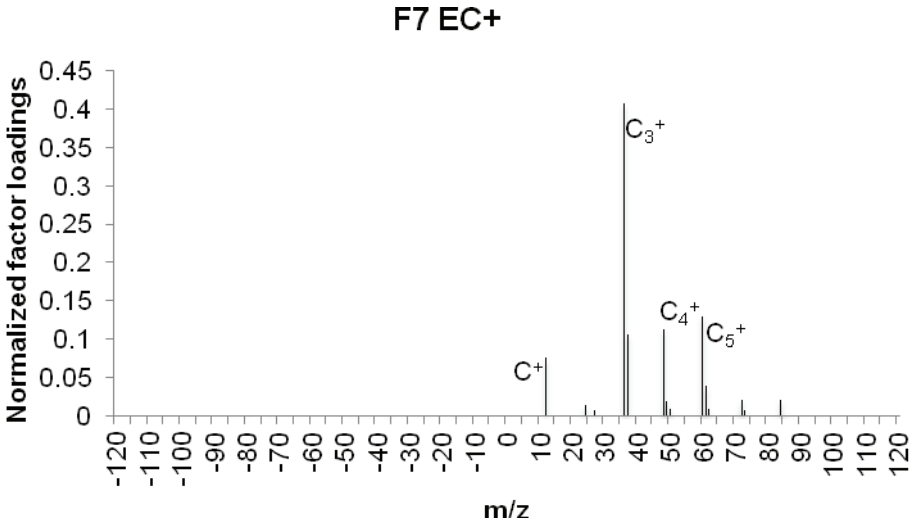
F7 EC+
Normalized factor loadings
0.45
0.4
0.35
0.3
0.25
0.2
0.15
0.1
0.05
0
C3+
C4+
C5+
C+
-120 -110 -100 -90 -80 -70 -60 -50 -40 -30 -20 -10 0 10 20 30 40 50 60 70 80 90 100 110 120
m/z

Figure 5.2

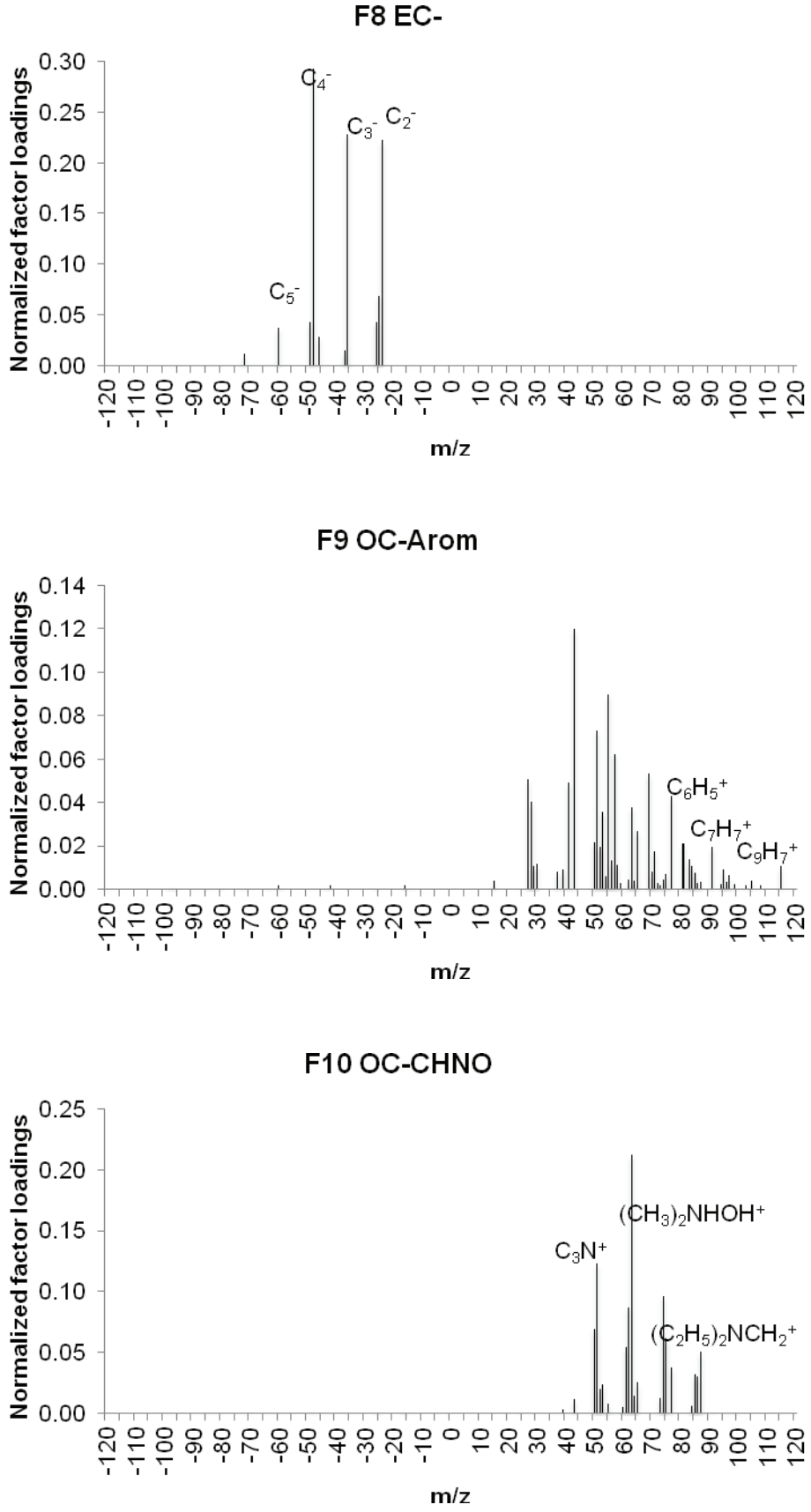

Figure 5.2. Factor chemical profiles (normalized matrix of loadings), PMF analysis on single particles divided by groups of days

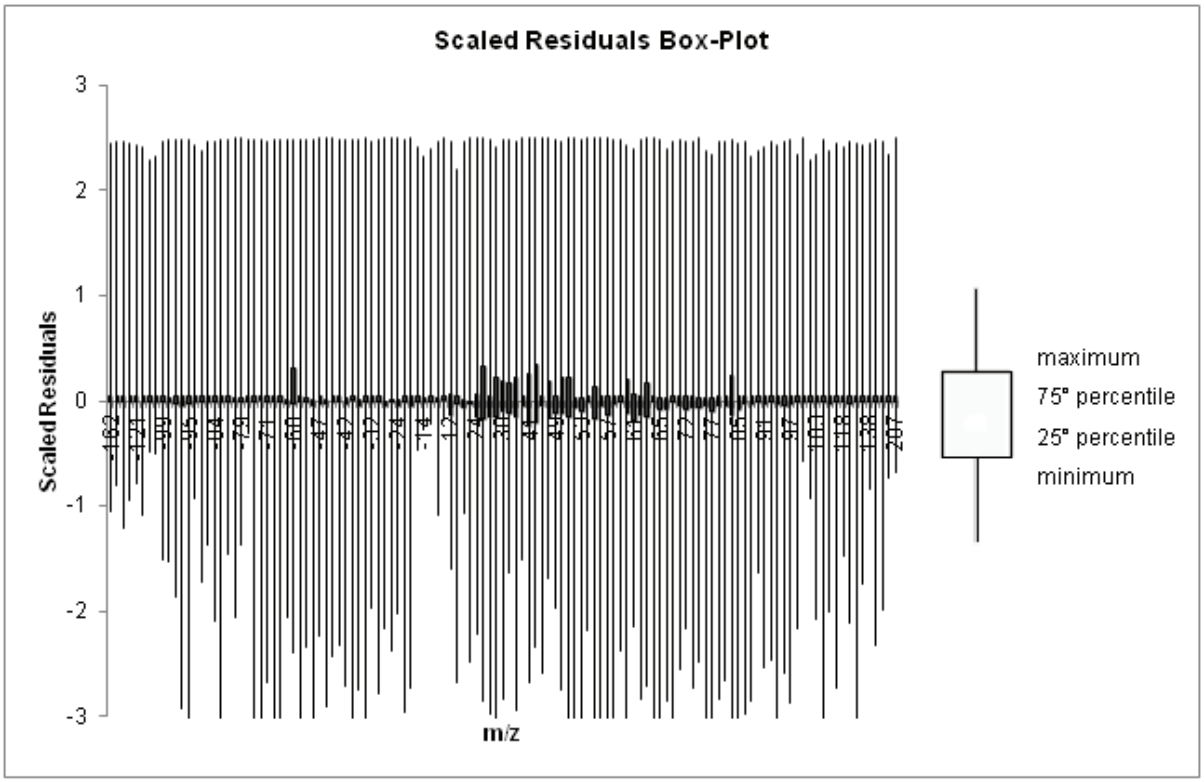

Figure 5.3. Scaled residuals box-plot for every variable (m/z)

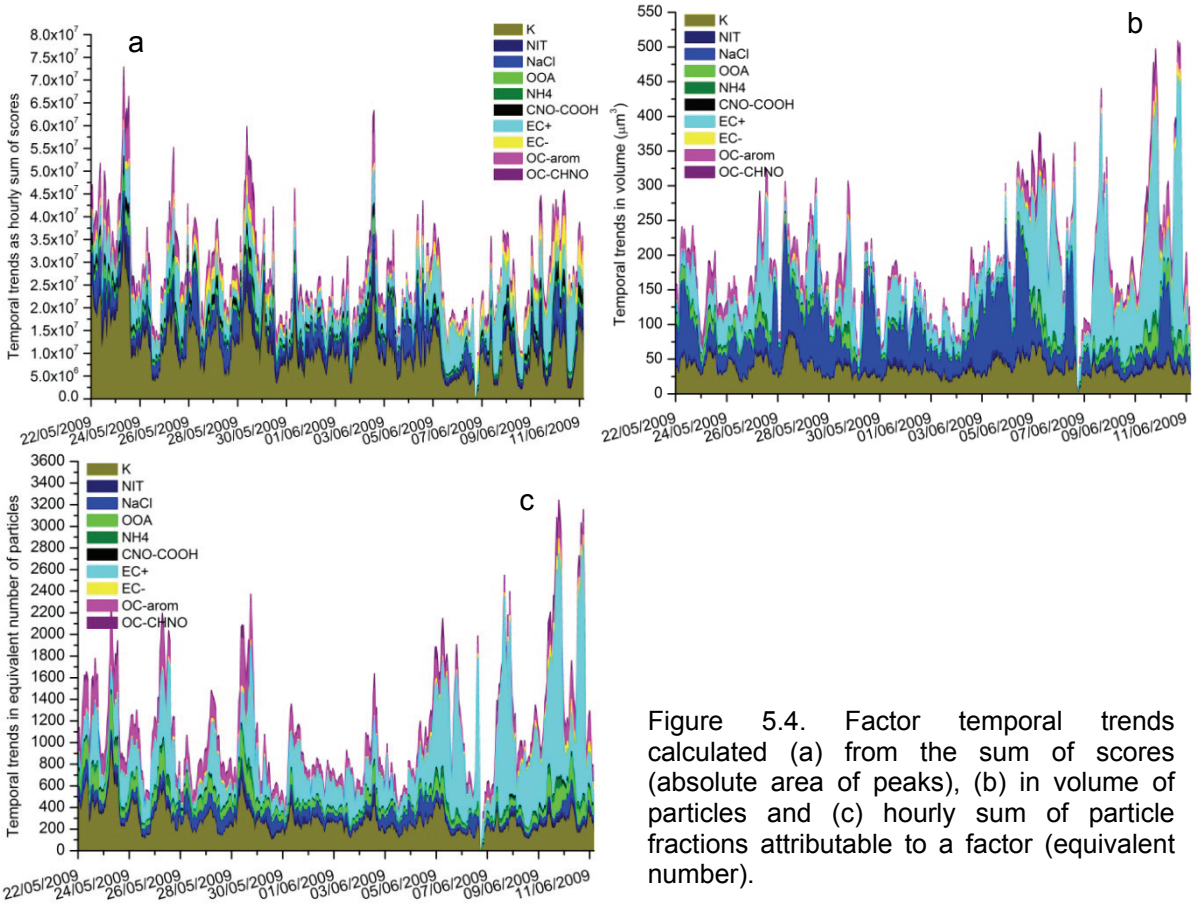

Figure 5.4. Factor temporal trends calculated (a) from the sum of scores (absolute area of peaks), (b) in volume of particles and (c) hourly sum of particle fractions attributable to a factor (equivalent number).

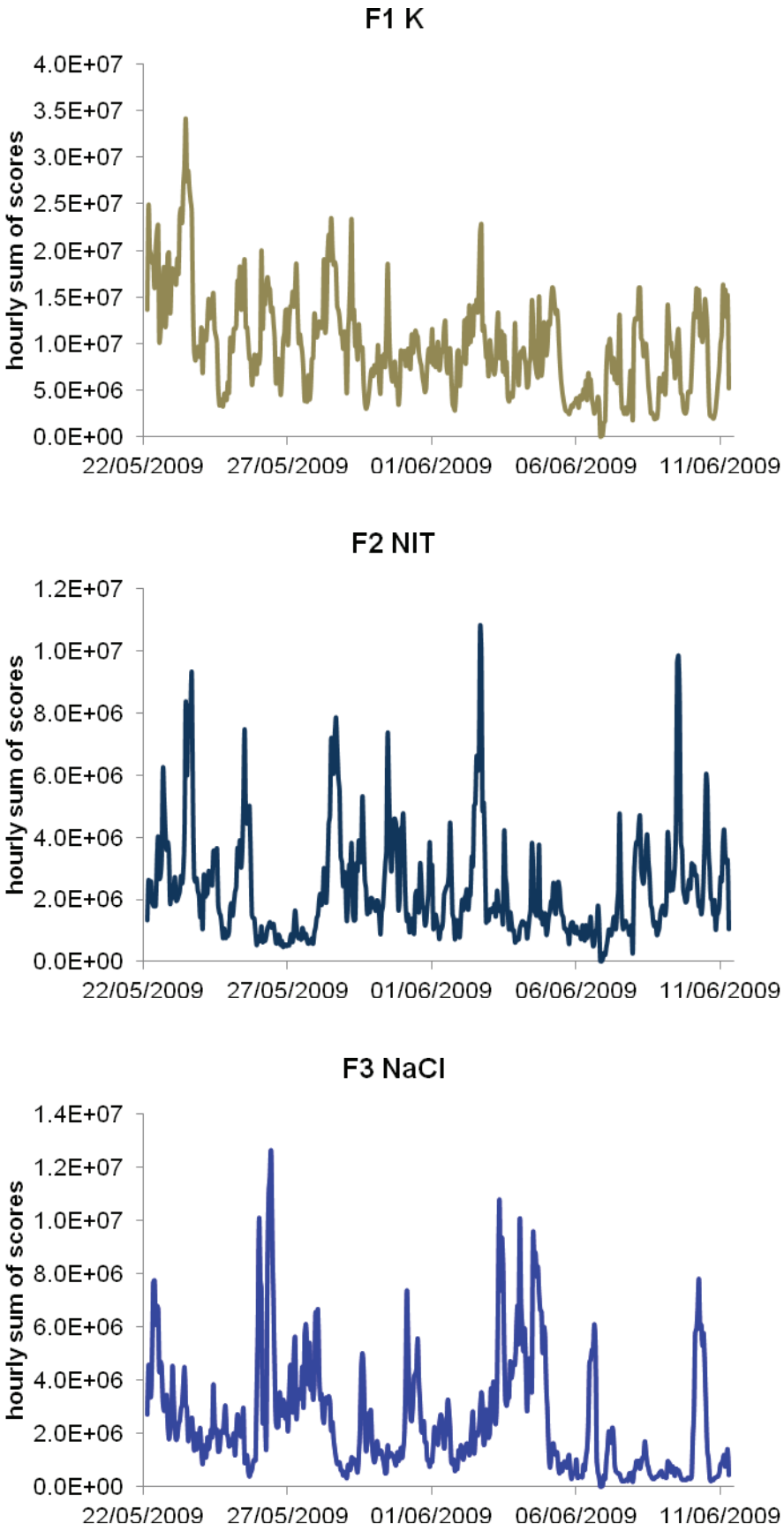
F1 K
hourly sum of scores
4.0E+07
3.5E+07
3.0E+07
2.5E+07
2.0E+07
1.5E+07
1.0E+07
5.0E+06
0.0E+00
22/05/2009
27/05/2009
01/06/2009
06/06/2009
11/06/2009
F2 NIT
hourly sum of scores
1.2E+07
1.0E+07
8.0E+06
6.0E+06
4.0E+06
2.0E+06
0.0E+00
22/05/2009
27/05/2009
01/06/2009
06/06/2009
11/06/2009
F3 NaCl
hourly sum of scores
1.4E+07
1.2E+07
1.0E+07
8.0E+06
6.0E+06
4.0E+06
2.0E+06
0.0E+00
22/05/2009
27/05/2009
01/06/2009
06/06/2009
11/06/2009

Figure 5.5

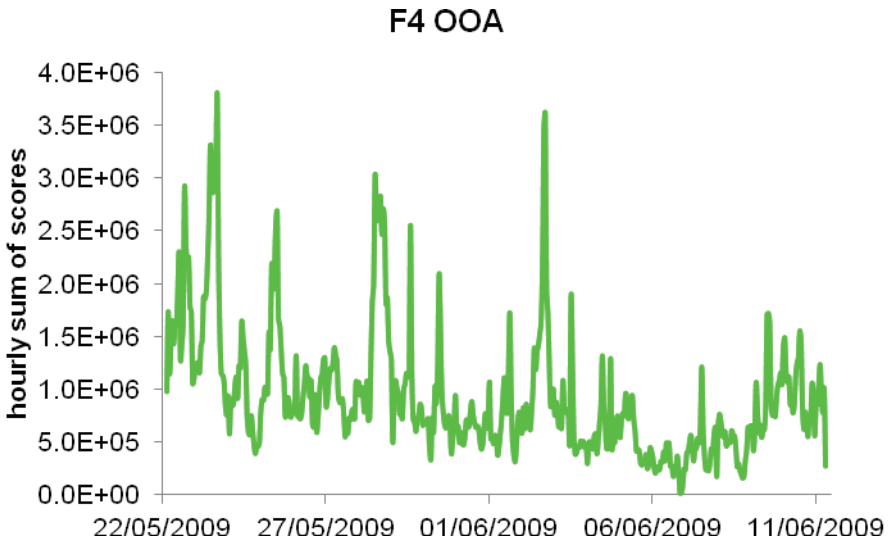
F4 OOA
hourly sum of scores
4.0E+06
3.5E+06
3.0E+06
2.5E+06
2.0E+06
1.5E+06
1.0E+06
5.0E+05
0.0E+00
22/05/2009
27/05/2009
01/06/2009
06/06/2009
11/06/2009

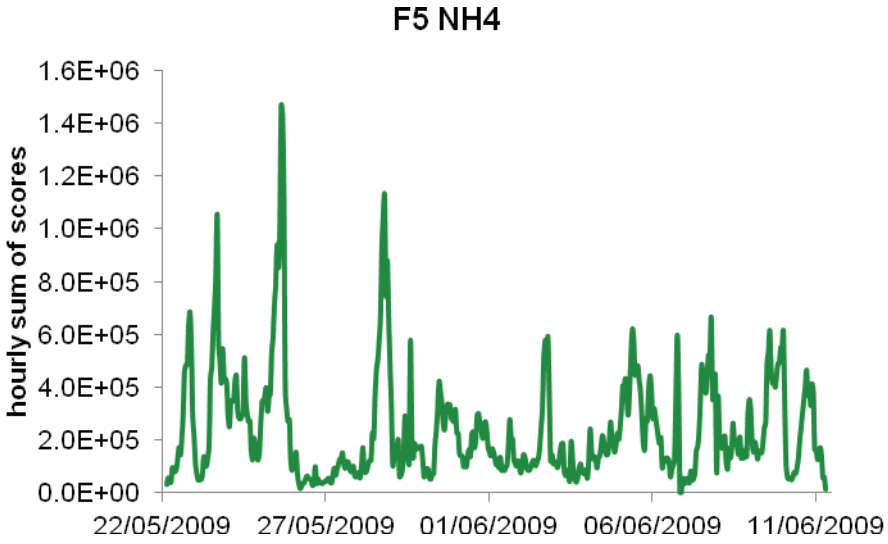
F5 NH4
hourly sum of scores
1.6E+06
1.4E+06
1.2E+06
1.0E+06
8.0E+05
6.0E+05
4.0E+05
2.0E+05
0.0E+00
22/05/2009
27/05/2009
01/06/2009
06/06/2009
11/06/2009

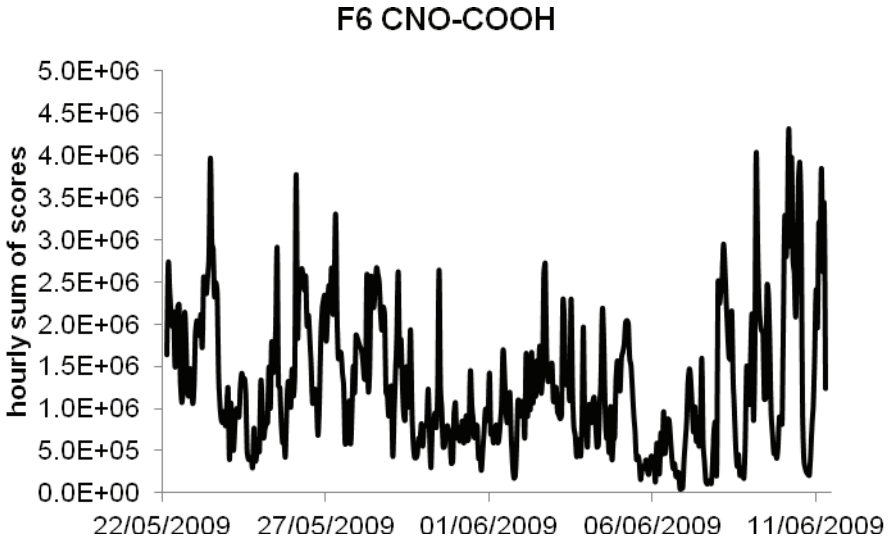
F6 CNO-COOH
hourly sum of scores
5.0E+06
4.5E+06
4.0E+06
3.5E+06
3.0E+06
2.5E+06
2.0E+06
1.5E+06
1.0E+06
5.0E+05
0.0E+00
22/05/2009
27/05/2009
01/06/2009
06/06/2009
11/06/2009

Figure 5.5

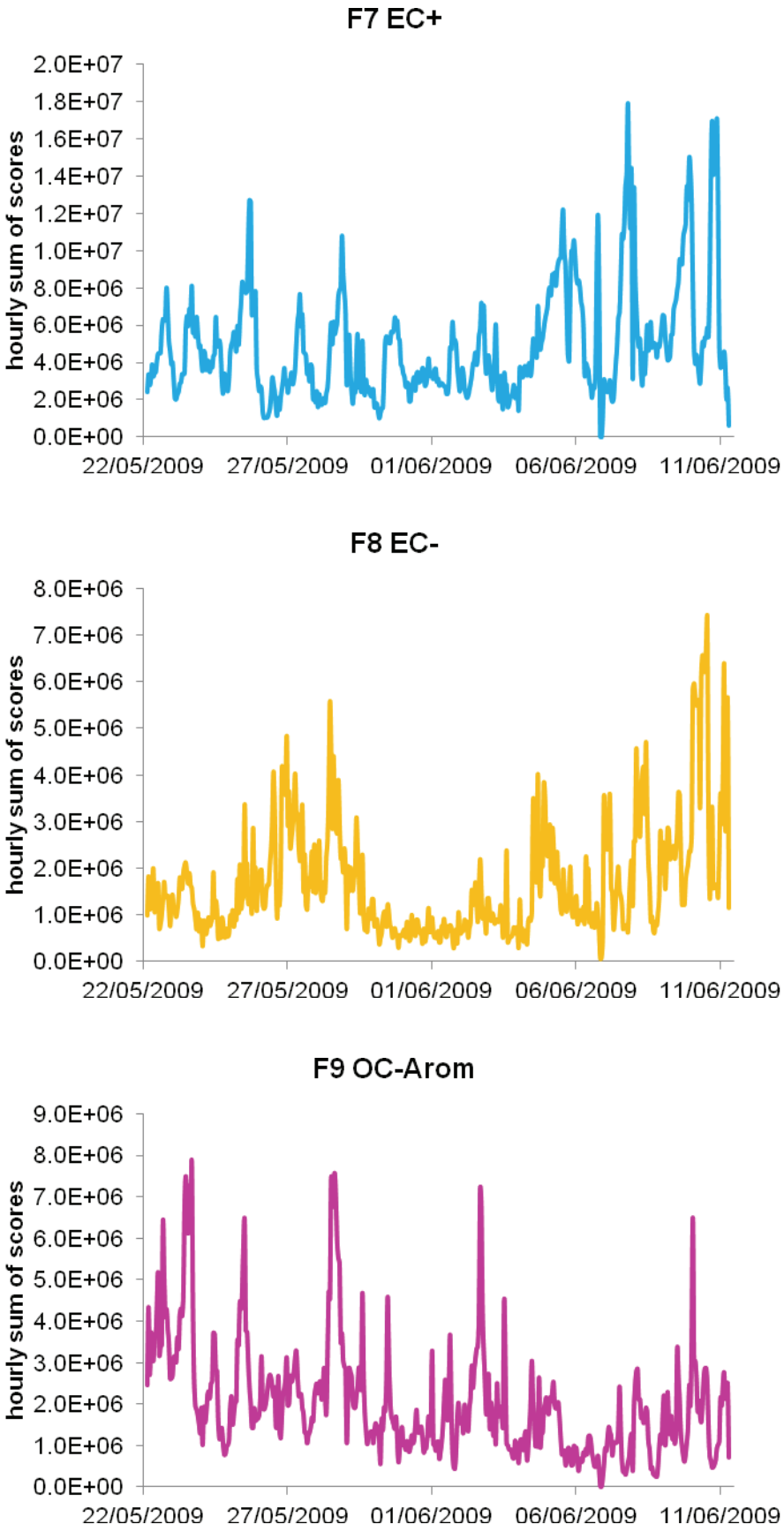
F7 EC+
hourly sum of scores
2.0E+07
1.8E+07
1.6E+07
1.4E+07
1.2E+07
1.0E+07
8.0E+06
6.0E+06
4.0E+06
2.0E+06
0.0E+00
22/05/2009
27/05/2009
01/06/2009
06/06/2009
11/06/2009
F8 EC-
hourly sum of scores
8.0E+06
7.0E+06
6.0E+06
5.0E+06
4.0E+06
3.0E+06
2.0E+06
1.0E+06
0.0E+00
22/05/2009
27/05/2009
01/06/2009
06/06/2009
11/06/2009
F9 OC-Arom
hourly sum of scores
9.0E+06
8.0E+06
7.0E+06
6.0E+06
5.0E+06
4.0E+06
3.0E+06
2.0E+06
1.0E+06
0.0E+00
22/05/2009
27/05/2009
01/06/2009
06/06/2009
11/06/2009

Figure 5.5

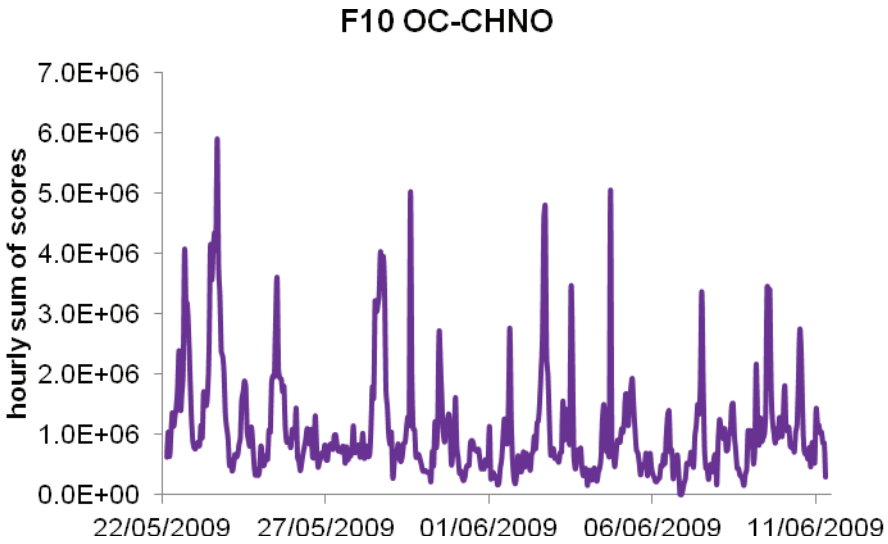

Figure 5.5. Hourly temporal trends of the factors in scores.

Chemical species that contribute to high m/z values, which always present a poor explained variation, are not extracted by the PMF analysis. The road traffic contribution is characterized by a wide range of both organic substances and metals in traces which do not give an high contribution to the total PM, if considered singularly. Thus the extraction of each single component could be very challenging.

The scaled residuals inspection reveals that a few variables, related to miscalibrated signals, were not extracted. All the other variables, which were not extracted by factors, present very low scaled residues and thus could be considered as bad variables.

Hourly temporal trends of the factors, in terms of scores, equivalent number of particles and in volume are reported in figure 5.4.

F1-K and F7-EC+ are the most contributing factors, both in terms of scores, equivalent number of particles and in volume. Concerning volume, NaCl is another dominant factor because of its coarse distribution (figure 5.6).

Size distributions (sum of scores in each size bin) of PMF factors are reported in figure 5.6. The majority of factors are characterized by an accumulation mode predominant. NaCl presents a coarse distribution because it is generated from sea spray. NIT, unlike for Harwell campaign, is characterized by a monomodal size distribution indicating that aged marine particles contribution could be considered negligible.

More interesting are the two EC factors. EC- presents a fine distribution centred to ca. 150 nm of diameter, while EC+ presents a size distribution centred on ca. 500 nm

of diameter which is typical of aged particles. This confirms what already seen in Harwell campaign. In fact, EC- seems to represent freshly emitted elemental carbon particles while EC+ represents aged elemental carbon probably internally mixed with secondary species. In fact, as advanced by Reinard and Johnston (Reinard and Johnston, 2008) secondary species like nitrate and sulphate could limit the electron availability, leading to a suppression of elemental carbon fragments negatively charged, while potassium and sodium, on the contrary, could lead to an enhancement of them. Still, this is the first time in which the separation of different elemental and organic carbon components from ATOFMS dataset is achieved. In fact, PMF analysis applied to single particles could separate the contribution of fresh EC from aged EC, and the different organic families including aromatic (OC-Arom), oxidized organic aerosol (OOA), and two organic nitrogen components: fresh (OC-CHNO) and aged (CNO-COOH).

OC-CHNO, which contains organic carbon enriched in nitrogen compounds, presents a size distribution centred at 300 nm of diameter while all the other factors are commonly centred on 400 nm with the exception of NH4 which is centred on 500 nm similarly to EC+ factor. NH4 size distribution seems to refuse the hypothesis of its origin from ammonia emitted by vehicles' catalytic converters. It is likely, indeed, that NH4 and EC+ come from long-range transports from central Europe, probably emitted in coal-burning power plants and then aged.

NIT, OOA, OC-Arom and OC-CHNO present similar diurnal trends (figure 5.7) which increase during night time probably because of lower temperature which favours condensation of semi-volatile compounds. K and CNO-COOH present a peak around 17h-18h while EC+ and NH4 seems to contribute more in the morning. Contrarily to what expected none of them presents a clear traffic signature, characterized by peaks on rush hours.

Correlation analysis among factors (hourly temporal trends in scores) reveals a strong correlation between OOA, OC-Arom and OC-CHNO which in turn are strongly correlated also with K and NIT factors. EC+ is strongly correlated only with NH4, while EC- is strongly correlated with CNO-COOH.

This analysis confirm that EC+ and EC- are different and in fact they are weakly correlated to each other ($r=0.13$, p-value=4E-03). NaCl is an independent factor as it is not strongly correlated to any other factor. From this analysis (figure 5.8) it seems that EC- is primarily emitted from vehicle exhaust which undergoes a progressive

oxidation with enrichment in aromatics, amines and other nitrogen compounds like CN, CNO and nitrate. The final product could be the aged elemental carbon particles represented by the EC+ factor. In fact, OOA and OC-Arom are strongly correlated to each other, which are progressively correlated with OC-CHNO, NIT and K, and finally with CNO-COOH factor. EC- is then connected to all this group of factors. EC+ and NH4, on the contrary, form an independent group which is then linked to the others but in a less extent.

The cross correlation analysis shows also that nitrate is related to NO_x local emissions instead of long-range transports of secondary aerosol. OOA, at the same way, seems to be related to traffic emissions because of its aromatic content.

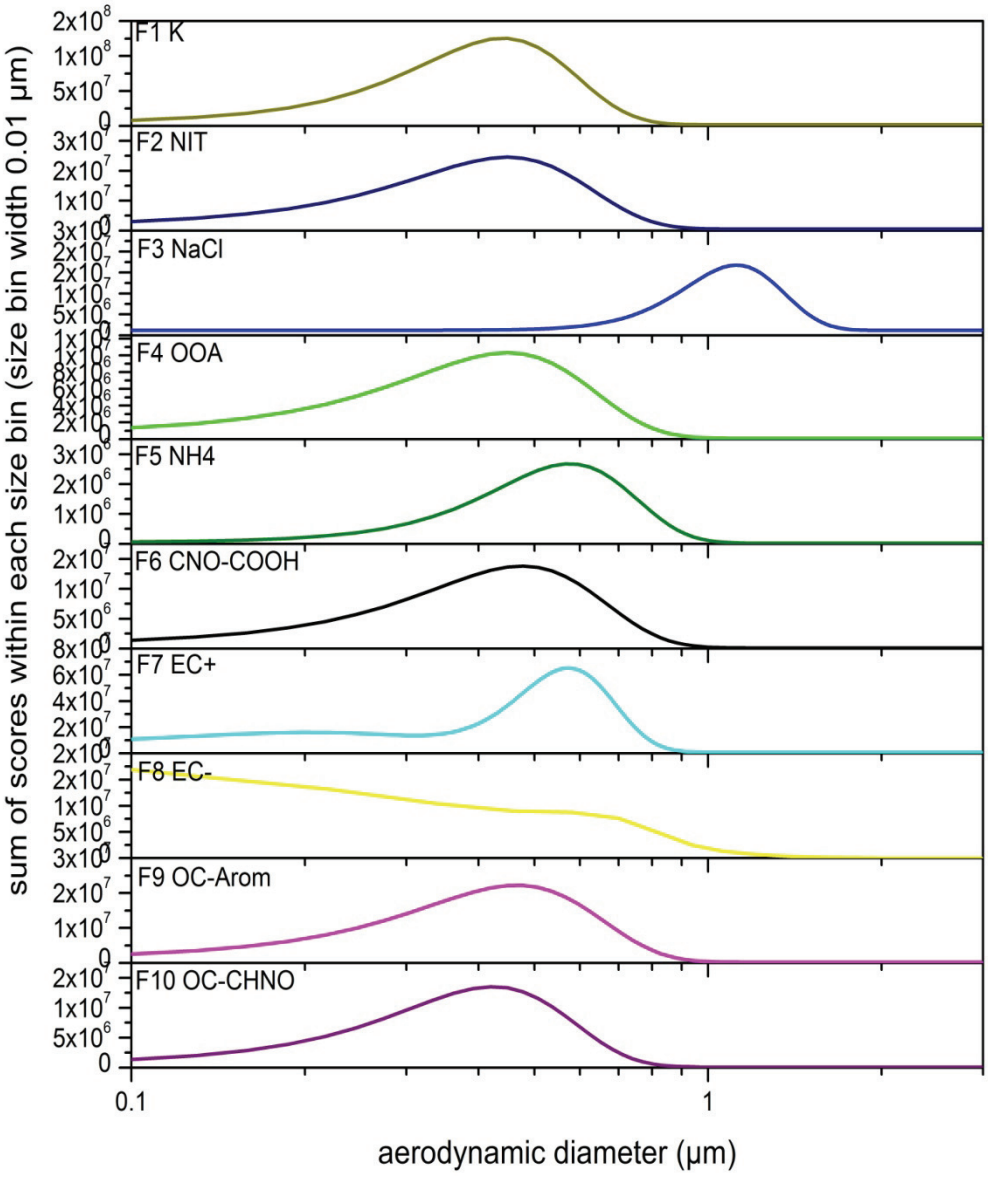

Figure 5.6. Size distributions of PMF factors as sum of scores in each size bin (size bin width 0.01 µm)

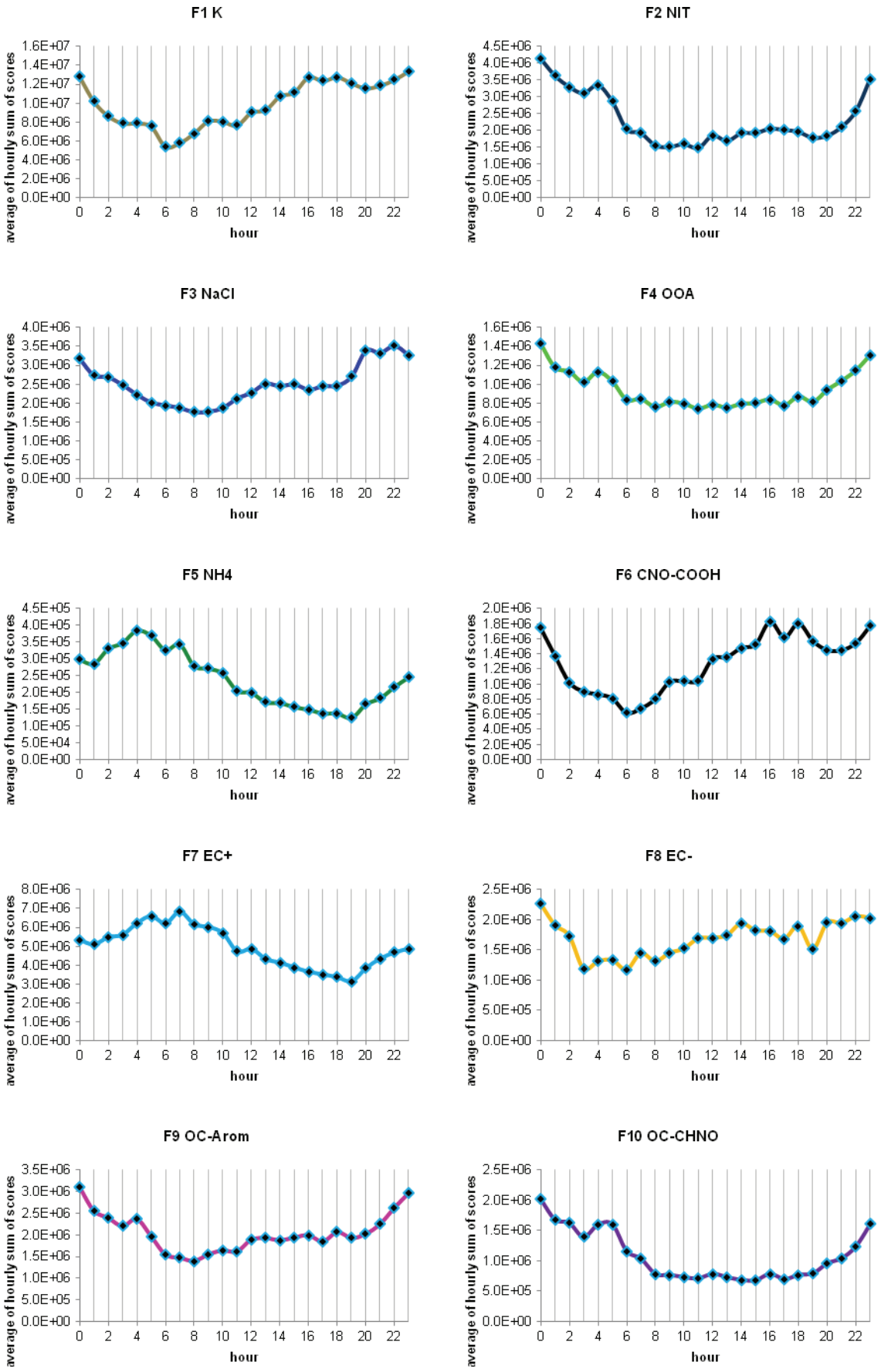

Figure 5.7. Diurnal trends of the PMF factors

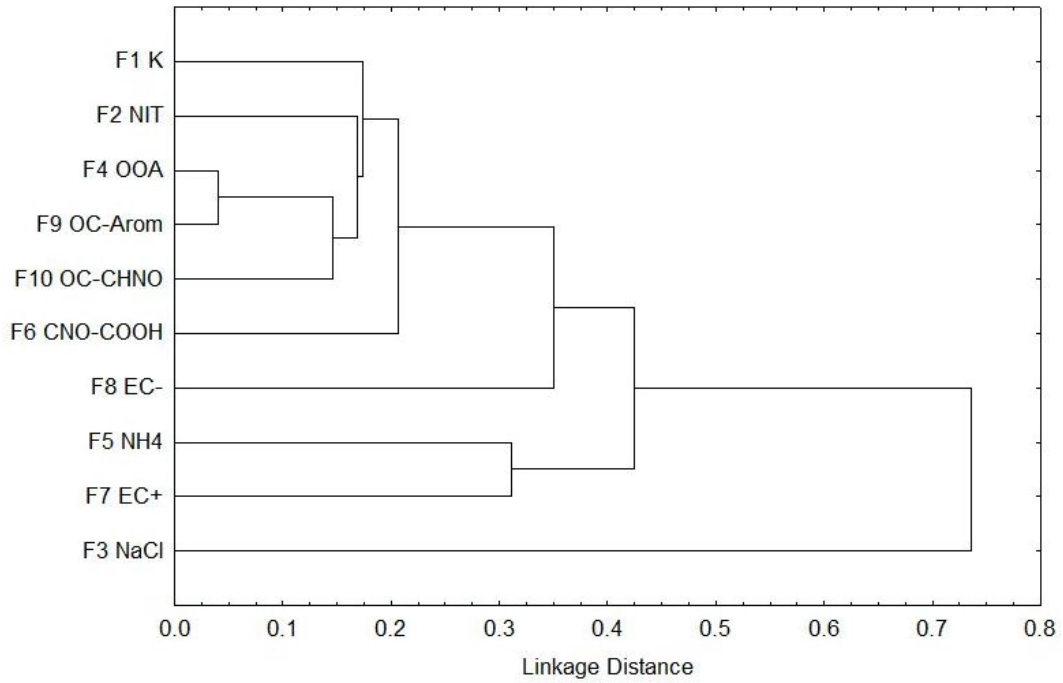

Figure 5.8. Tree diagram of the 10 factors' hourly temporal trends (sum of scores) extracted from PMF analysis on single particles mass spectra, single linkage, distance measure r-Pearson correlation coefficient.

Table 5.5. Correlation coefficients of the linear regression analysis among the hourly temporal trends (sum of scores) of the PMF factors

	K	NIT	NaCl	OOA	NH4	CNO-COOH	EC+	EC-	OC-arom	OC-CHNO
K	1.00	0.55	0.26	0.77	0.11	0.79	0.17	0.31	0.83	0.56
NIT	0.55	1.00	0.15	0.78	0.56	0.45	0.21	0.24	0.74	0.83
NaCl	0.26	0.15	1.00	0.10	0.35	0.25	0.40	0.11	0.13	0.02
OOA	0.77	0.78	0.10	1.00	0.48	0.59	0.11	0.27	0.96	0.85
NH4	0.11	0.56	0.35	0.48	1.00	0.04	0.69	0.01	0.39	0.57
CNO-COOH	0.79	0.45	0.25	0.59	0.04	1.00	0.15	0.65	0.66	0.46
EC+	0.17	0.21	0.40	0.11	0.69	0.15	1.00	0.13	0.02	0.21
EC-	0.31	0.24	0.11	0.27	0.01	0.65	0.13	1.00	0.32	0.25
OC-arom	0.83	0.74	0.13	0.96	0.39	0.66	0.02	0.32	1.00	0.80
OC-CHNO	0.56	0.83	0.02	0.85	0.57	0.46	0.21	0.25	0.80	1.00

Table 5.6. p-values of the r-Pearson correlation test among the hourly temporal trends (sum of scores) of PMF factors

	K	NIT	NaCl	OOA	NH4	CNO-COOH	EC+	EC-	OC-arom	OC-CHNO
K	*									
NIT	2E-39	*								
NaCl	5E-09	9E-04	*							
OOA	4E-98	4E-99	2E-02	*						
NH4	1E-02	1E-40	4E-15	1E-28	*					
CNO-COOH	1E-105	7E-26	2E-08	6E-46	0.38	*				
EC+	2E-04	4E-06	6E-20	2E-02	5E-69	7E-04	*			
EC-	3E-12	7E-08	2E-02	2E-09	0.88	5E-59	4E-03	*		
OC-arom	6E-122	1E-83	4E-03	2E-266	5E-19	4E-63	0.68	6E-13	*	
OC-CHNO	1E-40	3E-125	0.59	9E-139	8E-44	3E-27	2E-06	3E-08	2E-109	*

5.7. k-means cluster analysis

From the k-means cluster analysis applied to the entire dataset (693462 particles) the 15 clusters solution was selected. A cluster made of miscalibrated mass spectra was eliminated and 14 clusters were then considered for the results (table 5.7 and figure 5.9).

Table 5.7. K-means cluster analysis solution

	Number of particles	% of particles
1-K	163166	23.5
2-OOA	52693	7.6
3-Ca-EC	35192	5.1
4-OC-CN-SUL	10749	1.6
5-NaCl	54093	7.8
6-EC+	235954	34.0
7-Amines+58	3925	0.6
8-OC-NIT-SUL	23444	3.4
9-OC-K-SOA	46927	6.8
10-K-NIT	23130	3.3
11-Na-EC	16685	2.4
12-Fe-V	11974	1.7
13-Amines+59	4421	0.6
14-N-EC-	2291	0.3
Miscalibrated	8818	1.3
TOTAL	693462	100

The main clusters are: “1-K” characterized by the main signals of potassium (m/z=+39/+41); “2-OOA” which is characterized by secondary organic ions ($C_2H_3^+$ and $C_2H_3O^+$) and some fragments due to aromatics (m/z=+51/+55/+63); “3-Ca-EC” characterized mainly by Ca^+ (m/z=+40) and $CaOH^+$ (m/z=+57) and organic and elemental carbon signals; “4-OC-CN-SUL” characterized by organic aromatic fragments in the positive mass spectrum and CN^-, CNO^-, nitrate and sulphate in the negative mass spectrum; “5-NaCl” representing freshly emitted sea spray; “6-EC+” characterized by elemental carbon fragments in the positive mass spectrum principally; “8-OC-NIT-SUL” characterized by $C_2H_3^+$, $C_2H_3O^+$, nitrate and sulphate; “9-OC-K-SOA” whose main signals are K^+, $C_2H_3^+$ and $C_2H_3O^+$; “10-K-NIT” composed by potassium and nitrate; “11-Na-EC” composed by Na^+ (m/z=+23) and elemental carbon fragments which are more intense in the negative mass spectrum and “12-Fe-V” formed by V^+, Fe^+ and VO^+ (m/z=+51/+56/+67). Besides those clusters, other

three small clusters were considered: “7-Amines+58” with a strong signal at m/z=+58 which could be associated to $[C_2H_5NCH_2]^+$ and a signal at m/z=+84 probably associated to piperidines [Angelino 2001]; “13-Amines+59” with a strong signal associated to trimethylamine [Angelino 2001] and “14-N-EC-” composed by elemental carbon signal in the negative mass spectrum and m/z=+42/+84/+112/+127 which could be linked to $[C_2H_4N]^+$, piperidine, methylhexamethyleneimine and ethylhexamethyleneimine.

The temporal trends of clusters are reported in figure 5.10 and figure 5.11 and their diurnal trends are reported in figure 5.12.

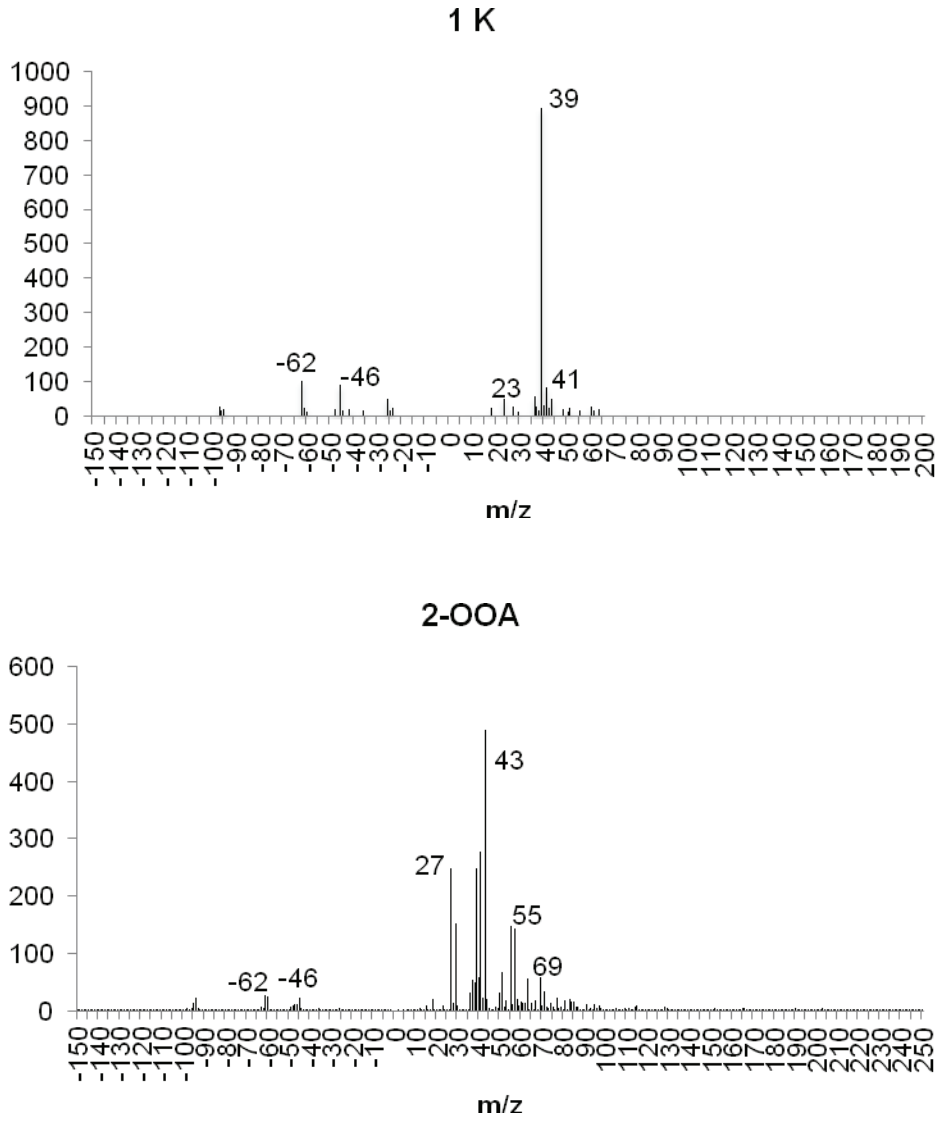

Figure 5.9

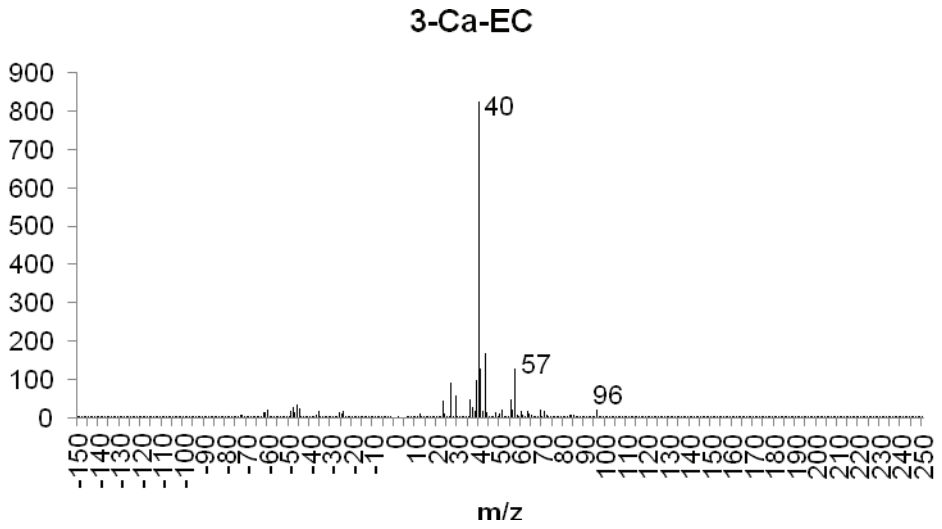
3-Ca-EC
40
57
96
m/z

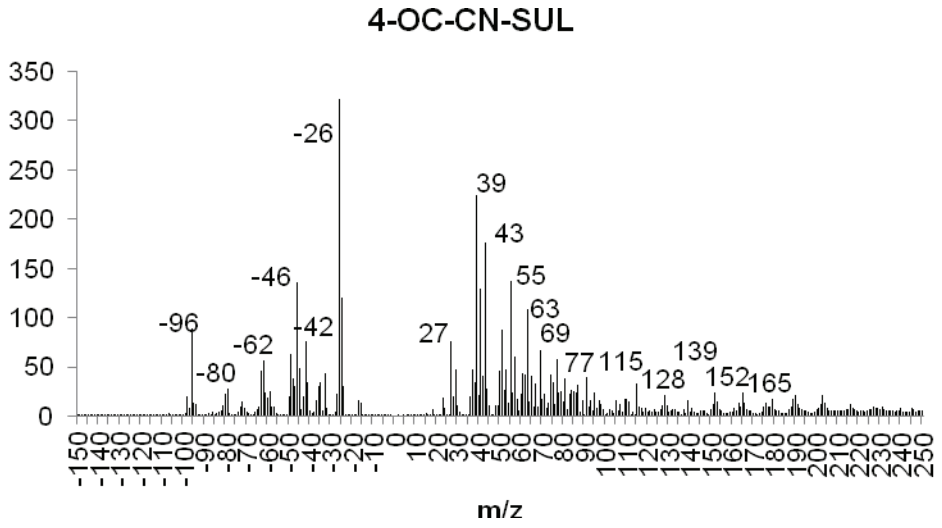
4-OC-CN-SUL
-26
39
43
-46
55
63
-96
-42
27
69
-62
77
115
139
-80
128
152
165
m/z

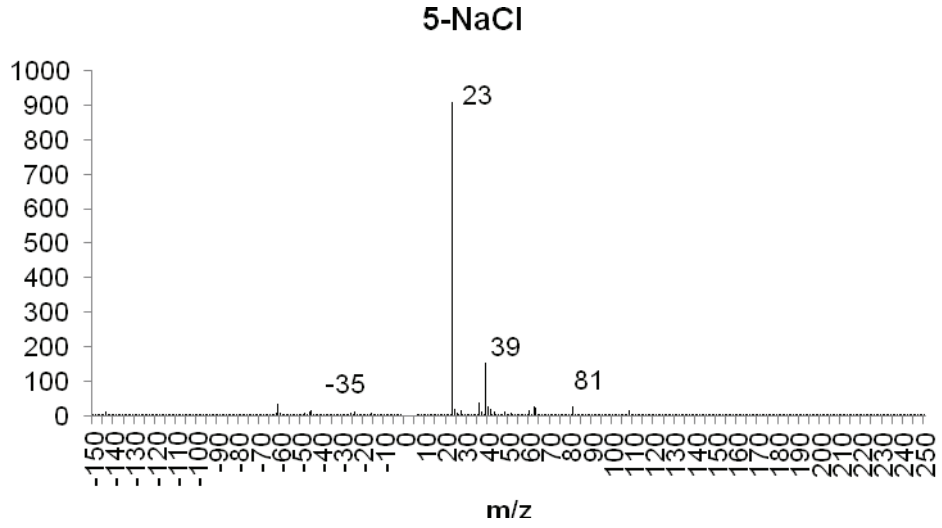
5-NaCl
23
39
-35
81
m/z

Figure 5.9

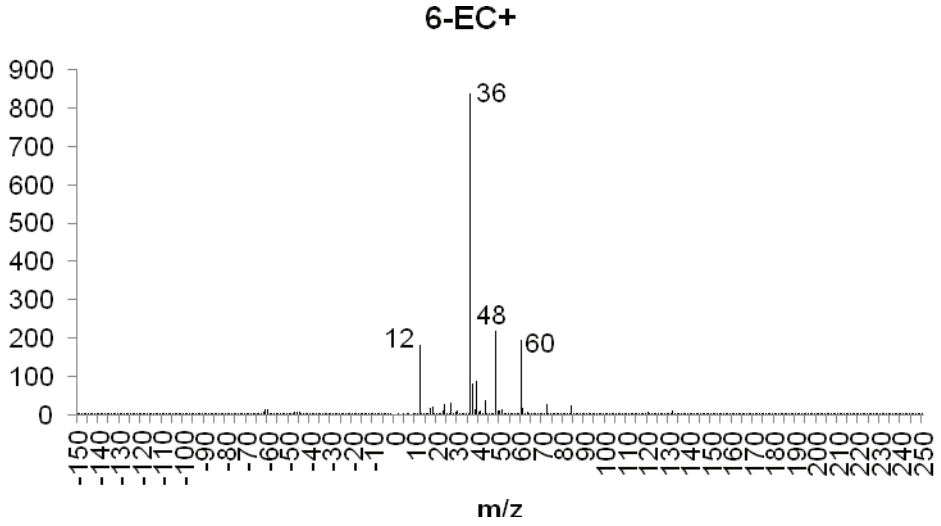
6-EC+
36
48
12
60
m/z

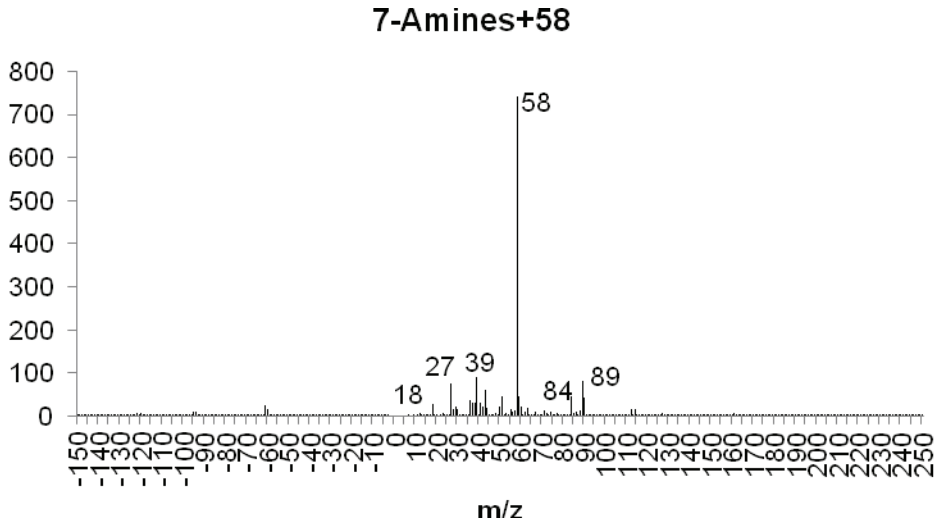
7-Amines+58
58
27
39
18
84
89
m/z

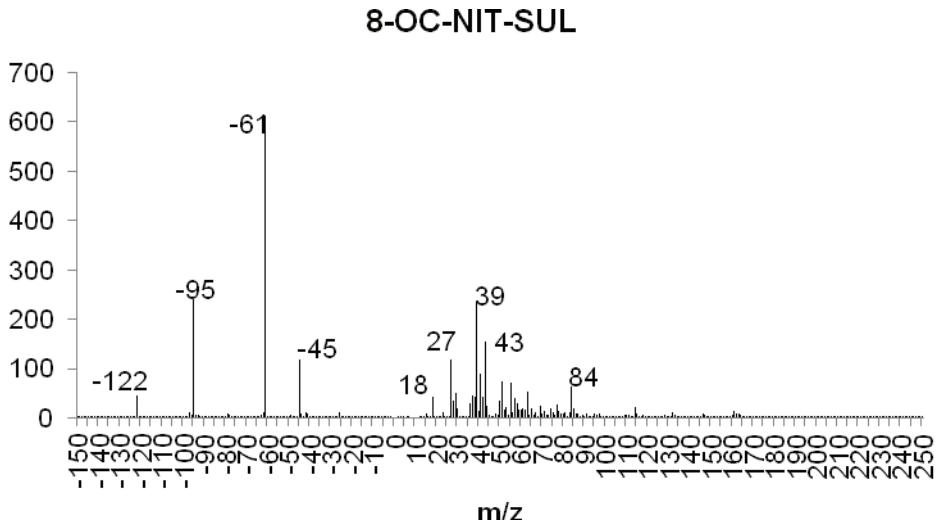
8-OC-NIT-SUL
-61
-95
39
-45
27
43
-122
18
84
m/z

Figure 5.9

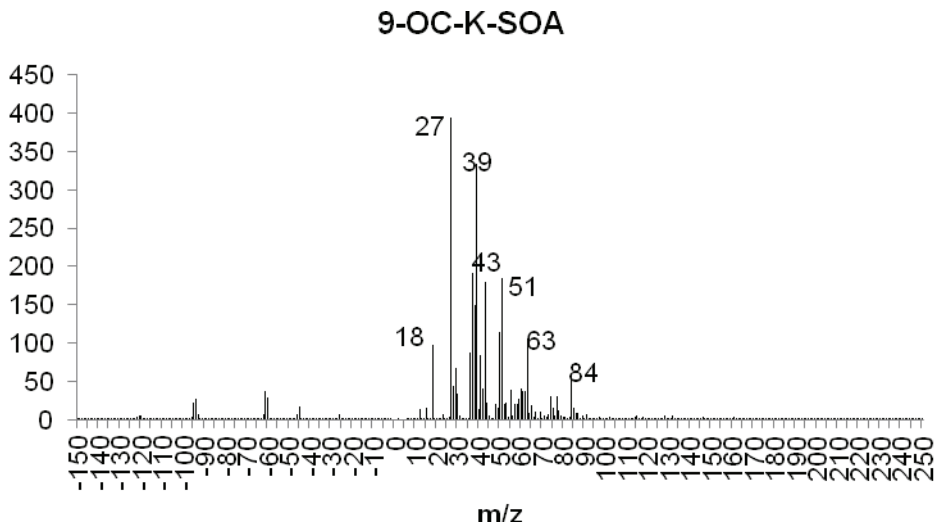
9-OC-K-SOA
27
39
43
51
18
63
84
m/z

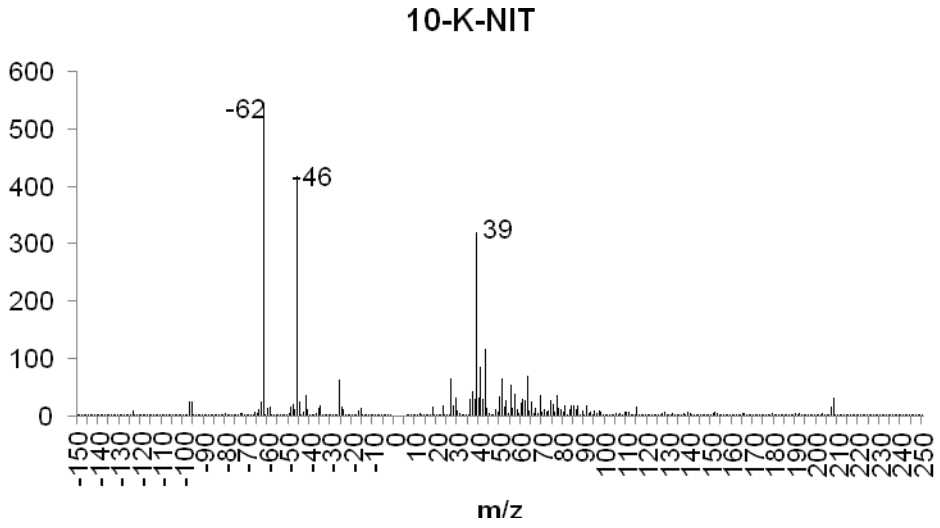
10-K-NIT
-62
-46
39
m/z

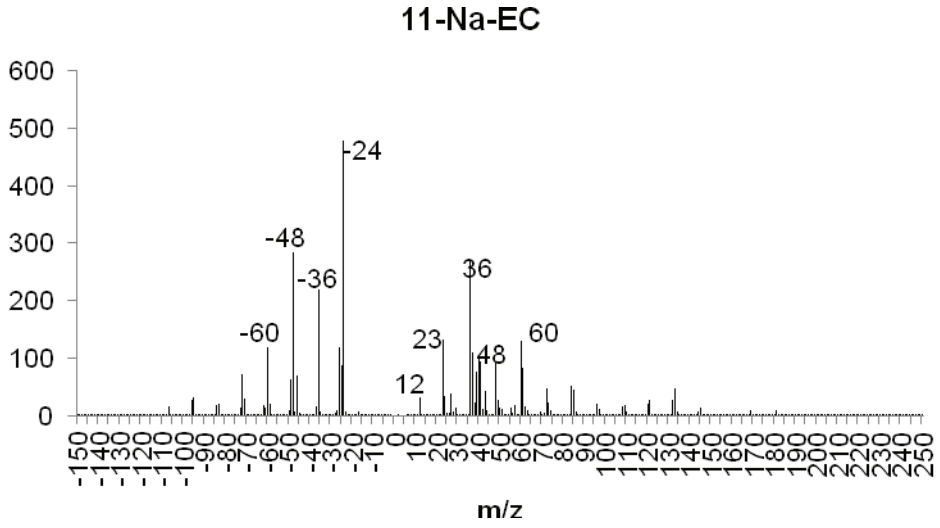
11-Na-EC
-24
-48
-36
36
-60
23
48
60
12
m/z

Figure 5.9

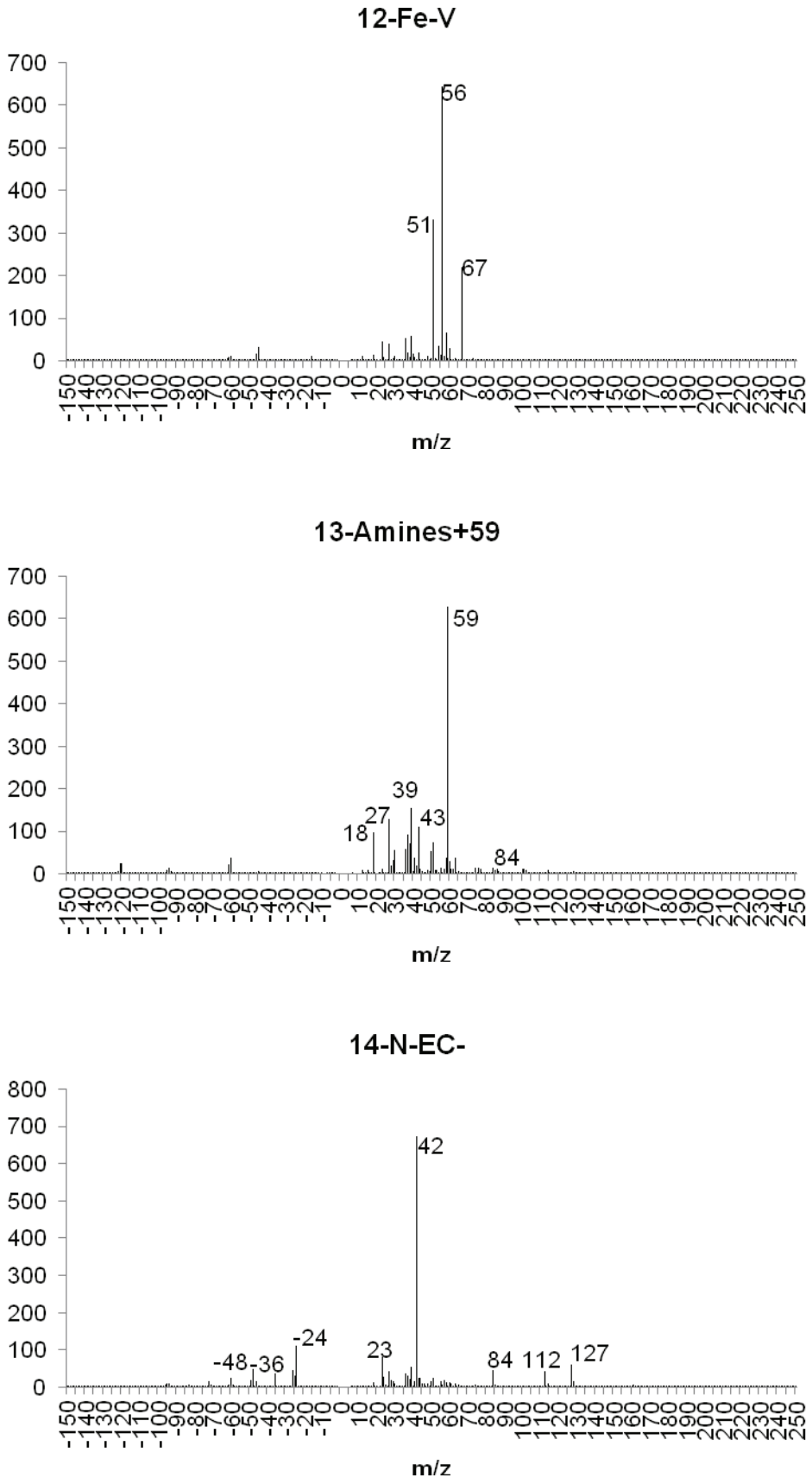

Figure 5.9. Mass spectra of the 14 K-means clusters (London Marylebone Road 2009).

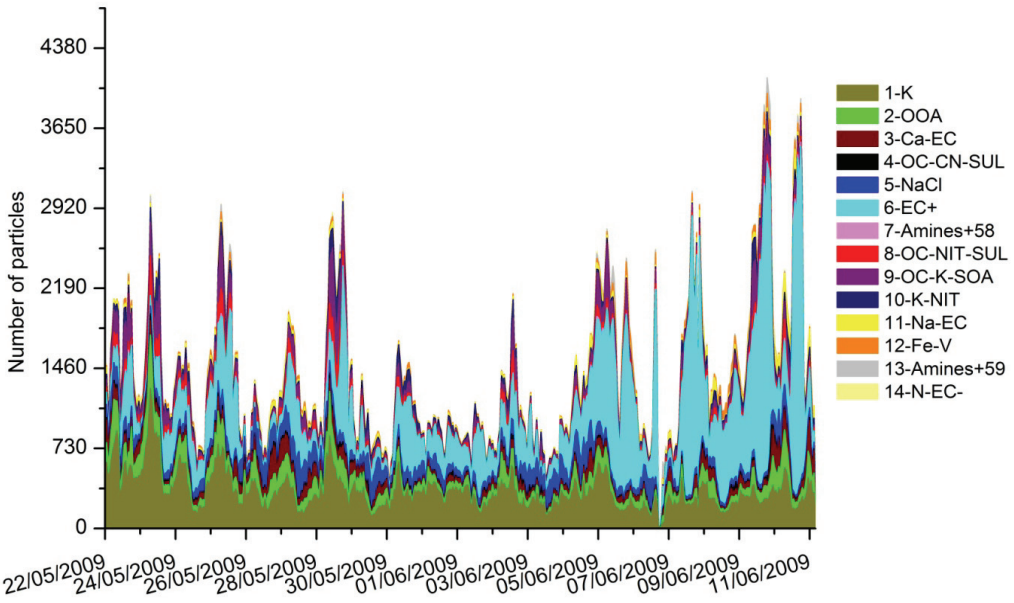

Figure 5.10. Hourly temporal trends in number of particles of clusters obtained from k-means cluster analysis on London Marylebone Road 2009 dataset.

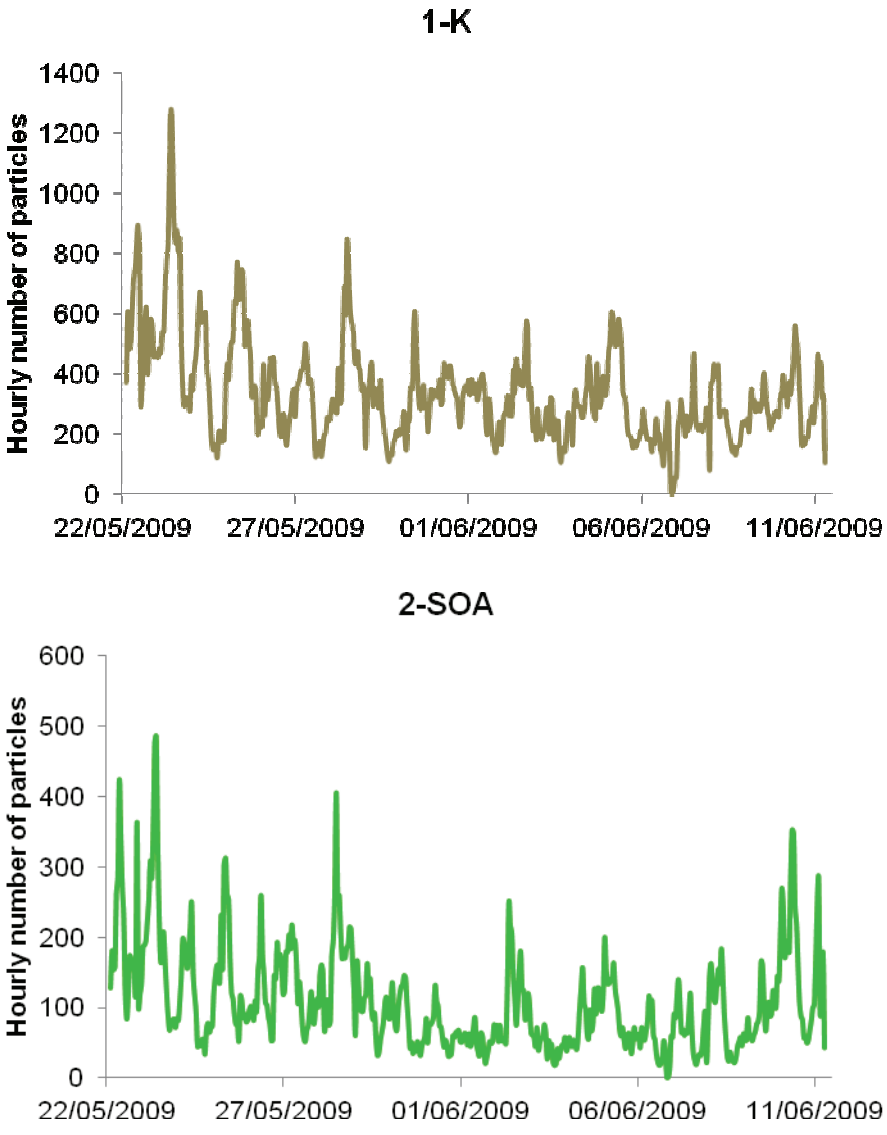

Figure 5.11

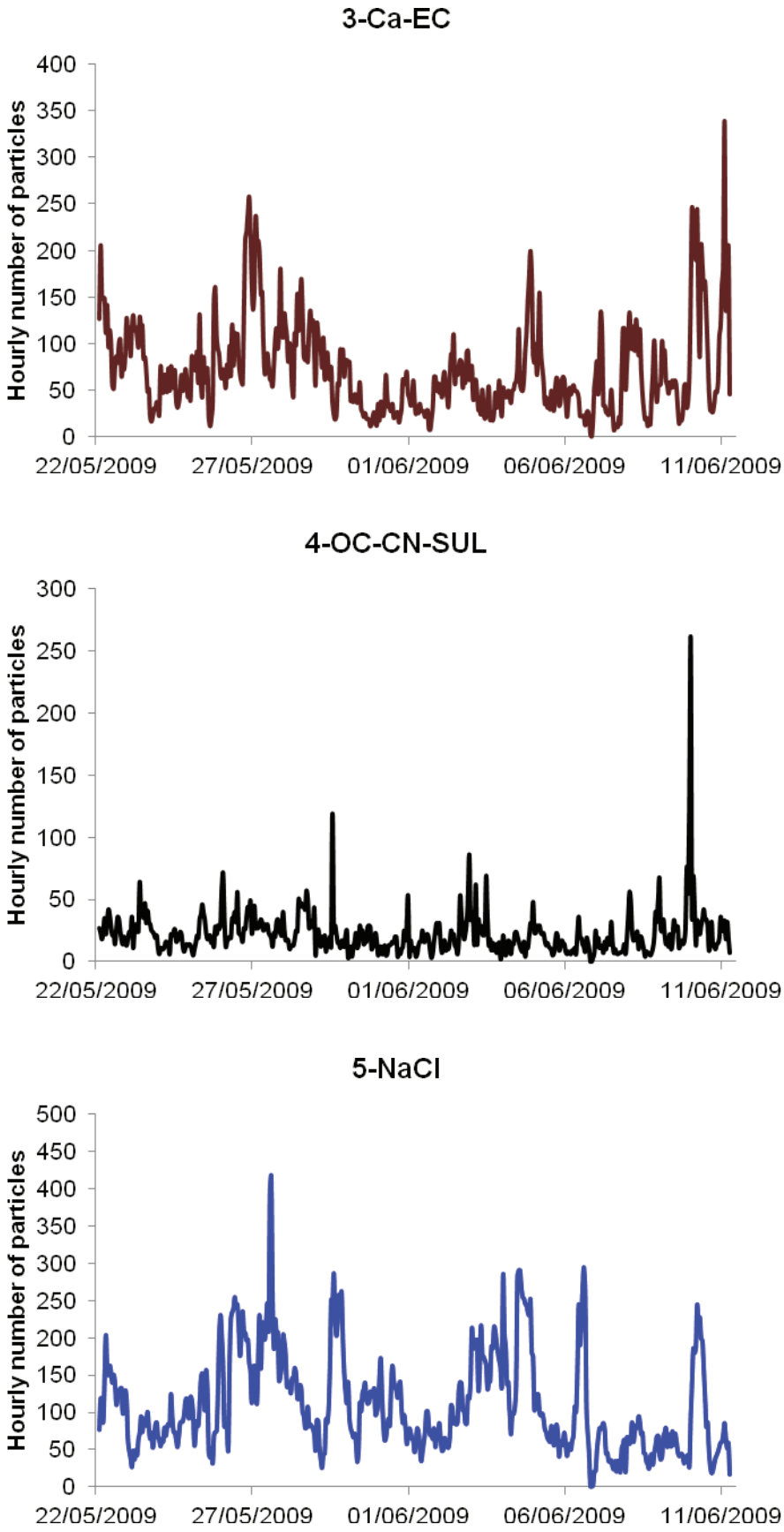
3-Ca-EC
Hourly number of particles
400
350
300
250
200
150
100
50
0
22/05/2009
27/05/2009
01/06/2009
06/06/2009
11/06/2009
4-OC-CN-SUL
Hourly number of particles
300
250
200
150
100
50
0
22/05/2009
27/05/2009
01/06/2009
06/06/2009
11/06/2009
5-NaCl
Hourly number of particles
500
450
400
350
300
250
200
150
100
50
0
22/05/2009
27/05/2009
01/06/2009
06/06/2009
11/06/2009

Figure 5.11

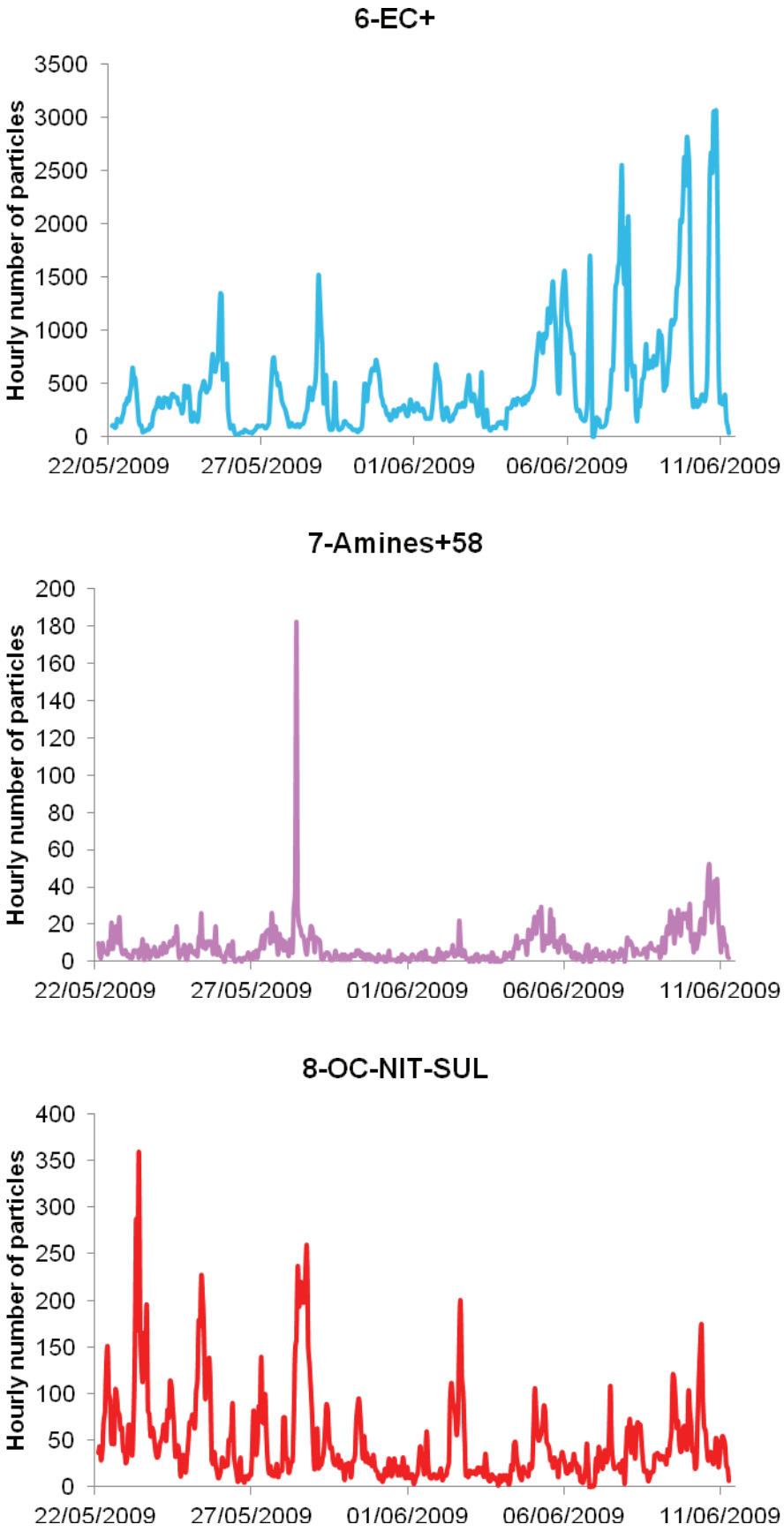
6-EC+
Hourly number of particles
3500
3000
2500
2000
1500
1000
500
0
22/05/2009
27/05/2009
01/06/2009
06/06/2009
11/06/2009
7-Amines+58
Hourly number of particles
200
180
160
140
120
100
80
60
40
20
0
22/05/2009
27/05/2009
01/06/2009
06/06/2009
11/06/2009
8-OC-NIT-SUL
Hourly number of particles
400
350
300
250
200
150
100
50
0
22/05/2009
27/05/2009
01/06/2009
06/06/2009
11/06/2009

Figure 5.11

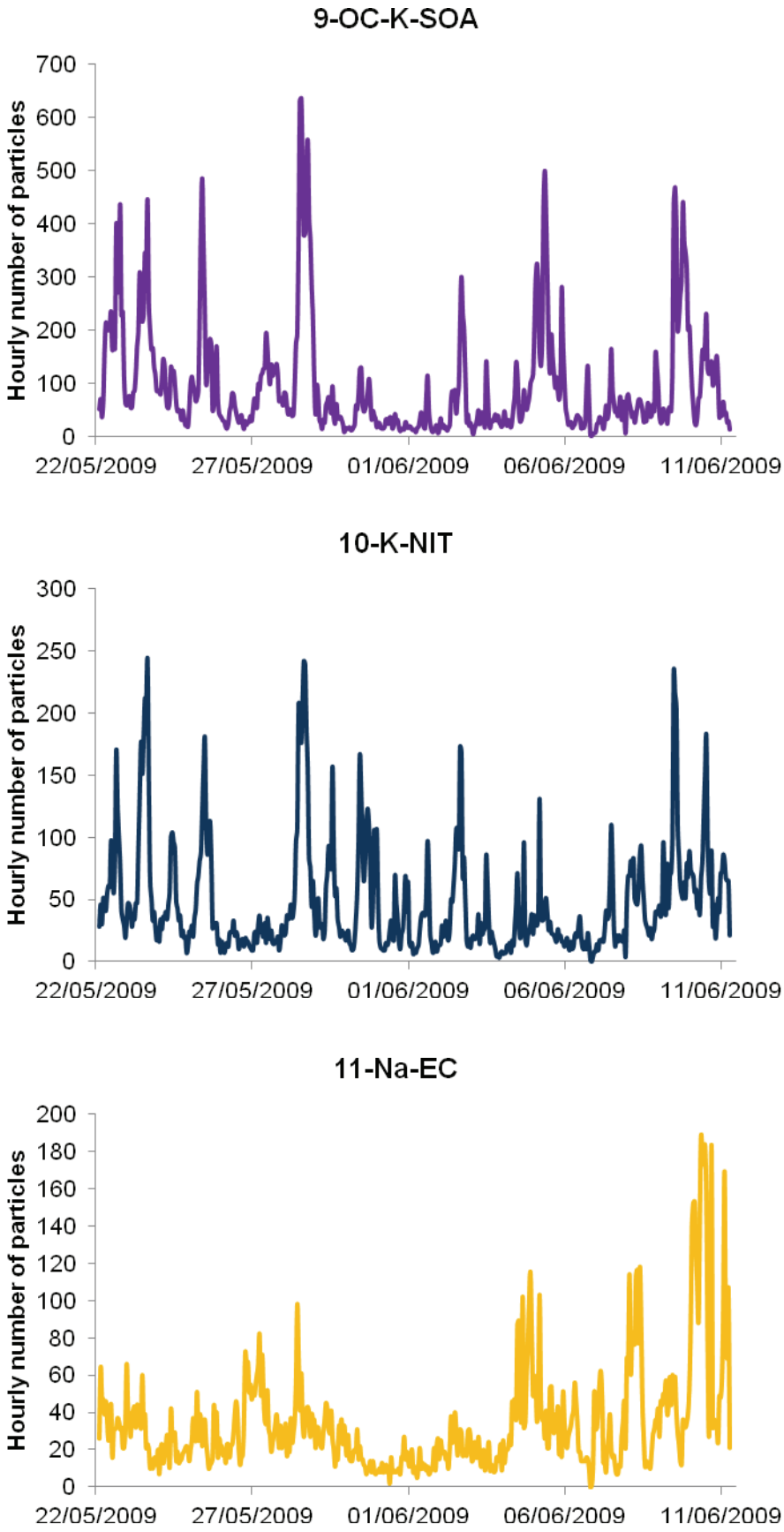
9-OC-K-SOA
Hourly number of particles
700
600
500
400
300
200
100
0
22/05/2009
27/05/2009
01/06/2009
06/06/2009
11/06/2009
10-K-NIT
Hourly number of particles
300
250
200
150
100
50
0
22/05/2009
27/05/2009
01/06/2009
06/06/2009
11/06/2009
11-Na-EC
Hourly number of particles
200
180
160
140
120
100
80
60
40
20
0
22/05/2009
27/05/2009
01/06/2009
06/06/2009
11/06/2009

Figure 5.11

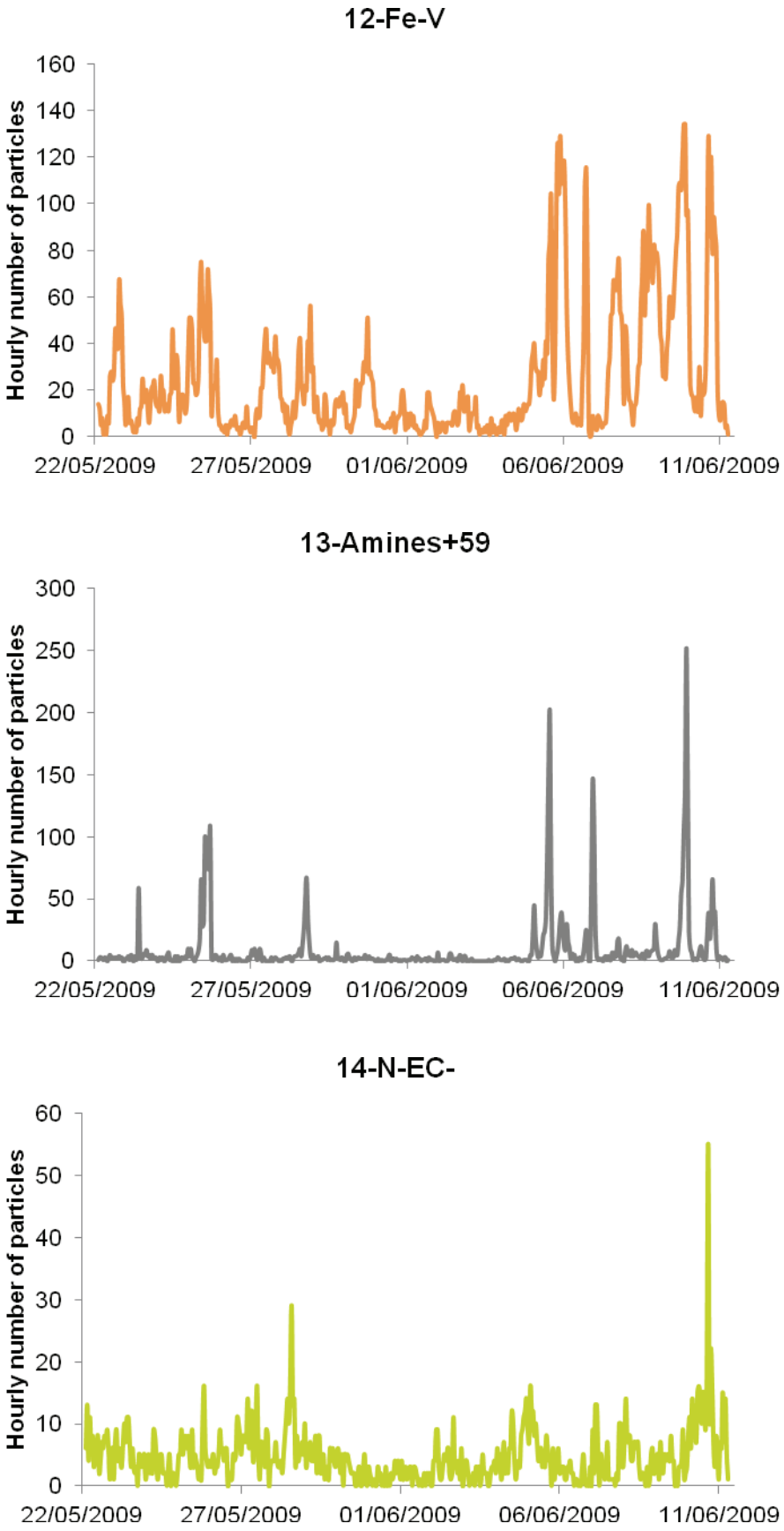

Figure 5.11. Hourly temporal trends in number of particles of single clusters obtained from k-means cluster analysis on London Marylebone Road 2009 dataset.

EC+ and Fe-V present the same diurnal trend, probably because of a common origin partially from long-range transports from central Europe or produced and then aged locally. Ca-EC, Na-EC and OC-CN-SUL are majorly present during day-time while the other most important factors, composed by organic compounds and nitrate are principally present during night-time because of condensation due to lower temperatures (figure 5.12).

The cross correlation analysis among temporal trends of clusters (figure 5.13, Tables 5.8, 5.9 and 5.10) shows that NaCl is an independent cluster, which could be linked to fresh sea spray transported by breezes. “EC+” and “Fe-V” are strongly correlated, and could be partially associated to long-range transports of air-masses from central Europe, confirming what already seen for EC+ PMF factor. EC+, which is one of the major contributing component in this campaign could be also produced and aged locally. “Na-EC” and “Ca-EC” are strongly correlated and in fact the former could be associated to emissions from vehicle exhaust, and the latter from lubricating oils used to protect internal combustion engine of vehicles [Spencer 2006]. Therefore, these two particle-type could be directly linked to traffic confirming the conclusion made about EC- PMF factor. Organic carbon clusters, nitrate and potassium are strongly correlated to each other forming a group of substances which are then connected (in a less extent) with traffic related clusters.

These results are similar to those already seen from cross correlation analysis of PMF factors. In fact, it seems that EC-, primarily emitted from vehicular traffic, undergoes progressive oxidative reaction with enrichment in aromatics, N-containing organic compounds and nitrate to form aged elemental carbon particles. Nitrate could be associated to local NO_x emissions as it is strongly correlated to clusters characterized by aromatic compounds. “7-Amines+58”, “13-Amines+59” and “14-N-EC-” are constituted by few particles and their temporal trends are characterized by a few peaks event during the entire campaign. Those signals, which are not explained by a specific PMF factor, are present in OC-CHNO factor.

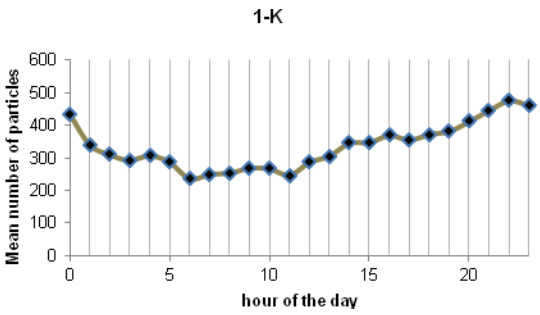
1-K
Mean number of particles
hour of the day

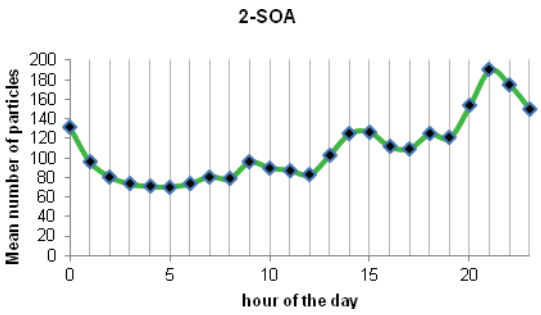
2-SOA
Mean number of particles
hour of the day

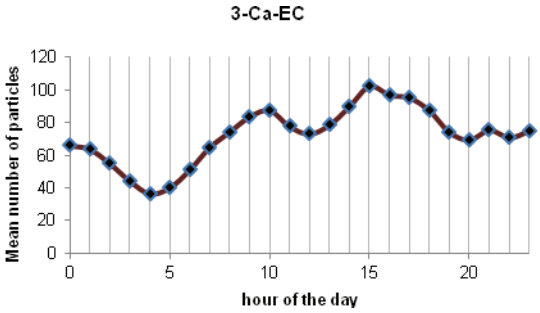
3-Ca-EC
Mean number of particles
hour of the day

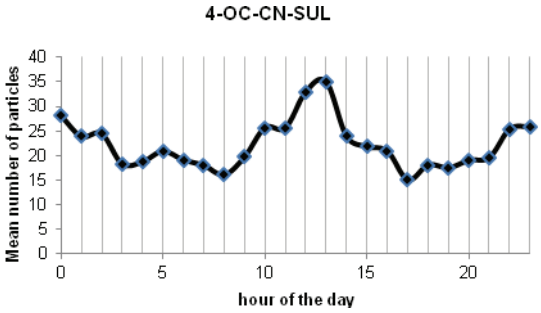
4-OC-CN-SUL
Mean number of particles
hour of the day

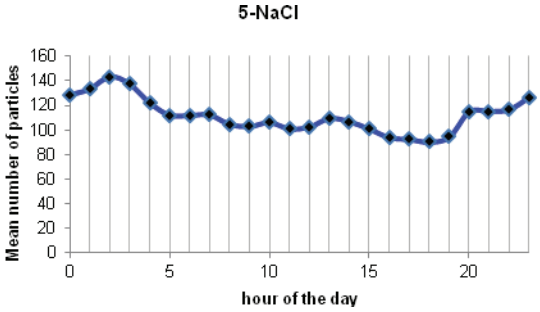
5-NaCl
Mean number of particles
hour of the day

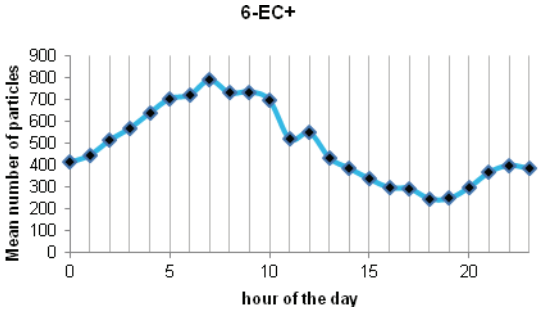
6-EC+
Mean number of particles
hour of the day

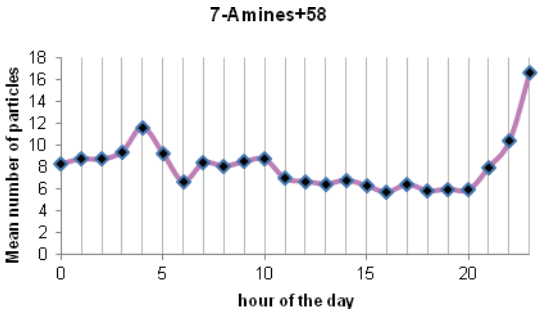
7-Amines+58
Mean number of particles
hour of the day

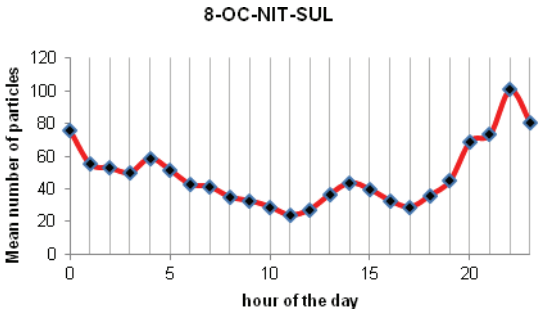
8-OC-NIT-SUL
Mean number of particles
hour of the day

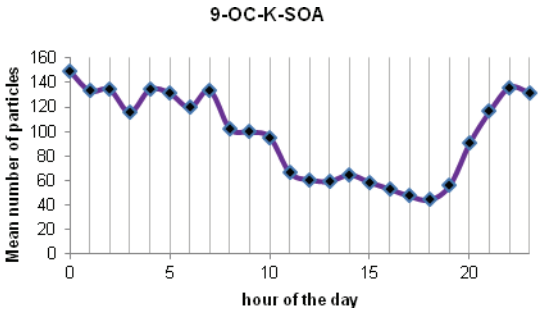
9-OC-K-SOA
Mean number of particles
hour of the day

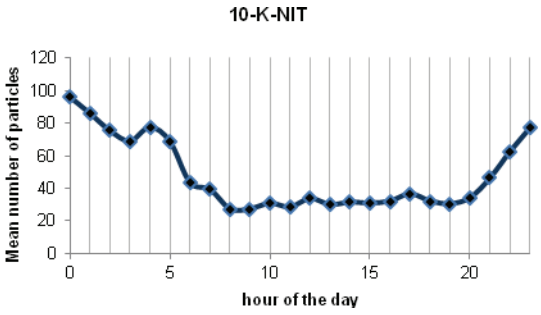
10-K-NIT
Mean number of particles
hour of the day

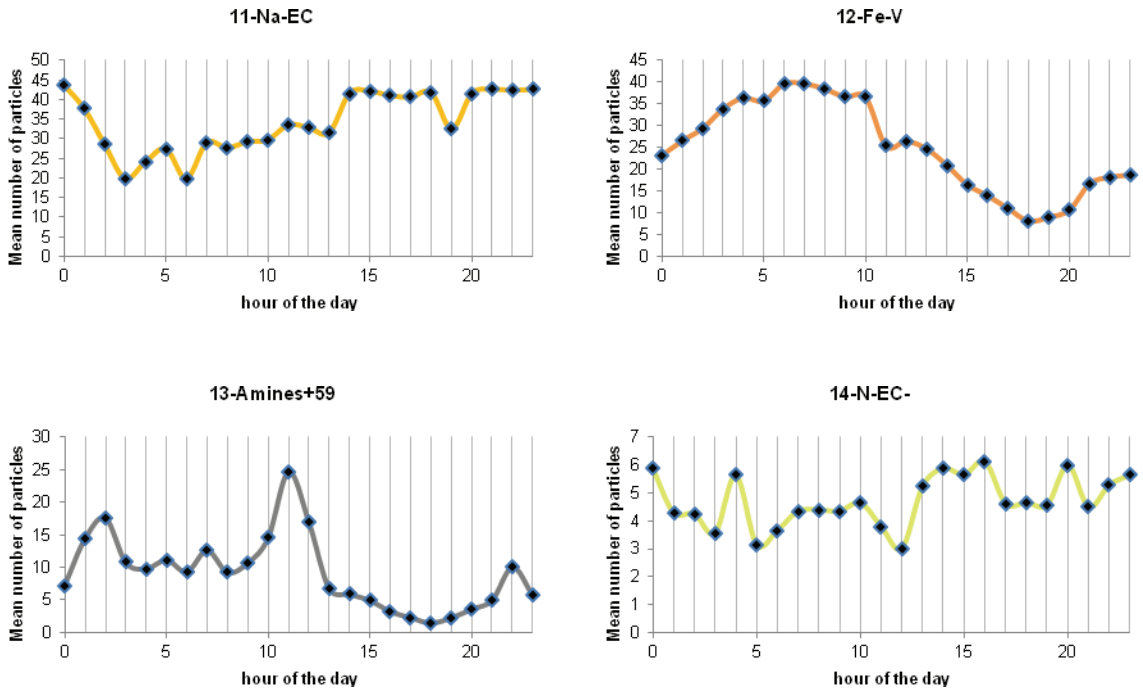

Figure 5.12. Diurnal trends (average number of particles) of k-means clusters, London Marylebone Road campaign.

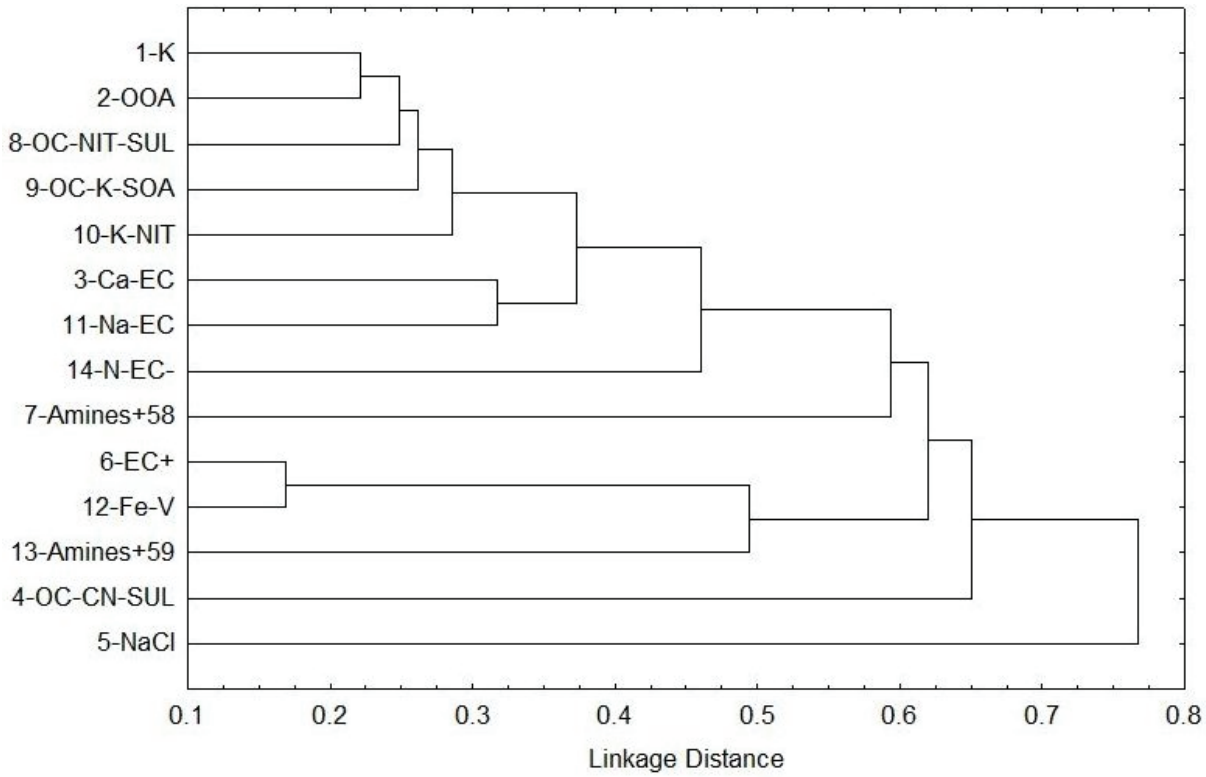

Figure 5.13. Tree diagram of the 14 clusters' hourly temporal trends (number of particles), single linkage, distance measure r-Pearson correlation coefficient.

Table 5.8. Correlation coefficients (r) among hourly temporal trends of k-means clusters

	1-K	2-OOA	3-Ca-EC	4-OC-CN-SUL	5-NaCl	6-EC+	7-Amines+58	8-OC-NIT-SUL	9-OC-K-SOA	10-K-NIT	11-Na-EC	12-Fe-V	13-Amines+59	14-N-EC-
1-K	1													
2-OOA	0.78	1												
3-Ca-EC	0.33	0.63	1											
4-OC-CN-SUL	0.24	0.34	0.32	1										
5-NaCl	-0.04	0.08	0.23	0.13	1									
6-EC+	-0.09	-0.13	-0.20	0.05	-0.37	1								
7-Amines+58	0.15	0.23	0.17	0.14	-0.06	0.38	1							
8-OC-NIT-SUL	0.75	0.73	0.25	0.34	-0.07	0.07	0.27	1						
9-OC-K-SOA	0.53	0.48	0.11	0.30	-0.07	0.35	0.36	0.74	1					
10-K-NIT	0.55	0.42	0.12	0.35	-0.09	0.11	0.26	0.71	0.67	1				
11-Na-EC	0.18	0.47	0.68	0.27	0.13	0.07	0.33	0.22	0.13	0.24	1			
12-Fe-V	-0.12	-0.12	-0.20	0.04	-0.32	0.83	0.35	0.08	0.37	0.12	0.02	1		
13-Amines+59	0.00	0.02	-0.11	0.14	-0.22	0.51	0.21	0.17	0.29	0.10	0.03	0.46	1	
14-N-EC-	0.30	0.44	0.50	0.19	0.07	0.15	0.41	0.33	0.30	0.22	0.54	0.13	0.05	1

*strong correlations (r>0.5) highlighted in green

Table 5.9. Determination coefficients (r^2) among hourly temporal trends of k-means clusters

	1-K	2-OOA	3-Ca-EC	4-OC-CN-SUL	5-NaCl	6-EC+	7-Amines+58	8-OC-NIT-SUL	9-OC-K-SOA	10-K-NIT	11-Na-EC	12-Fe-V	13-Amines+59	14-N-EC-
1-K	1													
2-OOA	0.61	1												
3-Ca-EC	0.11	0.39	1											
4-OC-CN-SUL	0.06	0.12	0.10	1										
5-NaCl	0.00	0.01	0.05	0.02	1									
6-EC+	0.01	0.02	0.04	0.00	0.14	1								
7-Amines+58	0.02	0.05	0.03	0.02	0.00	0.14	1							
8-OC-NIT-SUL	0.57	0.54	0.06	0.11	0.00	0.01	0.07	1						
9-OC-K-SOA	0.28	0.23	0.01	0.09	0.00	0.12	0.13	0.54	1					
10-K-NIT	0.30	0.17	0.02	0.12	0.01	0.01	0.07	0.51	0.45	1				
11-Na-EC	0.03	0.22	0.47	0.07	0.02	0.00	0.11	0.05	0.02	0.06	1			
12-Fe-V	0.01	0.01	0.04	0.00	0.10	0.69	0.12	0.01	0.14	0.01	0.00	1		
13-Amines+59	0.00	0.00	0.01	0.02	0.05	0.26	0.04	0.03	0.08	0.01	0.00	0.21	1	
14-N-EC-	0.09	0.19	0.25	0.04	0.00	0.02	0.17	0.11	0.09	0.05	0.29	0.02	0.00	1

*r^2>0.5 highlighted in green

Table 5.10. p-values of the *r*-Pearson correlation test among hourly temporal trends of k-means clusters

	1-K	2-OOA	3-Ca-EC	4-OC-CN-SUL	5-NaCl	6-EC+	7-Amines+58	8-OC-NIT-SUL	9-OC-K-SOA	10-K-NIT	11-Na-EC	12-Fe-V	13-Amines+59	14-N-EC-
1-K														
2-OOA	7E-100													
3-Ca-EC	2E-13	2E-54												
4-OC-CN-SUL	9E-08	9E-15	4E-13											
5-NaCl	4E-01	9E-02	2E-07	4E-03										
6-EC+	4E-02	5E-03	1E-05	3E-01	2E-17									
7-Amines+58	9E-04	5E-07	2E-04	2E-03	2E-01	4E-18								
8-OC-NIT-SUL	2E-89	3E-83	5E-08	2E-14	1E-01	1E-01	1E-09							
9-OC-K-SOA	1E-35	1E-28	1E-02	2E-11	1E-01	1E-15	5E-16	2E-84						
10-K-NIT	2E-39	1E-21	6E-03	2E-15	4E-02	1E-02	6E-09	7E-77	7E-64					
11-Na-EC	6E-05	3E-28	1E-67	3E-09	3E-03	1E-01	2E-13	1E-06	4E-03	2E-07				
12-Fe-V	8E-03	8E-03	1E-05	3E-01	3E-13	6E-125	2E-15	6E-02	2E-17	9E-03	6E-01			
13-Amines+59	1E+00	7E-01	2E-02	2E-03	1E-06	8E-33	3E-06	1E-04	7E-11	2E-02	4E-01	2E-26		
14-N-EC-	1E-11	7E-24	1E-32	2E-05	2E-01	6E-04	9E-21	9E-14	1E-11	7E-07	6E-38	3E-03	3E-01	

*absence of correlation highlighted in red

5.8. Comparison between PMF and K-means cluster analysis

From the joint deployment of PMF and cluster analysis to study urban particulate matter in a kerbside site, it was possible to highlight the differences in the two approaches and outcomes in characterizing such a complex PM mixture.

Cluster analysis techniques, such as K-means, give a rapid outcome on particle's heterogeneity by extracting the different particle-types allowing the study at detail level including peak events. For example, k-means was able to separate amines+58, amines+59 and N-EC particle-types which are constituted by a limited number of particles and contributes significantly only in a few peak events. Those clusters contribute to the OC-CHNO PMF factor, so their contribution is not separated from the one of other organic nitrogen compounds. At the same extent, species like iron and vanadium, which contribute to Fe-V cluster, are not extracted by PMF, again because of the limited number of particles.

Moreover, considering k-means results which show a Ca-EC cluster contributing to the 5.1% of the entire dataset, associated with lubricating-oil from traffic emissions, PMF analysis was run again including m/z=+40 to the input matrix. It is worth to specify that, at the same m/z value, there is a strong contribution of K^+ because of

the well-known miscalibration problem. In fact, PMF analysis failed to separate the Ca^+ and miscalibrated K^+ contributions to m/z=+40. On the contrary, it extracts a factor which explains all the variance associated to the m/z=+40. For this reason, the results obtained were not further considered. In this connection, an improvement to solve this problem could come from PMF analysis selecting a large number of factors, which is unlikely because it would cause a multiple splitting of the other factors. Moreover, PMF analysis could be applied to ATOFMS data *after* clustering with another technique, but not as previously done in the literature. In fact, clustering techniques could be used to separate the dataset in a few different particle types and the PMF analysis could be applied to single particle mass spectra differently for each particle-type.

The results of the correlation analysis among hourly temporal trends of clusters and PMF factors (equivalent number of particles) are reported in tables 5.11, 5.12 and 5.13.

The correlation analysis confirms what already seen in Harwell campaign. PMF factors in equivalent number of particles are strongly correlated to the corresponding k-mean cluster with similar chemical profile. In fact, K cluster is strongly correlated with K PMF factor (r=0.99). EC+ cluster is strongly correlated to EC+ PMF factor (r=1), NaCl factor is strongly correlated to NaCl cluster (r=0.96) and NIT factor is strongly correlated to K-NIT cluster (r=0.96).

Other particle-types, which present an higher internal mixing state, correlate with many factors. For example, OOA particle-type correlates with K, OOA, CNO-COOH and OC-Arom factors. OC-NIT-SUL cluster correlates with K, NIT, OOA and OC-Arom factors, while OC-K-SOA correlates with OOA, NH4, OC-Arom and OC-CHNO. Fe-V is correlated to EC+ factor, while Na-EC presents its larger but medium correlations with EC- (r=0.64) and CNO-COOH (r=0.58).

The OC-CN-SUL cluster is correlated to CNO-COOH factor. N-EC- cluster presents correlation of medium intensity with OOA, CNO-COOH, EC- and OC-Arom.

EC- factor does not present a diurnal trend typical of primary emission from vehicular traffic however it presents correlations of strong and medium intensities with clusters associated to vehicular traffic, i.e. Na-EC (r=0.64), Ca-EC (r=0.37), N-EC- (r=0.46). It is worth to highlight that it is correlated also with EC+ cluster (r=0.65) and Fe-V (r=0.56). It is likely that, EC- is present in particles which are not internally mixed with nitrate and sulphate but it may be originated by multiple sources.

Table 5.11. Correlation coefficients (r) among hourly temporal trends of PMF factors in equivalent number of particles and of k-means clusters.

	1-K	2-OOA	3-Ca-EC	4-OC-CN-SUL	5-NaCl	6-EC+	7-Amines+58	8-OC-NIT-SUL	9-OC-K-SOA	10-K-NIT	11-Na-EC	12-Fe-V	13-Amines+59	14-N-EC-
F1 K	0.99	0.81	0.38	0.28	-0.01	-0.04	0.19	0.78	0.59	0.57	0.23	-0.08	0.04	0.35
F2 NIT	0.61	0.44	0.09	0.31	-0.16	0.20	0.28	0.74	0.68	0.96	0.17	0.18	0.14	0.23
F3 NaCl	0.06	0.15	0.23	0.13	0.96	-0.36	-0.05	-0.03	-0.07	-0.10	0.16	-0.33	-0.22	0.08
F4 OOA	0.73	0.85	0.46	0.40	-0.04	0.25	0.39	0.82	0.78	0.59	0.35	0.23	0.26	0.45
F5 NH4	0.26	0.14	-0.12	0.16	-0.28	0.74	0.37	0.48	0.78	0.48	0.04	0.66	0.56	0.18
F6 CNO-COOH	0.65	0.72	0.69	0.53	0.09	-0.03	0.27	0.59	0.44	0.51	0.58	-0.06	0.03	0.48
F7 EC+	-0.06	-0.11	-0.19	0.05	-0.37	1.00	0.38	0.10	0.38	0.14	0.08	0.83	0.50	0.16
F8 EC-	0.10	0.32	0.37	0.35	-0.14	0.65	0.51	0.28	0.43	0.35	0.64	0.56	0.41	0.46
F9 OC-arom	0.81	0.87	0.52	0.42	0.05	0.04	0.32	0.89	0.75	0.65	0.35	0.04	0.13	0.46
F10 OC-CHNO	0.37	0.35	0.08	0.34	-0.18	0.63	0.43	0.58	0.86	0.63	0.27	0.57	0.44	0.31

Table 5.12. Determination coefficients (r^2) among hourly temporal trends of PMF factors in equivalent number of particles and of k-means clusters.

	1-K	2-OOA	3-Ca-EC	4-OC-CN-SUL	5-NaCl	6-EC+	7-Amines+58	8-OC-NIT-SUL	9-OC-K-SOA	10-K-NIT	11-Na-EC	12-Fe-V	13-Amines+59	14-N-EC-
F1 K	0.98	0.66	0.14	0.08	0.00	0.00	0.04	0.61	0.34	0.32	0.05	0.01	0.00	0.12
F2 NIT	0.38	0.20	0.01	0.10	0.03	0.04	0.08	0.54	0.46	0.91	0.03	0.03	0.02	0.05
F3 NaCl	0.00	0.02	0.05	0.02	0.91	0.13	0.00	0.00	0.01	0.01	0.02	0.11	0.05	0.01
F4 OOA	0.53	0.72	0.21	0.16	0.00	0.06	0.15	0.67	0.61	0.35	0.12	0.05	0.07	0.20
F5 NH4	0.07	0.02	0.01	0.03	0.08	0.54	0.13	0.23	0.60	0.23	0.00	0.44	0.31	0.03
F6 CNO-COOH	0.43	0.52	0.47	0.28	0.01	0.00	0.07	0.34	0.19	0.26	0.34	0.00	0.00	0.23
F7 EC+	0.00	0.01	0.04	0.00	0.14	1.00	0.15	0.01	0.14	0.02	0.01	0.69	0.25	0.03
F8 EC-	0.01	0.10	0.14	0.12	0.02	0.42	0.26	0.08	0.19	0.12	0.41	0.31	0.17	0.22
F9 OC-arom	0.66	0.76	0.27	0.18	0.00	0.00	0.10	0.80	0.56	0.42	0.13	0.00	0.02	0.21
F10 OC-CHNO	0.14	0.12	0.01	0.12	0.03	0.40	0.18	0.34	0.75	0.40	0.07	0.33	0.20	0.10

Table 5.12. p-values of the *r*-Pearson correlation test among hourly temporal trends of PMF factors in equivalent number of particles and of k-means clusters.

	1-K	2-OOA	3-Ca-EC	4-OC-CN-SUL	5-NaCl	6-EC+	7-Amines+58	8-OC-NIT-SUL	9-OC-K-SOA	10-K-NIT	11-Na-EC	12-Fe-V	13-Amines+59	14-N-EC-
F1 K	0E+00	3E-116	1E-17	4E-10	9E-01	4E-01	2E-05	1E-100	6E-46	2E-42	2E-07	8E-02	4E-01	4E-15
F2 NIT	2E-51	8E-25	4E-02	2E-12	5E-04	9E-06	5E-10	5E-84	7E-66	5E-258	2E-04	6E-05	2E-03	5E-07
F3 NaCl	2E-01	8E-04	4E-07	4E-03	3E-260	3E-16	2E-01	5E-01	1E-01	3E-02	5E-04	8E-14	2E-06	1E-01
F4 OOA	3E-82	7E-136	3E-26	2E-20	4E-01	4E-08	4E-19	1E-117	3E-100	2E-47	3E-15	4E-07	1E-08	3E-25
F5 NH4	3E-09	2E-03	8E-03	4E-04	5E-10	2E-83	7E-17	1E-28	3E-99	7E-29	4E-01	5E-63	6E-41	5E-05
F6 CNO-COOH	1E-60	2E-79	6E-69	9E-37	6E-02	5E-01	2E-09	5E-46	3E-24	9E-34	9E-46	2E-01	5E-01	2E-29
F7 EC+	2E-01	2E-02	3E-05	2E-01	3E-17	0E+00	2E-18	3E-02	8E-18	3E-03	7E-02	2E-126	2E-32	3E-04
F8 EC-	3E-02	5E-13	3E-17	4E-15	2E-03	2E-58	2E-33	2E-10	1E-23	1E-15	8E-57	4E-41	3E-21	2E-27
F9 OC-arom	8E-116	3E-150	7E-35	2E-22	3E-01	4E-01	9E-13	1E-169	5E-88	6E-60	9E-16	4E-01	4E-03	2E-26
F10 OC-CHNO	4E-17	3E-15	8E-02	1E-14	5E-05	6E-56	9E-23	2E-45	5E-146	6E-56	2E-09	3E-43	1E-24	3E-12

5.9. Marylebone Road aerosol characterization

Marylebone Road site is a street canyon in which when the winds blow from the south-westerly direction a strong vehicular traffic contribution arrive to the sampling site while if the winds blow perpendicular to the street there is a mix of traffic and background contributions [Harrison 2011]. The meteorological data were collected from the Heathrow Airport site on the outskirts of London which represent winds above the street canyon, rather than those within.

Air masses back-trajectories show a regional/continental contribution in the following periods: 25-26/05/2009, 31/05-03/06/2009 and 10-11/06/2009 (figure 5.14). In those periods PM is enriched in EC+ and NH4 factors and EC+ and Fe-V clusters, confirming their long-range transports origin of aged particles. NaCl (factor and cluster), on the contrary, seems more freshly emitted by marine breezes.

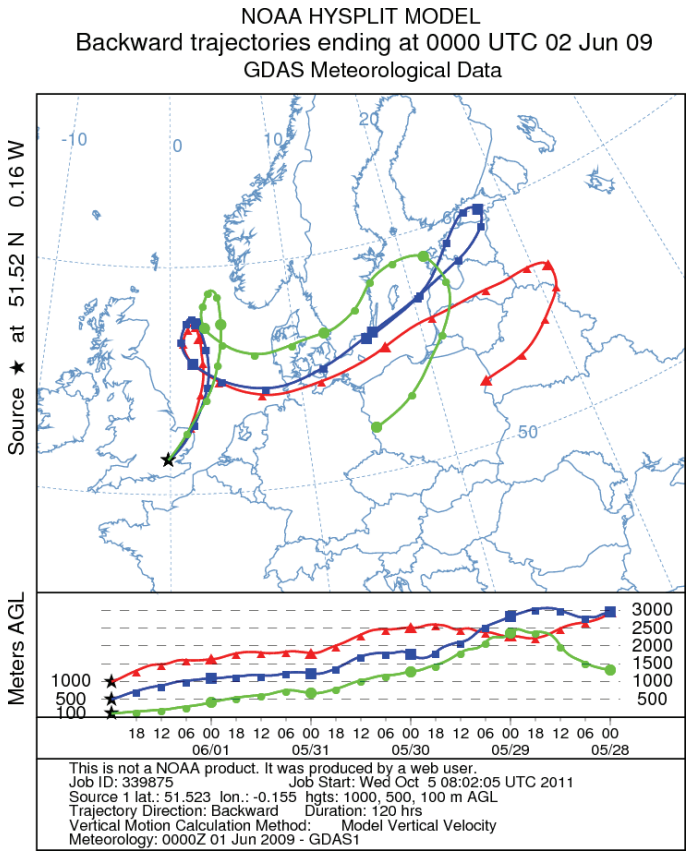

Figure 5.14. Example of air masses back-trajectories of regional/continental origin contributing during the periods 25-26/05/2009, 31/05-03/06/2009 and 10-11/06/2009.

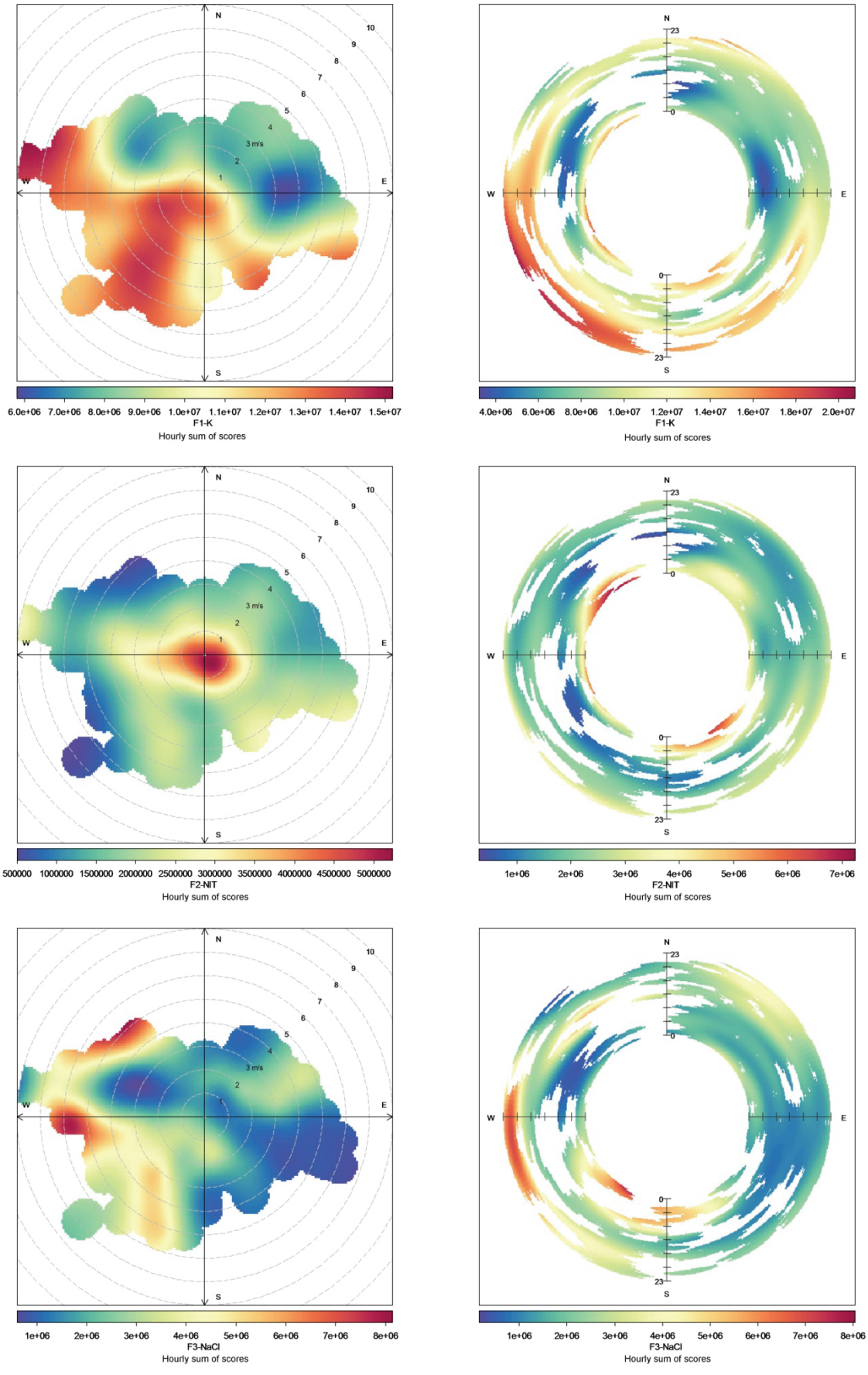
N
S
W
E
3 m/s
6.0e+06 7.0e+06 8.0e+06 9.0e+06 1.0e+07 1.1e+07 1.2e+07 1.3e+07 1.4e+07 1.5e+07
F1-K
Hourly sum of scores
4.0e+06 6.0e+06 8.0e+06 1.0e+07 1.2e+07 1.4e+07 1.6e+07 1.8e+07 2.0e+07
F1-K
Hourly sum of scores
500000 1000000 1500000 2000000 2500000 3000000 3500000 4000000 4500000 5000000
F2-NIT
Hourly sum of scores
1e+06 2e+06 3e+06 4e+06 5e+06 6e+06 7e+06
F2-NIT
Hourly sum of scores
1e+06 2e+06 3e+06 4e+06 5e+06 6e+06 7e+06 8e+06
F3-NaCl
Hourly sum of scores
1e+06 2e+06 3e+06 4e+06 5e+06 6e+06 7e+06 8e+06
F3-NaCl
Hourly sum of scores

Figure 5.15

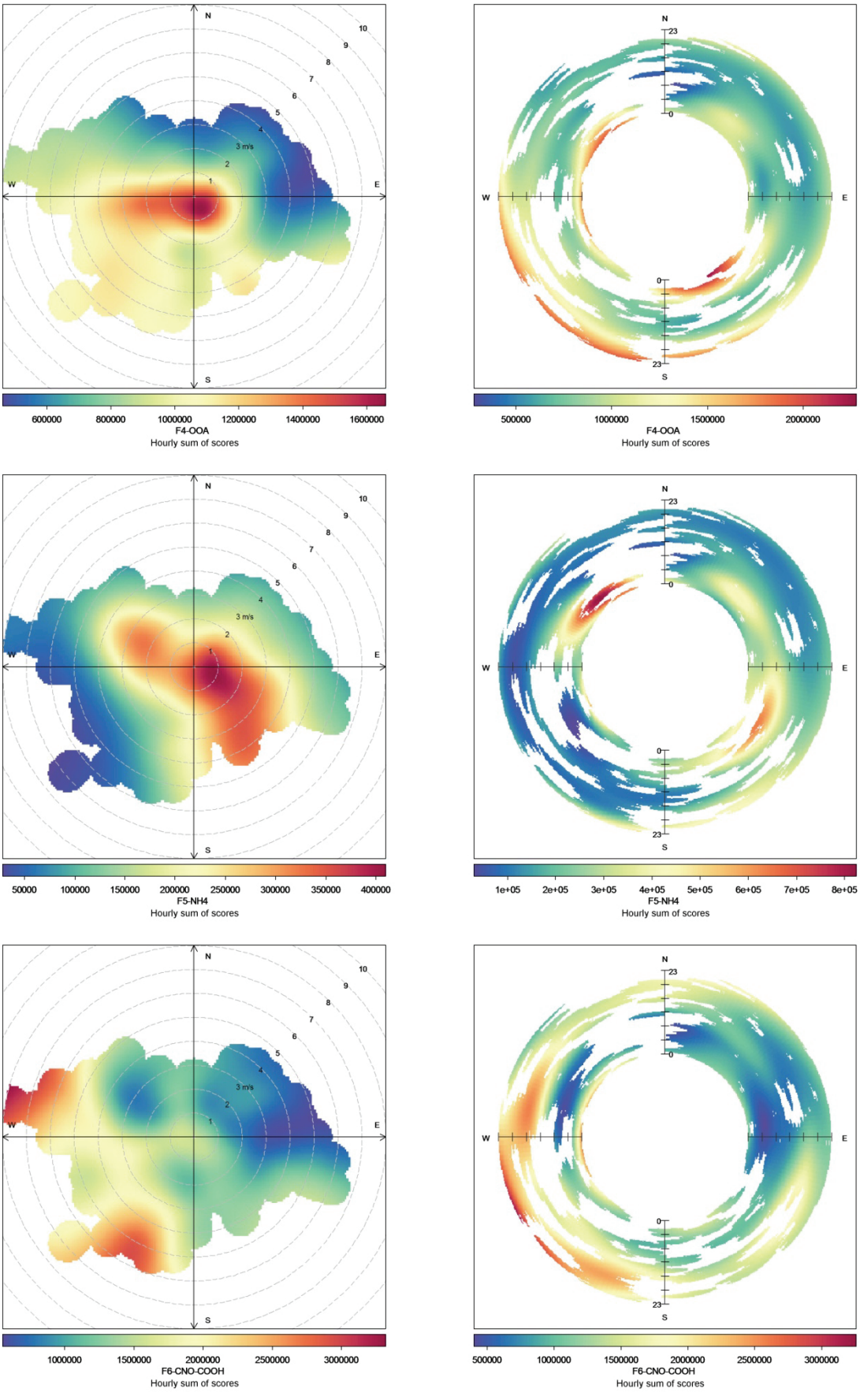
N
S
W
E
3 m/s
600000 800000 1000000 1200000 1400000 1600000
F4-OOA
Hourly sum of scores
500000 1000000 1500000 2000000
F4-OOA
Hourly sum of scores
50000 100000 150000 200000 250000 300000 350000 400000
F5-NH4
Hourly sum of scores
1e+05 2e+05 3e+05 4e+05 5e+05 6e+05 7e+05 8e+05
F5-NH4
Hourly sum of scores
1000000 1500000 2000000 2500000 3000000
F6-CNO-COOH
Hourly sum of scores
500000 1000000 1500000 2000000 2500000 3000000
F6-CNO-COOH
Hourly sum of scores

Figure 5.15

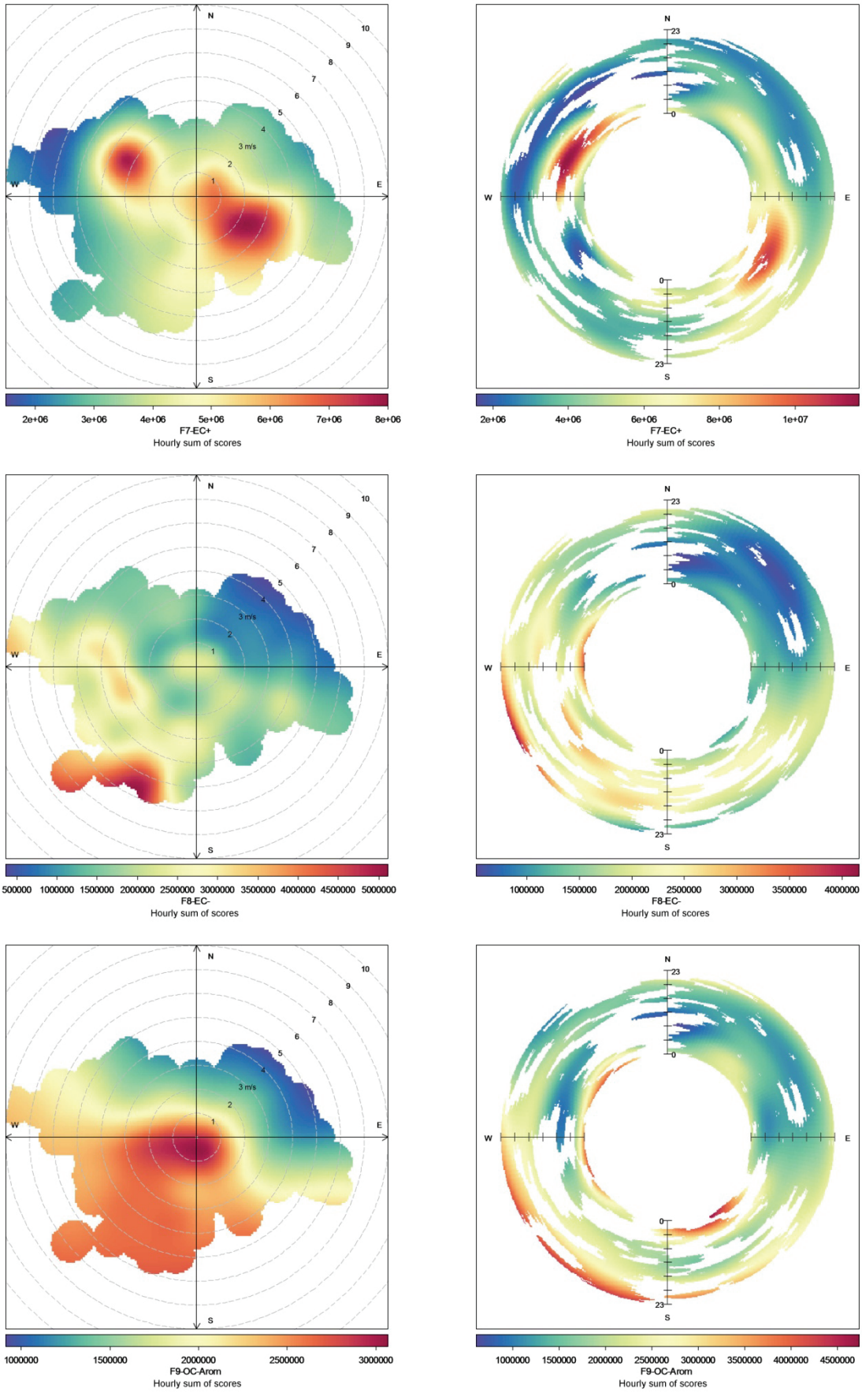
N
S
W
E
3 m/s
2e+06 3e+06 4e+06 5e+06 6e+06 7e+06 8e+06
F7-EC+
Hourly sum of scores
2e+06 4e+06 6e+06 8e+06 1e+07
F7-EC+
Hourly sum of scores
500000 1000000 1500000 2000000 2500000 3000000 3500000 4000000 4500000 5000000
F8-EC-
Hourly sum of scores
1000000 1500000 2000000 2500000 3000000 3500000 4000000
F8-EC-
Hourly sum of scores
1000000 1500000 2000000 2500000 3000000
F9-OC-Arom
Hourly sum of scores
1000000 1500000 2000000 2500000 3000000 3500000 4000000 4500000
F9-OC-Arom
Hourly sum of scores

Figure 5.15

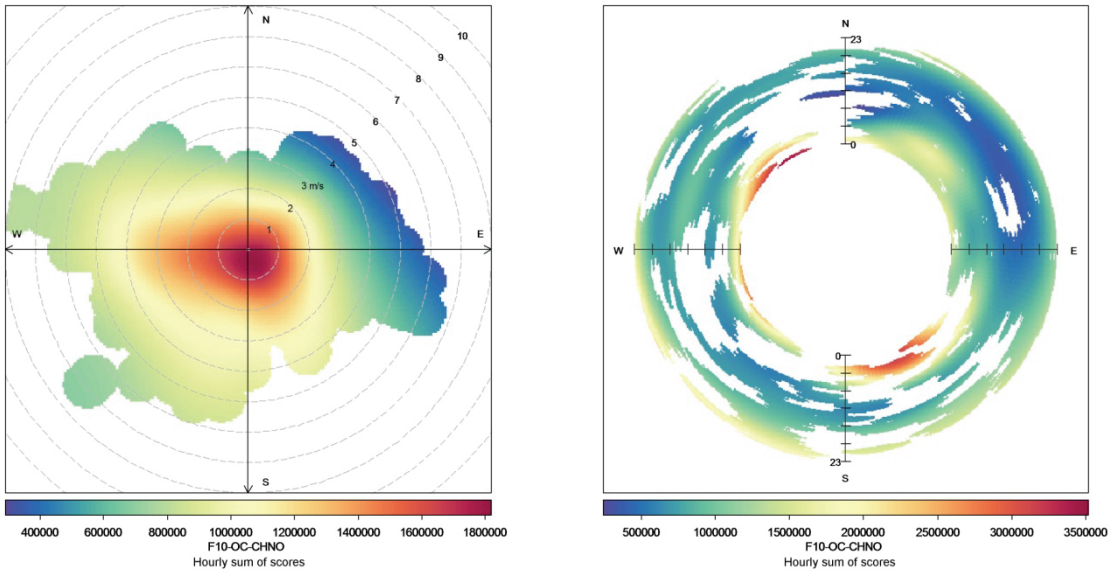

Figure 5.15. Wind roses depicting the trends in scores with wind direction and speed (on the left side) and with wind direction and time for a typical day (on the right side) of the PMF factors.

From the wind roses (figure 5.15), it is observed that K, CNO-COOH, EC- and OC-Arom increase when the winds blow from the south-westerly direction, when the traffic contribution is enhanced. On the contrary, EC+ and NH4 factors increase when the winds are perpendicular to the street canyon and thus there is more mixing with background air.

NIT, OOA, OC-CHNO and in some extent OC-Arom too, present the higher concentrations when the winds are calm, confirming their local origin.

It is likely that organic carbon compounds are in a complex mixture which origins from local emissions and then ages through many concurrent reactions and processes which at the moment are difficult to outline. In fact, the precise mechanisms of formation and evolution of secondary organic aerosol are still highly uncertain [Dall'Osto 2011, Hallquist 2009]. EC- seems to be local, even if it does not present a typical diurnal trend that could be related to vehicular traffic emissions. It could be related to many types of particles from those freshly emitted from vehicular exhaust to particles internally mixed with organic nitrogen compounds.

EC+ and NH4 factors are associated to urban background air. They could be transported from central Europe, however the particles depleted from sulphate, which is transported from central Europe too [Martin 2011], and the high contribution of EC+ to the total measured PM seems to indicate that the long-range transport could have a role but EC+ and NH4 factors are not only due to it.

In conclusion, k-means cluster analysis confirms that EC+ and EC- factors are different. From this campaign it seems that EC- is locally emitted probably from vehicle exhaust, however its diurnal trend, not typical of a traffic-related pollutant seems to indicate that it could be related to a multitude of particle-types and processes, especially those which involve organic nitrogen compounds.

OOA factor, counter to Harwell campaign, is associated to aromatic fragments and thus it is probably related to traffic emissions. At the same extent, nitrate is produced locally from traffic related NO_x emissions. Sulphate and carboxylic acids are scarcely present in this campaign. In addition, biomass burning contribution which was pointed out in Harwell with the K-EC cluster, did not contribute significantly in Marylebone Road.

EC+ and NH4 are related to urban background air, and are partially originated from long-range transports from central Europe. The latter, could not be the unique source of EC+ which is one of the major contributing factor and PM is depleted in sulphate which would have the same origin.

6. Conclusions

In the present work of thesis, for the first time, Positive Matrix Factorization (PMF) analysis has been directly applied to single particle ATOFMS spectra collected during two ambient sampling campaigns conducted in Harwell (UK), a rural background site in the Oxfordshire, and in a kerbside site, at Marylebone Road, a major traffic route in London (UK) city centre.

PMF analysis, applied to single particle mass spectra, leads to the deconvolution of particle mass spectra and the extraction of their major contributing components. In fact, in both campaigns, PMF factors present very clear, well defined and characterized chemical profiles. Thus, for every extracted component (PMF factor), its temporal trend, both in terms of scores, equivalent number of particles and volume, contemporarily with its size distribution have been calculated.

Regarding Harwell sampling campaign, PMF analysis was able to extract 10 factors, explaining 45% of data variation. The 10 factors extracted represent specific chemical species (K, NIT and SUL) or important classes of substances (NaCl, CNO-COOH, NH4-OOA, OC-Arom, OC-CN, EC+ and EC-).

From the cross correlation analysis among temporal trends of PMF factors two elemental carbon components were identified: the EC- factor, correlated to OC-CHNO, probably related to anthropogenic primary emissions and the EC+ factor present in aged particles internally mixed with secondary species. Furthermore, this is the first time in which different families of organic carbon are extracted from ATOFMS data, including aromatic, oxidized organic compound and two different organic nitrogen components: primary (OC-CHNO) and oxidized (CNO-COOH). Oxidized carbon such as oxidised organic nitrogen and carboxylic acids are found only in aged aerosol while nitrate and sulphate are found in different proportions: the former is less aged and it is mixed with urban plumes while sulphate came from long-range transport.

Concerning Marylebone Road campaign, PMF analysis was able to extract 10 factors, explaining the 55% of variance. The 10 factors extracted represent specific chemical species or important classes of substances and are similar to those extracted in Harwell, with the following exceptions: NH4-OOA splits into NH4 factor and OOA factor, CNO-COOH presents a less amount of carboxylic acids and SUL factor is not extracted. In fact, the particles sampled are depleted in sulphate.

EC-, K, CNO-COOH and OC-Arom factors seems to be related to traffic emissions, despite their diurnal trends do not present a typical traffic signature. OOA, is not related to NH4 and is strongly correlated indeed with OC-Arom factor. At the same extent, nitrate is produced locally from traffic related NO_x emissions. Sulphate and carboxylic acids are scarcely present in this campaign confirming the low contribution of long-range transports of aged particles. EC+ and NH4 factor could be transported from central Europe. However, it is unlikely that this is the unique source because EC+ is one of the most abundant factor.

The two elemental carbon different contributions are confirmed in this campaign. While EC+ factors is present in aged particles from urban background air and long-range transports, EC- seems locally emitted probably from vehicle exhaust, however its diurnal trend, not typical of a traffic-related pollutant indicates that it could be related to a multitude of particle-types and processes, especially those which involve organic nitrogen compounds. EC- is correlated to Na-EC, N-EC- and Ca-EC cluster, the latter representing lubricating-oil emissions. Moreover, its fine size distribution confirm that it is not present in aged particles. PMF failed to extract calcium contribution from lubricating-oil because of the presence of miscalibrated potassium signal at the same m/z value.

PMF results were compared to K-means cluster analysis results, finding strong correlations between temporal trends of PMF factors and the corresponding cluster temporal trends which present the most similar chemical profile. Still, while cluster analysis has the effect of dividing particles into classes of similarity, PMF makes a deconvolution of single particle mass spectra and it extracts their main contributing components.

In fact, K-means cluster analysis has the ability to give a rapid outcome on particle heterogeneity and mixing state by extracting the different particle-types. Moreover, it can easily isolate low contributing particle types characterized by peak events whose components are unlikely to be extracted by PMF. On the contrary, PMF analysis could turn to be useful for quantification purposes. As a matter of fact, the comparison among PMF factors and cluster temporal trends with independent ion and organic measurements shows in general a good agreement. In the case of highly internally mixed particles, a loss of correlation is observed for clusters but not for PMF factors. Thus PMF analysis could turn to be useful for the quantification of the main components of PM in view of a future development of the ATOFMS instrument.

Of course, better repeatability of the ionization patterns and efficiency in particles detection would improve its quantification capability. Conversely, the first attempt to obtain quantitative data from ATOFMS PMF factors seems encouraging despite factors have not been corrected for size-dependent transmission losses.

PMF analysis could be further improved by its application to ATOFMS data *after* clustering with another technique, but not as previously done in the literature. In fact, clustering techniques could be used to separate the dataset in a few different particle types and the PMF analysis could be applied to single particle mass spectra differently for each particle-type. On the other hand, large peaks could be scaled through square root or cube root in order to downweight their contribution and possibly extracts minor contributing components which can be indeed important source markers.

7. References

Adachi M., Okuyama K., Kousaka Y. (**1983**) Electrical neutralization of charged aerosol particles by bipolar ions. *Journal of Chemical Engineering of Japan* 16(3), 229-235.

Aiken A.C., DeCarlo P.F., Kroll J.H., Worsnop D.R., Huffman J.A., Docherty K.S., Ulbrich I.M., Mohr C., Kimmel J.R., Sueper D., Sun Y., Zhang Q., Trimborn A., Northway M., Ziemann P.J., Canagaratna M.R., Onasch T.B., Alfarra M.R., Prevot A.S.H., Dommen J., Duplissy J., Metzger A., Baltensperger U., Jimenez J.L. (**2008**) O/C and OM/OC Ratios of Primary, Secondary, and Ambient Organic Aerosols with High-Resolution Time-of-Flight Aerosol Mass Spectrometry. *Environmental Science & Technology* 42, 4478-4485.

Aiken A.C., Salcedo D., Cubison M.J., Huffman J.A., DeCarlo P.F., Ulbrich I.M., Docherty K.S., Sueper D., Kimmel J.R., Worsnop D.R., Trimborn A., Northway M., Stone E.A., Schauer J.J., Volkamer R.M., Fortner E., de Foy B., Wang J., Laskin A., Shutthanandan V., Zheng J., Zhang R., Gaffney J., Marley N.A., Paredes-Miranda G., Arnott W.P., Molina L.T., Sosa G., Jimenez J.L. (**2009**) Mexico City aerosol analysis during MILAGRO using high resolution aerosol mass spectrometry at the urban supersite (T0)-Part 1: Fine particle composition and organic source apportionment. *Atmospheric Chemistry and Physics* 9, 6633-6653.

Albrecht B.A. (**1989**) Aerosols, Cloud Microphysics, and Fractional Cloudiness. *Science* 245(4923), 1227-1230.

Alleman L.Y., Lamaison L., Perdrix E., Robache A., Galloo J.C. (**2010**) PM10 metal concentrations and source identification using positive matrix factorization and wind sectoring in a French industrial zone. *Atmospheric Research* 96, 612-625.

Allen J.O., Fergenson D.P., Gard E.E., Hughes L.S., Morrical B.D., Kleeman M.J., Gross D.S., Gälli M.E., Prather K.A., Cass G.R. (**2000**) Particle detection efficiencies of aerosol time of flight mass spectrometers under ambient sampling conditions. *Environmental Science & Technology* 34, 211-217.

Allen J.O., Bhave P.V., Whiteaker J.R., Prather K.A. (**2006**) Instrument Busy Time and Mass Measurement using Aerosol Time-of-Flight Mass Spectrometry. *Aerosol Science and Technology* 40, 615-626.

Angelino S., Suess D.T., Prather K.A. (**2001**) Formation of aerosol particles from reactions of secondary and tertiary alkylamines: Characterization by aerosol time-of-flight mass spectrometry. *Environmental Science & Technology* 35 (15), 3130-3138.

Bae M.S., Schauer J.J., Turner J.R. (**2006**) Estimation of the Monthly Average Ratios of Organic Mass to Organic Carbon for Fine Particulate Matter at an Urban Site. *Aerosol Science and Technology* 40, 1123–1139.

Bari M.A., Baumbach G., Kuch B., Scheffknecht G. (**2009**) Wood smoke as a source of particle-phase organic compounds in residential areas. *Atmospheric Environment* 43, 4722-4732.

Baron P.A., Mazumder M.K., Cheng Y.S. (**1993**) Direct-reading techniques using optical particle detection. *Aerosol Measurement: Principles, Techniques, and Applications*. K. Willeke and P.A. Baron. New York, Van Norstrand Reinhold.

Bhave P.V., Allen J.O., Morrical B.D., Fergenson D.P., Cass G.R., Prather K.A. (**2002**) A Field-Based Approach for Determining ATOFMS Instrument Sensitivities to Ammonium and Nitrate. *Environmental Science & Technology* 36 (22), 4868-4879.

Bi X., Zhang G., Li L., Wang X., Li M., Sheng G., Fu J., Zhou Z. (**2011**) Mixing state of biomass burning particles by single particle aerosol mass spectrometer in the urban area of PRD, China. *Atmospheric Environment* 45, 3447-3453.

Biswas P., Jones C.L., Flagan R.C. (**1987**) Distortion of size distributions by condensation and evaporation in aerosol instruments. *Aerosol Science and Technology* 7(2), 231-246.

Blifford I.H., Lockhart L.B., Rosenstock H.B. (**1952**) On the natural radioactivity in the air. *Journal of Geophysical Research* 57, 499-509.

Bricard J., Delattre P., Madelaine G., Pourprix M. (**1976**) Detection of ultra-fine particles by means of a continuous flux condensation nuclei counter. In: Liu, B.Y.H.

(Ed.), *Fine Particles: Aerosol Generation, Measurement, Sampling, and Analysis*. Academic Press, New York, pp. 565-580.

CAFE Working Group on Particulate Matter; Second position paper on particulate matter; **2004** December.

CAFE (**2011**) CAFE reference documents. Available from: http://ec.europa.eu/environment/archives/cafe/general/keydocs.htm.

Canagaratna M.R., Jayne J.T., Jimenez J.L., Allan J.D., Alfarra M.R., Zhang Q., Onasch T.B., Drewnick F., Coe H., Middlebrook A., Delia A., Williams L.R., Trimborn A.M., Northway M.J., DeCarlo P.F., Kolb C.E., Davidovits P., Worsnop D.R. (**2007**) Chemical and microphysical characterization of ambient aerosols with the aerodyne aerosol mass spectrometer. *Mass Spectrometry Reviews* 26, 185– 222.

Charlson R.J., Schwartz S.E., Hales J.M., Cess R.D., Coakley J.A., Hansen J.E., Hofmann D.J. (**1992**) Climate Forcing by Anthropogenic Aerosols. *Science* 255, 423-430.

Christie W.H., Eby R.E., Warmack R.J., Landau L. (**1981**) The determination of boron and lithium in nuclear materials by secondary ion mass spectrometry. *Analytical Chemistry* 53(1), 13-17.

Cohen J.W. (**1988**) Statistical power analysis for the behavioral sciences, pp. 79-81.

Cooke D.D., Kerker M. (**1975**) Response calculations for light scattering aerosol particle counters. *Applied Optics* 14, 734-739.

Cote V., Kos G., Mortazavi R., Ariya P.A. (**2008**) Microbial and de novo transformation of dicarboxylic acids by three airborne fungi. *The Science of the Total Environment* 390, 530-537.

Cotter R. J. (**1997**) Time-of-Flight Mass Spectrometry: Instrumentation and Applications in Biological Research. *ACS Professional Reference Books*: Washington, DC.

Dahneke B.E., Friedlander S.K. (**1970**) Velocity characteristics of beams of spherical polystyrene particles. *Journal of Aerosol Science* 1, 325-339.

Dahneke B.E. (**1973**) Aerosol beam spectrometry. *Nature Physical Science* 244, 54-55.

Dahneke B., Padliya D. (**1977**) Nozzle-inlet design for aerosol beam. *Instruments in Rarefied Gas Dynamics* 51 Part II, 1163-1172.

Dall'Osto M., Beddows D.C.S., Kinnersley R.P., Harrison R.M. (**2004**) Characterization of individual airborne particles by using aerosol time-of-flight mass spectrometry at Mace Head, Ireland. *Journal of Geophysical Research* 109, D21302.

Dall'Osto M., Harrison R.M. (**2006**) Chemical characterisation of single airborne particles in Athens (Greece) by ATOFMS. *Atmospheric Environment* 40, 7614-7631.

Dall'Osto M., Harrison R.M., Beddows D.C.S. (**2006**) Single-Particle Efficiencies of Aerosol Time-of Flight Mass Spectrometry during the North Atlantic Marine Boundary Layer Experiment. *Environmental Science & Technology* 40 (16), 5029-5035.

Dall'Osto M., Harrison R.M. (**2011**) Urban organic aerosols measured by single particle mass spectrometry in the megacity of London. *Atmospheric Chemistry and Physics Discussions* 11, 5043-5078, doi:10.5194/acpd-11-5043-2011.

De Angelo L., Black B. "London smog disaster, England". In: Encyclopedia of Earth. Eds. Cutler J. Cleveland (Washington, D.C.: Environmental Information Coalition, National Council for Science and the Environment). Published in the Encyclopedia of Earth February 8, **2008**; Available at: http://www.eoearth.org/article/London_smog_disaster,_England.

DeCarlo P.F., Kimmel J.R., Trimborn A., Northway M.J., Jayne J.T., Aiken A.C., Gonin M., Fuhrer K., Horvath T., Docherty K.S.,Worsnop D.R., Jimenez J.L. (**2006**) Field-deployable, high-resolution, time-of-flight aerosol mass spectrometer. *Analitical Chemistry* 78, 8281-8289.

DeCarlo P.F., Ulbrich I.M., Crounse J., de Foy B., Dunlea E.J., Aiken A.C., Knapp D., Weinheimer A.J., Campos T., Wennberg P.O., Jimenez J.L. (**2010**) Investigation of the sources and processing of organic aerosol over the Central Mexico Plateau from aircraft measurments during MILAGRO. *Atmospheric Chemistry and Physics* 10, 5257-5280.

Dockery D.W., Pope C.A., Xu X.P., Spengler J.D., Ware J.H., Fay M.E., Ferris B.G., Speizer F.E. (**1993**) An association between air-pollution and mortality in six US cities. *The New England Journal of Medicine* 329, 1753-1759.

Doğan G., Güllü G., Tuncel G. (**2008**) Sources and source regions effecting the aerosol composition of the Eastern Mediterranean. *Microchemical Journal* 88, 142-149.

Draxler R.R., Rolph G.D. (**2003**) HYSPLIT (Hybrid Single-Particle Lagrangian Integrated Trajectory) model v 4.9, NOAA Air Resource Laboratory, Silver Spring MD., http://ready.arl.noaa.gov/HYSPLIT.php

Drewnick F., Hings S.S., DeCarlo P.F., Jayne J.T., Gonin M., Fuhrer K.,Weimer S., Jimenez J.L., Demerjian K.L., Borrmann S., Worsnop D.R. (**2005**) A new Time-of-Flight Aerosol Mass Spectrometer (ToF-AMS) - Instrument description and first field deployment. *Aerosol Science and Technology* 39, 637–658.

Drewnick F., Dall'Osto M., Harrison R.M. (**2008**) Characterization of aerosol particles from grass mowing by joint deployment of ToF-AMS and ATOFMS instruments. *Atmospheric Environment* 42, 3006-3017.

Eades D.M., Johnson J.V., Yost R.A. (**1993**) Nonlinear resonance effects during ion storage in a quadrupole ion trap. *Journal of the American Society for Mass Spectrometry* 4, 917-929.

Easter R.C., Peter L.K. (**1994**) Binary homogeneous nucleation: temperature and relative humidity fluctuations, nonlinearity, and aspects of new particles production in the atmosphere. *Journal of Applied Meteorology* 33, 775-784.

Eatough D.J., Grover B.D., Woolwine W.R., Eatough N.L., Long R., Farber R. (**2008**) Source apportionment of 1h semi-continuous data during the 2005 Study of Organic Aerosols in Riverside (SOAR) using positive matrix factorization. *Atmospheric Environment* 42, 2706-2719.

El-Zanan H.S., Zielinska B., Mazzoleni L.R., Hansen D.A. (**2009**) Analytical Determination of the Aerosol Organic Mass-to-Organic Carbon Ratio. *Journal Of The Air & Waste Management Association* 59(1), 58-69.

EU 2008/50/EC, DIRECTIVE 2008/50/EC OF THE EUROPEAN PARLIAMENT AND OF THE COUNCIL of 21 May 2008 on ambient air quality and cleaner air for Europe.

Finlayson-Pitts B.J., Pitts J.N. (**1999**) Chemistry of the upper and lower atmosphere. Theory, experiments and applications. *Academic Press*, San Diego, CA, USA.

Forina M. (**2010**) V-PARVUS 2010 manual.

Forster P., Ramaswamy V., Artaxo P., Berntsen T., Betts R., Fahey D.W., Haywood J., Lean J., Lowe D.C., Myhre G., Nganga J., Prinn R., Raga G., Schulz M., Van Dorland R. (**2007**) Changes in Atmospheric Constituents and in Radiative Forcing. In: Climate Change 2007: The Physical Science Basis. Contribution of Working Group I to the Fourth Assessment Report of the Intergovernmental Panel on Climate Change [Solomon S., Qin D., Manning M., Chen Z., Marquis M., Averyt K.B., Tignor M., Miller H.L. (eds.)]. Cambridge University Press, Cambridge, United Kingdom and New York, NY, USA.

Franzetti A., Gandolfi I., Gaspari E., Ambrosini R., Bestetti G. (**2011**) Seasonal variability of bacteria in fine and coarse urban air particulate matter. *Environmental Biotechnology* 90, 745-753.

Fraser M.P., Cass G.R. (**1998**) Detection of Excess Ammonia Emissions from In-Use Vehicles and the Implications for Fine Particle Control. *Environmental Science & Technology* 32, 1053-1057.

Fujii T., Hayashi S., Hogg J.C., Mukae H., Suwa T., Goto Y., Vincent R., van Eeden S.F. (**2002**) Interaction of Alveolar Macrophages and Airway Epithelial Cells Following Exposure to Particulate Matter Produces Mediators that Stimulate the Bone Marrow. *American Journal of Respiratory Cell and Molecular Biology* 27, 34-41.

Fuzzi S., Mandrioli P., Perfetto A. (**1997**) Fog droplets-an atmospheric source of secondary biological aerosol particles. *Atmospheric Environment* 31, 287-290.

Gard E., Mayer J.E., Morrical B.D., Dienes T., Fergenson D.P., Prather K.A. (**1997**) Real-time analysis of individual atmospheric aerosol particles: design and performance of a portable ATOFMS. *Analytical Chemistry* 69 (20), 4083-4091.

Gebhart J., Heyder J., Roth C., Stahlhofen W. (**1976**) Optical aerosol size spectrometry below and above the wavelength of light - a comparison. In: Liu, B.Y.H. (Ed.), *Fine Particles: Aerosol Generation, Measurement, Sampling, and Analysis*. Academic Press, New York.

Giorio C., Tapparo A., Dall'Osto M., Harrison R.M., Beddows D.C.S., Nemitz E. (**2012**) Comparison of three techniques for analysis of data from an aerosol time-of-flight mass spectrometer. In preparation.

Gross D.S., Galli M.E., Silva P.J., Prather K.A. (**2000**) Relative Sensitivity Factors for Alkali Metal and Ammonium Cations in Single-Particle Aerosol Time-of-Flight Mass Spectra. *Analytical Chemistry* 72 (2), 416-422.

Gross D.S., Atlas R., Rzeszotarski J., Turetsky E., Christensen J., Benzaid S., Olson J., Smith T., Steinberg L., Sulman J., Ritz A., Anderson B., Nelson C., Musicant D.R., Chen L., Snyder D.C. Schauer J.J. (**2010**) Environmental chemistry through intelligent atmospheric data analysis. *Environmental Modelling & Software* 25, 760-769.

Guan S., Marshall A.G. (**1994**) Equilibrium space charge distribution in a quadrupole ion trap. *Journal of the American Society for Mass Spectrometry* 5, 64-71.

Hallquist M., Wenger J.C., Baltensperger U., Rudich Y., Simpson D., Claeys, M., Dommen J., Donahue N.M., George C., Goldstein A.H., Hamilton J.F., Herrmann H., Hoffmann T., Iinuma Y., Jang M., Jenkin M. E., Jimenez J. L., Kiendler-Scharr A., Maenhaut W., McFiggans G., Mentel Th.F., Monod A., Prévôt A.S.H., Seinfeld J.H., Surratt J.D., Szmigielski R., Wildt J. (**2009**) The formation, properties and impact of secondary organic aerosol: current and emerging issues. *Atmospheric Chemistry and Physics* 9, 5155-5236.

Harrison R.M., Yin J. (**2000**) Particulate matter in the atmosphere: which particle properties are important for its effects on health? *The Science of the Total Environment* 249, 85-101.

Harrison R.M., Beddows D.C.S., Dall'Osto M. (**2011**) PMF Analysis of Wide-Range Particle Size Spectra Collected on a Major Highway. *Environmental Science & Technology* 45, 5522-5528.

Haxel U., Schumann G. (**1955**) Selbstreinigung der Atmosphäre. *Zeitschrift für Physik A Hadrons and Nuclei* 142, 127-132.

Healy R.M., Hellebust S., Kourtchev I., Allanic A., O'Connor I.P., Bell J.M., Sodeau J.R., Wenger J.C. (**2010**) Source apportionment of PM2.5 in Cork Harbour, Ireland using a combination of single particle mass spectrometry and quantitative semi-continuous measurements. *Atmospheric Chemistry and Physics* 10, 9593-9613.

Healy R.M., O'Connor I.P., Hellebust S., Allanic A., Sodeau J.R., Wenger J.C. (**2009**) Characterisation of single particles from in-port ship emissions. *Atmospheric Environment* 43, 6408-6414.

Heinen H.J. (**1981**) On ion formation in laser desorption mass spectrometry with LAMMA. *International Journal on Mass Spectrometry and Ion Physics* 38, 309-322.

Hinds W.C. (**1982**) Aerosol Technology: Properties, Behavior, and Measurement of Airborne Particles. *Wiley*, New York.

Husar R.B. (**1974**) Atmospheric particulate mass monitoring with a beta radiation detector. *Atmospheric Environment* 8, 183-188.

Jeong C.-H., McGuire M.L., Godri K.J., Slowik J.G., Rehbein P.J.G., Evans G.J. (**2011**) Quantification of aerosol chemical composition using continuous single particle measurements. *Atmospheric Chemicstry and Physics* 11, 7027-7044.

Jia Y., Clements A.L., Fraser M.P. (**2010**) Saccharide composition in atmospheric particulate matter in the southwest US and estimates of source contributions. *Aerosol Science* 41, 62-73.

Jimenez J.L., Jayne J.T., Shi Q., Kolb C.E. (**2002**) Aerosol Mass Spectrometry: Instrumentation & Applications. Graduate Course on Mass Spectrometry & Chromatography, University of Colorado at Boulder.

Jimenez J.L., Jayne J.T., Shi Q., Kolb C.E., Worsnop D.R., Yourshaw I., Seinfeld J.H., Flagan R.C., Zhang X., Smith K.A., Morris J.W., Davidovits P. (**2003**) Ambient aerosol sampling with an Aerosol Mass Spectrometer. *Journal of Geophysical Research* 108, 8425, doi:8410:1029/2001JD001213.

Jobson B.T., Parrish D.D., Goldan P., Kuster W., Fehsenfeld F.C., Blake D.R., Blake N.J., Niki H. (**1998**) Spatial and Temporal Variability Of Nonmethane Hydrocarbon Mixing Ratios and Their Relation to Photochemical Lifetime. *Journal of Geophysical Research Atmosphere* 103, 13557-13567.

Jobson B.T., McKeen S.A., Parrish D.D., Fehsenfeld F.C., Blake D.R., Goldstein A.H., Schauffler S.M., Elkins J.W. (**1999**) Trace Gas Mixing Ratio Variability vs. Lifetime in the Troposphere and Stratosphere-Observations. *Journal of Geophysical Research* 104, D13, 16091-16113.

Kanakidou M., Seinfeld J.H., Pandis S.N., Barnes I., Dentener F.J., Facchini M.C., van Dingenen R., Ervens B., Nenes A., Nielsen C.J., Swietlicki E., Putaud J.P., Balkanski Y., Fuzzi S., Horth J., Moortgat G.K., Winterhalter R.M. (**2005**) Organic aerosol and global climate modelling: a review. *Atmospheric Chemistry and Physics* 5, 1053-1123.

Knutson E.O., Whitby K.T. (**1975**) Aerosol classification by electric mobility: Apparatus, theory, and application. *Journal of Aerosol Science* 6, 443-451.

Koop T. (**2004**) Homogeneous ice nucleation in water and aqueous solutions. *Zeitschrift für physikalische Chemie* 218(11), 1231-1258.

Korn et al. (**2007**) Atomic spectrometric methods for the determination of metals and metalloids in automotive fuels - A review. *Talanta* 73, 1-11.

Kulkarni P., Baron P.A., Willeke K. (**2011**) Aerosol Measurement: Principles, Techniques and Applications. Ed. John Wiley & Sons.

Lanz V.A., Henne S., Staehelin J., Hueglin C., Vollmer M.K., Steinbacher M., Buchmann B., Reimann S. (**2009**) Statistical analysis of anthropogenic non-methane VOC variability at a European background location (Jungfraujoch, Switzerland). *Atmospheric Chemistry and Physics* 9, 3445-3459.

Lee E., Chan C.K., Paatero P. (**1999**) Application of positive matrix factorization in source apportionment of particulate pollutants in Hong Kong. *Atmospheric Environment* 33, 3201-3212.

Liu B.Y.H., Pui D.Y.H. (**1974**) A submicron aerosol standard and the primary, absolute calibration of the condensation nuclei counter. *Journal of Colloid and Interface Science* 47, 155-171.

Liu B.Y.H., Pui Y.H. (**1974**) Electrical neutralization of aerosols. *Aerosol Science* 5, 465-472.

Liu P.; Ziemann P.J.; Kittelson D.B.; McMurry P.H. (**1995**) Generating particle beams of controlled dimensions and divergence: I. theory of particle motion in aerodynamic lenses and nozzle expansions. *Aerosol Science and Technology* 22, 293-313.

Liu P.; Ziemann P.J.; Kittelson D.B.; McMurry P.H. (**1995**) Generating particle beams of controlled dimensions and divergence: II. experimental evaluation of particle motion in aerodynamic lenses and nozzle expansions. *Aerosol Science and Technology* 22, 314-324.

Liu S., Takahama S., Russell L.M., Gilardoni S., Baumgardener D. (**2009**) Oxygenated organic functional groups and their sources in single and submicron organic particles in MILAGRO 2006 campaign. *Atmospheric Chemistry and Physics* 9, 6849-6863.

MacQueen J.B. (**1967**) Some methods for classification and analysis of multivariate observations. *Proceedings of 5-th Berkeley Symposium on Mathematical Statistics and Probability*, Berkeley, University of California Press, 1, 281-297.

Marchand G., Lavoie J., Lazure L. (**1995**) Evaluation of bioaerosols in a municipal solid waste recycling and composting plant. *Journal of the Air and Waste Management Association* 45, 778-781.

Martin C.L., Allan J.D., Crosier J., Choularton T.W., Coe H., Gallagher M.W. (**2011**) Seasonal variation of fine particulate composition in the centre of a UK city. *Atmospheric Environment* 45, 4379-4389.

McGuire M., Jeong C.H., Rehbein P., Corbin J., Slowik J.G., Chang R.Y.W., Abbatt J.D.P., Brook J.R., Evans G.J. (**2009**) Integrating ATOFMS and AMS mass Spectra in a Receptor Model for an Enhanced Understanding of Aerosol Sources. *American Association of Aerosol Research Annual Conference*, Minneapolis Minnesota.

McGuire M.L., Jeong C.H., Slowik J.G., Chang R.Y.W., Corbin J.C., Lu G., Mlhele C., Rehbein P.J.G., Sills D.M.L., Abbatt J.P.D., Brook J.R., Evans G.J. (**2011**) Elucidating determinants of aerosol composition through particle-type-based receptor modelling. *Atmospheric Chemistry and Physics Discussions* 11, 9831-9885.

McMurry P.H., Stolzenburg M.R. (**1989**) On the sensitivity of particle size to relative humidity for Los Angeles aerosols. *Atmospheric Environment* 23(2), 497-507.

McMurry P.H. (**2000**) A review of atmospheric aerosol measurements. *Atmospheric Environment* 34, 1959-1999.

Miller P.E., Denton M.B. (**1986**) The quadrupole mass filter: basic operating concepts. *Journal of Chemical Education* 63(7), 617-622.

Monn C., Becker S. (**1999**) Cytotoxicity and Induction of Proinflammatory Cytokines from Human Monocytes Exposed to Fine ($PM_{2.5}$) and Coarse Particles ($PM_{10–2.5}$) in Outdoor and Indoor Air. *Toxicology and Applied Pharmacology* 155, 245-252.

Murphy W.K., Sears G.W. (**1964**) Production of Particulate Beams. *Journal of Applied Physics* 35, 1986.

Nel A. (**2005**) Air Pollution-Related Illness: Effects of Particles. *Science* 308, 804-806.

Nel A., Xia T., Mädler L., Li N. (**2006**) Toxic Potential of Materials at the Nanolevel. *Science* 311, 622-627.

Ng N.L., Canagaratna M.R., Jimenez J.L., Zhang Q., Ulbrich I.M., Worsnop D.R. (**2011**) Real-time methods for estimating organic component mass concentrations from aerosol mass spectrometer data. *Environmental Science & Technology* 45(3), 910–916.

Norton S.A., Kahl J.S., Brakke D.F., Brewer G.F., Haines T.A., Nodvin S.C. (**1988**) Regional patterns and local variability of dry and occult deposition strongly influence sulfate concentrations in Maine lakes. *The Science of the Total Environment* 72, 183-196.

Owega S., Khan B.U.Z., D'Souza R., Evans G.J., Fila M., Jervis R.E. (**2004**) Receptor Modeling of Toronto PM2.5 Characterized by Aerosol Laser Ablation Mass Spectrometry. *Environmental Science & Technology* 38, 5712-5720.

Paatero P., Tapper U. (**1994**) Positive Matrix Factorization: a non-negative factor model with optimal utilization of error estimates of data values. *Environmetrics* 5, 111-126.

Paatero P. (**1998**) User's Guide for Positive Matrix Factorization programs PMF2 and PMF3.

Patashnick H., Rupprecht E.G. (**1991**) Continuous PM-10 measurements using the tapered element oscillating microbalance. *Journal of the Air and Waste Management Association* 41(8), 1079-1084.

Pekney N.J., Davidson C.I., Bein K.J., Wexler A.S., Johnston M.V. (**2006**) Identification of sources of atmospheric PM at the Pittsburgh Supersite, Part I: Single particle analysis and filter-based positive matrix factorization. *Atmospheric Environment* 40, S411-S423.

Pio C., Cerqueira M., Harrison R.M., Nunes T., Mirante F., Alves C., Oliveira C., Sanche de la Campa A., Artíñano B., Matos M. (**2011**) OC/EC ratio observations in Europe: Re-thinking the approach for apportionment between primary and secondary organic carbon. *Atmospheric Environment* 45, 6121-6132.

Pope C.A., Thun M.J., Namboodiri M.M., Dockery D.W., Evans J.S., Speizer F.E., Heath C.W. (**1995**) Particulate air pollution as a predictor of mortality in a prospective study of U.S. adults. *American Journal of Respiratory and Critical Care Medicine* 151, 669-674.

Pöschl U. (**2005**) Atmospheric Aerosols: Composition, Transformation, Climate and Health Effects. *Angewandte Chemie* 44, 7520-7540.

Pósfai M., Buseck P.R. (**2010**) Nature and Climate Effects of Individual Tropospheric Aerosol Particles. *Annual Review of Earth and Planetary Sciences* 38, 17-43.

Quaas J. (**2011**) The soot factor. *Nature* 471, 456-457.

Rader D.J., McMurry P.H. (**1986**) Application of the tandem differential mobility analyzer to studies of droplet growth or evaporation. *Journal of Aerosol Science* 17(5), 771-787.

Ramanathan V., Crutzen P.J., Kiehl J.T., Rosenfeld D. (**2001**) Aerosols, Climate, and the Hydrological Cycle. *Science* 294, 2119-2124.

Ramanathan V., Ramana M.V., Roberts G., Kim D., Corrigan C., Chung C., Winker D. (**2007**) Warming trends in Asia amplified by brown cloud solar absorption. *Nature* 448:575–78.

Rasool S.I., Schneider S.H. (**1971**) Atmospheric Carbon Dioxide and Aerosols: Effects of Large Increases on Global Climate. *Science* 173, 138-141.

Ravindra K., Sokhi R., Van Grieken R. (**2008**) Atmospheric polycyclic aromatic hydrocarbons: Source attribution, emission factors and regulation. *Atmospheric Environment* 42, 2895-2921.

Rebotier T.P., Prather K.A. (**2007**) Aerosol time-of-flight mass spectrometry data analysis: A benchmark of clustering algorithms. *Analytica Chimica Acta* 585, 38-54.

Reilly P.T.A., Lazar A.C., Gieray R.A., Whitten W.B., Ramsey J.M. (**2000**) The elucidation of charge-transfer-induced matrix effects in environmental aerosols via real-time aerosol mass spectral analysis of individual airborne particles. *Aerosol science and Technology* 33, 135-152.

Reinard M.S., Johnston M.V. (**2008**) Ion formation mechanism in laser desorption ionization of individual particles. *Journal of the American Society for Mass Spectrometry* 19(3), 389-399.

Reisen F., Meyer C.P., McCaw L., Powell J.C., Tolhurst K., Keywood M.D., Gras J.L. (**2011**) Impact of smoke from biomass burning on air quality in rural communities in southern Australia. *Atmospheric Environment* 45(24), 3944-3953.

Reiss R., Anderson E.L., Cross C.E., Hidy G., Hoel D., McClellan R., Moolgavkar S. (**2007**) Evidence of health impacts of sulfate-and nitrate-containing particles in ambient air. Inhalation toxicology 19(5), 419-449.

Seinfeld J.H., Pandis S.N. (**1998**) Atmospheric chemistry and physics: from air pollution to climate change. Wiley-Interscience publications.

Simon H., Bhave P.V., Swall J.L., Frank N.H., Malm W.C. (**2011**) Determining the spatial and seasonal variability in OM/OC ratios across the US using multiple regression. *Atmospheric Chemistry and Physics* 11, 2933-2949.

Sinclair D., Hoopes G.S. (**1975**) A continuous flow condensation nucleus counter. *Aerosol Science* 6, 1-7.

Spencer M.T., Shields L.G., Sodeman D.A., Toner S.M., Prather K.A. (**2006**) Comparison of oil and fuel particle chemical signatures with particle emissions from heavy and light duty vehicles. *Atmospheric Environment* 40, 5224-5235.

Sportisse B. (**2010**) Fundamentals in Air Pollution: From Processes to Modelling. Ed. Springer, 2010.

Stevens B., Feingold G. (**2009**) Untangling aerosol effects on clouds and precipitation in a buffered system. *Nature* 461, 607-613.

Stortini A.M., Freda A., Cesari D., Cairns W.R.L., Contini D., Barbante C., Prodi F., Cescon P., Gambaro A. (**2009**) An evaluation of the PM2.5 trace elemental composition in the Venice Lagoon area and an analysis of the possible sources. *Atmospheric Environment* 43, 6296-6304.

Su Y., Sipin M.F., Furutani H., Prather K.A. (**2004**) Development and Characterization of an Aerosol Time-of-Flight Mass Spectrometer with Increased Detection Efficiency. *Analytical Chemistry* 76, 712-719.

Suess D.T., Prather K.A. (**1999**) Mass Spectrometry of Aerosols. *Chemical Reviews* 99, 3007-3035.

Stoffels J.J., Ells D.R., Bond L.A., Freedman P.A., Tattersall B.N., Lagergren C.R. (**1994**) A triple-sector mass spectrometer with high transmission efficiency and 10^{-11} isotope-abundance sensitivity. *International Journal of Mass Spectrometry and Ion Processes* 132, 217-224.

Sutton M.A., Dragosits U., Tang Y.S., Fowler D. (**2000**) Ammonia emissions from non-agricultural sources in the UK. *Atmospheric Environment* 34, 855-869.

Tanner P.A. (**2009**) Vehicle-related ammonia emissions in Hong Kong. *Environmental Chemistry Letters* 7, 37-40.

Tauler R. (**1995**) Multivariate curve resolution applied to second order data. *Chemometrics and Intelligent Laboratory Systems* 30, 133-146.

Thomas R.M., Trebs I., Otjes R., Jongejan P.A.C., Brink H.T., Phillips G., Kortner M., Meixner F.X., Nemitz E. (**2009**) An automated analyzer to measure surface-atmosphere exchange fluxes of water soluble inorganic aerosol compounds and reactive trace gases. *Environmental Science & Technology* 43 (5), 1412-1418.

Thomson D.S., Murphy D.M. (**1993**) Laser-induced ion formation thresholds of aerosol particles in a vacuum. *Applied Optics* 32, 6818-6826.

Thomson D.S., Middlebrook A.M., Murphy D.M. (**1997**) Thresholds for laser-induced ion formation from aerosols in a vacuum using ultraviolet and vacuum-ultraviolet laser wavelengths. *Aerosol Science and Technology* 26, 544-559.

Thornhill D.A., Williams A.E., Ornasch T.B., Wood E., Herndon S.C., Kolb C.E., Knighton W.B., Zavala M., Molina L.T., Marr L.C. (**2010**) Application of positive matrix factorization to on-road measurements for source apportionment of diesel- and gasoline-powered vehicle emissions in Mexico City. *Atmospheric Chemistry and Physics* 10, 3629-3644.

Topinka J., Rossner P.Jr, Milcova A., Schmuczerova J., Svecova V., Sram R.J. (**2011**) DNA adducts and oxidative DNA damage induced by organic extracts from PM2.5 in an acellular assay. *Toxicology Letters* 202, 186-192.

Trautner F., Frank G., Tschiersch J., Voigt G. (**1990**) A method to quantify wet and occult deposition of aerosol to wheat plants. *Journal of Aerosol Science* 21 (S1), S295-S298.

Tsimpidi A.P., Karydis V.A., Zavala M., Lei W., Molina L., Ulbrich I.M., Jimenez J.L., Pandis S.N. (**2010**) Evaluation of the volatility basis-set approach for the simulation of organic aerosol formation in the Mexico City metropolitan area. *Atmospheric Chemistry and Physics* 10, 525-546.

Turpin B.J., Huntzicker J.J., Adams K.M. (**1990**) Intercomparison of photoacoustic and thermal-optical methods for the measurement of atmospheric elemental carbon. *Atmospheric Environment* 24A (7), 1831-1836.

Ulbrich I.M., Canagaratna M.R., Cubison M.J., Zhang Q., Ng N.L., Aiken A.C., Jimenez J.L. (**2011**) Three-dimensional factorization of size-resolved organic aerosol mass spectra from Mexico City. *Atmospheric Measurement Techniques Discussion* 4, 4561–4630. doi:10.5194/amtd-4-4561-2011.

van Eeden S.F., Tan W.C., Suwa T., Mukae H., Terashima T., Fujii T., Qui D., Vincent R., Hogg J.C. (**2001**) Cytokines Involved in the Systemic Inflammatory Response Induced by Exposure to Particulate Matter Air Pollutants (PM_{10}). *American Journal of Respiratory and Critical Care Medicine* 164, 826-830.

Vlasenko A., Slowik J.G., Bottenheim J.W., Brickell P.C., Chang R.Y.-W., MacDonald A.M., Shantz N.C., Sjostedt S.J., Wiebe H.A., Leaitch W.R., Abbatt J.P.D. (**2009**) Measurements of VOCs by proton transfer reaction mass spectrometry at a rural Ontario site: Sources and correlation to aerosol composition. *Journal of Geophysical Research* 114, D21305.

Wang S.C., Flagan R.C. (**1990**) Scanning electrical mobility spectrometer. *Aerosol Science and Technology* 13, 230-240.

Wang J., Yang S., Zhao Q., Cui S. (**2012**) Analyses of aerosol properties in Hefei based on polarization measurements of a sun photometer. *International Journal of Remote Sensing* 33(1), in press. Available on-line: http://www.tandfonline.com/doi/abs/10.1080/01431161.2011.562254

Warneck P. (**1987**) Chemistry of the natural atmosphere. *International Geophysics Series*, vol.41. Academy press, pp757.

Wenzel R.J., Liu D.Y., Edgerton E.S., Prather K.A. (**2003**) Aerosol time-of-flight mass spectrometry during the Atlanta supersite experiment: 2. scaling procedures. *Journal of Geophysical Research-Atmosphere* 108(D7), 8427.

Wexler, A. S. and Johnston, M. V. (**2008**) What have we learned from highly time-resolved measurements during EPA's supersites program and related studies?. *Journal of Air Waste Management* 58, 303-319.

Whitby K.T., Clark W.E. (**1966**) Electrical aerosol particle counting and size distribution measuring system for the 0.015 to 1.0 μm size range. *Tellus* 13, 573-586.

Whitby K.T., Cantrell B.K. (**1976**) Atmospheric aerosols: characteristics and measurement. *Proceedings of the International Conference on Environmental Sensing and Assessment (ICESA)*, Institute of Electrical and Electronic Engineers (IEEE). IEEE #75-CH 1004-1, ICESA paper 29-1, Washington, DC: IEEE. p. 6.

WHO (**2005**) WHO Air quality guidelines for particulate matter, ozone, nitrogen dioxide and sulfur dioxide Global update 2005 Summary of risk assessment; available at: http://whqlibdoc.who.int/hq/2006/WHO_SDE_PHE_OEH_06.02_eng.pdf

Willeke K., Liu B.Y.H. (**1976**) Single particle optical counter: principle and application. In: Liu, B.Y.H. (Ed.), *Fine Particles: Aerosol Generation, Measurement, Sampling and Analysis*, Academic Press Inc., New York, pp. 698-729.

Williams J., de Reus M., Krejci R., Fischer H., Ström J. (**2002**) Application of the variability-size relationship to atmospheric aerosol studies: estimating aerosol lifetimes and ages. *Atmospheric Chemistry and Physics* 2, 133-145.

Wilson W.E., Chow J.C. (**2002**) Monitoring of particulate matter outdoors. *Chemosphere* 49, 1009-1043.

Zhang X., Smith K.A., Worsnop D.R., Jimenez J., Jayne J.T., Kolb C.E. (**2002**) A Numerical Characterization of Particle Beam Collimation by an Aerodynamic Lens-Nozzle System: Part I. An Individual Lens or Nozzle. *Aerosol Science and Technology* 36, 617-631.

Zhang X., Smith K.A., Worsnop D.R., Jimenez J., Jayne J.T., Kolb C.E., Morris J., Davidovits P. (**2004**) Numerical Characterization of Particle Beam Collimation: Part II Integrated Aerodynamic-Lens–Nozzle System. *Aerosol Science and Technology* 38, 619-638.

Zhang T., Claeys M., Cachier H., Dong S., Wang W., Maenhaut N., Liu X. (**2008**) Identification and estimation of the biomass burning contribution to Beijing aerosol using levoglucosan as a molecular marker. *Atmospheric Environment* 42(29), 7013-7021.

Zhang Q., Jimenez J.L., Canagaratna M.R., Ulbrich I.M., Ng N.L., Worsnop D.R., Sun Y. (**2011**) Understanding atmospheric organic aerosols via factor analysis of aerosol mass spectrometry: a review. *Analytical and Bioanalytical Chemistry* 401, 3045-3067.

Zhang X., Li J., Yang W., Blasiak W. (**2011**) Formation Mechanism of Levoglucosan and Formaldehyde during Cellulose Pyrolysis. *Energy & Fuels* 25, 3739-3746.

Zhao Y., Gao Y. (**2008**) Acidic species and chloride depletion in coarse aerosol particles in the US east coast. *Science of the Total Environment* 407(1), 541-547.

Zhuang B., Jiang F., Wang T., Li S., Zhu B. (**2011**) Investigation on the direct radiative effect of fossil fuel black-carbon aerosol over China. *Theoretical and Applied Climatology* 104, 301-312.

Zimmermann R. (**2011**) Ambient aerosols and human health: working towards a combined analytical and toxicological approach. *Analytical and Bioanalytical Chemistry* 401, 3041-3044.

Annex 1. Codes

1. Data pre-treatment

Regarding PMF analysis, single particle mass spectra exported from MS-Analyze into MS-Access database were treated using the following approach:

1. From MS-Access database, in which, inside “peaks” table data are organized in the following fields: “Filename”, “MassToCharge”, “PeakArea”, “RelPeakArea” and “PeakHeight”, the fields “Filename”, “MassToCharge”, “PeakArea” were exported in a *.txt file;

2. the *.txt file obtained were imported into R in order to make a cross-tabulation obtaining the matrix to subject to PMF analysis, in which row names are “Filename”, column names are “MassToCharge” and values are “PeakArea”. The R-codes utilized are:

- *Emep08 <- read.table("C:/.../*.txt", header=TRUE, sep=",", na.strings="NA", dec=".", strip.white=TRUE)*
- *write.table(xtabs(PeakArea~Filename+MassToCharge, data=Emep08), "C:/.../*.txt", sep=",", col.names=TRUE, row.names=TRUE, quote=FALSE, na="NA").*

2. Random selection of particles

For the PMF on sub-datasets obtained from random sampling of particles, 3 matrices representing the 10% of the entire dataset (68159 particles) were random selected using the software R:

- *MR09 <- read.table("C:/.../*.txt", header=TRUE, sep=",", na.strings="NA", dec=".", strip.white=TRUE)*
- *s <- sample(1:nrow(MR09), trunc(nrow(MR09)*0.1))*
- *write.table(MR09[s,]), "C:/.../*.txt", sep=",", col.names=TRUE, row.names=TRUE, quote=FALSE, na="NA").*

Annex 2. List of Abbreviations

AFL	Aerodynamic focusing lens
ALS-MCR	Alternating Least Square-Multivariate Curve Resolution
AMS	Aerosol Mass Spectrometer
APS	Aerodynamic Particle Sizer
ATOFMS	Aerosol Time Of Flight Mass Spectrometer
BBOA	Biomass Burning Organic Aerosol
CMB	Chemical Mass Balance
CPC	Condensation Particle Counter
DMA	Differential Mobility Analyzer
EC	Elemental Carbon
GRAEGOR	GRadient of AErosol and Gases Online Registrator
HOA	Hydrocarbon-like Organic Aerosol
HTDMA	Hygroscopic Tandem Differential Mobility Analyzer
LAMMS	Laser Microprobe Mass Spectrometry
LDI	Laser Desorption/Ionization
NIT	Nitrate
OA	Organic Aerosol
OC	Organic Carbon
OOA	Oxidized Organic Aerosol
Org	Non-refractory organic aerosol
OPC	Optical Particle Counter
PAHs	Polycyclic Aromatic Hydrocarbons
PCA	Principal Component Analysis
PCFA	Principal Component Factor Analysis
PM	Particulate Matter
PMF	Positive Matrix Factorization
PTR-MS	Proton Transfer Reaction Mass Spectrometry
RH	Relative Humidity
SIMS	Secondary Ion Mass Spectrometry
SMPS	Scanning Mobility Particle Sizer
SOA	Secondary Organic Aerosol
SUL	Sulphate

TOFMS	Time Of Flight Mass Spectrometer
VOCs	Volatile Organic Compounds

Annex 3. Study of atmospheric particles deposition into human lungs

Particulate air pollution represents one of the most urgent worldwide problems for human health. Epidemiological studies have evidenced the association between exposure to PM and health outcomes. A recent meta-analysis of epidemiological data and measured PM concentration in Europe, by the Clean Air For Europe (CAFE) steering group of the European Commission, has depicted the estimating loss of life expectancy due to exposure to fine particulate matter. The estimated loss of life expectancy can exceed 12 months in European urbanized areas and 36 months in Holland and in the Po Valley [Zimmermann 2011, CAFE 2011].

However, epidemiological studies so far, has been based principally to measurements of PM_{10} and $PM_{2.5}$ concentrations typically taken from a single central monitoring location.

The hazard caused by aerosol particles depends both on their chemical composition and on the site at which they deposit within the respiratory system which is likewise related to their size distributions. From the standpoint of respiratory deposition, the respiratory system could be divided into three regions, each covering several anatomic units. The first unit is the extrathoracic region (ET) comprising the anterior nose (ET1) and the posterior nasal passages, larynx, pharynx and mouth (ET2). The second unit is the tracheobronchial region (TB) consisting of the trachea and main bronchi (BB) and bronchioles and terminal bronchioles (bb). The third unit is the alveolar-interstitial region (AI) consisting of the respiratory bronchioles, the alveolar ducts and sacs with their alveoli and their interstitial connective tissue [ICRP 66, Hinds 1999]. Predicting the deposition from basic theory is very difficult because respiratory deposition occurs in a system of changing geometry, with a flow that changes with time and cycles in direction [Hinds 1999]. Anyway, lung deposition is a function of particle size. Size distributions influence total depositions but they also determine the regional deposition which will turn in different health outcomes.

In this study, conducted during a visit to the research group of Professor Roy M. Harrison of the Department of Geography, Earth & Environmental Sciences at the University of Birmingham (UK), particle counts and size distributions were measured by a Scanning Mobility Particle Sizer (SMPS) and Aerodynamic Particle Sizer (APS) in different locations during the REPARTEE II project [Harrison 2011]. APS and SMPS size distributions were merged using a computer program developed for the

purpose [Beddows 2010], which calculates an effective density of particles that can be used to estimate the mass concentration. The particle concentration for each size bin was then multiplied by the lung deposition efficiency calculated at the corresponding size (figure A3.1) from the ICRP66 deposition model [ICRP66]. The deposition in the three major respiratory regions was then integrated across all the size distributions and compared to the measured ambient PM concentrations.

The results of this study show that PM_{10} mass concentration could be a good predictor of the mass dose in all regions of the lung but, on the contrary it is not a good predictor of surface area and particle number dose. On the other hand, measurement of total ambient particle number concentration do not well predict mass dose [Harrison 2010]. Thus, epidemiological studies are critically dependent upon the metric used and it is likely that the public health impacts from PM exposure have been so far underestimated [Harrison 2010].

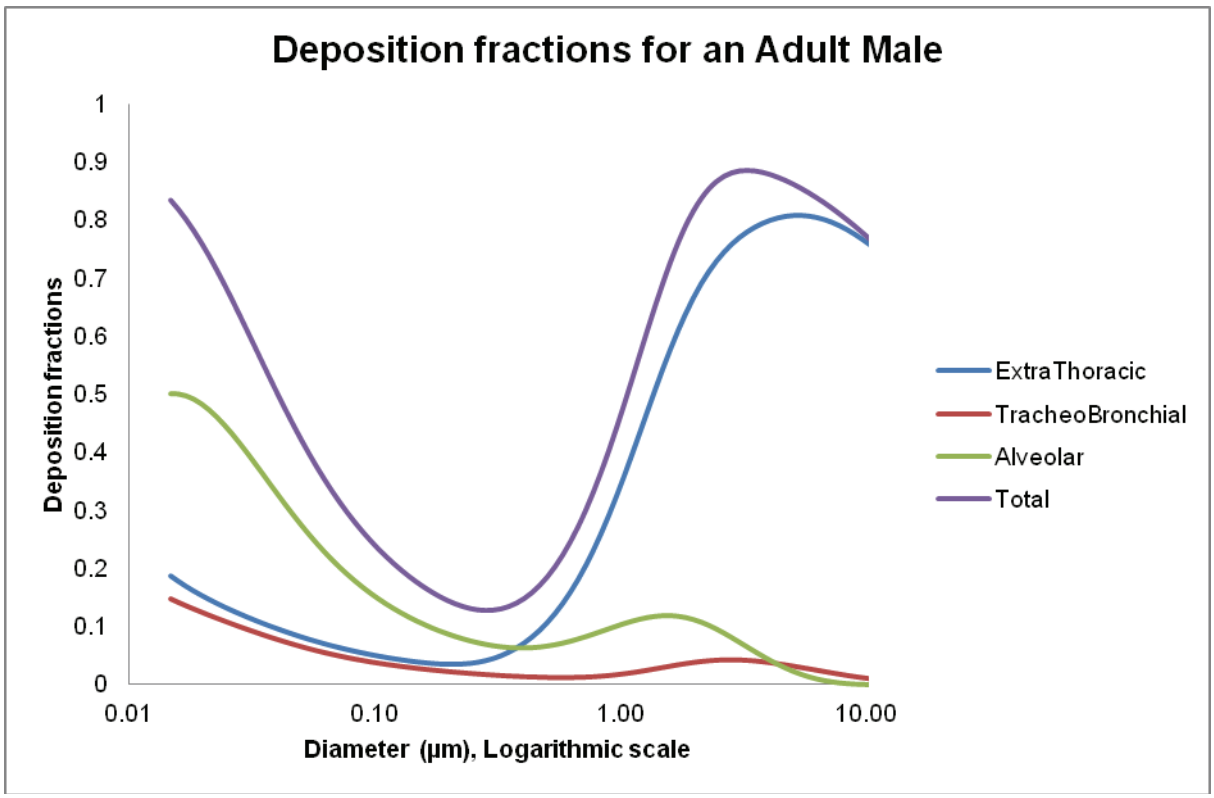

Figure A3.1. Size segregated deposition fractions for an adult male, who breath from the nose and is engaged in a light exercise (representative of outdoor exposure).

References

Beddows D.C.S., Dall'Osto M., Harrison R.M. (**2010**) An enhanced procedure for the merging of atmospheric particle size distribution data measured using electrical mobility and time-of-flight analysers. *Aerosol Science and Technology* 44, 930-938.

Harrison R.M., Giorio C., Beddows D.C.S., Dall'Osto M. (**2010**) Size distribution of airborne particle controls outcome of epidemiological studies. *Science of the Total Environment* 409, 289-293.

Harrison R.M., Dall'Osto M., Beddows D.C.S., Thorpe A.J., Bloss W.J., Allan J.D., Coe H., Dorsey J.R., Gallagher M., Martin C., Whitehead J., Williams P.I., Jones R.L., Langridge J.M., Benton A.K., Ball S.M., Langford B., Hewitt C.N., Davison B., Martin D., Petersson K., Henshaw S.J., White I.R., Shallcross D.E., Barlow J.F., Dunbar T., Davies F., Nemitz, E., Phillips G.J., Helfter C., Di Marco C.F., Smith S. (**2011**) Atmospheric chemistry and physics in the atmosphere of a developed megacity (London): an overview of the REPARTEE experiment and its conclusions. *Atmospheric Chemistry and Physics Discussions* 11, 30145-30271.

Hinds W.C. (**1999**) Aerosol technology: properties, behavior, and measurement of airborne particles. *Wiley-Blackwell*, 2nd Edition, 1999.

International Commission on Radiological Protection (**1994**) "Human Respiratory Tract Model for Radiological Protection", *Annals of the ICRP*, Publication 66, Elsevier Science, Inc. Tarrytown, NY.

Annex 4. SOA aging experiment in a smog chamber-preliminary results

The experiment was carried out at the CESAM smog chamber, in the laboratory of LISA (Laboratoire Interuniversitaire des Systèmes Atmosphériques - Université de Paris Diderot, Université de Paris Est-Créteil, CNRS Créteil-France) in collaboration with the research groups of Professor Jean François Doussin (LISA), dr Paola Formenti (LISA) and Professor Anne Monod of the University of Provence (France).
The aim of the project was to produce secondary organic aerosol (SOA) from the reaction of α-pinene and ozone, in a smog chamber, and to study the modification of optical and hygroscopic properties of particles after two aging processes carried out through the reaction of SOA with an excess of ozone and through irradiation with lights.

1. α-pinene+O_3 reaction

VOCs are emitted into the atmosphere from natural sources in marine and terrestrial environments, as well as from anthropogenic sources. On a global basis the emissions of biogenic volatile organic compounds (BVOCs), which are emitted mainly by vegetation, are estimated to exceed those from anthropogenic emissions. Isoprene accounts for about half of all natural VOC emissions and is, on a mass basis, the dominant emitted biogenic VOC. However isoprene is generally not considered as a major producer of SOA. Most important terpenes - after isoprene - are monoterpenes which represent a significant fraction of BVOCs emitted with contributions ranging from 10 to 50% [Kanakidou 2005]. The most naturally abundant monoterpene in the troposphere is α-pinene. The atmospheric oxidation of α-pinene is known to form low-volatility products which can be incorporated into SOA, and initiation by ozonolysis is the most efficient reaction respect to initiation with OH and NO_3 radicals [Ma 2007, Ma 2008].
The higher molecular weight carboxylic acids and dicarboxylic acids, including pinic and pinonic acids, have been suggested as key species in gas-to-particle conversion processes [Ma 2008].
The first steps of the reaction mechanism, generally accepted, is reported in figure A4.1. Briefly, the initial step of α-pinene ozonolysis follows the ‘Criegee mechanism’ [Criegee 1975].

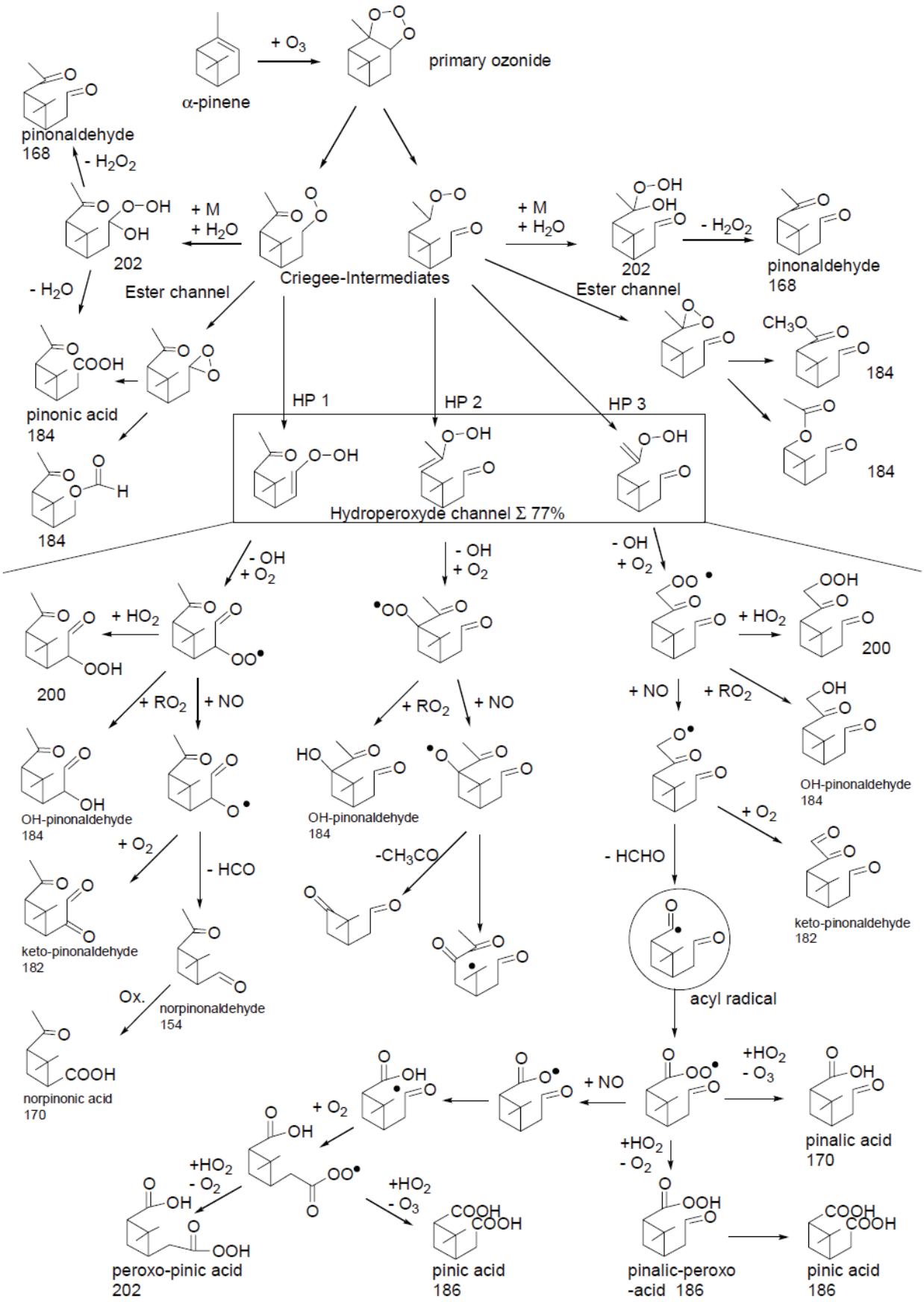

Figure A4.1. α-pinene with ozone reaction mechanism [Winterhalter 2003]

The cycloaddition of ozone to the α-pinene double bond leads initially to an energy-rich primary ozonide (POZ), which promptly decomposes to two excited carbonyl substituted Criegee intermediates (CIs), CI1 and CI2. The most important pathways of the two intermediates are suggested to be stabilisation by collisions and decomposition via hydroperoxide channel and ester channel. Moreover they could react with other species, including water, alcohols, acids, carbonyls, etc. often named as SCI (Stabilised Criegee Intermediates) scavengers [Ma 2007, Ma 2008, Winterhalter 2003].

2. Materials and Methods

2.1. Smog chamber

The CESAM chamber (Experimental Multiphase Atmospheric Simulation Chamber) is designed to allow researchs in atmospheric chemistry and photo-chemistry which involves both gas phase and condensed phase processes including aerosol and cloud chemistry [Wang 2011].

Figure A4.2. CESAM (Chambre Expérimentale de Simulation Atmosphérique Multiphasique)

It consists of a 4.2 m^3 stainless steel vessel equipped with three 4-KW high pressure xenon arc lamps (MH-Diffusion®, MacBeam™ 4000) positioned above the chamber which are able to simulate the solar irradiation in the boundary layer. The chamber is connected to the ground to prevent any electrical charge build-up. The reactor body

is made of double layers which may allow circulating a warm or cold fluid around in order to control the reactor temperature. The inner wall is polished in order to minimize the specific surface area and to provide a good light reflection inside the chamber. The chamber is equipped with a vacuum system which consists of two pumps for both gas and aerosol evacuation: a screw pump (Bush® Cobra™ N0100-0300B) and a secondary turbo pump (Leybold® Turbovac 361®). The vacuum limit falls in the range of 10^{-4} mbar. A 4-wing stainless steel fan of 50 cm of diameter is installed inside the reactor, at the bottom of the chamber to mix gas and particles. The mixing time for an homogeneous concentration inside the chamber is less than 60 seconds.

In the chamber it is possible to generate clouds by fast expansion or saturation in order to have a multiphase aerosol-droplet interaction. Particles lifetime in the chamber ranges from 10 hours to 4 days depending on PM size distribution which indicates that the chamber is perfectly suitable for aging processes studies since it simulates particles lifetime in the atmosphere.

CESAM is equipped with a large panel of analytical instruments for both gas and particles monitoring and speciation. Moreover, a number of available ports provide the possibility to connect other instruments. During each experiment it is possible to measure the pressure inside the chamber (two capacitance manometers MKS® Baratrons® 622A and 626A), temperature and relative humidity (HMP234 Vaisala® transmitter equipped with a capacitive thin-film polymer sensor Humicap®). Different monitors are installed for gaseous species measurements: ozone (APOA-370 Horiba®), NO and NO_2 (APNA-370 Horiba®). Moreover a Fourier transform infra-red spectrometer Bruker® Tensor37™ is installed. The aerosol phase measurements utilize SMPS (Scanning Mobility Particle Sizer TSI® 3010) to monitor particles number concentration and size distribution in the range of 10-500 nm diameter and an optical particle counter (Palas® Welas digital 2000™) for particles in the range of 0.1-20 µm diameter. Moreover, in the experiments of interest an aerosol mass spectrometer (AMS) was connected to the smog chamber.

2.2. AMS

The AMS, Aerosol Mass Spectrometer (Figure A4.3a), uses aerodynamic lens inlet technology together with thermal vaporization and electron-impact mass

spectrometry to measure the real-time non-refractory chemical speciation and mass loading as a function of particle size of fine aerosol particles with aerodynamic diameters between 50 and 1000 nm [Canagaratna 2007]. The instrument has three main sections: the aerosol inlet, the particle sizing chamber, and the particle composition detection section (Figure A4.3b). The aerosol inlet samples sub-micron aerosol particles into the AMS which pass through a series of aerodynamic lenses, forming a narrow particle beam which is transmitted into the detection chamber where the non-refractory components are flash vaporized upon impact on a hot surface (600°C) under high vacuum (10^{-5} Pa) and chemically analyzed via EI ionization and time-of-flight mass spectrometry. The beam transmission to the particle detector can be modulated with a mechanical chopper that is operated at 100-150 Hz. The chopper could be placed in one of the three positions: “closed” position which blocks the beam completely, “open” position which transmits the beam continuously, and “chopped” position which modulates the beam transmission with 1-4% duty cycle that is determined by the width of the chopper slit [Canagaratna 2007, Drewnick 2005].

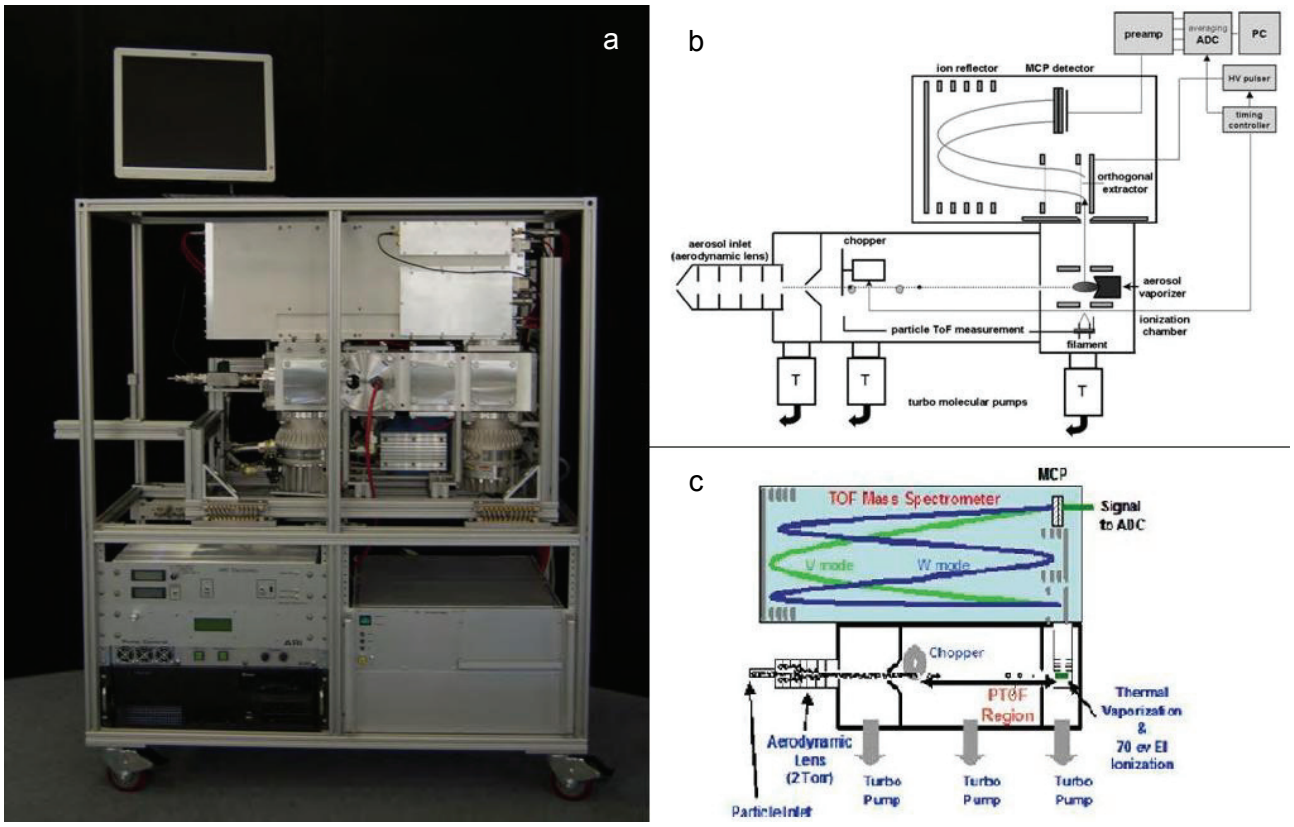

Figure A4.3. Aerodyne High Resolution Time-of-Flight Aerosol Mass Spectrometer (HR-ToF-AMS) (a) picture, (b) operation scheme and (c) V/W path of ions into the time-of-flight analyzer.

The AMS is typically alternated between two modes of operation: mass spectrum (MS) mode and particle ToF (PToF) mode [Jimenez 2003]. In MS mode, the chopper is in open position to obtain an ensemble averaged MS of the sampled aerosol. Signals from the ionization of background gases in the detection region are accounted for by subtracting the background MS obtained with the chopper in closed position. In the PToF mode, the chopper modulates the particle beam in order to measure particle flight times from the chopper to the detector [Jayne 2000]. The velocity acquired by particles when they exit the aerodynamic lenses system and expand into vacuum is directly related to their vacuum aerodynamic diameter. The opening of the chopper slit, detected with a LED and photodiode, provides the start time for each PToF measurement cycle. Particle arrival is indicated by the burst of ion signal at the detector.

The instrument has two ion optical modes: a single–reflection configuration (V-MODE) offers higher sensitivity and lower resolving power (up to ~2100 at m/z 200), and a two-reflectron configuration (W-MODE) yields higher resolving power (up to ~4300 at m/z 200) with lower sensitivity (Figure A4.3c) [De Carlo 2006].

The signals measured with the AMS (I ion rate in counts per second) can be converted into mass concentrations of aerosol chemical species:

$$C_s = \frac{10^{12} MW_s}{IE_s Q N_A} \sum_{all\ i} I_{s,i}$$

where MW is the molecular weight of the species in g/mol, N_A is Avogadro's number, Q is the volumetric sample flow rate into the instrument in cm^3/s, IE is the ionization efficiency, a dimensionless quantity equalling the number of ions detected per molecule of the parent species, 10^{12} is a factor for unit conversion and the summation is over all fragment ion rates constituting the species after subtraction of the interferences [Jimenez 2003].

While explicit calibrations can be performed for a small number of species, individual calibrations are not practical for the hundreds of known molecular organic species in ambient aerosol. The ionization cross section of a molecule, σ, is linearly related to the number of electrons it contains and since molecules with similar chemical structure and functionality have similar EI cross section-to-electrons ratios, only three distinct proportionality constants, corresponding to inorganic, hydrocarbon and oxygenated organic species are needed to estimate these ratios for a range of molecules. Experiments with lab-generated particles show a linear relationship

between IE and MW [Alfarra 2004]. These results suggest that the IE/MW of any organic or inorganic substance can be expressed as:

$$\frac{IE_S}{MW_S} = RIE_S \frac{IE_{NO_3}}{MW_{NO_3}}$$

RIEs is defined as the relative ionization efficiency of the species respect to nitrate. Nitrate is chosen as the primary mass calibration species for the AMS because it is a common aerosol constituent that produces most of its signal at only two m/z (30 and 46) and it is volatile enough that it evaporates with close to 100% efficiency in a few microseconds upon contact with the tungsten filament [Jayne 2000, Allan 2003, Drewnick 2009, Canagaratna 2007].

2.3. SMPS

The Scanning Mobility Particle Sizer, (SMPS+C, Grimm Aerosol Technik®), consisting of a DMA (Differential Mobility Analyzer, L-DMA type Vienna) and a CPC (Condensation Particle Counter, CPC 5403), measures the size distributions of particles of diameter between 10 and 500 nm. Larger particles are blocked by an impactor mounted upstream of the DMA. Smaller particles enter in the charger region where diffusion charging occurs as a result of random thermal motion of ions and particles, which leads to ion/particle collisions and particles charge by capturing ions. The aerosol sample is exposed to a high ion concentration which are generated by a radioactive source, effective enough to generate stationary state charging conditions. When exiting the charger, the particles have a well-defined charging state as a function of their size. The effects of particle morphology and composition are usually assumed to have only secondary importance and are therefore neglected [Reischl 1996]. The mean charge of particles leaving the charger is close to zero, but a fraction of the particles contain ±1, ±2 charges etc. Multiply charged particles increase with increasing size [McMurry 2000].

Figure A4.4. Scanning Mobility Particle Sizer (SMPS+C, Grimm Aerosol Technik®)

The DMA consists of two coaxial cylinder electrodes, in which particles, that enter through a hole in the outer cylinder (ground connected), are deflected towards the inner cylinder (negatively charged) under the effect of an electric field. The potential of the applied electric field is varied continuously to obtain a scan along the entire size range. Then particles selected are revealed by a CPC. This instrument consists primarily of a saturator, a condenser, and an optical detector. The working fluid is usually an alcohol (butanol in the SMPS+C Grimm). In the CPC particles are grown by condensation of butanol until they are sufficiently large to be detected optically. In the saturator, particles flow into a tank of heated butanol in which they are saturated with its vapours. Supersaturation is then achieved when saturated aerosol enters a laminar-flow cylindrical condenser, the walls of which are typically maintained at ~10°C. In this way particles grow to a diameter in the order of μm and could be detected by an optical system, generally consisting of a laser beam and a photodetector [Reischl 1997, Winkelmair 1991, McMurry 2000].

3. Experiment set-up

The reaction was conducted starting from 100 ppb of both α-pinene and ozone in dark conditions, in atmosphere of N_2 and O_2. The reaction was left occurring for 16 hours. After that there were about 1 hour and a half of samplings, 6 hours of aging processes followed by 2 hours of samplings, and finally the %RH was risen by injecting water vapour into the smog chamber. Throughout the experiment, the

chamber was not thermostated while, on the contrary, humidity and pressure were always monitored. Humidity was maintained at 0% - except during the injection of water vapour - and pressure was maintained at least 10 mbar above the external pressure in order to avoid contaminations during instruments connection. The AMS and the SMPS have been connected for almost the entire duration of the experiments while the other instruments have been used for about 1 hour and a half before the aging processes and for about 2 hours after the aging processes. During the samplings, the outgoing airflow has been compensated by an ingoing airflow of N_2.

The aging processes, of about 6 hours of duration, consisted in: 1. no aging (or time aging), 2. aging through the reaction of SOA with an excess of ozone (~1 ppm), 3. photochemical aging (irradiation with lamps simulating the solar irradiation in the atmospheric boundary layer).

The experimental data are currently under analysis by the various research groups involved in the experiments. My contribution to the project has been focused primarily on the calculation of two parameters: the oxidation grade of particulate matter expressed as the O/C ratio and particles density. By using the AMS and SMPS simultaneously, it is possible to obtain these two parameters which will be used in the study of particles optical and hygroscopic properties.

4. AMS data treatment and O/C calculation

Data collected through the AMS were elaborated using the software ToF-AMS Analysis Toolkit 1.51B (Squirrel) and ToF-AMS HR Analysis 1.10B (Pika).

In order to obtain the mass concentration of every species, the calibration has been optimized and some signals were taken as reference to define the integration parameters such as peak shape and width. The signals considered for the m/z calibration are OH^+, O_2^+, Ar^+, CO_2^+, SO_2^+, $^{182}W^+$, $^{184}W^+$, $^{186}W^+$; with the chopper position closed. Regarding the integration parameters definition - peak width and shape - the signals, taken as reference, are CH^+, OH^+, C_2H^+, O_2^+, $C_3H_2^+$, CO_2^+, $C_4H_2^+$, $C_6H_5^+$.

Usually, N_2^+ signal is used to monitor ionization efficiency decreasing as the N_2 concentration remains constant in the atmosphere. However, this is not the case because during instrumental sampling, the outgoing air flow is compensated with an

ingoing air flow of N_2. Thus, the N_2^+ signal did not remain constant and it was not used to correct species concentration.

After that, all the organic signals (species containing C, H and O) with m/z up to 180 were integrated for a total of 662 ions, including two isotopic species $^{13}CO_2^+$ and $^{15}NN^+$.

A critical point in AMS quantification regards the so call “fragmentation table” that is a table in which all the possible signal interferences are taken into account in order to assign the right contribution to every chemical component. This table is used in the software to calculate the final concentration of every chemical species and it was optimized by the AMS developers during several sampling campaigns in outdoor environment [Allan 2004]. However, in the case of a smog chamber experiment, the interferences contribution could be different and thus the fragmentation table has been modified for the purpose.

The modifications ported to the fragmentation table are:

- deletion of the dependence of O_2 signals from N_2 signal (m/z=28) and their assignment to the air concentration (N_2/O_2 was not constant during the experiments);
- deletion of CO_2 contribution from air (there was not injection of CO_2 in the smog chamber) and assignment of its signal to organic compounds concentration;
- calculation of H_2O^+ signal due to organic as H2O_organic=C_2H_3O during the last part of each experiment (during water injection);
- calculation of OH^+ signal due to organic as OH_organic=0.25*H2O_organic;
- calculation of CO^+ due to organic as CO_organic=CO_2.

These modifications are due to the following reasons. Usually, as the default fragmentation table have been optimized to be used in open field conditions, interferences due to air signals are taken into account by measuring the N_2 signal and by reporting all the other species as fractions of the N_2, taking into account the relative abundance in the atmosphere. This is not possible in our smog chamber experiment as the N_2 concentration was not constant. Therefore, m/z=16 and 32 were assigned to O_2.

Gaseous CO_2 was not injected in the smog chamber. Thus, m/z=44 signal could be considered originated by organic compounds fragmentation. Of course the reaction could produce CO_2. However, its contribution should be not high enough to produce an interference in the AMS measurement.

The H_2O^+ and OH^+ fragments followed the same temporal trend of $C_2H_3O^+$ when the chamber conditions were at 0% RH while they increased during the last hour of each experiment, when water vapour was injected into the chamber. It is likely that H_2O^+ and OH^+ are produced from organic compounds (i.e. hydroperoxides) fragmentation in the ionization step or thermo-decomposition in the vaporization step [Chen 2011]. Therefore, H_2O^+ and OH^+ due to organic compounds were calculated from $C_2H_3O^+$ signal in order to take into account their contribution even during water injection.

The fragment CO^+ signal is completely covered by N_2^+ signal and thus it needs to be estimated. CO^+ is usually estimated from CO_2^+ signal. The ratio between the two has been optimized in open field and chamber experiments, in which a variation between 0.9-1.25 was observed in the ratio CO^+/CO_2^+ [Aiken 2008]. However, this is representative of open field conditions, and in our case should be different. Other studies are necessary in order to better quantify this ratio for SOA from α-pinene and ozone reaction in smog chamber facilities. For the moment, the ratio CO^+/CO_2^+ was left to 1 (default value).

It was experimentally observed that SOA concentration decreased during the three experiments (figure A4.5). This unattended decreasing could be due to a leak or to SOA loss on chamber walls in which residuals of ethanol used during chamber cleaning could have been present. The organic fragments which present the highest concentrations are: CH_3^+, $C_2H_2^+$, $C_2H_3^+$, OH^+, H_2O^+, CO^+, CHO^+, $C_2H_5^+$, $C_3H_3^+$, $C_3H_4^+$, $C_3H_5^+$, C_2HO^+, $C_2H_2O^+$, $C_3H_6^+$, $C_2H_3O^+$, CO_2^+, $C_4H_5^+$, $C_3H_3O^+$, $C_4H_7^+$ and they account for about 70% of the total SOA concentration. The O/C ratio (atomic ratio calculated considering all the 662 fragments) presents an initial decreasing, registered in all the three experiments (figure A4.6). It is still unclear if this initial decreasing of O/C is due to physical/chemical processes or to an instrumental issue. It could be explained by the fact that, at the beginning of each experiment, as there are not particles inside the chamber, particles could be formed only by nucleation which occurs for less volatile/more oxidize organic compounds. Once particles are formed, another mechanism could take place, the condensation of species on already existing particles which could interest even less oxidized/more volatile compounds. Another mechanism that could take place is the dehydration of the most oxidized species in particulate phase.

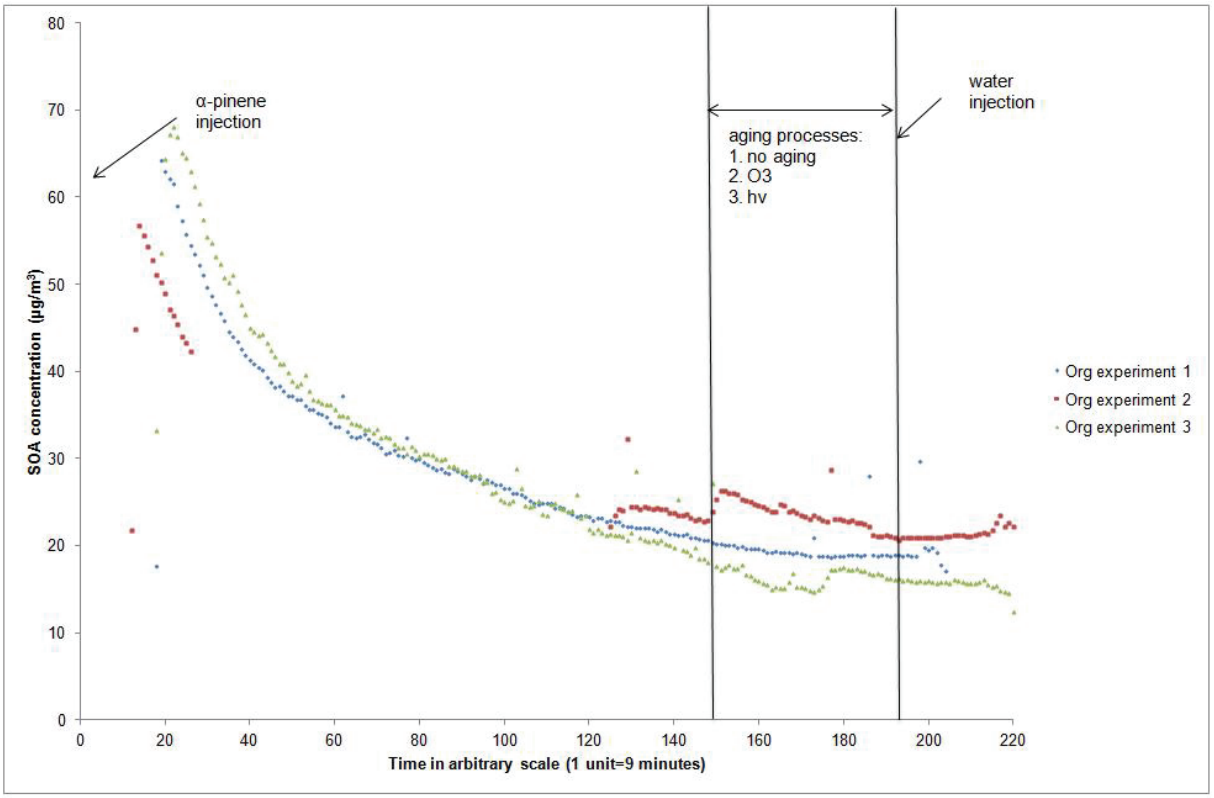

Figure A4.5. Secondary Organic Aerosol concentration during the three experiments

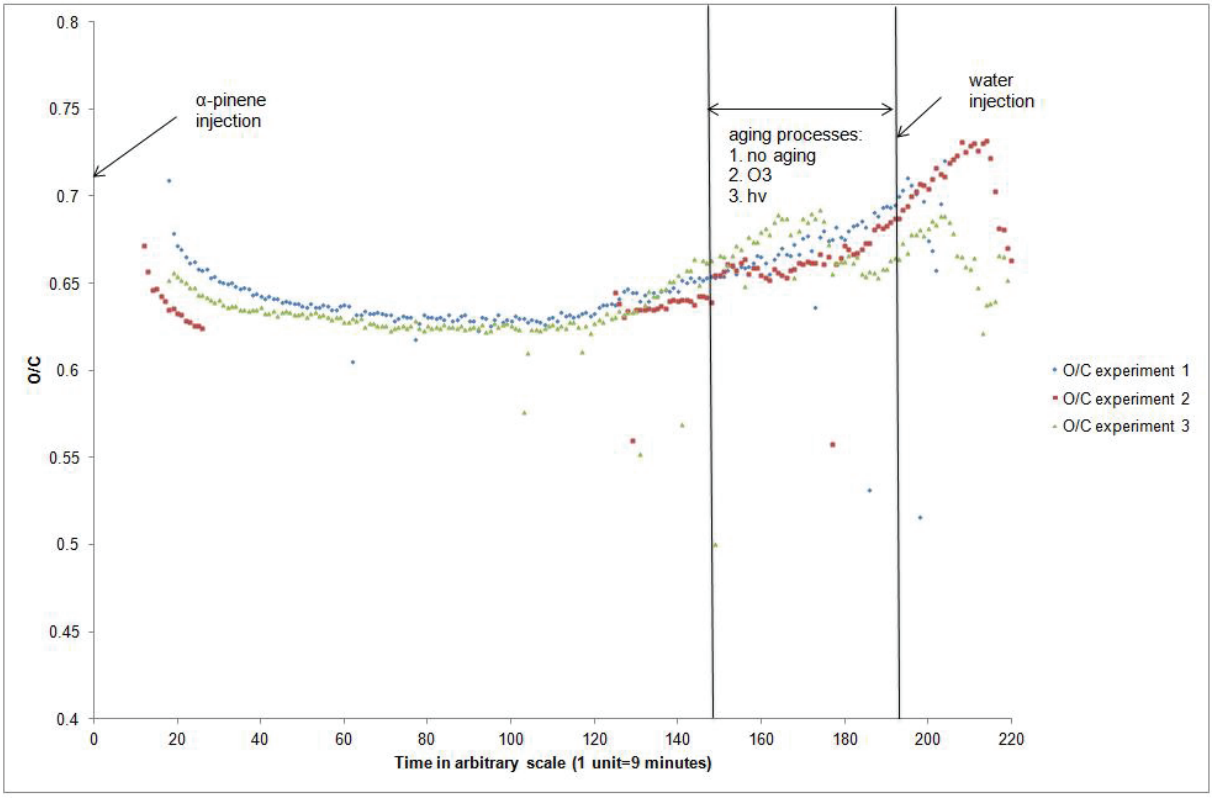

Figure A4.6. O/C ratio during the three experiments

During the aging processes an increasing of both O/C and SOA concentration is registered (figure A4.5 and A4.6). This increasing is rapid and immediate during SOA

aging through reaction with an excess of ozone while it is slower and delayed during the photochemical aging. The increasing in SOA concentration and O/C ratio could be due to chemical reaction of VOCs producing low-volatility compounds which partition in the particulate phase. It is worth to say that during the injection of the excess of O_3, there was some α-pinene left unreacted (due to loss of O_3 from reaction in chamber's walls).

5. Calculation of particle density

An estimation of aerosol effective density (ρ_{eff}) is obtainable by comparing parallel AMS mass distribution measurements in vacuum aerodynamic diameter (d_{va}) and SMPS volume distributions in electrical mobility diameter (d_m). The vacuum aerodynamic diameter is the diameter of a sphere, in the free molecular regime, with unit density (1 g/cm^3) and the same terminal velocity as the particle of interest. The mobility diameter is the diameter of a sphere with the same migration velocity of the particle of interest in a constant electric field at atmospheric pressure. These two measures of particle size are related by "effective density" (ρ_{eff}) or "material density" (ρ_m) as follows:

$$\rho_{eff} = \frac{d_{va}}{d_m}\rho_0 = \rho_m \frac{C_c(d_{ve})}{\delta^3 X_t X_v C_c(d_m)}$$

where ρ_0 is unit density (1 g/cm^3), C_c is the Cunningham slip correction factor, d_{ve} is the volume equivalent diameter, δ is the internal void fraction, χ_t is the dynamic shape factor in the transition regime, and χ_v is the dynamic shape factor in the free molecular regime [Bahreini 2005, Kostenidou 2007].

In order to estimate particle density, first of all, AMS size distributions of SOA (sum of all organic fragments) in mass were exported using the software "Squirrel". SMPS size distributions in number of particles were converted in volume distributions under the assumption of particle sphericity $\frac{dV}{dLogD_m} = \frac{dN}{dLogD_m}\frac{\pi}{6}(d_m)^3$.

As the AMS and SMPS data were collected with different time intervals, they were synchronized by calculating for every SMPS time the corresponding AMS size distribution and the other way round by using a linear interpolation. Once synchronized, the size distributions were normalized. Normalized AMS and SMPS size distributions were log-normally fitted using the software Microcal Origin 8:

$$y = y_0 + \frac{A}{\sqrt{2\pi}wx} e^{-\frac{\left[ln\frac{x}{x_c}\right]^2}{2w^2}}$$

where y is the normalized concentration, y_0 (offset), A (area under the curve), x_c (mean) and w (standard deviation) are the fitting parameters and x is the diameter.

After that, for every SMPS and AMS size distribution, fitting parameters and the fitting equations have been inserted in MS Excel. Mobility diameter and vacuum aerodynamic diameter are linked by $\rho = \frac{d_{va}}{d_m}\rho_0$, which is valid under the assumption of particle sphericity, where ρ is the density in g/cm^3 and ρ_0 is the reference density of 1 g/cm^3. In order to calculate the density, from AMS and SMPS size distributions the following equation cycle has been created in MS Excel:

1- $y_{SMPS} = y_0 + \frac{A}{\sqrt{2\pi}wd_m} e^{-\frac{\left[ln\frac{d_m}{x_c}\right]^2}{2w^2}}$

2- $d_{va} = \frac{\rho d_m}{\rho_0}$

3- $y_{AMS} = y'_0 + \frac{A'}{\sqrt{2\pi}w' d_{va}} e^{-\frac{\left[ln\frac{d_{va}}{x'_c}\right]^2}{2w'^2}}$

4- $\Delta = y_{SMPS} - y_{AMS}$

The density values were modified in order to minimize Δ, using the MS Excel add-in "solver". Thus, the densities in correspondence to each mobility diameter were optimized, by optimizing the overlap between the AMS and SMPS fitted size distributions. In order to repeat the same operation automatically to all the parallel size distributions, a macro has been created.

Using the approach aforementioned, particle density was calculated using the mode diameter of the two parallel size distributions, and then using 12 mobility diameters: 87.5 nm, 100 nm, 112.5 nm, 125 nm, 137.5 nm, 150 nm, 162.5 nm, 175 nm, 187.5 nm, 200 nm, 212.5, 225 nm. To be sure to have obtained the correct densities the calculation has been repeated starting from different initial values of the density (1 and 2 g/cm^3).

In figure A4.7 the results of the three experiments are reported, in figure A4.8 the comparison between the calculated density and the AMS sampling flow rate is reported.

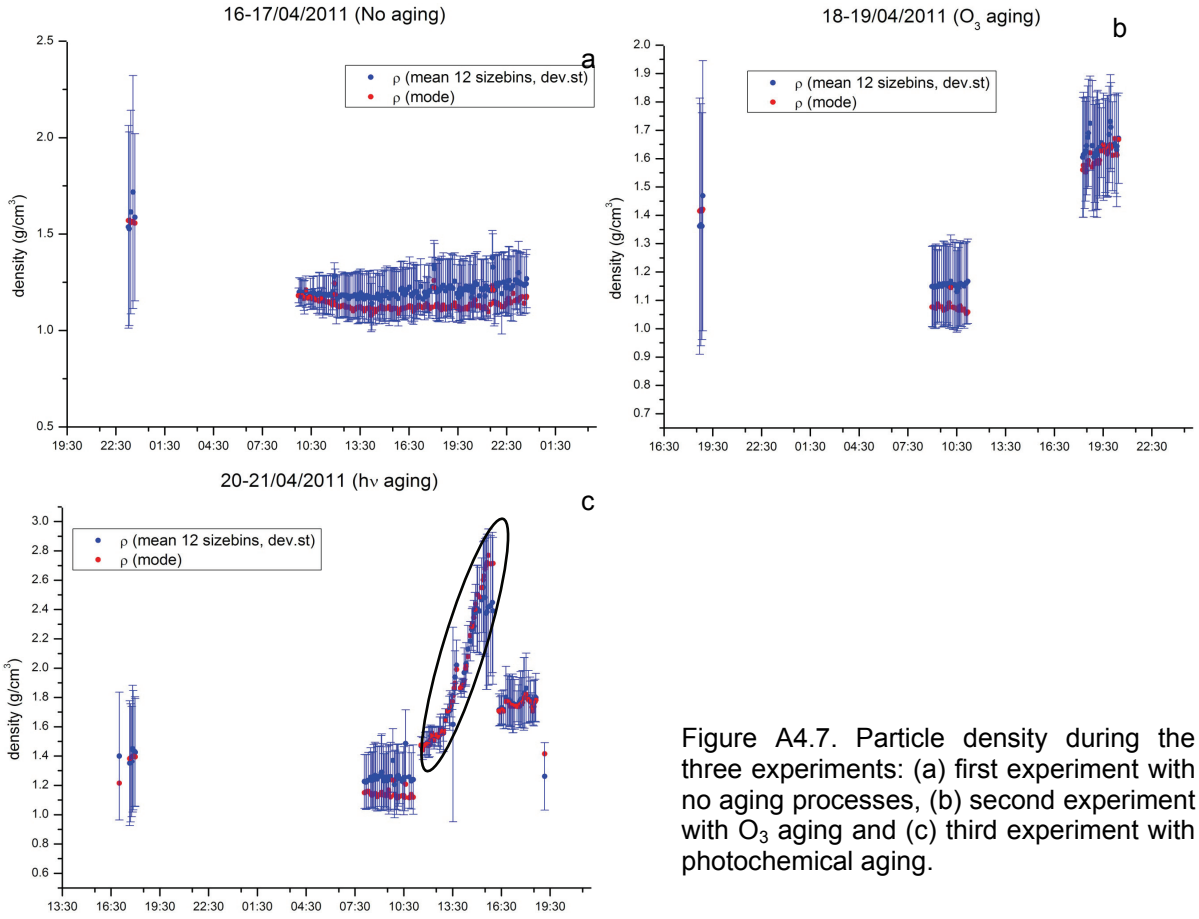

Figure A4.7. Particle density during the three experiments: (a) first experiment with no aging processes, (b) second experiment with O_3 aging and (c) third experiment with photochemical aging.

The calculated densities, using the mode diameter of the distributions or the mean of the 12 selected size bins, are very closed to each other and could be considered equal inside the calculated uncertainties. During the photochemical aging process there was a decreasing of the sampling flow rate of the AMS, probably due to an obstruction of the inlet, so the calculated density during that period of time could not be considered reliable (figure A4.7c and A4.8c).

During the three experiments density seems to decrease at the beginning, when the particulate matter begins to be produced and the AMS was just connected to the chamber. This could confirm the consideration made for O/C ratio, however it is still not clear if it is due to a chemical or an instrumental reason. Considering the second day of each experiment, during the first experiment the SOA density remains constant all the day while during the second and third experiments we can notice an increasing of the density after the aging processes.

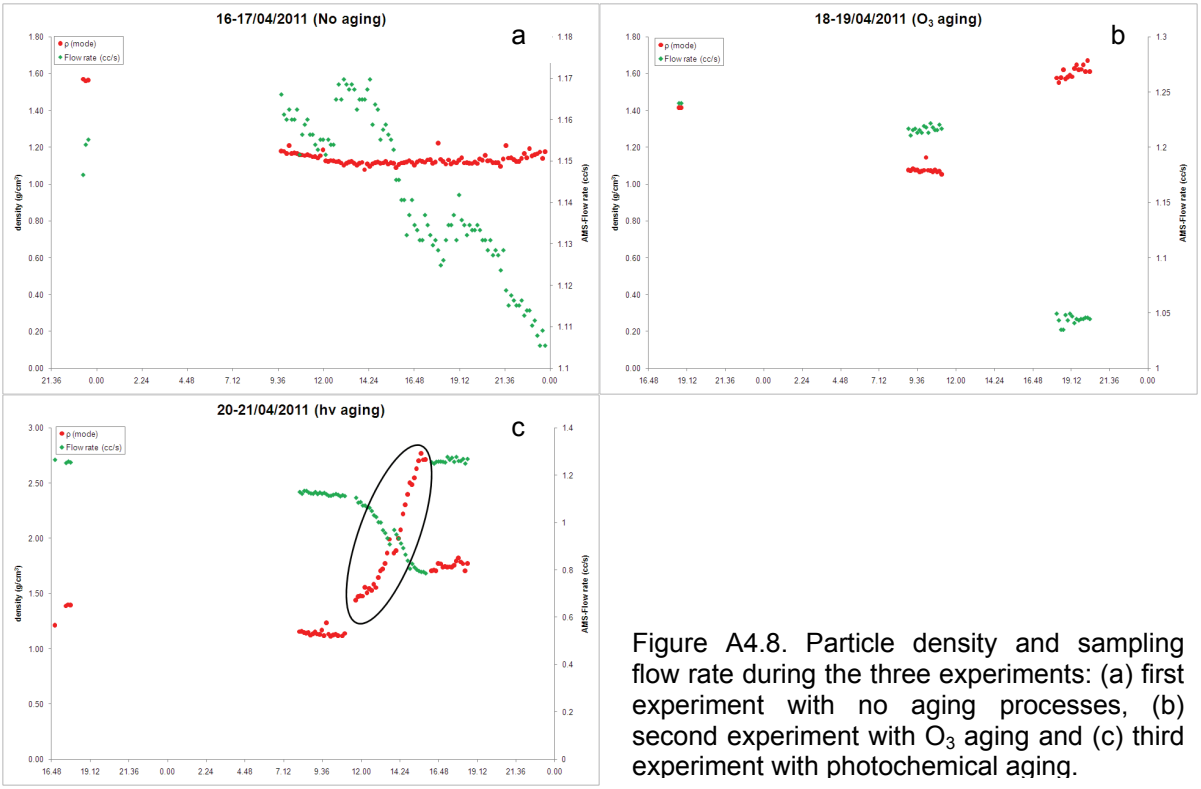

Figure A4.8. Particle density and sampling flow rate during the three experiments: (a) first experiment with no aging processes, (b) second experiment with O_3 aging and (c) third experiment with photochemical aging.

It is worthwhile to notice that during the first experiment the sampling flow rate of AMS decreased of about 0.06 cm^3/s, however the calculated density remain constant while during the second experiment, the sampling flow rate decreased of about 0.15 cm^3/s. It is difficult to understand if this decreasing is enough to affect the measure of the diameter and in this case how much it affects the measure. A strong and evident linear anti-correlation between the calculated density and the sampling flow rate could be seen only for the aforementioned period during the third experiment. In order to see if this difference between the calculated densities before and after the aging processes is significant, a t-test was applied to compare the mean densities. The details of the t-test are reported in table A4.1. In both cases the density before the aging process is statistically different from the density after the aging process.

Table A4.1. t-test

	2° experiment O_3 aging	**3° experiment hv aging**
mean density before the aging	1.075	1.141
mean density after the aging	1.605	1.751
σ of the mean*	0.025	0.027
p-value	<0.0001	<0.0001

*** values of means calculated before and after aging appertain to the same distribution (verified by F test)**

6. Conclusions

Through the joint deployment of an HR-TOF-AMS and an SMPS, it was possible to evaluate the oxidation grade (O/C) of SOA and particles density produced in the smog chamber from the reaction of α-pinene with ozone.

The O/C ratio was calculated from the concentration of 662 fragments determined in HR-TOF-AMS. The particles effective density was calculated from PM size distributions measured in terms of vacuum aerodynamic diameter and electrical mobility diameter.

At the beginning of each experiment, a decreasing of the O/C ratio and density was observed. This phenomenon could be due to the fact that, at the beginning, as there are not particles inside the chamber, particles could be formed only by nucleation which occurs for less volatile/more oxidized organic compounds. Once particles are formed there is a second mechanism that could take place, the condensation of substances on already existing particles. This second mechanism which is thermodynamically favoured, could interest also more volatile/less oxidize species. Another mechanism which could explain the decreasing of O/C and density is the dehydration reaction of more oxidized species.

In order to confirm or refuse the hypotheses, further experiments are needed. These could be done through discrete sampling of SOA on filters, in successive time from the beginning of the reaction (possibly with higher SOA concentrations), and LC-MS analysis.

During the aging processes (1-excess of ozone, 2-photochemical aging), an increasing of O/C, SOA concentration and density is observed probably due to oxidation of VOCs to form less volatile compounds. This phenomenon took place immediately during the aging with an excess of ozone, and it is slower and less intense during the photochemical aging.

7. Future activities and proposals

O/C and density calculation will be refined by porting further adjustments to the fragmentation table and by correcting PToF data as a function of lenses pressure in order to obtain reliable density values even during flow rate decreasing [Bahreini 2003].

Positive Matrix Factorization (PMF) analysis will be applied to HR-TOF-AMS data in order to disaggregate the contribution of different chemical/physical processes, i.e. nucleation/condensation.

8. References

Aiken A.C., DeCarlo P.F., Kroll J.H., Worsnop D.R., Huffman J.A., Docherty K.S., Ulbrich I.M., Mohr C., Kimmel J.R., Sueper D., Sun Y., Zhang Q., Trimborn A., Northway M., Ziemann P.J., Canagaratna M.R., Onasch T.B., Alfarra M.R., Prevot A.S.H., Dommen J., Duplissy J., Metzger A., Baltensperger U., Jimenez J.L. (**2008**) O/C and OM/OC Ratios of Primary, Secondary, and Ambient Organic Aerosols with High-Resolution Time-of-Flight Aerosol Mass Spectrometry. *Environmental Science & Technology* 42, 4478-4485.

Alfarra M.R., Coe H., Allan J.D., Bower K.N., Boudries H., Canagaratna M.R., Jimenez J.L., Jayne J.T., Garforth A., Li S.-M., Worsnop D.R. (**2004**) Characterization of urban and regional organic aerosols in the lower Fraser Valley using two Aerodyne Aerosol Mass Spectrometers. *Atmospheric Environment* 38, 5745–5758.

Allan J.D., Jimenez J.L., Williams P.I., Alfarra M.R., Bower K.N., Jayne J.T., Coe H., Worsnop D.R. (**2003**) Quantitative sampling using an Aerodyne aerosol mass spectrometer 1. Techniques of data interpretation and error analysis. *Journal of Geophysiacl Research* 108, D3, doi: 10.1029/2002JD002358.

Allan J.D., Delia A.E., Coe H., Bower K.N., Alfarra M.R., Jimenez J.L., Middlebrook A.M., Drewnick F., Onasch T.B., Canagaratna M.R., Jayne J.T., Worsnop D.R. (**2004**) A generalised method for the extraction of chemically resolved mass spectra from Aerodyne aerosol mass spectrometer data. *Aerosol Science* 35, 909-922.

Bahreini R., Jimenez J.L., Wang J., Flagan R.C., Seinfeld J.H., Jayne J.T., Worsnop D.R. (**2003**) Aircraft-based aerosol size and composition measurements during ACE-Asia using an Aerodyne aerosol mass spectrometer. *Journal of Geophysical Research* 108, D23, 8645, doi:10.1029/2002JD003226.

Bahreini R., Keywood M.D., Ng N.L., Varutbangkul V., Gao S., Flagan R.C., Seinfeld J.H., Worsnop D.R., Jimenez J.L. (**2005**) Measurements of Secondary Organic

Aerosol from Oxidation of Cycloalkenes, Terpenes, and m-Xylene Using an Aerodyne Aerosol Mass Spectrometer. *Environmental Science & Technology* 39, 15, 5674-5688.

Canagaratna M.R., Jayne J.T., Jimenez J.L., Allan J.D., Alfarra M.R., Zhang Q., Onasch T.B., Drewnick F., Coe H., Middlebrook A., Delia A., Williams L.R., Trimborn A.M., Northway M.J., DeCarlo P.F., Kolb C.E., Davidovits P., Worsnop D.R. (**2007**) Chemical and microphysical characterization of ambient aerosols with the aerodyne aerosol mass spectrometer. *Mass Spectrometry Reviews* 26, 185– 222.

Chen Q., Liu Y., Donahue N.M., Shilling J.E., Martin S.T. (**2011**) Particle-Phase Chemistry of Secondary Organic Material: Modeled Compared to Measured O:C and H:C Elemental Ratios Provide Constraints. *Environmental Science & Technology* 45, 4763-4770.

Criegee R. (**1975**) Mechanism of Ozonolysis. *Angewandte Chemie International Edition in English* 14, 745–752.

DeCarlo P.F., Kimmel J.R., Trimborn A., Northway M.J., Jayne J.T., Aiken A.C., Gonin M., Fuhrer K., Horvath T., Docherty K.S., Worsnop D.R., Jimenez J.L. (**2006**) Field-Deployable, High-Resolution, Time-of-Flight Aerosol Mass Spectrometer. *Analytical Chemistry* 78, 8281-8289.

Drewnick F., Hings S.S., DeCarlo P., Jayne J.T., Gonin M., Fuhrer K., Weimer S., Jimenez J.L., Demerjian K.L., Borrmann S., Worsnop D.R. (**2005**) A new time-of-flight aerosol mass spectrometer (TOF-AMS)-instrument description and first filed deployment. *Aerosol Science and Technology* 39, 637-658.

Drewnick F., Hings S.S., Alfarra M.R., Prevot A.S.H., Borrmann S. (**2009**) Aerosol quantification with the Aerodyne Aerosol Mass Spectrometer: detection limits and ionizer background effects. *Atmospheric Measurement Techniques* 2, 33-46.

Jayne J.T., Leard D.C., Zhang X., Davidovits P., Smith K.A., Kolb C.E., Worsnop D.R. (**2000**) Development of an aerosol mass spectrometer for size and composition analysis of submicron particles. *Aerosol Science & Technology* 33, 49–70.

Jimenez J.L., Jayne J.T., Shi Q., Kolb C.E., Worsnop D.R., Yourshaw I., Seinfeld J.H., Flagan R.C., Zhang X., Smith K.A., Morris J.W., Davidovits P. (**2003**) Ambient

aerosol sampling using the Aerodyne Aerosol Mass Spectrometer. *Journal of Geophysical Research* 108, D7, doi: 10.1029/2001JD001213.

Kanakidou M., Seinfeld J.H., Pandis S.N., Barnes I., Dentener F.J., Facchini M.C., Van Dingenen R., Ervens B., Nenes A., Nielsen C.J., Swietlicki E., Putaud J.P., Balkanski Y., Fuzzi S., Horth J., Moortgat G.K., Winterhalter R., Myhre C.E.L., Tsigaridis K., Vignati E., Stephanou E.G., Wilson J. (**2005**) Organic aerosol and global climate modelling: a review. *Atmospheric Chemistry and Physics* 5, 1053-1123.

Kostenidou E., Pathak R.K., Pandis S.N. (**2007**) An Algorithm for the Calculation of Secondary Organic Aerosol Density Combining AMS and SMPS Data. *Aerosol Science and Technology* 41, 1002-1010.

Ma Y., Luciani T., Porter R.A., Russell A.T., Johnson D., Marston G. (**2007**) Organic acid formation in the gas-phase ozonolysis of α-pinene. *Physical Chemistry Chemical Physics* 9, 5084-5087.

Ma Y., Russell A.T., Marston G. (**2008**) Mechanisms for the formation of secondary organic aerosol components from the gas-phase ozonolysis of α-pinene. *Physical Chemistry Chemical Physics* 10, 4294-4312.

Reischl G.P., Makela J.M., Karch R., Necid J. (**1996**) Bipolar charging of ultrafine particles in the size range below 10 nm. *Journal of Aerosol Science* 27 (6), 931-949.

Reischl G.P., Mäkelä J.M., Necid J. (**1997**) Performance of the Vienna type differential mobility analyser at 1.2 – 20 nm. *Aerosol Science and Technology* 27, 651-672.

Wang J., Doussin J.-F., Perrier S., Perraudin E., Katrib Y., Pangui E., Picquet-Varrault B. (**2011**) Design of a new multi-phase experimental simulation chamber for atmospheric photosmog, aerosol and cloud chemistry. *Atmospheric Measurement Techniques Discussions* 4, 315-384.

Winkelmair W., Reischl G.P., Lindner A.O., Berner A. (**1991**) A new electromobility spectrometer for the measurement of aerosol size distributions in the size range from 1 to 1000 nm. *Journal of Aerosol Science* 22, 289–296.

Winterhalter R., Van Dingenen R., Larsen B.R., Jensen N.R., Hjorth J. (**2003**) LC-MS analysis of aerosol particles from the oxidation of α-pinene by ozone and OH radicals. *Atmospheric Chemistry and Physics Discussions* 3, 1–39.

Annex 5. Assessment of the environmental exposure of honeybees to neonicotinoid insecticides used in corn seeds treatment.

Colony Collapse Disorder (CCD), the sudden loss of most honeybees failing to return to the hive represents a worldwide crisis of increasing proportions. The consequent losses in crops productivity and plant pollination constitute a major emergency from both economical and ecological standpoints. Although on the causes of CCD several hypothesis have been advanced (parasitic mites, viruses, insecticides, etc.) up to the present no one has been clearly supported by experimental results. In several countries the phenomenon is mainly observed in the period of corn sowing (spring), that generally occurs using corn seeds coated with neonicotinoid insecticides [Greatti 2003]. Neonicotinoid insecticides act as neurotoxic agents by binding to nicotinic acetylcholine receptors in the insects central nervous system. Most of them present a high solubility in water, i.e. Thiamethoxam, Clothianidin and Imidacloprid. As a consequence, seed-coating neonicotinoid insecticides, that are extensively utilized in corn crops, have been blamed for CCD.

During the sowing operations, the seeds are sucked into the pneumatic drilling machine causing the erosion of the seed coating and the fragments are then expelled through a waste pipe. In a first hypothesis, bees uptake neonicotinoids through the nectar and pollen of the contaminated vegetation at field margins. However, the insecticides content on the surrounding vegetation was shown to be not sufficient to cause acute toxicity in foraging bees [Greatti 2006]. In this connection, novel routes of exposure and intoxication of honeybees to neonicotinoids have been proposed: 1) the translocation of the systemic neonicotinoids from the coated seed to guttation drops of young corn plants [Girolami 2009, Tapparo 2011] and 2) the atmospheric emission of particulate matter containing the insecticide by the pneumatic drilling machine [Marzaro 2011, Girolami 2011, Tapparo 2012, Girolami 2012]. Quantitative measurements conducted both in laboratory and in the field demonstrated that both mechanisms of neonicotinoids environmental release can produce high exposure levels for bees. While the first one is limited to specific environmental conditions, we have demonstrated that the second mechanism depicts a scenario compatible with CCD phenomenon. In fact, honeybees in free flight conditions are directly exposed to particulate matter containing neonicotinoid insecticides, they assume doses

consistently above the LD_{50} and die within few hours even after a single flight in the proximity of the drilling machine [Girolami 2011, Girolami 2012, Tapparo 2012].
In conclusion, this emission source of particles with acute toxic effects on bees is a widespread ecological problem which should require a deeper analysis of the related agricultural policies and the realization of suitable devices for an efficient emission reduction.

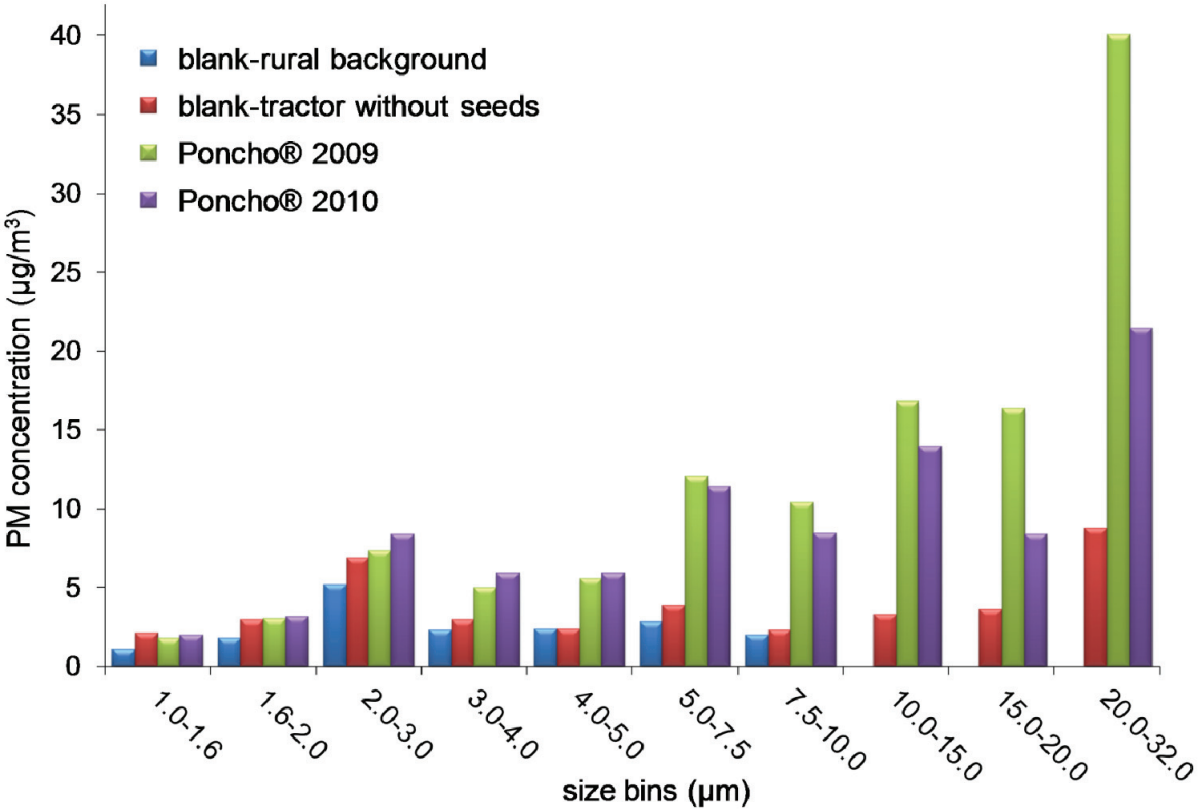

Figure A5.1. Example of the dimensional distribution of particles emitted by the drilling machine during the sowing of corn coated seeds with Poncho® (p.a. Clothianidin), measured by OPC instrumentation 5 m from the outlet of the air fan.

References

Girolami V., Mazzon L., Squartini A., Mori N., Marzaro M., Di Bernardo A., Greatti M., Giorio C., Tapparo A. (**2009**) Translocation of neonicotinoid insecticides from coated seeds to seedling guttations: a novel way of intoxication for bees. *Journal of Economic Entomology Ecotoxicology* 102(5), 1808-1815.

Girolami V., Marzaro M., Vivan L., Mazzon L., Greatti M., Giorio C., Marton D., Tapparo A. (**2011**) Fatal powdering of bees in flight with particulates of

neonicotinoids seed coating and humidity implication. *Journal of Applied Entomology*, in press. DOI: 10.1111/j.1439-0418.2011.01648.x.

Girolami V., Marzaro M., Vivan L., Giorio C., Marton D., Tapparo A. (**2012**) Aerial powdering of bees inside mobile cages and the extent of the toxic neonicotinoid cloud surrounding corn drillers. *Journal of Applied Entomology*, in press.

Greatti M., Sabatini A.G., Barbattini R., Rossi S., Stravisi A. (**2003**) Risk of environmental contamination by the active ingredient imidacloprid used for corn seed dressing. Preliminary results. *Bulletin of Insectology* 56(1), 69-72.

Greatti M., Barbattini R., Stravisi A., Sabatini A.G., Rossi S. (**2006**) Presence of the a.i. imidacloprid on vegetation near corn fields sown with Gaucho® dressed seeds. *Bulletin of Insectology* 59(2), 99-103.

Marzaro M., Vivan L., Targa A., Mazzon L., Mori N., Greatti M., Petrucco Toffolo E., Di Bernardo A., Giorio C., Marton D., Tapparo A., Girolami V. (**2011**) Lethal aerial powdering of honey bees with neonicotinoids from fragments of maize seed coat. *Bulletin of Insectology* 64(1), 119-126.

Tapparo A., Giorio C., Marzaro M., Marton D., Soldà L., Girolami V. (**2011**) Rapid analysis of neonicotinoid insecticides in guttation drops of corn seedlings obtained from coated seeds. *Journal of Environmental Monitoring* 13(6), 1564-1568.

Tapparo A., Marton D., Giorio C., Zanella A., Soldà L., Marzaro M., Vivan L., Girolami V. (**2012**) Assessment of the environmental exposure of honeybees to particulate matter containing neonicotinoid insecticides coming from corn coated seeds. *Environmental Science & Technology*, in press.

Annex 6. List of Publications of Chiara Giorio

1. Girolami V., Mazzon L., Squartini A., Mori N., Marzaro M., Di Bernardo A., Greatti M., Giorio C., Tapparo A. (**2009**) Translocation of neonicotinoid insecticides from coated seeds to seedling guttations: a novel way of intoxication for bees. *Journal of Economic Entomology Ecotoxicology* 102(5), 1808-1815.
2. Harrison R.M., Giorio C., Beddows D.C.S., Dall'Osto M. (**2010**) Size distribution of airborne particle controls outcome of epidemiological studies. *Science of the Total Environment* 409, 289-293.
3. Marzaro M., Vivan L., Targa A., Mazzon L., Mori N., Greatti M., Petrucco Toffolo E., Di Bernardo A., Giorio C., Marton D., Tapparo A., Girolami V. (**2011**) Lethal aerial powdering of honey bees with neonicotinoids from fragments of maize seed coat. *Bulletin of Insectology* 64(1), 119-126.
4. Tapparo A., Giorio C., Marzaro M., Marton D., Soldà L., Girolami V. (**2011**) Rapid analysis of neonicotinoid insecticides in guttation drops of corn seedlings obtained from coated seeds. *Journal of Environmental Monitoring* 13(6), 1564-1568.
5. Girolami V., Marzaro M., Vivan L., Mazzon L., Greatti M., Giorio C., Marton D., Tapparo A. (**2012**) Fatal powdering of bees in flight with particulates of neonicotinoids seed coating and humidity implication. *Journal of Applied Entomology* 136, 17-26.
6. Girolami V., Marzaro M., Vivan L., Giorio C., Marton D., Tapparo A. (**2012**) Aerial powdering of bees inside mobile cages and the extent of the toxic neonicotinoid cloud surrounding corn drillers. *Journal of Applied Entomology*, in press.
7. Tapparo A., Marton D., Giorio C., Zanella A., Soldà L., Marzaro M., Vivan L., Girolami V. (**2012**) Assessment of the environmental exposure of honeybees to particulate matter containing neonicotinoid insecticides coming from corn coated seeds. *Environmental Science & Technology*, in press.
8. Giorio C., Tapparo A., Dall'Osto M., Harrison R.M., Beddows D.C.S., Nemitz E. (**2012**) Comparison of three techniques for analysis of data from an aerosol time-of-flight mass spectrometer. In preparation.

Acknowledgements

First of all, I would like to thank my supervisor, prof. Andrea Tapparo, who has always been supportive. This thesis would not have been possible without him.

I would like to thank the group of analytical chemistry of the Department of Chemical Sciences of the University of Padova, and the 6th floor in particular, for support and for the time spent together.

I owe my deepest gratitude to all the people that have been involved in my PhD during these three years: Professor Roy M. Harrison, for the opportunity to work with him during these years, to have made possible for me to work with ATOFMS data and for helpful discussions, Johanna K. Gietl for London data, David C.S. Beddows for Harwell data, helpful discussion and technical support in data analysis and Manuel Dall'Osto for help in data interpretation. Moreover, I am grateful to Eiko Nemitz, for Harwell 2008 AMS data.

It is a pleasure to thank those who revised my thesis, prof. Hugh Coe and prof. John Sodeau for the scientific revision and helpful comments to improve my thesis and Francesca Ramanzin for language revision.

I would like to show my deepest gratitude to those who made possible the experience in Paris at LISA: prof. Jean-François Doussin, dr. Paola Formenti, Cyrielle Denjean, prof. Anne Monod, Brice Temime-Roussel, Sylvain Ravier and Frank Siekmann. Working with you at the smog chamber have been very interesting and exciting.

Last, but not least I would like to thank my family and all my friends. A special thank for "Mamma e Papà".